Department of Physics
Technical University of Ostrava

Spectral Interferometry of Polarization-Maintaining Optical Fibers

(Habilitation Thesis)

Ostrava 2016

RNDr. Dalibor Ciprian, PhD

Contents

Part I

Habilitation Thesis

Chapter 1

Introduction

Specialty optical fibers have been an important part of fiber optic technology for last four decades. They find their usage in diverse application domains as fiber optic laser sources, optical amplifiers, dispersion-compensating devices for optic communications, fiber optic gyroscopes used in aerospace systems, or in design of various fiber optic sensors. The last mentioned area is a leading consumer of specialty optical fibers. The application of fiber optic sensors of physical quantities includes the detection of strain, pressure, mechanical vibrations, flow, temperature, and electric or magnetic field sensing. As to the application in chemistry, fiber optic sensors based on refractive index change detection are often used for concentration measurements. Other application potential is connected with the possibility to combine multiple features in the same specialty fiber. Such fiber allows to detect for example stress and temperature changes simultaneously.

The term 'specialty' is used to distinguish such fibers from standard telecommunication fibers. It refers to some unique features obtained either by special dopant application or by specific geometry of the fiber. Typical examples of the first group are rare earth-doped fibers used for optical fiber amplifiers and fiber laser sources, or fluoride, chalcogenide or heavy metal oxide glass fibers designed for mid-infrared or infrared applications. Other examples are photosensitive fibers whose core index of refraction can be permanently modified when exposed to irradiation by ultraviolet light. Photosensitivity allows to realize various optical components based on fiber Bragg gratings or long-period gratings. Concerning the second group, various types of elliptical fibers ranging from elliptical core to D-shaped elliptical fibers are worth mentioning together with microstructured fibers, which are manufactured using only one material and whose dispersion properties can be optimized just by the change of their geometry. Because of broken circular symmetry, elliptical fiber waveguides exhibit ability to preserve the polarization state of a guided wave. This feature is often used in design of fiber optic sensors where polarimetric detection setup is exploited. The microstructured fiber with proper geometry design can possess the same feature.

The fibers with above mentioned ability to keep and transmit the polarization of the light launched into it are called *polarization maintaining fibers* (PMFs). They are important part of specialty optical fiber technology and the measurement methods for characterization of their parameters are the subject of presented text. Polarization maintaining fibers were developed for the purposes of coherent communication systems as one of the first applications of specialty fiber technology in beginning of eight decade of last century. Even if the development of commercial coherent communication systems based on PMFs effectively ceased ten years after when simpler and more versatile solutions to high-bandwidth transmission were presented, they found their usage in several others optical systems as fiber optic gyroscopes, current sensors or laser Doppler anemometry devices. The ability to transmit the polarization modes is created through the introduction of anisotropy to the fiber cross-section.

Such anisotropy can be created either by application of uniaxial stress leading to the refractive index changes via the photo-elastic effect, or by appropriate geometric design. The first case is referred to as *stress birefringence*, the second one as *form birefringence*.

The stress birefringent polarization maintaining fibers have usually one of the used geometries: PANDA, bow tie or elliptical jacket. All three designs are based on the same mechanism, where some stress applying parts consisting of high-expanding glass are placed in the vicinity of the fiber core. The thermal expansion coefficient difference leads to the residual tension acting as the source of birefringence.

As to the presented text, the experiments were oriented on characterization of fiber samples belonging to the second mentioned design - form birefringence fiber. The measurements were carried out for elliptical core fibers and microstructured fibers. Historically, elliptical core fibers were first studied as the case of imperfection of standard circular fibers. Now they are mostly used in sensing applications, where the elliptical core design offers lower temperature variation of birefringence and better mechanical properties than the stress induced birefringence design.

The other type of experimentally studied form birefringence fibers were photonic crystal fibers. Such fibers, sometimes called microstructured fibers, can be manufactured from a single material and their characteristics can be manipulated just by the change of several geometric parameters. The guiding mechanism of optical waves in the mentioned fibers differs from the waveguiding in conventional fibers operating on total internal reflection the waves undergo on boundary between core and cladding. Instead of cladding consisting of the glass with different refractive index, the core is surrounded by periodic array of microstructured air holes. The periodic arrangement of the holes leads to the formation of *photonic band-gap*. The waves whose frequencies fall into such a photonic band-gap can not propagate in the air-hole array and so they are forced to propagate in the core region. In addition, the core itself is not necessary solid and the waveguiding can take place in an air hole in located in the core. Thus, the photonic band-gap waveguiding offers a rich variety of possible fiber designs. Polarization maintaining properties of such fibers can be controlled via the geometry of the holes too. Introduction of some "defects" in the location and geometry of the holes, leading to the circular core symmetry break, induces the polarization maintaining ability of such fibers.

Proper design of fiber optic devices requires the knowledge of dispersion characteristics of used fibers. Considering the sensors of various chemical or physical quantities based on interferometric techniques and employing the polarization maintaining fibers, the phase and group birefringence behavior in spectral domain plays an important role. On the other side, chromatic dispersion is an important parameter for the design of supercontinuum sources. The type of the used characterization method depends on the length of investigated fiber. The dispersion characteristics of long length optical fibers are usually determined by time-of-flight method, or by modulation phase shift method. The first technique is based on the measurement relative temporal delay for pulses generated at different wavelengths. The second one measures the phase delay of a modulated signal as a function of wavelength. The other choice is wavelength scanning method usually used for short length fibers, but the technique can be applied to long length fibers as well. One of the most versatile tools considered for the dispersion characterization of short length fiber samples is *spectral interferometry*. Presented work deals with spectral interferometric techniques developed and applied to the characterization of polarization maintaining fibers.

The thesis begins with an introduction followed by two chapters where the basic facts and methods used in for description of elliptical core fibers and photonic crystal fibers are presented. Then the basic concepts of spectral interferometry methods used for characterization of polarization maintaining fibers are given. The results of research work are discussed in the chapter five. Finally, chapter six contains the summary of the thesis and some ideas for further research.

Chapter 2

Elliptical core fibers

2.1 Problem formulation

Wave propagation in optical elliptical core fibers is based on *index guiding* mechanism. It means that the refractive index value n_{cr} in core region (see Fig.2.1) is higher then the refractive index value n_{cl} in cladding region and the waves are confined within core by total reflection on the core-cladding boundary. Materials in both regions are assumed to be lossless, homogeneous dielectrics, forming a step refractive index profile. Besides the total reflection, other condition enforced by the fact that the waves in the core propagate in a bounded region has to be fulfilled as well. Both condition lead to the discrete character of the spectrum of waves guided in the waveguide structure. In the following text, the core is represented by the ellipse with the semi-major and semi-minor

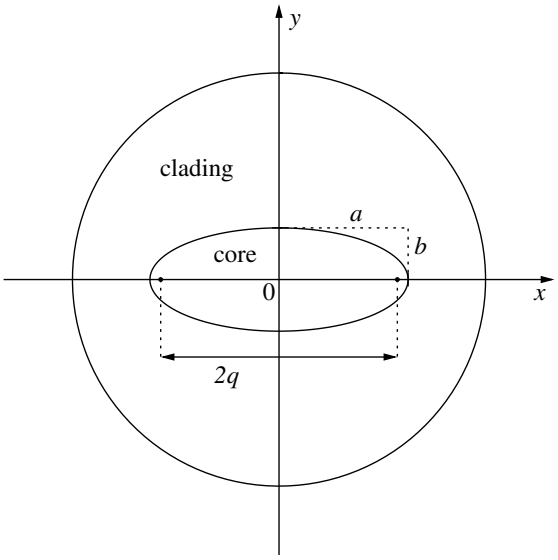

Figure 2.1: Elliptical core fiber cross-section

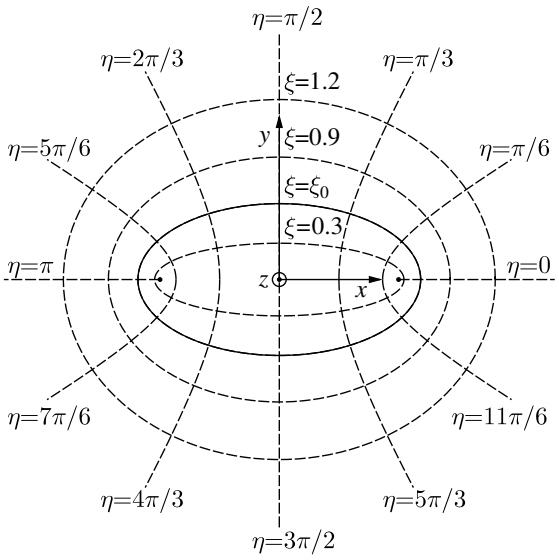

Figure 2.2: Schematic drawing of elliptical coordinates, core boundary at $\xi = \xi_0$.

axes a and b, where the semi-major axis is parallel to x-axis of Cartesian coordinate system. The geometry of the problem naturally leads to elliptical coordinate system schematically depicted in Figure 2.2. The elliptical coordinates ξ, η and z are related to Cartesian coordinates x, y and z by transformation:

$$x = q \sinh\xi \cos\eta \qquad y = q \cosh\xi \sin\eta \qquad z = z\,, \tag{2.1}$$

where $q = \sqrt{a^2 - b^2}$ is the semi-focal distance. The core boundary is then simply defined by a constant value of radial coordinate $\xi = \xi_0$. The semi-major and semi-minor axes of the core ellipse are then expressed as $a = q\cosh\xi_0$ and $b = q\sinh\xi_0$. The task is to find the solution to Maxwell equations in lossless, isotropic, non-magnetic ($\mu = \mu_0$) media, characterized by permittivity ϵ:

$$\boldsymbol{\nabla} \times \boldsymbol{E} = -\mu_0 \frac{\partial \boldsymbol{H}}{\partial t} \tag{2.2}$$

$$\boldsymbol{\nabla} \times \boldsymbol{H} = \epsilon \frac{\partial \boldsymbol{E}}{\partial t} \tag{2.3}$$

$$\boldsymbol{\nabla} \cdot \boldsymbol{E} = 0 \tag{2.4}$$

$$\boldsymbol{\nabla} \cdot \boldsymbol{H} = 0 \tag{2.5}$$

transformed to elliptical coordinates in the core and cladding region and fulfilling appropriate boundary conditions on core-cladding boundary. For the purposes of following analysis, the cladding region is supposed to be infinite, $\boldsymbol{E}(\boldsymbol{r}, t)$ and $\boldsymbol{H}(\boldsymbol{r}, t)$ denote the intensity of electric and magnetic field. Instead of the set of first-order partial differential equations (2.2-2.5), the wave equations for $\boldsymbol{E}$ and $\boldsymbol{H}$ vectors can be derived by taking the curl of (2.2) and (2.3):

$$\Delta\boldsymbol{E} - \mu\epsilon\frac{\partial^2 \boldsymbol{E}}{\partial t^2} = 0 \qquad \Delta\boldsymbol{H} - \mu\epsilon\frac{\partial^2 \boldsymbol{H}}{\partial t^2} = 0\,. \tag{2.6}$$

Usual method in waveguide analysis is to separate the vector fields to transverse and longitudinal parts with respect to the direction of propagation along the waveguide axis ($z-$axis in our case). Because the transverse components can be expressed using the longitudinal one, the problem can be substantially simplified - instead of two vector wave equations (2.6), two scalar wave equations for longitudinal components are solved. Then the transverse components can be obtained and used when the boundary conditions are introduced. Further simplification comes from the assumption that our analysis is restricted to time-harmonic case only. The time dependence $\exp(i\omega t)$ of the electric and magnetic field intensity is supposed. So the fields are periodic in longitudinal direction as $\exp(-i\beta z)$, where β is the propagation constant.

Partial differential equations for electromagnetic field are transformed to the required coordinate system using appropriate metric coefficients (for details of the procedure see [1]). The Laplace operator in general curvilinear orthogonal system (u^1, u^2, u^3) acting on a scalar function $\Phi(u^1, u^2, u^3)$ takes the form:

$$\Delta\Phi = \frac{1}{h_1 h_2 h_3}\left[\frac{\partial}{\partial u^1}\left(\frac{h_2 h_3}{h_1}\frac{\partial\Phi}{\partial u^1}\right) + \frac{\partial}{\partial u^2}\left(\frac{h_3 h_1}{h_2}\frac{\partial\Phi}{\partial u^2}\right) + \frac{\partial}{\partial u^3}\left(\frac{h_1 h_2}{h_3}\frac{\partial\Phi}{\partial u^3}\right)\right], \tag{2.7}$$

where h_1, h_2 and h_3 are the mentioned metric coefficients. In our case of elliptic coordinate system, the metric coefficients are expressed as:

$$h_1 = h_2 = q\sqrt{\sinh^2\xi\cos^2\eta + \cosh^2\xi\sin^2\eta} \quad h_3 = 1\,, \tag{2.8}$$

and according to (2.1) the curvilinear coordinates are $u^1 = \xi\,, u^2 = \eta$ and $u^3 = z$. Thus the scalar wave equation for assumed time harmonic fields $\Phi = \Phi_\mathrm{t}(\xi, \eta)\exp(-i\beta z)$ in elliptical coordinates can be expressed as:

$$\left[\frac{\partial^2\Phi_\mathrm{t}}{\partial\xi^2} + \frac{\partial^2\Phi_\mathrm{t}}{\partial\eta^2}\right] + q^2[k^2 - \beta^2][\sinh^2\xi + \sin^2\eta]\Phi_\mathrm{t} = 0\,, \tag{2.9}$$

where $\Phi_{\mathrm{t}}(\xi,\eta)$ represents the transverse distribution of the field and k is the wavenumber in the appropriate media. Assuming that according to [2] the separation of variables $\Phi_{\mathrm{t}}(\xi,\eta) = R(\xi)\Theta(\eta)$ can be applied to (2.9), we obtain a pair of equations for radial and azimuthal variation of the field:

$$\frac{\partial^2 R}{\partial \xi^2} - \left[\Lambda - (k^2-\beta^2)\frac{q^2}{2}\cosh^2 2\xi\right] R = 0 \tag{2.10}$$

$$\frac{\partial^2 \Theta}{\partial \eta^2} + \left[\Lambda - (k^2-\beta^2)\frac{q^2}{2}\cos^2 2\eta\right] \Theta = 0\,, \tag{2.11}$$

where Λ denotes the separation constant. Equation (2.10) for the radial variation is the *modified Mathieu equation*, the equation (2.11) for azimuthal variation is the *Mathieu equation*. The following sections of this chapter are focused on basic methods of solution to the mentioned waveguiding problem, as the computation of the properties of elliptical core fibers is an important counterpart to the measurement methods used for determination of their parameters.

2.2 Exact approach

This type of analysis follows simple idea - find the appropriate eigensolutions to waveguide equation in the core and cladding regions and apply boundary conditions at the interface between them. The physics of the waveguiding problem requires continuity of tangent components of electromagnetic field intensities at the core/cladding boundary. This leads to a dispersion relation from which the propagation constant β can be obtained. The word 'exact' means that no additional assumptions considering the geometry of the boundary (for example low core ellipticity value), or refractive index difference value is used in order to simplify the analysis.

In order to compact the expressions in following text, it is useful to introduce the transverse propagation constant γ as:

$$\gamma_{\mathrm{d}}^2 = \frac{q^2}{4}(k_{\mathrm{d}}^2 - \beta^2) \tag{2.12}$$

where the indices $\mathrm{d} = \mathrm{cr}, \mathrm{cl}$ refers to the core and cladding regions. As to the azimuthal variation of the electromagnetic field along the boundary ellipse (given by $\xi = \xi_0$), it is obvious that the solution to Mathieu equation (2.11) must be single-valued or periodic with the azimuthal coordinate $\eta \in \langle 0, 2\pi\rangle$. According to the theory of Mathieu functions [3] that happens only when the separation constant Λ equals to one of the characteristic number of Mathieu equation:

$$\Lambda = \Lambda(\gamma_{\mathrm{d}}) = a_0(\gamma_{\mathrm{d}}^2),\, a_1(\gamma_{\mathrm{d}}^2),\, a_2(\gamma_{\mathrm{d}}^2),\, \ldots;\, b_0(\gamma_{\mathrm{d}}^2),\, b_1(\gamma_{\mathrm{d}}^2),\, b_2(\gamma_{\mathrm{d}}^2),\, \ldots\,. \tag{2.13}$$

Two sets of characteristic numbers $a_n(\gamma_{\mathrm{d}}^2)$ and $b_n(\gamma_{\mathrm{d}}^2)$ corresponds to even and odd eigensolutions to (2.11) denoted in literature as *angular Mathieu functions*: $\mathrm{ce}_n = \mathrm{ce}_n(\eta,\gamma^2)$ (even) and $\mathrm{se}_n = \mathrm{se}_n(\eta,\gamma^2)$ (odd). The characteristic numbers can be computed for a given value of γ using recursive formulae - for details see [3] or [4]. The angular Mathieu functions describe the electromagnetic field in the core as well as in the cladding.

Radial variations of the field are described by the solutions to modified Mathieu equation (2.10). Two types of solution can be distinguished. The first type are periodic functions called *associated Mathieu functions of the first kind*: $\mathrm{Ce}_n(\xi,\gamma^2)$ (cosine-like) and $\mathrm{Se}_n(\xi,\gamma^2)$ (sine-like). They correspond to the appropriate characteristic numbers (2.13). Those functions describe the field in the core (bounded) region. The other type of the solution exhibit non-periodic decrease for $\xi \to \infty$. If the wave is to be guided in the core, it has to be evanescent in the outer (cladding) region, which is here considered to be unbounded. Thus the non-periodic solutions to associated

Mathieu equation denoted as $\mathrm{Fek}_n(\xi,\gamma^2)$ and $\mathrm{Gek}_n(\xi,\gamma^2)$ are used for representation of the field in the cladding region. In comparison with the case of circular-core waveguide, the Mathieu function describing the azimuthal variation of the field does not depend on the azimuthal coordinate η only, but they also depend on material properties (refractive index) of the region. So the field components in the core and cladding regions have to be represented using *infinite* series of terms, each of them written as the product of appropriate azimuthal and radial eigensolutions [5]. According to the parity, the longitudinal field components E_z and H_z correspond either to even modes in core ($0 \le \xi \le \xi_0$):

$$H_z(\xi,\eta,z,\gamma_{\mathrm{cr}}^2) = \sum_{m=0}^{\infty} A_m \mathrm{Ce}_m(\xi,\gamma_{\mathrm{cr}}^2)\mathrm{ce}_m(\eta,\gamma_{\mathrm{cr}}^2)\exp(-i\beta z) \tag{2.14}$$

$$E_z(\xi,\eta,z,\gamma_{\mathrm{cr}}^2) = \sum_{m=1}^{\infty} B_m \mathrm{Se}_m(\xi,\gamma_{\mathrm{cr}}^2)\mathrm{se}_m(\eta,\gamma_{\mathrm{cr}}^2)\exp(-i\beta z) \tag{2.15}$$

and cladding region ($\xi_0 \le \xi < \infty$):

$$H_z(\xi,\eta,z,\gamma_{\mathrm{cl}}^2) = \sum_{r=0}^{\infty} L_r \mathrm{Fek}_r(\xi,-\gamma_{\mathrm{cl}}^2)\mathrm{ce}_r(\eta,-\gamma_{\mathrm{cl}}^2)\exp(-i\beta z) \tag{2.16}$$

$$E_z(\xi,\eta,z,\gamma_{\mathrm{cl}}^2) = \sum_{r=1}^{\infty} P_r \mathrm{Gek}_r(\xi,-\gamma_{\mathrm{cl}}^2)\mathrm{se}_r(\eta,-\gamma_{\mathrm{cl}}^2)\exp(-i\beta z)\,, \tag{2.17}$$

or to the odd modes in core:

$$H_z(\xi,\eta,z,\gamma_{\mathrm{cr}}^2) = \sum_{m=1}^{\infty} C_m \mathrm{Se}_m(\xi,\gamma_{\mathrm{cr}}^2)\mathrm{se}_m(\eta,\gamma_{\mathrm{cr}}^2)\exp(-i\beta z) \tag{2.18}$$

$$E_z(\xi,\eta,z,\gamma_{\mathrm{cr}}^2) = \sum_{m=0}^{\infty} D_m \mathrm{Ce}_m(\xi,\gamma_{\mathrm{cr}}^2)\mathrm{ce}_m(\eta,\gamma_{\mathrm{cr}}^2)\exp(-i\beta z) \tag{2.19}$$

and cladding region:

$$H_z(\xi,\eta,z,\gamma_{\mathrm{cl}}^2) = \sum_{r=1}^{\infty} G_r \mathrm{Gek}_r(\xi,-\gamma_{\mathrm{cl}}^2)\mathrm{se}_r(\eta,-\gamma_{\mathrm{cl}}^2)\exp(-i\beta z) \tag{2.20}$$

$$E_z(\xi,\eta,z,\gamma_{\mathrm{cl}}^2) = \sum_{r=0}^{\infty} F_r \mathrm{Fek}_r(\xi,-\gamma_{\mathrm{cl}}^2)\mathrm{ce}_r(\eta,-\gamma_{\mathrm{cl}}^2)\exp(-i\beta z)\,, \tag{2.21}$$

where A_m, B_m, C_m, D_m, L_r, P_r, F_r and G_r are arbitrary constants. The remaining transverse field components are determined from the longitudinal ones using Maxwell's curl equations in core and cladding regions distinguished by the region index $\mathrm{d} = \mathrm{cr}, \mathrm{cl}$:

$$E_{\xi,\mathrm{d}} = \frac{-i}{\gamma_d^2}\left(\frac{\beta}{h_1}\frac{\partial E_z}{\partial \xi} + \frac{\omega\mu_{\mathrm{d}}}{h_2}\frac{\partial H_z}{\partial \eta}\right) \qquad H_{\xi,\mathrm{d}} = \frac{-i}{\gamma_{\mathrm{d}}^2}\left(\frac{\beta}{h_1}\frac{\partial H_z}{\partial \xi} - \frac{\omega\epsilon_{\mathrm{d}}}{h_2}\frac{\partial E_z}{\partial \eta}\right) \tag{2.22}$$

$$E_{\eta,\mathrm{d}} = \frac{-i}{\gamma_{\mathrm{d}}^2}\left(\frac{\beta}{h_2}\frac{\partial E_z}{\partial \eta} - \frac{\omega\mu_{\mathrm{d}}}{h_1}\frac{\partial H_z}{\partial \xi}\right) \qquad H_{\eta,\mathrm{d}} = \frac{-i}{\gamma_{\mathrm{d}}^2}\left(\frac{\beta}{h_2}\frac{\partial H_z}{\partial \eta} + \frac{\omega\epsilon_{\mathrm{d}}}{h_1}\frac{\partial E_z}{\partial \xi}\right) \tag{2.23}$$

where h_1 and h_2 are the appropriate metric coefficients for elliptical coordinate system defined by (2.8). According to the boundary conditions, the tangential components of electric and magnetic

field intensity have to be continuous across the core-cladding boundary given by $\xi = \xi_0$. It can be written as:

$$\begin{aligned} H_{z,\mathrm{cr}}(\xi_0, \gamma_{\mathrm{cr}}^2) &= H_{z,\mathrm{cl}}(\xi_0, -\gamma_{\mathrm{cl}}^2) \\ E_{\eta,\mathrm{cr}}(\xi_0, \gamma_{\mathrm{cr}}^2) &= E_{\eta,\mathrm{cl}}(\xi_0, -\gamma_{\mathrm{cl}}^2) \\ H_{\eta,\mathrm{cr}}(\xi_0, \gamma_{\mathrm{cr}}^2) &= H_{\eta,\mathrm{cl}}(\xi_0, -\gamma_{\mathrm{cl}}^2) \\ E_{z,\mathrm{cr}}(\xi_0, \gamma_{\mathrm{cr}}^2) &= E_{z,\mathrm{cl}}(\xi_0, -\gamma_{\mathrm{cl}}^2)\,. \end{aligned} \tag{2.24}$$

In order to assemble this system of equations, Mathieu and modified Mathieu functions have to be expressed. Angular Mathieu functions are usually represented using the trigonometric function series [4]. The radial (modified) Mathieu functions can be obtained if the argument η in angular functions is replaced by $i\xi$. It leads to the expansion in terms of hyperbolic functions $\sinh\xi$ and $\cosh\xi$ [4], but such expansion is not suitable for numeric computation because of divergent nature of the mentioned functions. So the representation in terms of Bessel function series is usually employed [6–8]. Because the waveguiding problem in elliptical geometry requires the usage of infinite number of modes for field representation in both regions, the boundary conditions (2.24) lead to the infinite system of linear homogeneous equations (for details see [5]). Linear algebraic equation system has a non-trivial solution, if its determinant takes a zero value. Because the matrix elements of the mentioned system depend on γ_{cr} and γ_{cl} (see (2.24)), the roots of determinant provide the values from which the propagation constant β can be obtained. Because the structure of the infinite determinant is rather complex, the roots can be obtained only by numerical methods, such as the method of successive approximation [9].

It can be seen from (2.22) and (2.23) that to fulfill the boundary conditions (2.24), both longitudinal components E_z, H_z have to be present. The consequence is that all modes propagating in elliptical core waveguide are hybrid. Because of the asymmetry of the core two orientations of field configurations exists. The are denoted as *even* and *odd* waves corresponding to the fact that the longitudinal components are represented by even or odd Mathieu functions (2.15-2.21). Results obtained using the exact approach are often used as a trial or benchmark data for other methods, usually based on some simplification of waveguiding problem. As to the exact approach, the only inevitable approximation, besides the approximation used in numeric computing of Mathieu functions and their derivatives, is connected with the truncation of infinite matrix leading to the determinantal equation for propagation constants.

2.3 Approximate methods

Although the above described exact method should yield the most rigorous results when the propagation constant β or the modal field distribution is to be obtained, its practical implementation is difficult because of complexity of computational process. That is why various approximate methods have been developed in order to either simplify the formulation of waveguiding problem or to completely avoid the usage of Mathieu functions. Usually the assumption is made that the core refractive index differs only slightly from the refractive index of the cladding. This is valid in the most cases of practical interest. The other often used assumption is related to the core shape, where the slightly elliptical core can be treated as the perturbation of a circular one.

2.3.1 Perturbation approach

The method was developed for computation of mode parameters of waveguides with low dielectric contrast between the core and cladding media. Under the assumption $n_{\mathrm{cr}} \approx n_{\mathrm{cl}}$ the electromagnetic field components of an optical waveguide can be expressed using a critical angle $\theta_{\mathrm{c}} \approx \sin\theta_{\mathrm{c}} =$

$(1 - n_{\mathrm{cl}}^2/n_{\mathrm{cr}}^2)^{1/2}$ acting here as a "small" parameter used for perturbation. The other parameter $V = b(k_{\mathrm{cr}}^2 - k_{\mathrm{cl}}^2)^{1/2}$ is assumed to be independent with respect to θ_{c} when $\theta_{\mathrm{c}} \ll 1$. If a waveguide has a cylindrical symmetry and the material parameters do not change in the longitudinal (z) direction, the electromagnetic field of the modes can be decomposed to transverse and longitudinal components:

$$\boldsymbol{E} = (\boldsymbol{e}_{\mathrm{t}} + \boldsymbol{e}_z) \exp i\beta z \qquad \boldsymbol{H} = (\boldsymbol{h}_{\mathrm{t}} + \boldsymbol{h}_z) \exp i\beta z \tag{2.25}$$

for harmonic $\exp(-i\omega t)$ time dependence. It can be shown, that the transverse part $\boldsymbol{e}_{\mathrm{t}}$ of electric field intensity has to obey the reduced wave equation:

$$\nabla_{\mathrm{t}}^2 \boldsymbol{e}_{\mathrm{t}} + (k^2 - \beta^2)\boldsymbol{e}_{\mathrm{t}} = -\nabla_{\mathrm{t}}(\boldsymbol{e}_{\mathrm{t}} \cdot \nabla_{\mathrm{t}} \ln \epsilon)\,, \tag{2.26}$$

where ∇_{t}^2 is the transverse part of vector Laplacian operator, $k = 2\pi n(x, y)/\lambda$ is the wave and ϵ represents the transverse permittivity distribution. The idea of the method is to expand the field as a power series in θ_{c}, treating θ_{c} and V as independent variables [10]:

$$\boldsymbol{e}(V, \theta_{\mathrm{c}}) = \boldsymbol{e}_0(V, 0) \,+\, \theta_{\mathrm{c}} \boldsymbol{e}_1(V, 0) \,+\, \theta_{\mathrm{c}}^2 \boldsymbol{e}_2(V, 0) \,+\, \ldots$$

to simplify the waveguide equation and consequently obtain an approximation formula for propagation constant. From the point of view of physics, one first deals with the $n_{\mathrm{cr}} = n_{\mathrm{cl}}$ waveguide and then uses the results to approximate the field of $n_{\mathrm{cr}} \approx n_{\mathrm{cl}}$ waveguide. The zero-order approximation, given by $n_{\mathrm{cr}} = n_{\mathrm{cl}}$ condition appears to lead to unphysical consequence, that such a waveguide is incapable to guide the energy. But when we assume that the guiding properties remain unaffected (i.e. V can be an arbitrary constant), it is found that $\boldsymbol{e}(V, 0)$ is an excellent approximation to $\boldsymbol{e}(V, \theta_{\mathrm{c}})$. Because $n_{\mathrm{cr}} = n_{\mathrm{cl}}$ condition leads to $\beta = k_{\mathrm{cr}} = k_{\mathrm{cl}}$, the field in such a structure is purely transverse electromagnetic waves and all polarization-dependent effects vanish since they are related to $\nabla_{\mathrm{t}} \ln \epsilon$ term in (2.26). When $n_{\mathrm{cr}} = n_{\mathrm{cl}}$, this term is zero. Consequently, the field of $n_{\mathrm{cr}} = n_{\mathrm{cl}}$ waveguide is the solution of scalar wave equation:

$$\nabla_{\mathrm{t}}^2 \psi + (k^2 - \tilde{\beta}^2)\psi = 0\,. \tag{2.27}$$

The vector modal fields can be expressed in Cartesian coordinate system as $\tilde{\boldsymbol{e}}_x = \psi \boldsymbol{x}$ and $\tilde{\boldsymbol{e}}_y = \psi \boldsymbol{y}$, where $\boldsymbol{x}$ and $\boldsymbol{y}$ are the unit vectors, and the tilde is used to distinguish the quantities obtained using (2.27) from the ones obtained using (2.26). The solution ψ has to be bounded everywhere (waveguiding) and they have to obey the condition related to scalar wave equation that ψ and its normal derivative with respect to core boundary are continuous everywhere. The mentioned constraints are used to construct the eigenvalue equation for $n_{\mathrm{cr}} = n_{\mathrm{cl}}$ case in order to obtain the propagation constants $\tilde{\beta}$. The mentioned modal fields $\tilde{\boldsymbol{e}}_x$ and $\tilde{\boldsymbol{e}}_y$ of $n_{\mathrm{cr}} = n_{\mathrm{cl}}$ step index profile waveguide are uniformly polarized, thus they are referred in the literature as linearly polarized (LP) modes [11]. They can be used to approximate the modal fields of vector wave equation for the case of $n_{\mathrm{cr}} \approx n_{\mathrm{cl}}$, when the $\nabla_{\mathrm{t}}(\boldsymbol{e}_{\mathrm{t}} \cdot \nabla_{\mathrm{t}} \ln \epsilon)$ is no longer zero. The appropriate modal fields are then approximated by linear combinations of the mentioned LP modes. The way how to form them depends on the symmetry of the waveguide cross-section.

Under the low dielectric contrast assumption the longitudinal component of electric field intensity can be obtained from Maxwell's equations using approximation formula:

$$e_z \approx (i/\beta)\nabla_{\mathrm{t}} \cdot \boldsymbol{e}_{\mathrm{t}}\,. \tag{2.28}$$

Once the propagation constant $\tilde{\beta}$ and modal fields $\tilde{\boldsymbol{e}}_{\mathrm{t}}$ of scalar wave equation (2.27) are known and the vector wave equation modal fields $\boldsymbol{e}_{\mathrm{t}}$ are approximated using LP modes (assembled using

$\tilde{\boldsymbol{e}}_\mathrm{t}$), standard perturbation technique can be applied to find the approximation formula for β [12]. The idea is based on deviation computation used to obtain modal orthogonality, forming first the dot product of $\tilde{\boldsymbol{e}}_\mathrm{t}$ with vector wave equation (2.26) and the dot product of (2.27) with $\boldsymbol{e}_\mathrm{t}$. The dot products are then subtracted and the resulting equation integrated over the infinite waveguide cross-section $\mathcal{A}_\infty$. This leads to a formula:

$$\beta - \tilde{\beta} \approx \frac{\beta^2 - \tilde{\beta}^2}{2k} = \frac{\int_{\mathcal{A}_\infty} \tilde{\boldsymbol{e}}_\mathrm{t} \cdot \nabla_\mathrm{t}(\boldsymbol{e}_\mathrm{t} \cdot \nabla_\mathrm{t} \ln \epsilon)\,\mathrm{d}\mathcal{A}}{2k \int_{\mathcal{A}_\infty} \tilde{\boldsymbol{e}}_\mathrm{t} \cdot \boldsymbol{e}_\mathrm{t}\,\mathrm{d}\mathcal{A}} \tag{2.29}$$

for the required propagation constant β. Further simplification can be done for the step index waveguide, where the integral in the numerator can be converted to a line integral around the core boundary $\mathcal{B}$:

$$\int_{\mathcal{A}_\infty} \tilde{\boldsymbol{e}}_\mathrm{t} \cdot \nabla_\mathrm{t}(\boldsymbol{e}_\mathrm{t} \cdot \nabla_\mathrm{t} \ln \epsilon)\,\mathrm{d}\mathcal{A} = \theta_\mathrm{c}^2 \oint_{\mathcal{B}} (\nabla_\mathrm{t} \cdot \tilde{\boldsymbol{e}}_\mathrm{t})(\boldsymbol{e}_\mathrm{t} \cdot \boldsymbol{n})\,\mathrm{d}l$$

where $\boldsymbol{n}$ denotes the outer normal with respect to core boundary line.

In order to form the LP modes polarized along x or y axes, the linear combinations of proper waveguide modes are used. The procedure is usually demonstrated on the circular waveguide case. Here the fundamental modes (angular order $l = 0$) of a $n_\mathrm{cr} = n_\mathrm{cl}$ are exceptional - they are the same as fundamental modes $n_\mathrm{cr} \approx n_\mathrm{cl}$ waveguide and they are directly x or $y-$polarized. As to the elliptical waveguide, the situation is similar, except that the propagation constants for both polarizations are different - the elliptic shape of the core removes the degeneracy. The higher order modes have to be constructed as linear combinations. For example, in the case of $l = 1$ of circular waveguide they are: $\tilde{\boldsymbol{e}}_{xe} = {}_\mathrm{e}\mathrm{EH}_{01} + {}_\mathrm{e}\mathrm{HE}_{21}$, $\tilde{\boldsymbol{e}}_{xo} = {}_\mathrm{o}\mathrm{HE}_{21} - {}_\mathrm{o}\mathrm{EH}_{01}$, $\tilde{\boldsymbol{e}}_{ye} = {}_\mathrm{e}\mathrm{HE}_{21} + {}_\mathrm{e}\mathrm{EH}_{01}$, and $\tilde{\boldsymbol{e}}_{yo} = {}_\mathrm{o}\mathrm{EH}_{01} - {}_\mathrm{o}\mathrm{HE}_{21}$ (nomenclature of hybrid modes as in [12], the indices e and o stand for even and odd modes). Similar procedure can be used for elliptic waveguide case where for example $\boldsymbol{e}_{\mathrm{t},i} = a_i\psi^\mathrm{e}\boldsymbol{x} + b_i\psi^\mathrm{o}\boldsymbol{y} \approx a_i\tilde{\boldsymbol{e}}_{xe} + b_i\tilde{\boldsymbol{e}}_{yo}\,(i = 1, 2)$, formed using ψ^e and ψ^o, are the even and odd solution to scalar wave equation (2.27) in elliptical geometry. These combinations are then used in the perturbation formula for the propagation constants computation. It is important to mention that the LP modes are not individual modes of the waveguide - especially in the case of circular waveguide. That is because the propagation constants of the modes used to form them are different. Consequently the LP mode pattern rotates as the "mode" propagates, thus it is better to refer them as pseudo-modes. Nevertheless, when the core has a non-zero eccentricity (elliptical core), the LP pseudo-modes resemble the true modes of elliptical waveguide. That is why they are used for their approximation. Whether to use the solution to a scalar wave equation in circular or elliptical geometry for the mentioned approximation or not is given by the core eccentricity. For highly elliptical cores, the scalar wave equation is to be solved in elliptical geometry, whereas for the nearly-circular core cross-section the circular waveguide modes will do. For detailed discussion see [12].

2.3.2 Weakly guiding approximation

The low dielectric contrast assumption can be used to obtain a simplified version of dispersion relations, when applied to the above described exact approach. The procedure is often addressed as weakly guiding approximation because the low dielectric contract implies low confinement of guided optical waves in the core region. If the term $(1 - n_\mathrm{cl}^2/n_\mathrm{cr}^2)$ is very small, according to [10], a small parameter $\theta_\mathrm{p} = (1 - \beta^2/k_\mathrm{cr}^2)$ can be introduced to expand various quantities used in exact approach in order to simplify the analysis. Perhaps the most important result of this approach is that the angular Mathieu functions in the waveguide core and infinite cladding region are simply

related as [13]:

$$\mathrm{ce}_n(\eta,-\gamma_{\mathrm{cl}}^2)=\mathrm{ce}_n(\eta,\gamma_{\mathrm{cr}}^2)+O(\theta_{\mathrm{p}}^2)\qquad\text{and}\qquad \mathrm{se}_n(\eta,-\gamma_{\mathrm{cl}}^2)=\mathrm{se}_n(\eta,\gamma_{\mathrm{cr}}^2)+O(\theta_{\mathrm{p}}^2)\,. \tag{2.30}$$

In addition, $1+\gamma_{\mathrm{cr}}^2/\gamma_{\mathrm{cl}}^2=O(\theta_{\mathrm{p}}^2)$ holds for the transverse propagation constants. This approximation can be used when the linear equation system for mode amplitudes in exact analysis is constructed. Here, it is necessary to expand the angular Mathieu function in the cladding region using angular Mathieu functions of the core region using so called connection coefficients [5, 14]. For example $\mathrm{ce}_n(\eta,-\gamma_{\mathrm{cl}}^2)=\sum_r'^{\infty}\alpha_{nr}\mathrm{ce}_n(\eta,\gamma_{\mathrm{cr}}^2)$, where the prime indicates the summation over even values of r only. The connection coefficients α_{nr} are obtained using the orthogonality of $\mathrm{ce}_n(\eta,\gamma_{\mathrm{cr}}^2)$.

After a simple but tedious algebra one obtains an infinite system of linear equations whose matrix is full. Using (2.30) the situation can be simplified because now the orthogonality of the core and cladding functions leads to $\alpha_{nr}=\delta_{nr}+O(\theta_{\mathrm{p}}^2)$ (here, the normalization of ce_n and se_n is supposed). Thus the infinite system matrix is no longer full, but it is in block-diagonal form. In other words, the radial orders are treated as independent quantities in the computation process. Then the determinant of the whole matrix is in the form of the product of subdeterminants related to individual blocks and the approximate dispersion equations of $m-$th radial mode order can be written in explicit forms [13] for even:

$$\frac{1}{\gamma_{\mathrm{cr}}^2}\frac{\mathrm{Ce}_m'(\xi_0,\gamma_{\mathrm{cr}}^2)}{\mathrm{Ce}_m(\xi_0,\gamma_{\mathrm{cr}}^2)}+\frac{1}{\gamma_{\mathrm{cl}}^2}\frac{\mathrm{Fek}_m'(\xi_0,|\gamma_{\mathrm{cl}}^2|)}{\mathrm{Fek}_m(\xi_0,|\gamma_{\mathrm{cl}}^2|)}=0 \tag{2.31}$$

and odd modes:

$$\frac{1}{\gamma_{\mathrm{cr}}^2}\frac{\mathrm{Se}_m'(\xi_0,\gamma_{\mathrm{cr}}^2)}{\mathrm{Se}_m(\xi_0,\gamma_{\mathrm{cr}}^2)}+\frac{1}{\gamma_{\mathrm{cl}}^2}\frac{\mathrm{Gek}_m'(\xi_0,|\gamma_{\mathrm{cl}}^2|)}{\mathrm{Gek}_m(\xi_0,|\gamma_{\mathrm{cl}}^2|)}=0\,, \tag{2.32}$$

where the prime denotes the derivative of radial Mathieu function with respect to ξ in elliptical coordinate system. The value $\xi=\xi_0$ represents the core boundary. Thus, using the quasi-orthogonality implied by weakly guiding approximation, the dispersion relations for ${}_e\mathrm{HE}_{mn}$ and ${}_o\mathrm{HE}_{mn}$ hybrid waves of a step-index, elliptical core waveguide can be obtained.

The above described procedure can be used in analysis based on LP pseudo-mode concept too, as was shown in [15]. The scalar fields $\psi(\xi,\eta)$ in elliptical geometry are assumed to be x or $y-$polarized. The even and odd solutions to scalar wave equation (2.27) are $\mathrm{LP}_{mn}^{\mathrm{e,o}}$ modes, expressed in the core region ($0\le\xi\le\xi_0$) as:

$$\psi_{\mathrm{cr}}^{\mathrm{e}}(\xi,\eta) = \sum_{m=0}^{\infty}A_m\mathrm{Ce}_m(\xi,\gamma_{\mathrm{cr}}^2)\mathrm{ce}_m(\eta,-\gamma_{\mathrm{cr}}^2)e^{i\beta z} \tag{2.33}$$

$$\psi_{\mathrm{cr}}^{\mathrm{o}}(\xi,\eta) = \sum_{m=0}^{\infty}A_m\mathrm{Se}_m(\xi,\gamma_{\mathrm{cr}}^2)\mathrm{se}_m(\eta,-\gamma_{\mathrm{cr}}^2)e^{i\beta z}\,, \tag{2.34}$$

and in the infinite cladding as:

$$\psi_{\mathrm{cl}}^{\mathrm{e}}(\xi,\eta) = \sum_{m=0}^{\infty}B_m\mathrm{Fek}_m(\xi,\gamma_{\mathrm{cl}}^2)\mathrm{ce}_m(\eta,-\gamma_{\mathrm{cl}}^2)e^{i\beta z} \tag{2.35}$$

$$\psi_{\mathrm{cl}}^{\mathrm{o}}(\xi,\eta) = \sum_{m=0}^{\infty}B_m\mathrm{Gek}_m(\xi,\gamma_{\mathrm{cl}}^2)\mathrm{se}_m(\eta,-\gamma_{\mathrm{cl}}^2)e^{i\beta z}\,. \tag{2.36}$$

As stated in [12], the solution to scalar waveguide equation and its normal derivative have to be continuous at the core-cladding boundary:

$$\psi_{\mathrm{cr}}^{\mathrm{e,o}}(\xi_0,\eta)=\psi_{\mathrm{cl}}^{\mathrm{e,o}}(\xi_0,\eta)\qquad\left.\frac{\partial}{\partial\xi}\psi_{\mathrm{cr}}^{\mathrm{e,o}}(\xi,\eta)\right|_{\xi=\xi_0}=\left.\frac{\partial}{\partial\xi}\psi_{\mathrm{cl}}^{\mathrm{e,o}}(\xi,\eta)\right|_{\xi=\xi_0}. \tag{2.37}$$

After expansion using the connection coefficients, the solutions are inserted into (2.37) and subsequently the quasi-orthogonality relations (2.30) are applied. The results are dispersion equations:

$$\frac{\mathrm{Ce}'_m(\xi_0,\gamma_{\mathrm{cr}}^2)}{\mathrm{Ce}_m(\xi_0,\gamma_{\mathrm{cr}}^2)} = \frac{\mathrm{Fek}'_m(\xi_0,-\gamma_{\mathrm{cl}}^2)}{\mathrm{Fek}_m(\xi_0,-\gamma_{\mathrm{cl}}^2)}\,, \qquad \frac{\mathrm{Se}'_m(\xi_0,\gamma_{\mathrm{cr}}^2)}{\mathrm{Se}_m(\xi_0,\gamma_{\mathrm{cr}}^2)} = \frac{\mathrm{Gek}'_m(\xi_0,-\gamma_{\mathrm{cl}}^2)}{\mathrm{Gek}_m(\xi_0,-\gamma_{\mathrm{cl}}^2)} \tag{2.38}$$

for the even and odd LP_{mn} pseudo-modes. The equations are similar to (2.31) and (2.32), except of factors $1/\gamma_{\mathrm{cr}}^2$ and $1/\gamma_{\mathrm{cl}}^2$, but recalling that $1+\gamma_{\mathrm{cr}}^2/\gamma_{\mathrm{cl}}^2 = O(\theta_{\mathrm{p}}^2) \approx 0$, there is no discrepancy. The index m denotes the order of radial Mathieu function, whereas n is related to the root position of (2.38). The same dispersion equations can be obtained by direct using of boundary conditions for E_η, H_z, H_η and E_z components of electromagnetic field [16] in LP pseudo-mode analysis. Thus the correctness of the continuity conditions of ψ and its normal derivative merely stated in [12] were proved. Nevertheless, its worth mentioning that to obtain correct results, besides the weakly guiding condition, the value of the core eccentricity should be low - for discussion see [17].

2.3.3 Approximation by rectangular-core waveguide

Whereas the above described approximate methods will do for the elliptical core fibers with low core eccentricity, they may not cope with highly elliptical core fibers, but such fibers are often a subject of interest because of their polarization maintaining properties. Although their propagation characteristics can be in principle obtained using the exact analysis, its implementation is rather complicated (Mathieu functions implementation, truncation of infinite determinantal eigenvalue equation, etc). In such a case, the highly elliptical core fibers can be treated using rectangular core approximation. The idea of the method is simple - the highly eccentric core is approximated by a rectangular one. This geometry simplification leads to much simpler characteristic equations for propagation constant. Once its value and the appropriate modal fields are known, the propagation constant can be further improved by perturbation method [18]. Let us look at the step-index

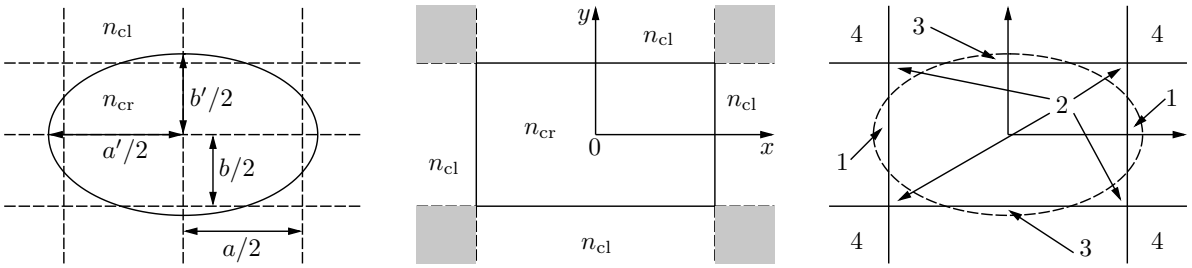

Figure 2.3: Approximation by rectangular core waveguide: (a) geometry of an elliptical core and a rectangular one, (b) rectangular waveguide geometry, (c) regions for perturbation method

elliptical core waveguide depicted in the figure 2.3a characterized by its semi-major and semi-minor axes $a'/2$, $b'/2$', and by the core and cladding dielectric constants n_{cr}^2 and n_{cl}^2. The dimensions a, b of an equivalent rectangular-core waveguide are chosen in such a way that its core area is kept the same and the axes aspect ratios equal to $a/a' = b/b' = \sqrt{\pi}/2$. Its dielectric constant distribution is then expressed as $n^2(x,y) = n'^2(x) + n''^2(y)$ [19], where:

$$\begin{aligned} n'(x)^2 &= n_{\mathrm{cr}}^2/2 \quad |x| < a/2 \\ &= n_{\mathrm{cl}}^2 - n_{\mathrm{cr}}^2/2 \quad |x| > a/2 \end{aligned} \qquad \begin{aligned} n''(y)^2 &= n_{\mathrm{cr}}^2/2 \quad |y| < b/2 \\ &= n_{\mathrm{cl}}^2 - n_{\mathrm{cr}}^2/2 \quad |y| > b/2\,. \end{aligned} \tag{2.39}$$

The basic steps of the rectangular-core waveguide follows the Marcatili's technique [20], omitting the corner regions (see fig. 2.3b - shaded areas). Then the distribution field of the components can be described using scalar function $\psi(x,y) = X(x)Y(y)$ [19]:

$$\begin{array}{rclcrclc} X(x) & = & A_1\cos(\mu_1 x+\alpha) & |x|<a/2 & Y(y) & = & B_1\cos(\nu_1 y+\gamma) & |y|<b/2 \\ & = & A_2\exp(-\mu_2|x|) & |x|>a/2 & & = & B_2\exp(-\nu_2|y|) & |y|>b/2\,. \end{array} \tag{2.40}$$

In order to keep the notation of (2.40) compact, the following parameters $\mu_1 = \sqrt{k_0^2 n_1^2/2 - \beta_1^2}$, $\mu_2 = 2a^{-1}\sqrt{V_1^2 - \mu_1^2 a^2/4}$, $\nu_1 = \sqrt{k_0^2 n_1^2/2 - \beta_2^2}$, $\nu_2 = 2b^{-1}\sqrt{V_2^2 - \nu_1^2 b^2/4}$ are used, where $V_1 = k_0 a\sqrt{n_{\rm cr}^2 - n_{\rm cl}^2}/2$ and $V_2 = V_1 b/a$ are the normalized frequencies, k_0 is the free space wavenumber. The propagation constant of a specific mode is obtained as $\beta_0 = (\beta_1^2 + \beta_2^2)^{1/2}$, the index 0 indicates that it will be subsequently used as the zero-order approximation in perturbation method. The constants $\alpha = 0, -\pi/2$, $\gamma = 0, -\pi/2$ refers to symmetric (antisymmetric) mode in x and $y-$directions.

The modal fields have to obey the appropriate boundary conditions on the core-cladding rectangular interface. The boundary conditions resulting from continuity relations yield the eigenvalue equations for β_1, β_2 and the relationship among the modal amplitude constants A_1, A_2 and B_1, B_2. As in the case of previously described LP mode-based approach, two types of modes polarized along the symmetry axes x, y are considered. One of them, E_{pq}^x, is predominantly polarized along the x-axis, the other one, E_{pq}^y is polarized along the y-axis. The other field components are therefore expressed using the dominant one. When we consider that $\psi(x,y)$ corresponds to E_x, the continuity relations require that E_x and $\partial E_x/\partial y$ are continuous at $y = \pm b/2$, and $n^2 E_x$ and $\partial E_x/\partial x$ are continuous at $x = \pm a/2$. In the case of E_{pq}^y, $\psi(x,y)$ corresponds to E_y and $n^2 E_y$ and $\partial E_y/\partial y$ have to be continuous at $y = \pm b/2$ whereas E_y and $\partial E_y/\partial x$ are continuous at $x = \pm a/2$. The results are the eigenvalue equations written in a compact form as:

$$\begin{array}{rcl} \kappa - \arctan\left[C\sqrt{\frac{V_1^2}{\kappa^2} - 1}\right] - (p-1)\frac{\pi}{2} & = & 0 \\ \zeta - \arctan\left[\frac{n_{\rm cr}^2}{n_{\rm cl}^2}\frac{1}{C}\sqrt{\frac{V_1^2}{\zeta^2} - 1}\right] - (q-1)\frac{\pi}{2} & = & 0 \end{array}\,, \tag{2.41}$$

where $\kappa = \mu_1 a/2$, $\zeta = \nu_1 b/2$. The constant C equals to $n_{\rm cr}^2/n_{\rm cl}^2$ for E_{pq}^x modes and 1 for E_{pq}^y modes. The relationship between $A_1\,, A_2$ and $B_1\,, B_2$ is expressed as:

$$\frac{A_2}{A_1} = C\cos(\kappa+\alpha)\exp(\mu_2 a/2) \qquad \frac{B_2}{B_1} = \frac{n_{\rm cr}^2}{n_{\rm cl}^2}\frac{1}{C}\cos(\zeta+\gamma)\exp(\nu_2 b/2)\,. \tag{2.42}$$

Instead of propagation constant β, we can define its normalized form using the following expression:

$$P^2 = \frac{\beta^2 - k_0^2 n_{\rm cl}^2}{k_0^2(n_{\rm cr}^2 - n_{\rm cl}^2)}\,. \tag{2.43}$$

The normalized propagation constant of an elliptic core waveguide can be then obtained using perturbation technique [18] applied on the rectangular-core waveguide. We consider its corrected value as $P^2 = P_0^2 + P'^2$, where P' is the first-order correction and the zero-order term P_0 is computed using β_0 obtained from eigenvalue equations (2.41) describing unperturbed rectangular-core waveguide. Assuming that $n_{\rm cr} \approx n_{\rm cl}$, the dielectric constant is perturbed by the amount of δn^2. The value of the perturbation is considered to be:

$$\begin{array}{rcll} \delta n^2 & = & n_{\rm cr}^2 - n_{\rm cl}^2 & \text{in regions 1, 3} \\ & = & n_{\rm cl}^2 - n_{\rm cr}^2 & \text{in region 2} \\ & = & 0 & \text{otherwise,} \end{array} \tag{2.44}$$

where the region numbers are related to figure 2.3c. According to the perturbation method, the first-order correction P' to normalized propagation constant is given by following expression:

$$P' = \frac{1}{(n_{\mathrm{cr}}^2 - n_{\mathrm{cl}}^2)} \frac{\int_{-\infty}^{\infty}\int_{-\infty}^{\infty} |\psi(x,y)|^2 \delta n^2 \mathrm{d}x\mathrm{d}y}{\int_{-\infty}^{\infty}\int_{-\infty}^{\infty} |\psi(x,y)|^2 \mathrm{d}x\mathrm{d}y}\,, \tag{2.45}$$

where the expressions (2.40) and (2.44) are used. After some lengthy but straightforward algebra, the normalized propagation constants P_x^2 and P_y^2 corresponding to E_{pq}^x and E_{pq}^y modes are obtained [19]. They can subsequently be used to express the modal birefringence $\Delta\beta$, which is an important characteristics of an elliptical-core fiber:

$$\Delta\beta = (\beta_x - \beta_y)/k_0 = [P_x^2(n_{\mathrm{cr}}^2 - n_{\mathrm{cl}}^2) + n_{\mathrm{cl}}^2]^{1/2} - [P_y^2(n_{\mathrm{cr}}^2 - n_{\mathrm{cl}}^2) + n_{\mathrm{cl}}^2]^{1/2}\,. \tag{2.46}$$

Thus, the technique leads to expressions using only elementary functions (sine, cosine or exponential function) instead of Mathieu or Bessel functions.

Chapter 3

Microstructured optical fibers

3.1 Basic concepts

Conventional optical fiber usually consists of a solid thread (core) surrounded by another material (cladding) where the refractive index of the cladding is lower than the core refractive index. That is because the guiding mechanism is based on total internal reflection (TIR). In order to achieve the required dielectric contrast, two materials (usually glasses) are needed. Moreover, because of the condition required by production process (drawing), the thermal expansion of those materials have to be similar. The alternative can be the usage of various dopants to change the refractive index value, but this may lead to unwanted increase of material absorption and to change of dispersion properties. The mentioned facts and some other factors limit the design possibilities of the optical fibers based on TIR waveguiding mechanism, so the question is how to avoid such difficulties.

The solution came from the research of artificial periodic structures known as *photonic crystals*. Photonic crystal is an analogue of solid state crystal where the atoms or molecules are replaced by macroscopic media with different dielectric constants and instead of periodic potential a periodic distribution of dielectric function (or refractive index) is considered. When the dielectric constant difference is sufficiently high and the absorption of light by the materials is minimal, the multiple reflections and refractions from all interfaces in the periodic structure can lead to similar phenomena for *photons* that the periodic atomic potential produces for *electrons*. Especially, it is possible to design a photonic crystal with so called *photonic band gaps* to prevent the light, whose wavelength (frequencies) falls to some specified range, from propagating in certain direction. The characteristics of such band gaps are given by dielectric contrast and lattice geometry, and so they offer the possibility to design and produce the fibers with parameters not achievable (for example dispersion) with conventional fiber design based mostly on material parameters.

In order to form the mode guided in the core region and not to rely on the total internal reflection phenomena, it is necessary to introduce the light wave into the core with such a value of propagating constant, that is not allowed to propagate in the cladding consisting of photonic band gap material. The photonic crystal cladding is usually formed by two-dimensional (2D) photonic crystal structure, although the one-dimensional structure can be used as well, effectively infinite in the third dimension (along the fiber axis). The fibers containing some type of photonic crystal structure can be roughly divided in two broad classes according to the sign of the difference between core and cladding refractive indices. If the core refractive index is higher then the "effective refractive index" of the photonic cladding, the fiber is denoted as solid core fiber. When the fiber core-cladding index difference is negative, such a fiber is usually referred to as photonic band gap guiding fiber.

The described optical fibers are usually called *photonic crystal fibers* (PCF) because the original objective was to make a periodic wavelength-scale cladding structure - photonic crystal, as described above. But other names are in use as well, such as *holey* or *microstructured* fibers, emphasizing other features. Since all those fibers have a microstructure, we adopted the term *microstructured optical fibers* (MOFs).

3.2 Guiding mechanisms in MOFs

As to the waveguiding in MOFs, usually two types of guiding mechanism are considered: index guiding mechanism referred to as *modified total internal reflection* (MTIR), and *photonic band gap guiding* (PBG) mechanism.

3.2.1 MTIR waveguiding

This type of waveguiding process takes place in MOFs whose core refractive index is higher then the refractive index of the cladding, as is usual in conventional optical fiber. However, in the case of MOF, the cladding consists of a periodic structure (photonic crystal) formed by low refractive index inclusions in higher-index dielectric matrix ($n_{\mathrm{inc}} < n_{\mathrm{mat}}$), and the core can be considered as a defect in the periodic structure created either by missing inclusion (see Fig.3.1), or by the inclusion with higher refractive index then the index of dielectric matrix, so $n_{\mathrm{cr}} \geq n_{\mathrm{mat}}$. The first possibility is usually preferred in manufacturing process because the MOF is produced using just *one* material. Such fibers are often called solid-core fibers.

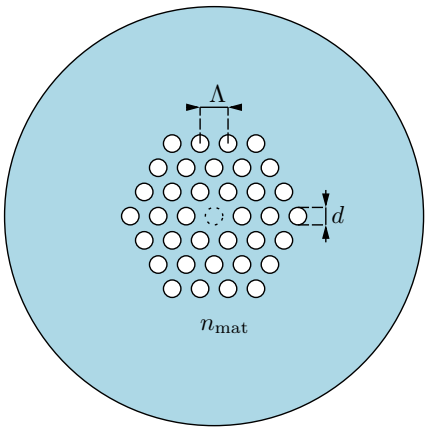

Figure 3.1: Example of solid-core MOF, triangular lattice microstructured cladding with pitch Λ, $n_{\mathrm{cr}} = n_{\mathrm{mat}}$.

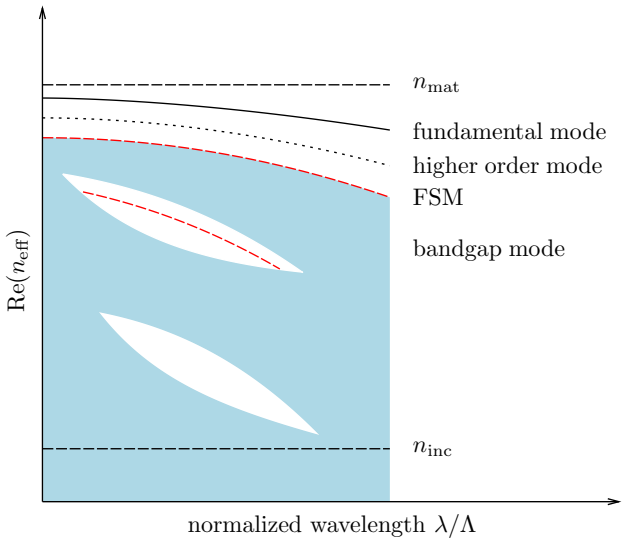

Figure 3.2: Schematic drawing of solid-core fiber band gap diagram and dispersion curves, Λ, $n_{\mathrm{cr}} = n_{\mathrm{mat}}$

The mechanism of waveguiding in the mentioned fiber can be qualitatively explained using the band diagram depicted in Fig. 3.2 related to microstructured cladding consisting of low-index inclusions (for example air holes) in homogeneous dielectric matrix. We are interested in the modes with the highest possible real part of the modal effective index n_{eff}, having in the same time the

lowest value of its imaginary part, and localized in the core region. It is clear that in our case when $n_{\mathrm{cr}} = n_{\mathrm{mat}}$, the highest possible value of real part of n_{eff} is limited by n_{mat}, so no guided mode is allowed above the n_{mat} line forming the upper bound of the guided mode region. The lower bound of that region is given by the dispersion curve of so called *fundamental space-filling mode* (FSM). This mode is the one with the highest effective modal index n_{fsm} allowed in the photonic crystal (infinite) structure used as microstructured cladding. Thus the modal effective indices have to be located in the region given by $n_{\mathrm{fsm}} < real(n_{\mathrm{eff}}) < n_{\mathrm{mat}}$ condition. From this point of view, such MOF can be considered as a waveguiding structure similar to conventional step index optical fiber where $n_{\mathrm{cl}} < n_{\mathrm{eff}} < n_{\mathrm{cr}}$. The microstructured cladding can be then considered as a region with an "average" refractive index (depending now on hole diameter d, lattice geometry and inclusion/matrix dielectric contrast) corresponding to n_{cl} in conventional step index fiber case, where the guiding mechanism is based on total internal reflection on core/cladding boundary. In a solid-core MOF, of course, the total internal reflection will be *modified* by the finite thickness of microstructured cladding, hence the waveguiding mechanism is often referred to as modified total internal reflection. It is worth mentioning that some modes can exist inside of the band gaps (see Fig. 3.2), but they are usually out of interest. As to the situation where the core refractive index exceeds the matrix refractive index, the situation is similar but the n_{mat} line is replaced by n_{cr} line, which is now shifted upward, and the dispersion curve shift can be now influenced by the core diameter too.

3.2.2 Photonic band gap waveguiding

The other type of MOFs are usually called "hollow core" fibers because their cores consist of low refractive index inclusion in high refractive index matrix, surrounded by microstructured cladding (see Fig. 3.3). The core can have a different size (or even the shape) and its refractive index value may not be the same as the value of low-index inclusions n_{inc} in the cladding region, but $n_{\mathrm{cr}} = n_{\mathrm{inc}}$ design is often preferred from technology point of view. The highest dielectric contrast is achieved when the inclusions are air holes, leading to the mentioned name of such MOFs.

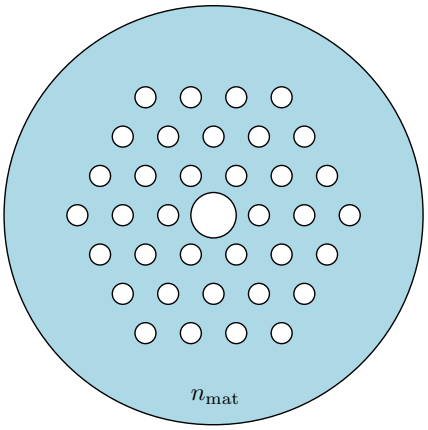

Figure 3.3: Example of hollow-core MOF with $n_{\mathrm{cr}} = n_{\mathrm{inc}}$.

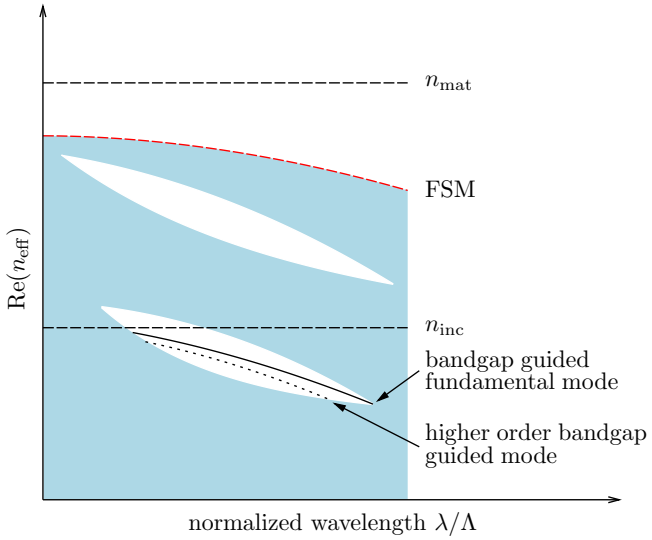

Figure 3.4: Schematic drawing of hollow-core fiber band gap diagram and dispersion curves.

Because the core refractive index is lower then the "average" cladding refractive index, the waves in the core region cannot be guided by MTIR mechanism. The alternative is to surround the core by microstructured cladding with the complete photonic band gap in the transverse direction of the fiber for required wavelength region and the guided modes have to be located in this band gap, as is schematically depicted in Fig. 3.4. Hence the name photonic crystal fibers. Guiding the modes in the air core offers the possibility to reduce the unwanted dispersion.

It should be noted that the band diagram point of view gives only a qualitative picture of waveguiding properties, because it is computed for the case of *infinite* periodic structure, whereas a real photonic crystal fiber has a microstructured cladding of *finite* thickness (finite number of inclusions). The result is that all guided modes are in fact leaky modes and there are losses even if the fiber material is lossless.

3.3 Modeling methods for microstructured optical fibers

The main task of the computational methods is to obtain dispersion relations $\beta(\lambda)$ (or $\beta(\omega)$, $\omega(\beta)$), electromagnetic field distribution and the other important modal characteristics. In contrast to the conventional optical fibers (with circular or elliptical core), even the dispersion relation cannot be expressed in a closed form because of complicated geometry of MOF and some sophisticated numerical techniques are needed. In following text the methods mainly used to model MOFs properties are briefly introduced.

3.3.1 Effective index method

This approach is the simplest of the modeling methods and it can be applied to solid core MOFs operating on modified total reflection. The method can be considered as a "bridge" between the convention optical fibers and MOFs. The idea is simple: because the microstructured cladding consists of low-index inclusions in high-index dielectric matrix, it is possible to introduce some "average" refractive index in the cladding region which is lower than the refractive index of the core (usually formed by missing inclusion). Then instead of complicated microstructure geometry, the fiber is treated as a conventional step-index optical fiber. Even if the effective index method (EIM) is not a real theory but an auxiliary trick, it was successfully used to explain the possibility of endlessly single-mode guiding phenomenon in solid core MOFs [21].

Effective index of microstructure cladding

Considering the conventional optical fibers, the values of guided mode effective indices are in the range $n_{\mathrm{cl}} < n_{\mathrm{eff}} < n_{\mathrm{cr}}$. In the case of MOF, the effective index n_{fsm} of fundamental space-filling mode is used instead of cladding material refractive index, so $n_{\mathrm{cl}} < n_{\mathrm{eff}} < n_{\mathrm{fsm}}$ (see Fig. 3.2). Assuming an infinite cladding, the microstructure can be analyzed by some of the methods developed for photonic crystals [22] to compute the value of n_{fsm} for a given λ, d and Λ, but it means to employ a computationally demanding numerical technique and the simplicity of EIM is lost. Instead of this, it is possible to consider the symmetry of the fundamental space-filling mode, which is the same as the symmetry of the photonic crystal, and to obtain n_{fsm} by solving the wave equation within a unit cell centered on one inclusion. Let us demonstrate it on a honeycomb array of circular low-index inclusions (usually air holes) in high-index (usually silica) matrix. Here, the unit cell has a hexagonal shape, but it can be approximated with a circular one as depicted in Fig. 3.5. The choice of the outer cell radius is not unique - often $R = \Lambda/2$, but the choice of $R = \Lambda(\sqrt{3}/(2\pi))^{1/2}$

based on the assumption that hexagonal and circular cell have the same area can be used as well (R_1 and R_2 in Fig. 3.5).

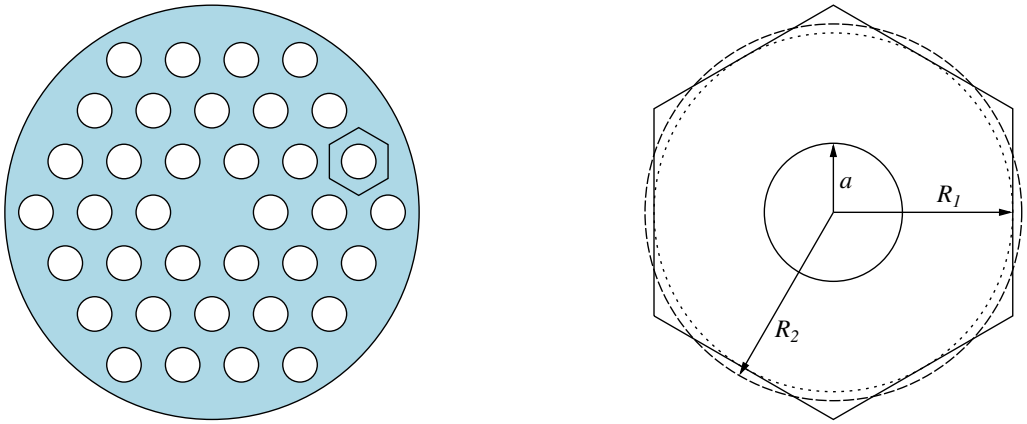

Figure 3.5: Solid core MOF with honeycomb cladding structure and hexagonal cell for EIM, circular cell approximation used for n_{fsm} computation, $R_1 = \Lambda/2$ (dotted), $R_2 = \Lambda(\sqrt{3}/(2\pi))^{1/2}$ (dashed).

In beginning the scalar wave equation with Neumann boundary conditions on the cell edges was used [21,23], but in most cases the dielectric contrast between the inclusion and matrix is high, so the vector wave equation has to be used. Hence this improved variant of EIM is called fully vectorial effective index method (FVEIM). The procedure for calculating n_{fsm} is well known [20] - the wave equation for longitudinal electromagnetic field components E_z, H_z is solved with appropriate boundary conditions. The continuity of tangential field components is required on inner boundary (inclusion boundary), whereas on the outer cell boundary, the condition $E_z(R) = H_z(R) = 0$ has to be fulfilled [24]. Then the E_z, H_z in the cell are expressed as (ϱ is the radial coordinate) [25]:

$$\begin{array}{ll} E_z(\varrho),\, H_z(\varrho) \sim I_l(\gamma_{\mathrm{inc}}\varrho) & 0 < \varrho < a = d/2 \\ E_z(\varrho),\, H_z(\varrho) \sim [J_l(\gamma_{\mathrm{mat}}\varrho)Y_l(\gamma_{\mathrm{mat}}R) - Y_l(\gamma_{\mathrm{mat}}\varrho)J_l(\gamma_{\mathrm{mat}}R)] & a < \varrho < R, \end{array} \tag{3.1}$$

where $\gamma_{\mathrm{inc}}^2 = \beta^2 - k_0^2 n_{\mathrm{inc}}^2$ and $\gamma_{\mathrm{mat}}^2 = \beta^2 - k_0^2 n_{\mathrm{mat}}^2$ are transverse propagation constants in the inclusion and rest of the cell (matrix), and I_l, J_l, Y_l are the Bessel functions. Applying the boundary conditions and defining $P_l(\gamma_{\mathrm{mat}}\varrho) = J_l(\gamma_{\mathrm{mat}}\varrho)Y_l(\gamma_{\mathrm{mat}}R) - Y_l(\gamma_{\mathrm{mat}}\varrho)J_l(\gamma_{\mathrm{mat}}R)$, the dispersion equation for the cell can be written [26]:

$$\begin{aligned} \left[\frac{P_l'(\gamma_{\mathrm{mat}}a)}{\gamma_{\mathrm{mat}}aP_l(\gamma_{\mathrm{mat}}a)} + \frac{I_l'(\gamma_{\mathrm{inc}}a)}{\gamma_{\mathrm{inc}}aI_l(\gamma_{\mathrm{inc}}a)}\right]\left[\frac{n_{\mathrm{mat}}^2 P_l'(\gamma_{\mathrm{mat}}a)}{\gamma_{\mathrm{mat}}aP_l(\gamma_{\mathrm{mat}}a)} + \frac{n_{\mathrm{inc}}^2 I_l'(\gamma_{\mathrm{inc}}a)}{\gamma_{\mathrm{inc}}aI_l(\gamma_{\mathrm{inc}}a)}\right] = \\ l^2\left[\left(\frac{1}{\gamma_{\mathrm{inc}}a}\right)^2 + \left(\frac{1}{\gamma_{\mathrm{mat}}a}\right)^2\right]^2\left(\frac{\beta}{k_0}\right)^2. \end{aligned} \tag{3.2}$$

When $l = 1$, the solution β to the above equation yields the value of the fundamental space-filling mode $n_{\mathrm{fsm}} = \beta/k_0$.

Dispersion equation

Because MOFs do not have a well defined boundary between the core and cladding regions, the choice of the waveguide core radius r_{cr} is to a certain extend arbitrary. One possibility is to define it as $r_{\mathrm{cr}} = \Lambda/2$ [23], or $r_{\mathrm{cr}} = \Lambda - a$ [25]. The other choices reported in the literature are $r_{\mathrm{cr}} = 0.64\Lambda$ [27]

and $r_{\mathrm{cr}} = 0.625\Lambda$ [28]. It should be noted that such a choice of *fixed* "effective" core radius does not reflect the influence of d/Λ and Λ/λ, so some attempts to introduce such a dependence were made, for example [29, 30], but these are mostly based on retro-fitting schemes, where the modal parameters are first computed using some numerical technique and then the EIM parameters are fitted to obtain the best agreement with the computed data.

Once the effective core radius r_{cr} and the effective cladding index $n_{\mathrm{cl}} = n_{\mathrm{fsm}}$ are determined, the equivalent step-index fiber is defined and its guided modes propagation constants β can be easily computed from well known dispersion equation [30]:

$$\left[\frac{J_l'(U)}{UJ_l(U)} + \frac{K_l'(W)}{WK_l(W)}\right]\left[\frac{n_{\mathrm{cr}}^2 J_l'(U)}{UJ_l(U)} + \frac{n_{\mathrm{cl}}^2 K_l'(W)}{WK_l(W)}\right] = l^2\left[\frac{1}{U^2} + \frac{1}{W^2}\right]\left[\frac{n_{\mathrm{cr}}^2}{U^2} + \frac{n_{\mathrm{cl}}^2}{W^2}\right], \tag{3.3}$$

where the parameters U and W are defined in usual way as $U^2 = r_{\mathrm{cr}}^2(k_0^2 n_{\mathrm{cr}}^2 - \beta^2)$ and $W^2 = r_{\mathrm{cr}}^2(\beta^2 - k_0^2 n_{\mathrm{cl}}^2)$. So the analogy between the photonic crystal fiber and step-index fiber is established, but one should not forget, that it is only an approximation and the choice of effective core radius can lead to slightly different results obtained for the same MOF [26].

3.3.2 Plane wave method

The method was originally developed for the analysis of photonic crystals and it was the first accurate technique to compute the photonic band structure in two-dimensional geometry. It is based on the assumption that the analyzed structure is periodic. Considering a typical MOF, its cross-section has a periodic structure (cladding) where the core forms a central defect. The structure consisting of infinitely long array of air holes embedded in a lossless dielectric matrix is supposed to be invariant along the fiber axis. To solve Maxwell's equations in such periodic media, the idea of the method is to expand the electromagnetic field intensities and material parameters on the same space period (primitive unit cell) using plane waves basis functions. Hence the method is referred to as plane wave expansion method (PWEM).

The governing equation can be obtained either for electric or magnetic field intensity vector, but the formulation in terms of $\boldsymbol{H}$ is mostly preferred. Assuming the time harmonic dependence of the form $e^{-i\omega t}$ and linear and non-magnetic media ($\mu = \mu_0$), we eliminate the electric field intensity from Maxwell's equations to obtain the *master* equation [22] of the problem:

$$\nabla \times \left(\frac{1}{\epsilon_{\mathrm{r}}}\nabla \times \boldsymbol{H}\right) = \frac{\omega^2}{c^2}\boldsymbol{H} \qquad\qquad \nabla \cdot \boldsymbol{H} = 0 \tag{3.4}$$

together with the divergence condition in order to get the correct solution (transverse waves) only. When analyzing the guiding properties of a MOF, two tasks can be distinguished. The first one is to compute the spectral band gaps of the microstructured cladding treated as an infinite two-dimensional photonic crystal, and the second one is related to the computation of guided mode propagation constant. In the theory of photonic crystals, the band structure computations are performed for the waves whose propagation direction lies in the cross-section plane. But that is not the case of MOF where the computation has to be performed for out of plane geometry [31] in order to analyze the wave guiding along the fiber axis. Further, PWEM can be formulated in two ways depending on the choice of required quantities. One method is to fix the wave vector $\boldsymbol{k}$ and compute the modes characterized by the angular frequency ω. This is similar to the computation of energy bands in solid state physics. The other choice, directly related to optics of MOF, is to fix the angular frequency (or wavelength) together with two perpendicular components of the wave vector and formulate the equations to determine the longitudinal wave vector component (β). This approach can be referred to as "fixed frequency" method.

The translation invariance along the $z-$axis of the fiber allows to express the magnetic field intensity as:

$$\boldsymbol{H}(x,y) = [\boldsymbol{h}_{\mathrm{t}}(x,y) + \boldsymbol{z}_0 h_z(x,y)] \exp(i\beta z)\,, \tag{3.5}$$

where $\boldsymbol{h}_{\mathrm{t}}$ and h_z are the transverse and longitudinal parts of $\boldsymbol{H}$ vector. For linear, non-magnetic media described by material parameters ε_{r} and μ_0, the equation (3.4) can be split in two equations. The problem of finding the propagation constant is obviously formulated using the equation for magnetic intensity transverse part [12]:

$$[\nabla_{\mathrm{t}}^2 + \varepsilon_{\mathrm{r}} k_0^2 + \nabla_{\mathrm{t}} \ln \varepsilon_{\mathrm{r}} \times \nabla_{\mathrm{t}} \times]\, \boldsymbol{h}_{\mathrm{t}} = \beta^2 \boldsymbol{h}_{\mathrm{t}}\,. \tag{3.6}$$

Here, ∇_{t}^2 is the transverse Laplacian operator, $k = \omega/c$ is the free-space wavenumber and $\varepsilon_{\mathrm{r}}(x,y)$ is the relative permittivity distribution. The computation of β from (3.6) leads to a non-Hermitian eigenproblem. In order to solve it, the field components have to be expanded using a finite basis set of periodic functions. The simplest natural choice is the plane wave basis.

As the relative permittivity ε_{r} is periodic in the fiber transverse cross-section plane, it satisfies the condition of discrete translational symmetry $\varepsilon_{\mathrm{r}}(\boldsymbol{r}_{\mathrm{t}}) = \varepsilon_{\mathrm{r}}(\boldsymbol{r}_{\mathrm{t}} + \boldsymbol{R})$ where $\boldsymbol{R} = l_1\boldsymbol{R}_1 + l_2\boldsymbol{R}_2$ ($l_1,\, l_2 \in \mathbb{Z}$) are the 2D primitive lattice vectors and $\boldsymbol{r}_{\mathrm{t}} = (x,y)$. Considering the appropriate primitive *reciprocal* lattice vectors $\boldsymbol{G}$ defined by the condition $\boldsymbol{G}_i \cdot \boldsymbol{R}_i = 2\pi\delta_{ij}\,(i,j = 1,2)$, the relative permittivity ε_{r} can be expanded together with $\eta_{\mathrm{r}} = \ln \varepsilon_{\mathrm{r}}$ using the plane wave basis set:

$$\varepsilon_{\mathrm{r}}(\boldsymbol{r}_{\mathrm{t}}) = \sum_{\boldsymbol{G}} [\varepsilon_{\mathrm{r}}]_{\boldsymbol{G}} \exp(i\boldsymbol{G}\cdot\boldsymbol{r}_{\mathrm{t}}) \qquad\qquad \eta_{\mathrm{r}}(\boldsymbol{r}_{\mathrm{t}}) = \sum_{\boldsymbol{G}} [\eta_{\mathrm{r}}]_{\boldsymbol{G}} \exp(i\boldsymbol{G}\cdot\boldsymbol{r}_{\mathrm{t}})\,, \tag{3.7}$$

where $\boldsymbol{G} = m_1\boldsymbol{G}_1 + m_2\boldsymbol{G}_2\,(m_1,\, m_2 \in \mathbb{Z})$. The same operation is then applied to the transverse component of magnetic field intensity $\boldsymbol{h}_{\mathrm{t}}$, so its components are expressed in the form:

$$h^{(j)}(\boldsymbol{r}_{\mathrm{t}}) = \sum_{\boldsymbol{G}} h^{(j)}_{\boldsymbol{k}_{\mathrm{t}},\boldsymbol{G}} \exp[i(\boldsymbol{k}_{\mathrm{t}} + \boldsymbol{G})\cdot\boldsymbol{r}_{\mathrm{t}}]\,. \tag{3.8}$$

The symbol $\boldsymbol{k}_{\mathrm{t}}$ denotes here the transverse (Bloch) wave vector. After the substitution of (3.7) and (3.8) to the master equation (3.6), the Laurent's theorem on series multiplication is applied formally to vector index $\boldsymbol{G}$, and the matrix representation of (3.6) is obtained in reciprocal-space form [32]:

$$\sum_{\boldsymbol{G}'} \begin{bmatrix} \mathbf{M}_{xx} & \mathbf{M}_{xy} \\ \mathbf{M}_{yx} & \mathbf{M}_{yy} \end{bmatrix} \begin{bmatrix} \boldsymbol{h}^{(x)}_{\boldsymbol{k}_{\mathrm{t}},\boldsymbol{G}'} \\ \boldsymbol{h}^{(y)}_{\boldsymbol{k}_{\mathrm{t}},\boldsymbol{G}'} \end{bmatrix} = \beta^2 \begin{bmatrix} \boldsymbol{h}^{(x)}_{\boldsymbol{k}_{\mathrm{t}},\boldsymbol{G}'} \\ \boldsymbol{h}^{(y)}_{\boldsymbol{k}_{\mathrm{t}},\boldsymbol{G}'} \end{bmatrix}. \tag{3.9}$$

The reciprocal-space expansion coefficients $h^{(j)}_{\boldsymbol{k}_{\mathrm{t}},\boldsymbol{G}'}$ are here arranged into column vectors, and $\mathbf{M}_{ij}$ elements have the form:

$$\begin{aligned}
\mathbf{M}_{xx} &= -|\boldsymbol{k}_{\mathrm{t}} + \boldsymbol{G}'|^2 \delta_{\boldsymbol{G},\boldsymbol{G}'} + k_0^2\,[\varepsilon_{\mathrm{r}}]_{\boldsymbol{G}-\boldsymbol{G}'} + (G_y - G'_y)(k_y + G'_y)[\eta_{\mathrm{r}}]_{\boldsymbol{G}-\boldsymbol{G}'}\,, \\
\mathbf{M}_{xy} &= -(G_x - G'_x)(k_y + G'_y)\,[\eta_{\mathrm{r}}]_{\boldsymbol{G}-\boldsymbol{G}'}\,, \\
\mathbf{M}_{yx} &= -(G_y - G'_y)(k_x + G'_x)\,[\eta_{\mathrm{r}}]_{\boldsymbol{G}-\boldsymbol{G}'}\,, \\
\mathbf{M}_{yy} &= -|\boldsymbol{k}_{\mathrm{t}} + \boldsymbol{G}'|^2 \delta_{\boldsymbol{G},\boldsymbol{G}'} + k_0^2\,[\varepsilon_{\mathrm{r}}]_{\boldsymbol{G}-\boldsymbol{G}'} + (G_x - G'_x)(k_x + G'_x)[\eta_{\mathrm{r}}]_{\boldsymbol{G}-\boldsymbol{G}'}\,.
\end{aligned} \tag{3.10}$$

Equation (3.9) represents an infinite equation set for the eigenvectors $\boldsymbol{v} = (h^{(x)}_{\boldsymbol{k}_{\mathrm{t}},\boldsymbol{G}'}, h^{(y)}_{\boldsymbol{k}_{\mathrm{t}},\boldsymbol{G}'})$. In practice, the sum is truncated restricting the expansion in the reciprocal space on the area given, for example, by the condition $|\boldsymbol{G}| < G_{\mathrm{cut}}$. The resulting finite set of equations forms a non-Hermitian (see (3.10)) matrix eigenproblem $\mathbf{M}\,\boldsymbol{v} = \beta^2\boldsymbol{v}$, where the square of propagation constant is the eigenvalue.

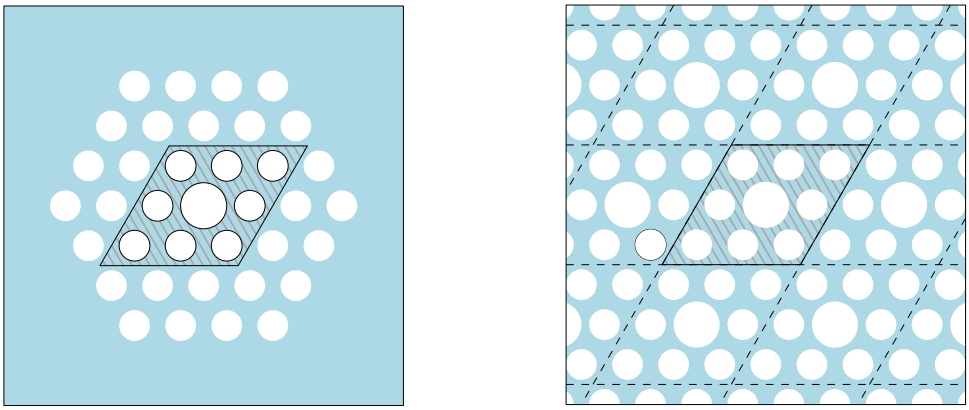

(a) (b)

Figure 3.6: Supercell approach: (a) supercell geometry, (b) artificial periodic structure used for computation of β

In principle, the computation is performed for the components of $\boldsymbol{k}_\mathrm{t}$ corresponding to all points inside and on the boundaries of the Brillouin zone. However, in order to prove the existence of photonic band gaps, it is widely accepted that the computation for $\boldsymbol{k}_\mathrm{t}$ vectors along the zone boundary is sufficient. So far, the periodicity of $\varepsilon_\mathrm{r}(\boldsymbol{r}_\mathrm{t})$ has been supposed. Such a case corresponds to infinite MOF cladding region, but the fiber core forms a defect in otherwise perfect structure. To use the above described formulation of PWEM, a slight modification has to be made. Instead of the primitive cell referring to the cladding structure, an auxiliary *supercell* is considered (see Fig. 3.6a), containing the core (defect) and several periods of surrounding cladding structure [33]. The real MOF structure is then approximated by an artificially periodic system of supercells, as depicted in Fig. 3.6b. The size of the supercell has to be large enough to guarantee that the neighboring defect interactions can be neglected.

3.3.3 Multipole method

Instead of treating the photonic cladding (and core) as a periodic, crystal-like structure, it is possible to consider it as a set of inclusions acting as *scatterers* of light and use a multiple scattering technique called *multipole method* (MPM). Since this method does not require the periodicity of the structure, it is capable to describe the guiding properties of MOFs with a finite cladding structure with generally irregular arrangement of inclusions (air holes). The only crucial restriction is that the inclusions has to be *non-overlapping*. The physics of the method is simple. At the boundary of each inclusion two different types of field can be distinguished. The first one is transmitted through the boundary from the region beyond it, the second one is reflected from the boundary itself and coming from all the other inclusions. That is why the boundary of each inclusion in MOF acts effectively as a source of radiation, even though no actual sources or sinks are present.

The basic idea of MPM is to formulate a *field identity* that relates the field incident on each inclusion to the field scattered from all the other inclusions and the jacket [34]. The fields on both sides of every inclusion and jacket (inside/outside) have to obey the continuity relations following from Maxwell's equations and therefore are coupled via reflection and transmission processes.

Consider the cross-section of a MOF as the set of circular inclusions of refractive index n_I embedded in a homogeneous matrix whose refractive index is n_M. The matrix domain has a circular shape and is surrounded by a jacket of refractive index n_J - see Fig. 3.7a. To derive the

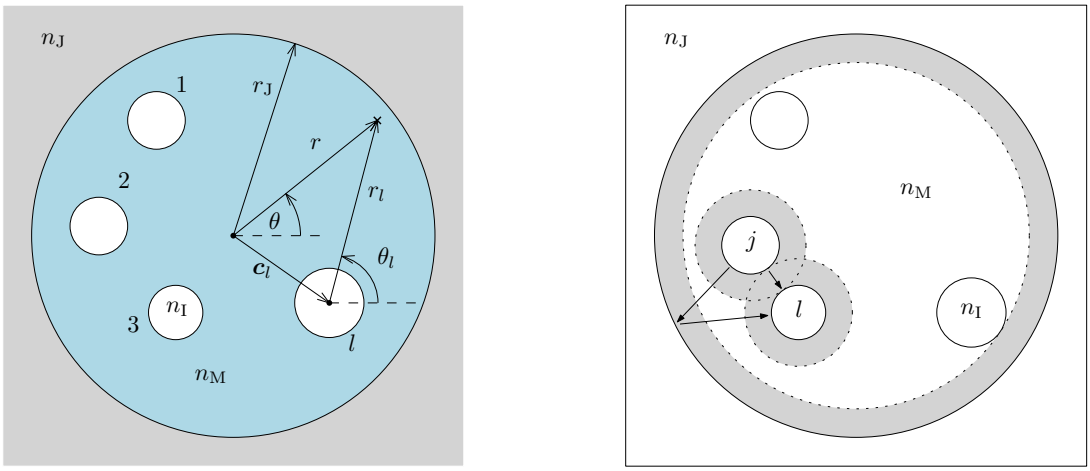

(a) (b)

Figure 3.7: Multipole method scheme: (a) local and global coordinate systems, (b) domains of Fourier-Bessel expansion

field identity, the time-harmonic longitudinal components of electromagnetic field E_z and H_z are considered. They are then expanded using a function basis set related to the geometry of the inclusion (or jacket) in the surrounding of each inclusion and jacket [35]. In our case of cylindrical shape, the basis are Bessel functions J_m and Hankel functions of first kind $H_m^{(1)}$. The field in the proximity of the $l-$th cylindrical inclusion is expressed in the local cylindrical coordinate system centered at $\boldsymbol{c}_l$ as:

$$V_l(r_l,\theta_l) = \sum_{m=-\infty}^{\infty} \left[{}^{V}A_m^l J_m(k_\mathrm{t}^\mathrm{M} r_l) + {}^{V}B_m^l H_m^{(1)}(k_\mathrm{t}^\mathrm{M} r_l) \right] e^{im\theta_l}, \quad V = E_z,\, H_z \tag{3.11}$$

where k_t^M is the transverse wavenumber in the matrix material and A_m^l, B_m^l are the coefficients of Fourier-Bessel expansion. This is a *local* expansion where the *regular* part of the field is described by Bessel functions (no singularity) whereas the Hankel functions describe the *outgoing* field propagating away from the cylinder boundary corresponding to the source placed in the inclusion center. The local expansion is valid in an annular region around the inclusion, and it extends to the perimeter of the nearest cylinder or jacket boundary - see Fig. 3.7b. Similar expansion can be written for jacket ($l = 0$) using (r, θ) coordinate system. On the other hand, the field throughout the uniform dielectric matrix can be expanded using *global* expansion. Here E_z, H_z at any point can be described as a superposition of outgoing waves from all the 'sources' in the matrix - i.e. jacket and all inclusions [36]. To keep the consistency of the field description, the local and global expansions near $l-$th inclusion has to be equal, forming the relation (N_I is the total number of inclusions):

$$\sum_{m=-\infty}^{\infty} {}^{V}A_m^l J_m(k_\mathrm{t}^\mathrm{M} r_l) e^{im\theta_l} = \sum_{\substack{j=1 \\ j\neq l}}^{N_\mathrm{I}} \sum_{m=-\infty}^{\infty} {}^{V}B_m^j H_m^{(1)}(k_\mathrm{t}^\mathrm{M} r_j) e^{im\theta_j} + \sum_{m=-\infty}^{\infty} {}^{V}A_m^0 J_m(k_\mathrm{t}^\mathrm{M} r) e^{im\theta} \tag{3.12}$$

called *Rayleigh identity*. In the vicinity of the jacket a similar relation can be found, connecting the field contributions from waves approaching the jacket from inside to the sum of the field

contributions corresponding the waves outgoing from all inclusions:

$$\sum_{m=-\infty}^{\infty} {}^{V}B_m^0 H_m^{(1)}(k_{\mathrm{t}}^{\mathrm{M}} r) e^{im\theta} = \sum_{l=1}^{N_{\mathrm{I}}} \sum_{m=-\infty}^{\infty} {}^{V}B_m^l H_m^{(1)}(k_{\mathrm{t}}^{\mathrm{M}} r_l) e^{im\theta_l} \,. \tag{3.13}$$

The equations (3.12) and (3.13) use different coordinate systems related to the l or $j-$th inclusion (local system), or to the jacket (global system). Thus the different changes of basis functions are needed: inclusion-to-inclusion, inclusion-to-jacket and jacket-to-inclusion conversion. The transformation can be performed using Graf's theorem [37]. According to this theorem, a displaced cylindrical harmonic function can be expressed as a superposition of undisplaced ones. Applying it to (3.12) and (3.13), the field identities can be cast in compact matrix form:

$$\boldsymbol{\mathcal{A}} = \tilde{\mathbb{H}}\,\boldsymbol{\mathcal{B}} + \tilde{\mathbb{T}}^{B0}\,\tilde{\boldsymbol{\mathcal{A}}}^{0} \qquad \text{and} \qquad \tilde{\boldsymbol{\mathcal{B}}}^{0} = \tilde{\mathbb{T}}^{0B}\,\boldsymbol{\mathcal{B}}\,, \tag{3.14}$$

where $\boldsymbol{\mathcal{A}} = [{}^{E}\tilde{\boldsymbol{\mathcal{A}}}^{l}, {}^{H}\tilde{\boldsymbol{\mathcal{A}}}^{l}]^{\mathrm{T}}$ and $\boldsymbol{\mathcal{B}} = [{}^{E}\tilde{\boldsymbol{\mathcal{B}}}^{l}, {}^{H}\tilde{\boldsymbol{\mathcal{B}}}^{l}]^{\mathrm{T}}$ are the column vectors of all expansion coefficients for all inclusions ($l \neq 0$) and $\tilde{\boldsymbol{\mathcal{A}}}^{0}$, $\tilde{\boldsymbol{\mathcal{B}}}^{0}$ for the jacket field (caused by all inclusions). The symbols $\tilde{\mathbb{H}}$, $\tilde{\mathbb{T}}^{B0}$ and $\tilde{\mathbb{T}}^{0B}$ correspond to the appropriate transformation matrices describing the mentioned changes of basis functions.

According to Maxwell's equations, the tangential components E_z, H_z, E_θ and H_θ have to be continuous at every boundary, thus the relations among the *internal* (inside the inclusion or jacket) and *external* (outside the inclusion or jacket) expansion coefficients are needed. Resulting reflection and transmission processes lead to general coupling between electric and magnetic field components. Considering the waveguiding process, there are no sources inside the inclusions and jacket, so the relation between the expansion coefficient vectors is simplified to

$$\boldsymbol{\mathcal{B}} = \mathbb{R}\,\boldsymbol{\mathcal{A}}\,, \tag{3.15}$$

where the block-diagonal matrix $\mathbb{R}$ describes the reflection on all inclusion boundaries. Combining (3.14) and (3.15), the Rayleigh identity (3.12) can be expressed in the form of homogeneous system of equations [34] using the expansion coefficient vector $\boldsymbol{\mathcal{B}}$ only:

$$\mathbb{M}\,\boldsymbol{\mathcal{B}} = 0, \qquad \mathbb{M} = \mathbb{I} - \mathbb{R}\left(\tilde{\mathbb{H}} + \tilde{\mathbb{T}}^{B0}\,\tilde{\mathbb{R}}^{0}\,\tilde{\mathbb{T}}^{0B}\right) \tag{3.16}$$

where $\mathbb{I}$ is the identity matrix and $\tilde{\mathbb{R}}^{0}$ is the reflection matrix on jacket boundary. The term $\tilde{\mathbb{H}}$ describes all direct inclusion-to-inclusion interactions, while $\tilde{\mathbb{T}}^{B0}\,\tilde{\mathbb{R}}^{0}\,\tilde{\mathbb{T}}^{0B}$ term is related to all indirect interactions among the inclusions caused by the reflections on jacket boundary. Considering a given fiber, whose geometry and wavelength-dependent material parameters are known, the field identity matrix $\mathbb{M}$ is then the function of mode propagation constant β. As the field identity leads to homogeneous equation system, its non-trivial solutions exist only if $\mathbb{M}$ is singular. Thus the propagation constants of guided modes are obtained as the solution to a determinant equation $\det \mathbb{M} = 0$. The expansion coefficient vector $\boldsymbol{\mathcal{B}}$ corresponding to a given β is then obtained using a singular value decomposition procedure, and it can be used to construct the associated longitudinal electric and magnetic field distribution allowing further computation of other important parameters as modal power distribution, etc. [38].

3.3.4 The finite element method

In contrast to the methods described in previous text, the finite element method (FEM) is extremely general, so there is no limitation of the analyzed fiber geometry. This can be very useful when

considering real photonic crystal fibers as their cross-section can exhibit some irregularities. The FEM implementation is usually based on one of the two methods used to solve boundary-value problems. A boundary-value problem is defined by a governing differential equation in a given domain Ω:

$$\mathcal{L}\,\phi = f \tag{3.17}$$

together with the boundary conditions on the domain boundary Γ. Here $\mathcal{L}$ is a differential operator and f is an excitation function. One way how to solve such a boundary-value problem is based on variational principle [39]. The problem is formulated in terms of an integral expression called *functional*. It can be shown that the stationarity condition for this functional corresponds to the governing differential equation under given boundary conditions. In order to be able to construct the functional, the operator $\mathcal{L}$ has to be self-adjoint $\langle\mathcal{L}\phi, \psi\rangle = \langle\phi, \mathcal{L}\psi\rangle$ and positive definite. The angular brackets denote the inner product defined as $\langle\phi, \psi\rangle = \int_\Omega \phi\,\psi^* \mathrm{d}\Omega$. Then the appropriate functional corresponding to equation (3.17) takes the following form:

$$F(\tilde{\phi}) = \frac{1}{2}\langle\mathcal{L}\tilde{\phi}, \tilde{\phi}\rangle - \frac{1}{2}\langle\tilde{\phi}, f\rangle - \frac{1}{2}\langle f, \tilde{\phi}\rangle\,, \tag{3.18}$$

where $\tilde{\phi}$ denotes the trial function. To formulate the conditions for stationarity of F, assume that the solution $\tilde{\phi}$ can be approximated by the expansion:

$$\tilde{\phi} = \sum_{j=1}^{n} c_j\, v_j = \{c\}^{\mathrm{T}}\{v\} = \{v\}^{\mathrm{T}}\{c\}\,, \tag{3.19}$$

where v_j are the expansion functions and c_j are the unknown coefficients. The $\{\}$ brackets denote a column vector and the superscript T means the vector transpose. To find a stationarity condition of $F(\tilde{\phi})$, the expansion (3.19) is inserted into (3.18) and the partial derivatives with respect to the coefficients c_i have to be zero. This operation leads to a set of linear algebraic equations:

$$[\mathbf{S}]\{c\} = \{b\}\,, \tag{3.20}$$

where the elements of the matrix $[\mathbf{S}]$ and vector $\{b\}$ are given as:

$$S_{ij} = \frac{1}{2}\int_\Omega (v_i\mathcal{L}v_j + v_j\mathcal{L}v_i)\,\mathrm{d}\Omega \quad \text{and} \quad b_j = \int_\Omega v_j f\,\mathrm{d}\Omega\,. \tag{3.21}$$

When the vector of expansion coefficients $\{c\}$ is computed, the approximate solution to original boundary-value problem (3.17) is given by the expansion (3.19).

The other way is to seek the solution by computing the weighted residual [40] of the governing differential equation. When the trial function ϕ is approximated by $\tilde{\phi}$, inserting it into the equation (3.17) results in a nonzero residual:

$$r = \mathcal{L}\tilde{\phi} - f \neq 0\,. \tag{3.22}$$

The best approximation of $\tilde{\phi}$ minimizes the residual at all points of the domain Ω. To this purpose, the weighted residual method enforce the condition:

$$R_i = \int_\Omega w_i r\,\mathrm{d}\Omega \qquad i = 1,\, 2, \ldots,\, n\,, \tag{3.23}$$

where R_i denote the weighted residual integrals and w_i are chosen weighting functions. When the weighting functions are the same as the expansion functions used in approximation (3.19), i.e. $w_i = v_i$, the method is referred to as Galerkin's method. Inserting those functions into (3.23) leads to the conditions:

$$R_i = \int_\Omega (v_i \mathcal{L}\{v\}^{\mathrm{T}}\{c\} - v_i f)\,\mathrm{d}\Omega = 0\,. \tag{3.24}$$

This results to the algebraic equation system in the form (3.20), but now the matrix $[\mathbf{S}]$ is in general not symmetric unless the operator $\mathcal{L}$ is self-adjoint. In this case the Galerkin method leads to the same equation system as obtained by the variational method. The alternative is to minimize the absolute square residual error $I = \frac{1}{2}\int_\Omega r^2\,\mathrm{d}\Omega$ with respect to the unknown coefficients in the expansion (3.19). This is equivalent to using the weighting functions $w_i = \mathcal{L}v_i$.

In the above described formulations, the trial functions $\tilde{\phi}$ were expressed as a combination of a basis function set defined over the *entire* domain Ω. Considering a general problem whose geometry can be complicated and can contain irregular boundaries, it is very difficult or even impossible to find any required entire-domain trial functions. To overcome this difficulty, the domain is divided into smaller domains, denoted as *elements*, hence the name *finite element method*. If the subdomains are small enough to assume that the solution does not change much inside them, the basis functions defined over a subdomain can have a simple form. This is the basic idea of FEM - to replace an entire continuous domain by a number of elements, where the solution to boundary-value problem is represented by simple interpolation functions with unknown coefficients called here *degrees of freedom* (DOFs).

The work-flow of FEM solution to a boundary-value problem starts with the division of continuous domains into elements - see Fig. 3.8a. Considering the waveguiding problem in PCF, the analysis is usually carried out on two-dimensional (2D) domain (fiber cross-section) and the fiber is assumed to be infinite along its axis. In this case the straight-edge elements as quadrilaterals and triangles are mostly used, the latter being more suitable for structures with curved boundaries (circular inclusions, etc). Overlaps and gaps among the elements are not allowed. The element size

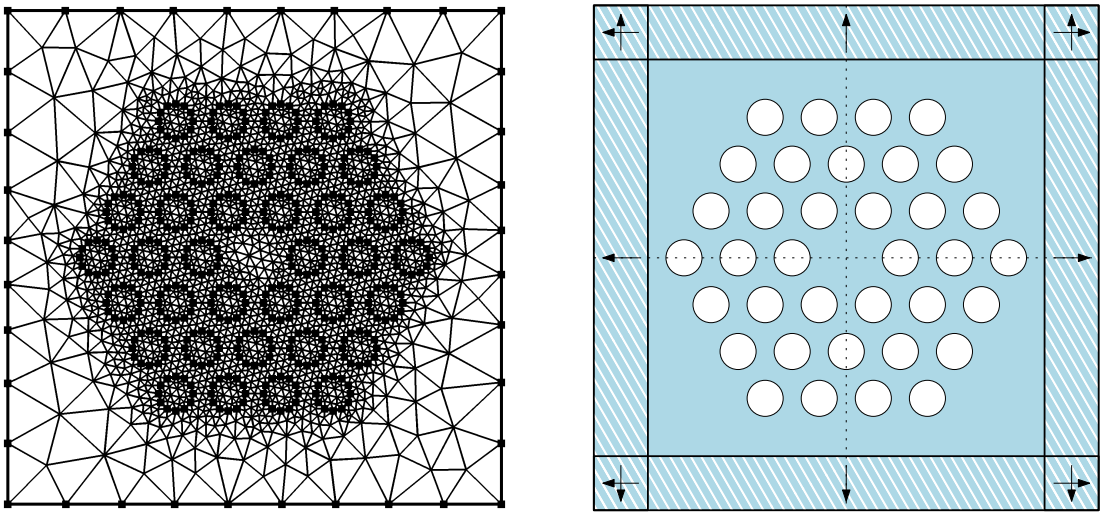

(a) (b)

Figure 3.8: Finite element method: (a) meshed cross-section of PCF, (b) infinite matrix terminated by perfect matching layers

can change - the smaller are generated in the vicinity of fine details, larger can be used where the abrupt changes of the solution (electromagnetic field components) are not assumed.

The next step is to choose some suitable elemental interpolation functions. Polynomials are the usual choice as they are simple and easy to implement. Lagrange interpolation polynomials can be used as well. Considering the standard FEM formulation, the basis polynomials are connected with the element nodes, so they have the property that they are equal to one in the appropriate node and zero in the other nodes. Then the DOFs are directly the solution values at the nodes. The simplest choice are linear polynomials. Increasing the order of polynomials (higher-order elements) leads to the solution accuracy, but more nodes have to be added on the edges and interior of elements. The above described so-called *nodal-based* elements are well suited for the cases, when the problem is described by scalar functions as is the waveguiding formulated using the longitudinal field components E_z, H_z only. But in general, the waveguide modes are hybrid modes and all field components are required. Here the usage of node-based elements often leads to non-physical results referred to as *spurious* solutions. The problem is related to the lack of divergence condition the electromagnetic waves has to obey. One way to overcome this difficulty, is to add the divergence condition as a penalty term or to reformulate the problem using transverse field components $\boldsymbol{E}_\mathrm{t}$, $\boldsymbol{H}_\mathrm{t}$ [41]. The other way leads to so called *edge-elements* constructed to ensure the continuity of vector field tangent component across element's edges. The DOFs are the associated with the edges and not with the nodes only [42].

When the choice of interpolation functions is done, the elemental matrices can be obtained using already described variational or Galerkin formulation. Then the sum of elemental equations over all elements is constructed to form the global system of equations. This process is called *assembly*. At this step, if necessary, the interface and boundary conditions given by the physics of the analyzed problem are imposed.

The waveguiding in PCF belongs to the open-domain problem class. To solve it using FEM the original exterior infinite domain has to be truncated by an artificial boundary to create a finite computational domain. Appropriate conditions on this boundary should have make it appear as transparent as possible to the field radiating out from the waveguiding structure. For this purpose, the so called *absorbing boundary conditions* (ABC) were designed. These pure mathematical conditions can be derived by combining the asymptotic form of wave equation solution valid for a large distance from the waveguide [43]. Unfortunately, the absorbing boundary created by this method has to be placed some distance away from the waveguide (source of radiation) because its transparency depends on angle of incidence and the best condition leading to lowest back-reflection are met close the normal incidence. The alternative to ABC based on physical approach to the problem is to truncate the domain by a fictitious absorber consisting of a conducting boundary (magnetic or electric) whose inner surface is coated by a system of several layers dielectrics with fictitious material parameters. Their thickness and material constants can be optimized to absorb the incident field for a wide incident angle range. The disadvantage of this technique is that fictitious absorbers are designed to work at some specific wavelength so the computation of PCF dispersion properties is difficult to implement.

In order to solve this problem, the concept of *perfectly matched layer* (PML) was proposed [44]. A perfectly matched interface between two domains does not reflect a plane wave incident from the first domain for all angles of incidence, frequencies and polarizations. In the second domain, the waves are supposed to be attenuated in the direction normal to the interface. Considering the material parameters to be the same in both domains, *the coordinate stretching* in the second domain is introduced [45]. It maps the space coordinates $x_i \rightarrow \tilde{x}_i$ using some stretching functions $s(x_i)$, specifically $s_x = s_x(x)$, $s_y = s_y(y)$, $s_z = s_z(z)$. Because of scaling properties of Maxwell's

equations, the wave impedance is the same in both domains and perfect matching is achieved. When for example the stretching function s_x is complex, the wave is attenuated in $x-$direction. The same holds for other two coordinates. The example of a domain truncated by PMLs is depicted in Fig. 3.8b - where a typical PCF structure consisting of air holes (inclusions) in homogeneous glass matrix is considered. As one is mainly interested in guided modes localized in the core region, the matrix is supposed to be infinite, but for the FEM computation is truncated by PMLs. The waves traveling in the PML regions are attenuated (the attenuation direction is marked by arrows) but not reflected. On the outer boundary of PML domains, the zero-condition or ABC can be applied. The PML concept can be extended to cylindrical or spherical coordinate systems as well as to anisotropic media [46].

The last step is to solve the assembled equation system. As to the waveguiding in optical fibers, the excitation of the fiber is not usually considered, so the formulation does not lead to the system of equations in the form of (3.20). Without the source, its right-hand side is zero and the system of equations is recast to following form:

$$[\mathbf{A}]\{\phi\} = \Lambda[\mathbf{A}]\{\phi\}\,, \tag{3.25}$$

which is a type of generalized eigenproblem. The primary aim is to compute the eigenvalue Λ. It is possible to formulate the eigenproblem (3.25) using k_0, or k_z as the eigenvalue. The former yields the allowed frequencies propagating in the waveguide whereas the latter leads to computation of the propagation constants $\beta = k_z$ of guided modes. This is usually the objective of the analysis of waveguiding in PCF, since it gives the information of modal effective indices n_{eff} and waveguide losses. The appropriate eigenvector (consisting of DOFs) can be then used to compute the field distribution of a given mode and subsequently the other required quantities as propagating power distribution, mode field diameter, etc., usually as a function of the wavelength and fiber geometry.

Chapter 4

Spectral interferometry

4.1 Dispersion in optical fibers

Dispersion phenomena play an important role in design of optical fibers as they limit the information transfer capacity of any optical communication system. The performance of optical fiber sensing schemes is influenced too. Dispersion inevitably distorts any signal of a finite bandwidth, leading to possible detection and decoding problems. In general, a medium exhibits *chromatic dispersion* when the propagation constant of a wave traveling inside it varies non-linearly with the frequency (wavelength). Considering an optical waveguide, this effect has two reasons: (1) refractive index of the medium depends on the wavelength and (2) waveguide-related effects. In polarization maintaining fibers an additional dispersion mechanism appears arising from polarization effects, as the principal polarization modes have different propagation constants.

4.1.1 Material dispersion

The origin of this type of dispersion is the variation of the media refractive index with the wavelength as the waves with different wavelengths travel at different velocities. The dielectric function of materials can be often expressed as a sum of oscillator functions describing electron transitions. Considering the glasses used to prepare the optical fibers, their losses are low in the required operational wavelength range. Moreover, this range usually lies between infrared and ultraviolet transitions (resonances), so the formula for the dielectric function can be simplified. Hence for a such type of material it is convenient to write the dependence of refractive index on the wavelength in the form:

$$n^2(\lambda) - 1 = \sum_i \frac{A_i \lambda^2}{\lambda^2 - B_i^2} \,. \tag{4.1}$$

This equation is referred to as *Sellmeier formula*, where the coefficients for a given material are obtained from a fit to experimentally measured refractive index data. The coefficients A_i can be considered as the magnitudes and B_i are resonance wavelengths. Sellmeier formula shows that in the spectral ranges away from any resonance, or between them, the refractive index decreases with the increasing wavelength. The most often used materials in optical fiber production are pure silica (SiO_2) and germanium dioxide (GeO_2) glasses. Their Sellmeier formula coefficients [47, 48] are summarized in Table 4.1.

The required changes of refractive index in the core or cladding regions can be achieved by adding of appropriate dopants (usually germanium dioxide or fluorine) to the host material (silica). In that case the refractive index $n(\lambda)$ of resulting composite is expressed using the refractive indices

Table 4.1: The coefficients for computing of the refractive index by Sellmeier formula

Material	A_1	$B_1\,[\mu\mathrm{m}]$	A_2	$B_2\,[\mu\mathrm{m}]$	A_3	$B_3\,[\mu\mathrm{m}]$
SiO_2	0.69611630	0.068404300	0.40794260	0.11624140	0.89747940	9.896161
GeO_2	0.80686642	0.068972606	0.71815848	0.15396605	0.85416831	11.841931

of all components and their concentrations using some mixing rule. The simplest model suggested for a two-component glass based on experimental data assumes that its refractive index can be represented by Sellmeier formula whose coefficients are obtained using a linear mixing rule applied to the Sellmeier coefficients of both constituents [49]:

$$n^2(\lambda) - 1 = \sum_i^3 \frac{[A_i^{(1)} + f(A_i^{(2)} - A_i^{(1)})]\lambda^2}{\lambda^2 - [B_i^{(1)} + f(B_i^{(2)} - B_i^{(1)})]^2}\,, \tag{4.2}$$

where f is the mole fraction of the dopant (constituent denoted by superscript (2)). A better model based on Clausius-Mossotti relation leads to the equation [50]:

$$\frac{n^2(\lambda) - 1}{n^2(\lambda) + 2} = (1 - f)\frac{n_1^2(\lambda) - 1}{n_1^2(\lambda) + 2} + f\frac{n_2^2(\lambda) - 1}{n_2^2(\lambda) + 2}\,, \tag{4.3}$$

which is in fact a form of Lorentz-Lorenz formula for a binary mixture and n_1, n_2 for a given wavelength are obtained using Eq. (4.1). When the concentration of germanium dioxide dopant is relatively low ($< 20\%$), the equation (4.3) can be simplified to the form [51]:

$$\frac{n^2(\lambda) - 1}{n^2(\lambda) + 2} = \sum_i^3 \frac{(A_m + fB_m)\lambda^2}{\lambda^2 - Z_m^2}\,, \tag{4.4}$$

where the coefficients (see table 4.2) were obtained by fitting the equation (4.4) to experimental data acquired for different $SiO_2 - GeO_2$ glass compositions.

Table 4.2: The coefficients for computing of the $SiO_2 - GeO_2$ glass refractive index.

	A_m	B_m	Z_m
$m = 1$	0.2045154578	−0.1011783769	0.06130807320
$m = 2$	0.06451676258	0.1778934999	0.1108859848
$m = 3$	0.1311583151	−0.1064179581	8.964441861

4.1.2 Waveguide-related dispersion effects

Even if the refractive index wavelength dependence is not taken into account (no material dispersion), the transmission properties of the waveguide are affected by other dispersion effect related to the *waveguide geometry*. Consider the single-mode transmission when only the fundamental mode propagates along the waveguide. The propagation constant β of a guided mode is obtained as a solution to the characteristic equation related to appropriate waveguide problem. Material constants and the wavelength are the parameters in this equation. Keeping the material parameters constant, the solution β still depends on the wavelength (or frequency). Considering the analogy between

the propagation of meridional rays in a step-index optical fiber and propagation in a dielectric slab, this effect referred to as *waveguide dispersion* can be interpreted as the dependence of a ray zig-zag path on the wavelength.

When a *set of guided modes* at a given wavelength propagates in the waveguide, another dispersion mechanism appears. Considering a light pulse which is coupled into the optical fiber, it propagates in the form of a set of discrete modes traveling with different propagation velocities. Using the ray model, the overall paths along a given length of the fiber are different for different modes. As a result, there is a delay among the modes and the input pulse is spread at the output. This distortion effect is called *modal dispersion* and it exists even for ideal monochromatic light source.

The propagation in the waveguide can be influenced by the birefringence too. Such a fiber is then denoted as *polarization maintaining* fiber. Two type of birefringence can be distinguished: material birefringence and form birefringence. Considering the case of an optical fiber, the first one is usually the result of an intentional or unwanted mechanical stress (stress applying part or residual stress). The second type of the birefringence is related to the break of circular symmetry of the fiber as in case of elliptical core fiber. Both mechanisms remove the polarization degeneracy. In an ideal circular fiber the fundamental mode can have two orthogonal polarizations propagating at the same speed. When the circular symmetry is broken, both polarizations travel at different speeds and a mutual delay appears having adverse effects on optical data transmission. This phenomenon is denoted as *polarization mode dispersion*.

4.1.3 Dispersion parameters

The propagation in an homogeneous medium is described by a wave vector $\boldsymbol{k}$. When a medium is unbounded, the magnitude of the wave vector k (the wave number) depends only on the wavelength and medium refractive index. Considering a waveguide, only the wave vectors meeting the transverse resonance condition can be guided and instead of wave vector the description using the propagation constant β is preferred. Propagation constant is the projection of the guided mode wave vector on the waveguide longitudinal axis. Instead of propagation constant, it is useful to define an *effective index* of a guided mode as

$$n_{\text{eff}} = \beta / k_0 \tag{4.5}$$

where k_0 is the free space wavenumber. The propagation constant is related to the *phase velocity* $v = \omega/\beta$ of a guided wave in the same way as the wave number in the case of a wave propagating in an unbounded medium, where $v = \omega/k$.

The transmitted information has often the form of pulses, so the spectrum of the propagating light is no more monochromatic, but is characterized by a finite spectral bandwidth. The pulse in an unbounded, homogeneous medium can be represented by a set of waves having different wavelengths and traveling at different phase velocities, as the refractive index generally depends on the wavelength (frequency). Assume such a pulse in the form of wave packet centered on a frequency ω_0 with sufficiently narrow spectral width in frequency domain, so its wave number dependence on frequency can be approximated by its Taylor expansion up to first order $k(\omega) \approx k(\omega_0) + \left(\frac{\mathrm{d}k}{\mathrm{d}\omega}\right)_{\omega_0} \omega$. Then the *group delay* of the packet propagating on the distance z is given by expression:

$$\tau_{\text{g}} = z\frac{\mathrm{d}k}{\mathrm{d}\omega} = z\frac{\mathrm{d}\lambda}{\mathrm{d}\omega}\frac{\mathrm{d}}{\mathrm{d}\lambda}(nk_0) = \frac{z}{c}\left(n - \lambda\frac{\mathrm{d}n}{\mathrm{d}\lambda}\right), \tag{4.6}$$

where $n(\lambda)$ is the refractive index of the medium. Using this expression, the *group velocity* can be

defined as:

$$v_{\mathrm{g}} = \frac{c}{n - \lambda(\mathrm{d}n/\mathrm{d}\lambda)} = \frac{c}{N} \qquad \Rightarrow \qquad N(\lambda) = n(\lambda) - \lambda \frac{\mathrm{d}n(\lambda)}{\mathrm{d}\lambda}\,, \tag{4.7}$$

where $N(\lambda)$ denotes the *group refractive index* of the medium. The group velocity can be interpreted as the velocity at which the envelope maximum of the wave packet propagates through the medium, or as the velocity at which the energy flows along a wave. The same concept can be applied to the case of a waveguide, where the propagation constant $\beta(\omega)$ is considered instead of $k(\omega)$. The resulting expression:

$$N_{\mathrm{eff}}(\lambda) = n_{\mathrm{eff}}(\lambda) - \lambda \frac{\mathrm{d}n_{\mathrm{eff}}(\lambda)}{\mathrm{d}\lambda}\,, \tag{4.8}$$

defines the group effective index of a given mode propagating in the waveguide.

Often the linear approximation of wave number (or propagation constant) variation with frequency does not describe the pulse propagation properly and higher-order terms in Taylor expansion of $k(\omega)$ have to be taken into account. Usually the the quadratic approximation is sufficient. Then it is useful to define the *dispersion parameter* $D(\lambda)$ relating the group delay changes to the changes in wavelength:

$$D(\lambda) = \frac{1}{c} \frac{\mathrm{d}N(\lambda)}{\mathrm{d}\lambda}\,. \tag{4.9}$$

The value of D parameter gives the information about the group delay spread in picoseconds per nanometer of light source bandwidth per unit of the propagation distance (usually kilometers). It is related to the second-order Taylor expansion coefficient in frequency domain as $D = -\frac{2\pi c}{\lambda} \frac{\mathrm{d}^2 k}{\mathrm{d}\omega^2}$. Often the expression in wavelength domain is preferred:

$$D(\lambda) = -\frac{\lambda}{c} \frac{\mathrm{d}^2 n(\lambda)}{\mathrm{d}\lambda^2} \tag{4.10}$$

as the measurement results are usually obtained in wavelength domain. Similarly, the dispersion parameter for a given mode can be obtained when the group index in Eq. (4.9) is replaced by the appropriate group index of a guided mode, or refractive index in Eq. (4.10) is replaced by modal effective index.

In a step-index optical fiber consisting of isotropic material, whose geometry has a circular symmetry, the guided modes can exhibit a *polarization degeneracy* - there exist two guided waves with different polarization states with the same propagation constant β. When the anisotropy is introduced, the polarization degeneracy is removed and the waveguide becomes *birefringent*. Then each mode is characterized by its unique propagation constant and polarization state. The effect have two sources: the material of the waveguide becomes to be anisotropic, or the symmetry of the structure is broken (for example by the change of the core shape from circular to elliptic). The anisotropy of originally isotropic material is induced by an external agent (mechanical or thermal stress, magnetic field, etc.) so the result is denoted as *induced birefringence*. The anisotropy related to the structure geometry is denoted as *form birefringence*.

Considering an unbounded, homogeneous, anisotropic medium, its birefringence is characterized by the difference of two refractive indices belonging to two polarization eigenmodes propagating along the same direction (for example $n_{\mathrm{e}} - n_{\mathrm{o}}$ in the case of an uniaxial crystal). As to the birefringent optical fiber (holey or elliptical core fiber), the guided modes can be often represented by LP mode approximation (see subsection 2.3.1). In this case the *phase modal birefringence* B_{mn} for the respective spatial LP_{mn} mode at a given wavelength is defined in the following way:

$$B_{mn}(\lambda) = \frac{\lambda}{2\pi} \left[\beta_{mn}^{(\mathrm{x})}(\lambda) - \beta_{mn}^{(\mathrm{y})}(\lambda) \right]\,, \tag{4.11}$$

where $\beta_{mn}^{(\mathrm{x})}$ and $\beta_{mn}^{(\mathrm{y})}$ are the wavelength-dependent propagation constants of the appropriate modes polarized along x and y directions. The $x-y$ coordinate frame is chosen along the principal axes of the waveguide anisotropy. Furthermore, one can define the *group modal birefringence* G_{mn} for respective spatial LP mode as:

$$G_{mn}(\lambda) = B_{mn}(\lambda) - \lambda \frac{\mathrm{d}B_{mn}(\lambda)}{\mathrm{d}\lambda} = -\lambda^2 \frac{\mathrm{d}}{\mathrm{d}\lambda}\left[\frac{B_{mn}(\lambda)}{\lambda}\right] \tag{4.12}$$

The birefringence of the fiber can be characterized in a different way. Once more assume an optical fiber whose principal axes of anisotropy coincide with x and y coordinate axes operated in single-mode regime. In fact, there are *two* orthogonally polarized modes. Considering the pair of modes linearly polarized along x and y directions, the resulting field is a wave whose polarization state changes with the z coordinate. As the value of z increases, the polarization state is evolving periodically from linear through elliptical and circular back to the linear polarization. The spatial periodicity of this evolution is known as the *beat length*, defined as:

$$L_{\mathrm{B}}(\lambda) = \frac{2\pi}{\Delta\beta(\lambda)}\,, \tag{4.13}$$

where $\Delta\beta$ is the difference of appropriate propagation constants [see Eq. (4.11)]. Obtaining the beat length from experiment, the modal birefringence for the pair of fundamental polarization modes can be determined as $B(\lambda) = \lambda / L_{\mathrm{B}}(\lambda)$.

4.2 Two-wave interference in the spectral domain

The measurement methods of spectral interferometry are based on two-wave interference concept in the spectral domain. Let us consider two beams from a broadband light source traveling along different optical paths and then combined. The result of their mutual interference at the angular frequency ω and arbitrary position $\boldsymbol{r}$ is given by the spectral interference law [52]:

$$S(\boldsymbol{r},\omega) = S_1(\boldsymbol{r},\omega) + S_2(\boldsymbol{r},\omega) + 2\sqrt{S_1(\boldsymbol{r},\omega)S_2(\boldsymbol{r},\omega)}\cos\left[\frac{\omega}{c}\Delta(\boldsymbol{r},\omega)\right], \tag{4.14}$$

where $S_1(\boldsymbol{r},\omega)$ and $S_2(\boldsymbol{r},\omega)$ are the contributions of both beams to the resultant spectral power density $S(\boldsymbol{r},\omega)$ and $\Delta(\boldsymbol{r},\omega)$ is the *optical path difference* (OPD). The interference in the spectral domain leads to spectral modulation of the source spectrum usually called as *spectral fringes*.

The resultant optical field is then launched into some detection device (for example detection optical fiber or input slit of a spectrometer) whose finite input aperture can affect the measured spectrum. This effect can be described by the following equation:

$$P(\omega) = \int S(\boldsymbol{R},\omega) A(\boldsymbol{R},\omega) \mathrm{d}^2\boldsymbol{R}\,, \tag{4.15}$$

representing the spatial integration over the input aperture area given by position $\boldsymbol{R}$ and described by an aperture function $A(\boldsymbol{R},\omega)$. Assuming that the aperture function varies slowly with ω, the equation (4.14) is substituted into (4.15) and the spectral interference law is then expressed as:

$$P(\omega) = P_1(\omega) + P_2(\omega) + 2\,V_{\mathrm{A}}(\omega)\,\sqrt{P_1(\omega)P_2(\omega)}\cos\left[\frac{\omega}{c}\Delta(\omega)\right], \tag{4.16}$$

where $P_1(\omega)$ and $P_2(\omega)$ are the contributions of both beams to the spectral power $P(\omega)$. The term $V_{\mathrm{A}}(\omega)$ denotes the *visibility* and it describes the influence of the input aperture of the detection system on the resultant spectral fringes.

In practice the spectrometer itself has an additional influence on the measured spectrum. The effect can be characterized by the spectrometer *response function* $R(\omega - \omega')$ reflecting its finite spectral bandpass. Thus the spectral intensity $I(\omega)$ detected at a given angular frequency ω adjusted by the spectrometer has to be expressed by the convolution of the input spectral power with the response function:

$$I(\omega) = \int P(\omega')R(\omega - \omega')\mathrm{d}\omega' \,. \tag{4.17}$$

The form of the response function depends on the used type of spectrometer. Suppose that a low-resolution fiber optic spectrometer is used to detect the spectral fringes. In this case the spectrometer response function is a Gaussian function characterized by its half-width Γ_R:

$$R(\omega - \omega') = \frac{R_0}{\sqrt{\pi}\Gamma_\mathrm{R}} \exp\left[-\frac{(\omega - \omega')^2}{\Gamma_\mathrm{R}^2}\right] \tag{4.18}$$

To compute the convolution expression (4.17), assume that the spectral phase function $\Phi(\omega) = \frac{\omega}{c}\Delta(\omega)$ can be represented by local Taylor expansion in the vicinity of a given angular frequency ω truncated to the first three terms:

$$\Phi(\omega') \approx \Phi(\omega) + \Phi'(\omega)(\omega' - \omega) + \frac{1}{2}\Phi''(\omega)(\omega' - \omega)^2 + \dots \,, \tag{4.19}$$

where the expansion coefficients $\Phi'(\omega) = \frac{\mathrm{d}\Phi}{\mathrm{d}\omega'}\Big|_\omega$ and $\Phi''(\omega) = \frac{\mathrm{d}^2\Phi}{\mathrm{d}\omega'^2}\Big|_\omega$ are related to the first and second order dispersion effect in the whole analyzed system. Suppose that $P_1(\omega)$, $P_2(\omega)$ and $V_\mathrm{A}(\omega)$ are slowly varying with the angular frequency, the equations (4.16), (4.18) and (4.19) can be substituted to the convolution relation (4.17), and the resultant spectral intensity $I(\omega)$ can be obtained:

$$I(\omega) = I_1(\omega) + I_2(\omega) + 2\,V_\mathrm{A}(\omega)\,V_\mathrm{R}(\omega)\,\sqrt{I_1(\omega)I_2(\omega)}\cos\left[\Phi_\mathrm{R}(\omega)\right] \,, \tag{4.20}$$

where $I_1(\omega)$, $I_2(\omega)$ are the contribution of both beams. The terms $V_\mathrm{R}(\omega)$ and $\Phi_\mathrm{R}(\omega)$ denote the spectral visibility and spectral phase of the resultant spectral fringes affected by the spectrometer. Computing the convolution integral [4], the spectral visibility can be expressed in the following form [53]:

$$V_\mathrm{R} = \frac{1}{\sqrt[4]{1 + \rho^2(\omega)}} \exp\left\{-\frac{1}{4}\Gamma_\mathrm{R}^2[\Phi'(\omega)]^2\frac{1}{1 + \rho^2(\omega)}\right\} \,. \tag{4.21}$$

To express the spectral visibility in a simple form, the parameter $\rho(\omega)$ which is related to second-order dispersion effects was used:

$$\rho(\omega) = \frac{1}{2}\Gamma_\mathrm{R}^2\Phi''(\omega) \,. \tag{4.22}$$

Similarly, the expression for spectral phase [53] can be written as

$$\Phi_\mathrm{R}(\omega) = \Phi(\omega) + \frac{1}{4}\,\Gamma_\mathrm{R}^2\,[\Phi'(\omega)]^2\,\frac{\rho(\omega)}{1 + \rho^2(\omega)} - \frac{1}{2}\arctan[\rho(\omega)] \,. \tag{4.23}$$

The equation (4.20) is usually expressed in a compact form:

$$I(\omega) = I_0(\omega)\left\{1 + V_\mathrm{I}(\omega)\cos[\Phi_\mathrm{R}(\omega)]\right\} \,, \tag{4.24}$$

where $I_0(\omega)$ is the reference spectrum of the used source (unmodulated) and $V_\mathrm{I}(\omega)$ denotes the *overall* visibility of detected spectral fringes:

$$V_\mathrm{I}(\omega) = 2\,V_\mathrm{A}(\omega)\,V_\mathrm{R}(\omega)\frac{\sqrt{I_1(\omega)I_2(\omega)}}{I_1(\omega) + I_2(\omega)} \tag{4.25}$$

Equation (4.24) is usually used to describe and analyze a given spectral interferometric experimental setup as well as to compute synthetic interferograms.

4.3 Measurement methods

The methods of spectral interferometry how to obtain the dispersion characteristics of various sample types can be roughly classified using two criteria. The first one refers to the type of recorded spectral interferogram and its evaluation, the second one is related to the configuration of the measuring setup. Considering the spectral interferograms, two types can be usually distinguished:

- the interferogram contains so called *stationary phase* point,
- the interferogram is recorded far from that point.

As to the second mentioned criterion, it is related to the location of analyzed sample with respect to the measurement setup:

- the sample is placed *inside* the interferometer - in the measuring arm,
- the sample is placed *outside* the interferometer - *tandem* configuration.

The mentioned features can be combined in order to tailor the measuring method to obtain the requested dispersion parameter.

4.3.1 Equalization wavelength method

The idea of the method can be explained using the analysis of an interferometer operated in the wavelength domain. Let us consider for example the Michelson interferometer depicted in Fig. 4.1. For the sake of clarity we can assume that the interferometer is compensated (assume an ideal beamsplitter BS) before the measured dispersive sample is inserted into it and a broad band (white light) source is used. The spectral interferogram recorded at the output of such a setup can be described by the expression (4.24). The phase function of the modulated spectral intensity distribution is in general given by the expression:

$$\Phi(\lambda) = \frac{2\pi}{\lambda}[\Delta_1(\lambda) - \Delta_2(\lambda)]\,, \tag{4.26}$$

where $\Delta_1(\lambda)$ and $\Delta_2(\lambda)$ are the *optical paths* in the reference and measuring arm respectively. In our case, when the sample is inserted into the measuring arm, the phase function takes the form:

$$\Phi(\lambda) = \frac{2\pi}{\lambda}\left\{2[n_\mathrm{s}(\lambda) - 1]t - 2L\right\}. \tag{4.27}$$

Here $L = L_2 - L_1$ is the *optical path difference* (OPD) in the air, t is the sample thickness and $n_\mathrm{s}(\lambda)$ is the sample refractive index. Without the sample, the phase function exhibit monotonous behavior (the dispersion in the air can be neglected). When the inserted sample exhibit dispersion, i. e. $n_\mathrm{s} = n_\mathrm{s}(\lambda)$, the phase function is no longer monotonous and it can have an extremum (or an inflection point) in the measured wavelength range. Its position depends on the value of L, so it can be in principle adjusted by the position of the M2 mirror in the reference arm. The extremum itself is often referred in the literature as the *stationary phase point* [54], the wavelength where it is located is denoted as *the equalization wavelength* [55]. Mathematically, the extremum can be located at the points where the first derivative of the phase function reaches zero. Applying this condition on equation (4.27) the following expression is obtained:

$$[N_\mathrm{s}(\lambda_\mathrm{eq}) - 1]t = L \qquad \Rightarrow \qquad N_\mathrm{s}(\lambda_\mathrm{eq}) = \frac{L}{t} + 1\,, \tag{4.28}$$

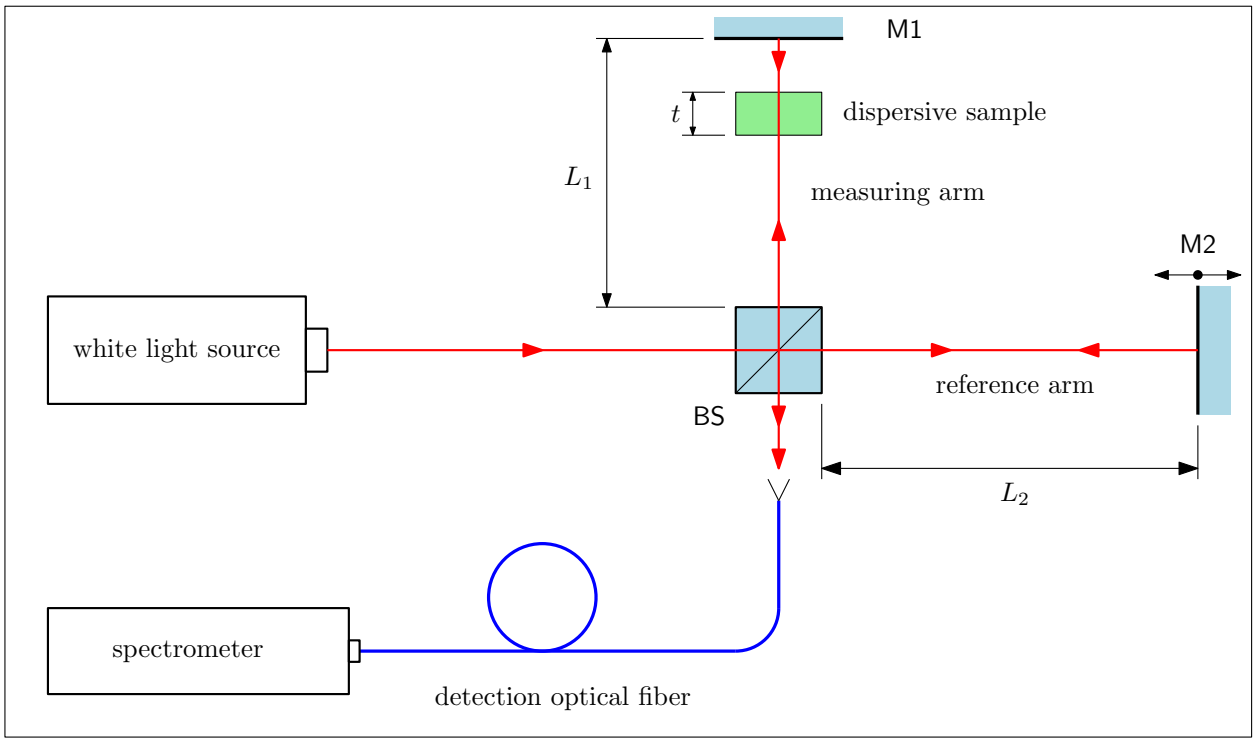

Figure 4.1: Schematic drawing of a Michelson interferometer with a dispersive sample inserted into the measuring arm, M1 and M2 are the mirrors, BS is an ideal (non-dispersive) beamsplitter

where $N_s(\lambda_{eq})$ is the value of the group refractive index of the sample at the appropriate equalization wavelength. So the group refractive index can be obtained provided the sample thickness and OPD in the air are known.

The presence of a stationary phase point in the recorded range of the spectral interferogram has an influence on the local period and visibility of spectral fringes. The density of spectral fringes (reciprocal period) is given by the rate of spectral phase change. So the period of spectral fringes is infinitely large at the zero points of the first derivative of spectral phase. To analyze the visibility, the expression (4.21) has to be written in the wavelength domain [56], neglecting the second-order effects ($\rho(\omega) \approx 0$):

$$V(\lambda) \approx \exp\left\{\frac{-\pi^2}{2}\left[\frac{\Delta_g(\lambda)\Delta\lambda_R}{\lambda^2}\right]^2\right\}, \tag{4.29}$$

where $\Delta_g(\lambda)$ is the group OPD of the interferometer and $\Delta\lambda_R$ is the width of the spectrometer Gaussian response function in the spectral domain. Excluding the case of an ideal spectrometer ($\Delta\lambda_R = 0$), the visibility function (4.29) has a maximum only when the group OPD between the beams in both arms of an interferometer is zero. As the group OPD can be expressed using optical path difference in the interferometer [57], the condition for the maximum visibility is:

$$\Delta_g(\lambda) = \Delta(\lambda) - \lambda\frac{\mathrm{d}[\Delta(\lambda)]}{\mathrm{d}\lambda} = 0\,. \tag{4.30}$$

Inserting the expression $\Delta(\lambda) = 2[n_s(\lambda) - 1]t - 2L$ for the OPD in analyzed case into (4.30), one obtains the equation which is same as the condition (4.28) for the spectral phase extremum. So the spectral fringes exhibit the highest visibility at the equalization wavelength.

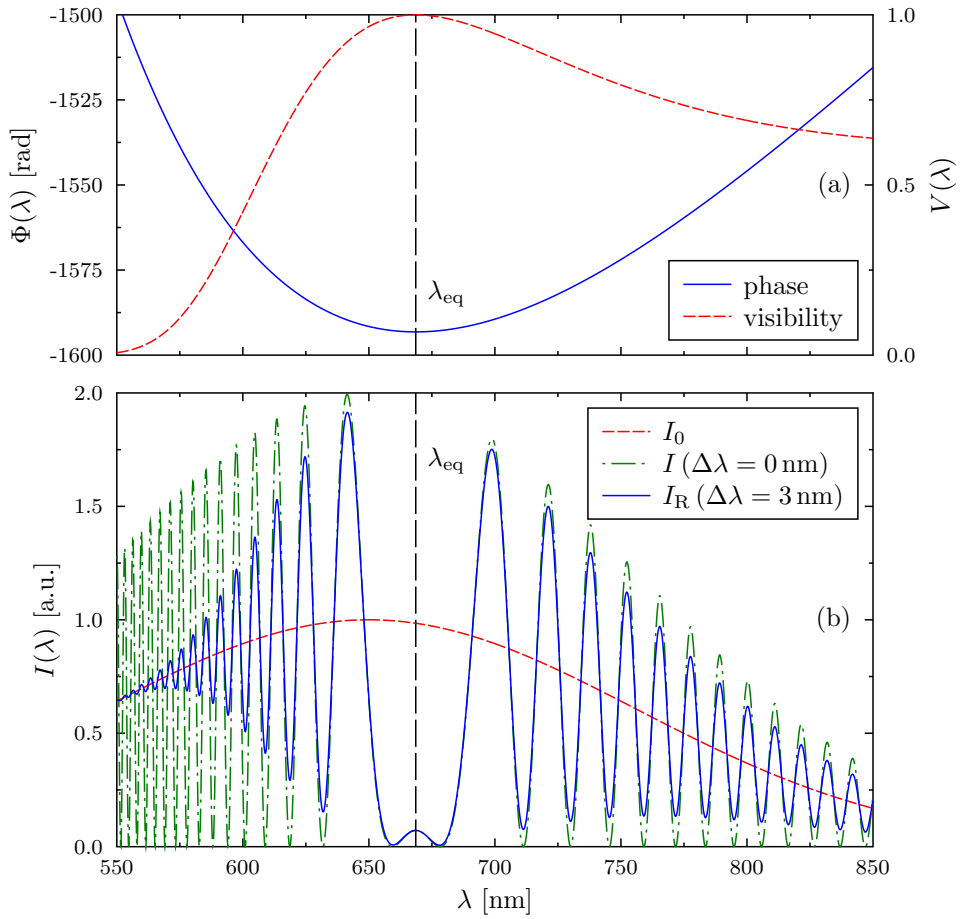

Figure 4.2: Spectral interferogram computed for analyzed Michelson interferometer: (a) phase and visibility functions, spectrometer Gaussian response function with $\Delta\lambda = 3\,\mathrm{nm}$ is assumed; (b) spectral interferogram $I(\lambda)$ for ideal ($\Delta\lambda = 0\,\mathrm{nm}$) and $I_\mathrm{R}(\lambda)$ for a real spectrometer, non-modulated (background) Gaussian spectrum $I_0(\lambda)$ of white light source ($\lambda_\mathrm{max} = 650\,\mathrm{nm}$, 150 nm half-width) was used for computation.

The mentioned features of the phase $\Phi(\lambda)$ and visibility functions $V(\lambda)$ are demonstrated in spectral interferogram (see Figs. 4.2a and 4.2b) computed using Eqs. (4.27), (4.29) and (4.24) for the case of analyzed Michelson interferometer where the dispersive sample consists of fused silica plate ($t = 5\,\mathrm{mm}$). The adjusted OPD value $L = 2365\,\mu\mathrm{m}$ in the air then leads to the stationary phase point at the equalization wavelength $\lambda_\mathrm{eq} = 668.6\,\mathrm{nm}$ whose position corresponding to the phase extremum and visibility maximum is marked by the dashed line. The effect of the spectrometer is clearly seen in Fig. 4.2b where the dash-dotted line was obtained for the case of an ideal spectrometer. In this case the half-width of the response function is zero and consequently the visibility equals to one in the whole measured spectral range. The finite half-width of the response function leads to decrease of the visibility of spectral fringes (see the full line in Fig. 4.2b corresponding to the interferogram $I_\mathrm{R}(\lambda)$ resolved by spectrometer), but the method is based on stationary phase point detection where the visibility reaches its maximum. In order to obtain $N_\mathrm{s}(\lambda)$, the OPD in the air L is changed in steps and corresponding spectral interferograms are recorded to determine $\lambda_\mathrm{eq}(L)$ and compute the sample group index using the Eq. (4.28).

4.3.2 Measurement far from stationary phase point

Sometimes it is not possible to adjust the position of stationary phase point inside of the measured wavelength range. Consequently, the position of the equalization wavelength can not be scanned to determine the dispersion parameters of the sample. In such a case, the required information can be obtained using the phase function whose values can be retrieved from the spectral interferogram. In contrast to the equalization wavelength method where the set of spectral interferograms corresponding to different OPDs has to be recorded, only *one* interferogram is needed to retrieve the phase function.

The analysis is usually performed in reciprocal wavelength domain [58] using the quantity $\sigma = 1/\lambda$, where the scaling is the same as angular frequency ω scaling used for the phase function expansion (4.19) except the multiplicative constant $1/(2\pi c)$. At first, the phase function $\Phi_\mathrm{r}(\sigma)$ is retrieved from the spectral interferogram using some of the signal processing methods. The resulting set of discrete values of the spectral phase is then usually fitted to a polynomial to obtain a continuous approximation $\Phi_\mathrm{app}(\sigma)$ in the analyzed wavenumber range. The approximation function can be used for computation of the sample group refractive index $N_\mathrm{s}(\sigma)$ as a function of the wavenumber. Considering the analyzed case of the Michelson interferometer depicted in Fig. 4.1, equation (4.27) for spectral phase is rewritten to express its dependence on the wavenumber:

$$\Phi(\sigma) = 4\pi t\sigma n_\mathrm{s}(\sigma) - 4\pi(t+L)\sigma\,. \tag{4.31}$$

The expression (see equation (4.7)) for the sample group refractive index is rewritten to wavenumber domain as well:

$$N_\mathrm{s}(\sigma) = n_\mathrm{s}(\sigma) + \sigma\frac{\mathrm{d}n_\mathrm{s}}{\mathrm{d}\sigma}\,. \tag{4.32}$$

Let us assume that the values of the sample thickness t and the optical path difference in the air L for the analyzed interferogram are known. Then one can express the sample refractive index $n_\mathrm{s}(\sigma)$ using equation (4.31) and insert it into equation (4.32). The result is the following expression

$$N_\mathrm{s}(\sigma) = \frac{1}{4\pi t}\frac{\mathrm{d}\,\Phi_\mathrm{app}(\sigma)}{\mathrm{d}\sigma} + \frac{L+t}{t}\,, \tag{4.33}$$

which can be used to compute the group refractive index of the sample using the approximation $\Phi_\mathrm{app}(\sigma)$ of the phase function.

The polynomial approximation of phase function can be deduced from the polynomial approximation of the sample refractive index in the wavenumber domain around the given wavenumber σ_0 chosen in the center of the inspected range. As the contribution of the dispersion is usually weak in comparison to the refractive index value at a given σ_0, the sample refractive index in the vicinity of this point can be approximated by Taylor series up to the first order:

$$n_\mathrm{s}(\sigma) = n_0 + \left[\frac{\mathrm{d}n_\mathrm{s}}{\mathrm{d}\sigma}\right]_{\sigma_0}(\sigma-\sigma_0) + \cdots\,, \tag{4.34}$$

where n_0 denotes the refractive index value $n_\mathrm{s}(\sigma_0)$. When this approximation is inserted into the expression (4.31), the resulting phase function takes a polynomial form $\Phi_\mathrm{app}(\sigma) = A_2\sigma^2 + A_1\sigma$ without the constant term [54]. The phase function $\Phi_\mathrm{r}(\sigma)$ retrieved from recorded spectral interferogram is obtained with $2m\pi$ ambiguity, where m is the order of the interference. To remove such an ambiguity, some additional information has to be used. When for example σ_0 is chosen to correspond to the intensity maximum, the phase value at that very point is $\Phi(\sigma_0) = 2m\pi$. Using this condition, the interference order can be estimated as $m = 2\sigma_0\Delta_0$, where the optical path

difference $\Delta_0 = \Delta(\sigma_0) = (A_2\sigma_0 + A_1)/4\pi$ is computed using the mentioned polynomial, whose coefficients are obtained from fit to the retrieved phase. The computed value of m is subsequently rounded to the nearest integer m' and Δ_0 is corrected to $\Delta_0' = m'/2\sigma_0$. The phase function can be then corrected to remove the ambiguity and written as follows:

$$\Phi(\sigma) = \Phi_{\text{app}}(\sigma) + \left[4\pi\sigma_0\Delta_0' - \Phi_{\text{app}}(\sigma_0)\right] . \tag{4.35}$$

Hence the ambiguity removal means the constant term addition to the approximation. According to the assumption about the weak contribution of the dispersion to n_0 in the considered spectral range, the dispersion effect can be described by *differential* refractive index of the sample as:

$$\Delta n_{\text{s}}(\sigma) = n_{\text{s}}(\sigma) - n_0 . \tag{4.36}$$

In order to compute this dispersion parameter, let us introduce the auxiliary phase function $\Phi_{\text{aux}}(\sigma) = 4\pi\sigma\Delta_0'$ using the corrected OPD corresponding to the given wavenumber σ_0. Such a phase is a linear function [54] in the considered spectral interval. Then the phase difference $\Delta\Phi(\sigma) = \Phi(\sigma) - \Phi_{\text{aux}}(\sigma)$ can be introduced. Considering the equation (4.31), the phase difference can be expressed in the following form:

$$\Delta\Phi(\sigma) = 4\pi t\sigma[n_{\text{s}}(\sigma) - n_0] = 4\pi t\sigma\Delta n_{\text{s}}(\sigma) . \tag{4.37}$$

So the spectral dependence of differential refractive index of the sample can be computed using the expression:

$$\Delta n_{\text{s}}(\sigma) = \frac{\Delta\Phi(\sigma)}{4\pi t\sigma} . \tag{4.38}$$

The dispersion of the refractive index can be subsequently obtained provided that its value at the given wavenumber σ_0 is known, or can be determined by some other measurement method. Once more it is worth mentioning, that only one spectral interferogram is needed to determine $\Delta n_s(\sigma)$, where the required intensity maximum at σ_0 can be obtained by a proper adjusting the path difference L in the air. The above described concept can be applied to other quantities with differential or difference nature as are the quantities related to birefringence.

4.3.3 Tandem configuration

The idea of the tandem methods is to use two sequentially connected systems where the interference takes place, so the optical field at the output of the first system is launched into the input of the second one. Then the OPD, or the group OPD, in one system can be compensated by a proper adjusting of the OPD in the other one. Tandem configuration usually comprises two interferometers with the sample under test inserted into an arm of one of them, or it can consist of one interferometer used for controlled OPD adjustment and measured sample placed behind (*outside*) it. The later configuration can be used to obtain the birefringence and group birefringence of an anisotropic dispersive sample as a piece of polarization maintaining fiber or birefringent crystal plate.

Let us demonstrate the idea of a tandem spectral interferometry method in the case of group birefringence measurement. Consider the configuration of Michelson interferometer (MI) and dispersive birefringent sample depicted in Fig. 4.3. For the sake of clarity the interferometer is assumed to be non-dispersive. The sample is placed at the output of MI between a pair of linear polarizers. The light beam from an unpolarized broad-band source is divided by an ideal beamsplitter in two beams with equal optical intensities having adjustable OPD given by the path difference between the arms (1) and (2). After transmission through the polarizer P the electric field intensity of

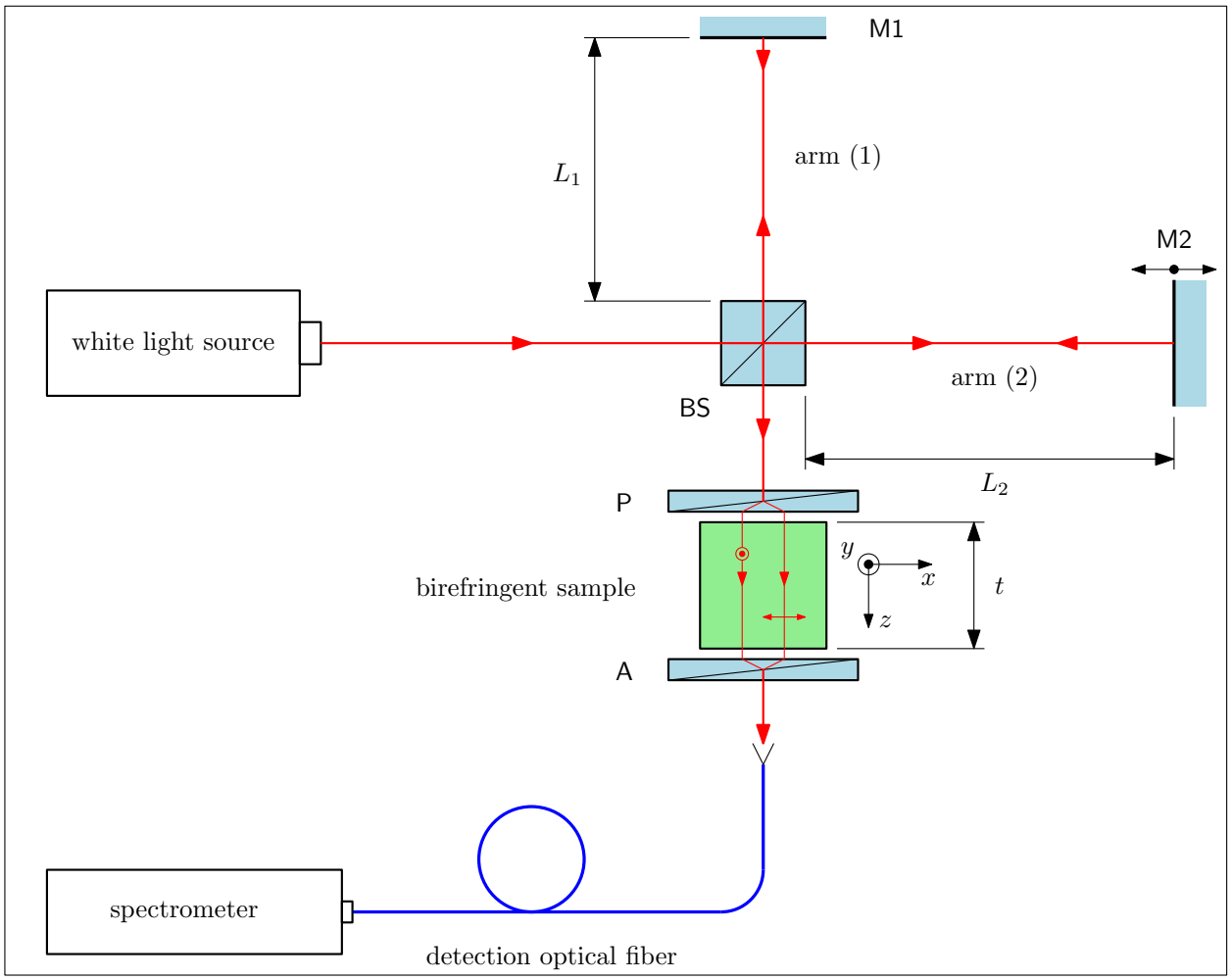

Figure 4.3: Schematic drawing of a tandem system: Michelson interferometer and dispersive birefringent sample, M1 and M2 are the mirrors, BS is an ideal (non-dispersive) beamsplitter, P and A are polarizer and analyzer

each wave is considered to be projected on its transmission axis and it can be decomposed into appropriate $x-$ and $y-$component with respect to the chosen coordinate system whose $x-z$ plane coincides with the plane given by the light beams in both arms of MI. The positions of transmission axes of the polarizer P and analyzer A are characterized by the angles α and β with respect to the $x-$axis. To keep the analysis simple, the principal axes of the sample coincide with the axes of coordinate system and the sample optical axis is parallel to the sample input face. In such a case, the normal modes of the sample are plane waves linearly polarized along $x-$ and $y-$ direction (crystal plate), or appropriate polarization modes (PMF described using LP mode approximation). As the optical axis of the sample is not parallel to the direction of propagation, the $x-$ and $y-$ polarized components of total field, consisting of the contributions from beams (1) and (2), travel inside the sample at different velocities. Passing through the analyzer A both components of electric field intensity are mixed by their projection on analyzer transmission axis and the interference takes place. The resulting optical field is then analyzed by a low-resolution spectrometer.

The analysis of this tandem system can be carried out using the two-wave interference formalism described in detail in section 4.2. Under the assumption that the influence of the second order

dispersion effects can be neglected and the Gaussian response function of the spectrometer is assumed, the resulting spectral intensity recorded by a low-resolution spectrometer at the output of the above described tandem configuration can be expressed in the wavelength domain as [59]:

$$\begin{aligned} I(\lambda) \;=\; & I_0(\lambda)\left\{1+\exp\left[-\frac{\pi^2}{2}\left(\frac{\Delta\lambda_{\mathrm{R}}}{\lambda^2}\right)^2\Delta_{\mathrm{g,I}}^2\right]\cos\left[\frac{2\pi}{\lambda}\Delta_{\mathrm{I}}\right]\right. \\ & +V(\alpha,\beta)\,\exp\left[-\frac{\pi^2}{2}\left(\frac{\Delta\lambda_{\mathrm{R}}}{\lambda^2}\right)^2\Delta_{\mathrm{g,S}}^2(\lambda)\right]\cos\left[\frac{2\pi}{\lambda}\Delta_{\mathrm{S}}(\lambda)\right] \\ & +\frac{1}{2}V(\alpha,\beta)\,\exp\left[-\frac{\pi^2}{2}\left(\frac{\Delta\lambda_{\mathrm{R}}}{\lambda^2}\right)^2\big(\Delta_{\mathrm{g,I}}+\Delta_{\mathrm{g,S}}(\lambda)\big)^2\right]\cos\left[\frac{2\pi}{\lambda}\big(\Delta_{\mathrm{I}}+\Delta_{\mathrm{S}}(\lambda)\big)\right] \\ & \left.+\frac{1}{2}V(\alpha,\beta)\,\exp\left[-\frac{\pi^2}{2}\left(\frac{\Delta\lambda_{\mathrm{R}}}{\lambda^2}\right)^2\big(\Delta_{\mathrm{g,I}}-\Delta_{\mathrm{g,S}}(\lambda)\big)^2\right]\cos\left[\frac{2\pi}{\lambda}\big(\Delta_{\mathrm{I}}-\Delta_{\mathrm{S}}(\lambda)\big)\right]\right\}, \end{aligned} \tag{4.39}$$

where Δ_{I} and $\Delta_{\mathrm{g,I}}$ are the OPD and group OPD adjusted in the interferometer (dispersion in the air is neglected). Similarly $\Delta_{\mathrm{S}}(\lambda) = B(\lambda)\,t$ and $\Delta_{\mathrm{g,S}}(\lambda) = G(\lambda)\,t$ are the OPD and group OPD related to the birefringent sample whose thickness is denoted as t. The term $V(\alpha,\beta)$ is the visibility function related to the angular position of polarizer and analyzer transmission axes. To obtain the highest contrast of resulting spectral fringes, both polarization eigenwaves (or polarization modes) have to be excited with the same amplitude of electric field intensity, so α is usually set to $\pi/4$ and consequently $\beta = \pi/4$. The resulting spectral intensity (4.39) is then the superposition of four spectral fringes with different periods, superimposed on the reference (unmodulated) spectrum $I_0(\lambda)$.

The technique itself is based on the determination of equalization wavelength λ_{eq} in the recorded spectral interferogram. At this very point the visibility reaches its maximum value, so the overall group OPD has to be zero [see Eq. (4.29)]. Considering the analyzed system, only two last terms in Eq. (4.39) can be used for such a measurement strategy, as the arguments in their visibility terms contain the expression $\Delta_{\mathrm{g,I}} \pm \Delta_{\mathrm{g,S}}(\lambda)$. Thus by the proper adjustment of the OPD in the interferometer, the equalization wavelength is moved across the measured spectral range in steps yielding the information about the group birefringence of the sample given by the condition $\Delta_{\mathrm{g,I}} = -G(\lambda_{\mathrm{eq}})\,t$. Once the discrete set of group birefringence values is known, it is possible to perform a fit to some approximation function. As the group birefringence can be expressed via birefringence $B(\lambda)$ using the relation $G(\lambda) = -\lambda^2\mathrm{d}[B(\lambda)/\lambda]/\mathrm{d}\lambda$, the *relative* wavelength dependence of sample birefringence can be obtained as well. When it is combined with the known value at some specific wavelength, the absolute values of $B(\lambda)$ can be then determined.

Chapter 5

Discussion of research work

5.1 Measurement and computation of birefringence dispersion of a microstructured fiber

Optical sensing of various physical quantities, as temperature or strain, is often based on the interaction of polarization modes in an optical fiber, so the conventional birefringent fibers supporting two stable polarization modes have received a considerable amount of interest for a long period of time. Taking into account the mentioned facts, the technology of microstructured fibers offers much higher flexibility in shaping of propagation and sensing characteristics than the conventional fiber technology. In order to properly develop a fiber optic sensing scheme operated in the spectral domain, the knowledge of the dispersion characteristics of the sensing fiber plays an important role in the design process.

The topics of experimental and theoretical investigation of dispersion properties of an birefringent microstructured fiber are studied in papers [I] and [II]. The investigated fiber was a commercially produced solid core fiber, made of fused silica. The core was surrounded by five rings of air holes in triangular lattice forming a microstructured cladding. Such an idealized structure belongs to C_{6v} symmetry group. It was shown [60] that in this case the fundamental mode exhibits double degeneracy. In order to remove it, the six-fold symmetry has to be broken. As to the studied sample, two opposite holes in the most inner ring have bigger diameter than the rest of the cladding holes. The fundamental mode of the resulting structure is then split in two polarization modes with different propagation constants and consequently the fiber exhibits the required polarization maintaining features.

The task was to obtain the wavelength dependence of the phase modal birefringence and group modal birefringence. Besides the fundamental mode, the fiber can support another spatial mode in some part of the investigated spectral range, so it was also possible to study the intermodal dispersion which is described by the wavelength dependence of the differences between the phase effective indices of the two modes having the same polarization. Furthermore, the differences between the appropriate group effective indices can be defined too. The mentioned modes are denoted as LP_{01} (fundamental mode) and *even* LP_{11} (higher-order mode) using the LP mode approach adopted from the approximate theory of conventional step-index, circular-core waveguides.

Besides the experimental work, the model computation of dispersion properties plays an important part in the analysis of the microstructured fibers, thus the proper choice of the computational method is essential. Let us examine the basic theoretical approaches introduced in section 3.3 with respect to the analyzed fiber structure. For the sake of clarity, the geometry is supposed to be ideal (no defects). It means that all the holes are perfect circles and the lattice is not distorted.

Even in this case, the effective index method cannot be applied because of the pair of holes whose diameter differs from the rest. Speaking in terms of EIM (or FVEIM), we have the effective "elliptical core" surrounded by the microstructure cladding, whereas the method was developed for circular core shape in order to use all the results of conventional fiber theory. Moreover, the change of the diameter of some holes inevitably leads to anisotropic "cladding" and there is no reasonable straightforward method how to obtain an "effective permittivity tensor" of such a structure. Thus the EIM (FVEIM) cannot be applied to such a polarization maintaining fiber.

The above described problem can be avoided using PWEM, where the plane-wave (Fourier) expansion is applied to the field and material parameters in the supercell (see subsection 3.3.2). For this method, the periodicity is essential. To obtain correct results, the central defects (formed in our case by the "core" and the most inner ring of holes), have to be well separated. In practice, it means to check the convergence of computed propagation constants with respect to increasing number of surrounding hole rings included to the supercell. This can lead to large supercells and subsequently to the increasing demand of computational resources as the scaling of the resulting matrix problem is poor with respect to the number of used plane waves [61]. On the other hand, the method is in principle capable to handle even the irregular MOF structure as the required Fourier expansion coefficients for the distribution of material parameters in the supercell can be computed numerically. However, any approximate method based on Fourier expansion is prone to a low convergence rate when the material parameters are represented by discontinuous functions. This problem is well known in the electromagnetic theory of diffraction gratings and its mathematics is related to the case when a product of two functions (one of them or both have a discontinuity) has to be represented using their Fourier expansion coefficients (factorization problem). As shown in [62], the proper usage of factorization theorems can help in some cases, but the application to two-dimensional structures representing MOFs is not straightforward. Nevertheless, recent study [63] claims that proper implementation of PWEM can achieve the same computational efficiency as finite element methods.

Summarizing the above mentioned facts, it is clear that the drawbacks of PWEM have two reasons. The first of them is related to the plane-wave basis used for the expansion, as it does not conform with the general characteristics of the inclusion geometry. Whereas the plane waves are highly general and mathematically easy to treat, they are consequently not efficient. The second reason is related to the inclusion boundaries, where the material parameters exhibit discontinuities, but the appropriate continuity relations are not incorporated into the method. To solve both problems, the multipole method was developed (see subsection 3.3.3). As the periodicity of the inclusion placement is not required for the field component expansion, the MPM can treat in general any irregular cross-section structure of MOF provided that the inclusions do not overlap. Moreover, because the microstructured cladding can be considered to be finite, the losses associated with the mode propagation are automatically obtained. For the inclusions arranged to regular lattice, the symmetry can be used to decrease the computational load. However, it should be noted that the key aspect of the method is the circularity of the inclusions leading to the proper choice of the Fourier-Bessel expansion which is natural for the circular geometry. Besides this, the continuity relations for the field components tangent to the inclusion boundary lead to reflection and transmission matrices whose elements can be expressed for circular inclusions in closed form. On the other hand, the assumption about the regularity of the inclusion shape brings some limitations to MPM. The non-circular inclusions can be in principle treated by this method [64] but the formulation of field identities will be more complicated. For example, even the simplest case of elliptical-shaped inclusions requires the usage of Mathieu functions, which are not easy to handle and implement to computations. As to the general inclusions shapes, some numerical estimates obtained from

differential or integral equation treatment have to be used [64].

Because the geometry of the real fiber is not ideal, the modeling method used for the computations of its guiding properties has to be capable to treat the inclusions with irregular shape arranged in the lattice exhibiting some imperfections. Considering this requirement, the finite element method (see 3.3.4) is an extremely powerful tool which allows to obtain the modal properties of fibers with arbitrary cross-section structures, so it was used for the model computations in papers [I] and [II]. The key to the determination of parameters, which have to be compared to the experimental results, was computation of effective indices of all guided polarization modes propagating in the fiber in the spectral range where the measurements were performed. The problem was formulated using all three component of electric field intensity, and full-vector mode solver, based on hybrid edge/nodal approach, was used to compute the propagation constants at a given wavelength. The model domain was terminated by PML. The governing equations led to generalized eigenproblem and the Arnoldi method was used as the eigensolver. Since the microstructured cladding in the real geometry is always finite, the guided modes are in principle leaky modes and their propagation constants are complex. Then the resulting system of linear equations is not symmetric, so an asymmetric multifrontal solver has to be used. The accuracy of the computed propagation constants (or effective indices) was checked versus the number of elements forming the mesh. In the considered case, to obtain the effective index values stable to six decimal places, the mesh consisting of approximately 2×10^5 triangular, curl-conforming elements had to be used. As the computations were performed in broad spectral range, the dispersion of refractive index of the fiber material (fused silica) had to be included into the model. Once the modal effective indices were computed, the phase or group modal birefringence as well as the intermodal dispersion parameters were easily obtained. The mask used for the mesh generation was obtained from scanning electron microscopy image by digital image processing methods.

The experimental study of the analyzed holey PMF was performed using the combination of several measurement techniques. In contrast to the modeling approach where the effective modal indices are computed at first and the phase and group modal birefringence (or the differences between the group effective indices used to characterize the intermodal dispersion) are obtained as the result of some post-processing of the computed data (for definition see subsection 4.1.3), the measurement strategy is different as it starts with the determination of group modal birefringence dispersion. In order to cover the required broad spectral range, two interferometric methods were used. First of them was the spectral-domain tandem interferometry employing a white-light source (halogen lamp). The tandem setup consisted of a Michelson interferometer with the PMF sample placed at its output between a pair of polarizers. The method is based on the fact that the OPD adjusted in the interferometer compensates the group OPD introduced by the fiber sample at the equalization wavelength (see subsections 4.3.1 and 4.3.3 for the idea of the method). The measurement was performed in the spectral range from 500 to 800 nm where it was possible to determine the equalization wavelengths by used a low-resolution spectrometer, and the group modal birefringence dispersion was obtained for both spatial modes. To perform the measurement for longer wavelengths, the wavelength scanning method employing four broadband SLEDs was applied and measurement range was extended to $\approx 1.6\,\mu$m. In both methods the polarizer and analyzer placed at both ends of measured fiber sample were oriented at 45° relative to fiber polarization axes to obtain the interference of polarization modes. Once the group modal birefringence was obtained as a function of the wavelength, it was used to determine the *relative* wavelength dependence of phase modal birefringence. To get the *absolute* values of phase modal birefringence, at least one its value at a specific wavelength is needed. For this purpose the lateral force method was used [65]. This method allowed to determine the absolute values of phase modal birefringence at several distinctive

wavelengths. When combined with the results yielded from spectral-domain tandem interferometry and wavelength scanning method, the dispersion of phase modal birefringence was obtained in a broad spectral range. Furthermore, the spectral-domain tandem interferometry allowed to determine the differences between the group effective indices of the identically polarized modes. As in previous case, the method based on the measurement of equalization wavelength was used, but this time the orientation of polarizer/analyzer pair was parallel to the fiber polarization axes to ensure that only the modes with the same polarization took part in the interference process.

All the results obtained from the measurement were compared to the data computed for the real fiber geometry. As the mutual discrepancy was low ($< 10\%$ in the worst case), consistency of the used experimental and computing methods was proved. The differences can be explained as a result of limited precision of the input data used to build the model geometry.

The substantially improved variant of the spectral tandem interferometry was later described in paper [II]. To obtain the wavelength dependence of the group modal birefringence in a broad spectral range, two different techniques had to be used, as was mentioned in the above text. As the considerable progress of the low-resolution fiber optic spectrometer technology allowed to extend their usage to near-infrared range, the setup described in [II] was equipped with two spectrometers: one for the measurement in $\langle 350, 1000\rangle$ nm spectral range and the other one for $\langle 850, 1700\rangle$ nm range. Such a combination allowed to perform effectively the measurement in the spectral interval from 480 nm to 1600 nm using the tandem interferometry in the spectral domain as the *only* technique. Moreover, the usage of the spectrometer in NIR led to the more dense and uniformly distributed data in this spectral interval and consequently to more precise polynomial representation of determined wavelength dependence of the group modal birefringence. Further improvement of the method was based on the usage of a birefringent crystal plate serving here as an additional delay line. When such a uniaxial crystal plate of suitable thickness and optical axis orientation is placed between the polarizer/analyzer pair behind the tested fiber, the shift of the spectral fringes resolvable in the vicinity of the equalization wavelength can be observed. Provided that the group birefringence and the thickness of the plate are known, the sign of the fiber group birefringence can be determined from the direction of that shift. For example, the elliptical core fiber analyzed in paper [II] exhibited positive birefringence whereas the holey PMF (the same type as analyzed in [I]) exhibited negative group modal birefringence. Using the fourth-order polynomial representation of $-G(\lambda)/\lambda^2$ the relative phase modal birefringence was then obtained. The described method offered the precision of $\approx 0.1\%$ in a broad spectral range obtained using cost-effective instrumentation.

5.2 Measurement of the group index dispersion

The knowledge of the group index of optical components over a broad spectral range plays an important role in various areas of optical research. Considering the model computation of parameters of PMFs, the knowledge of the dispersion properties of used materials is as important as the information about the fiber geometry. The producers often declare only the basic information on the materials (as its commercial name), but not the dispersion data itself. The similar situation arises when the material of fiber core is known but the material of the cladding is not. Therefore the measurement methods of dispersion characteristics of glasses of optical fibers are required. Spectral interferometry is considered as one of the best tools for the dispersion characterization of optical guiding media such as optical fibers. Such a measurement technique is the topic of paper [III].

The method utilizes an unbalanced Mach-Zehnder interferometer with the fiber sample inserted into one of its arms (referred to as the test arm). The other arm (reference arm) contains a delay

line, so the variable path difference in the air can be adjusted. The analysis of such a setup is similar to the analysis of a Michelson interferometer (see section 4.3), only the OPD (and appropriate group OPD) is one-half of the OPD in the Michelson interferometer. Considering practical implementation, the proper alignment of the components in a Mach-Zehnder interferometer is much simpler compared with the Michelson interferometer where the light passes both arms twice. As it is not possible to couple the light into the tested fiber directly, a lens or microscope objective has to be used to focus the beam on the entrance face of the sample. Similar components are placed behind the fiber. All the optics used in the test arm is the source of some dispersion as well as the fiber itself. Thus its influence has to be included into the condition for overall group OPD, where its phenomenologically represented by a product of an "effective" thickness and appropriate "effective" group refractive index.

Because the correct alignment of all parts of the setup is crucial, prior to the measurement a laser diode was used as the light source instead of the white-light source in order to adjust the excitation condition of the fiber - whether the light is coupled into the guided mode or to the cladding. As we want to measure the dispersion properties of the holey fiber material, the ring-shape optical field has to be seen at the output of the test arm in the far-field zone. The measurement, based on equalization wavelength determination, is carried out in two steps. At first the overall group dispersion of a combination of the sample and coupling optics is measured. The path length in the air is changed in steps and the spectral interferograms are recorded to determine the equalization wavelength values. Second, the sample is removed and the measurement is repeated on the previously determined set of equalization wavelengths. Because in this case it was not possible to obtain them directly using only the delay line in the Mach-Zehnder interferometer, the tandem configuration utilizing a Michelson interferometer placed between the light source and unbalanced Mach-Zehnder interferometer was used to resolve the spectral fringes at its output. Subsequently one specific equalization wavelength was used as a reference value and the path lengths differences with respect to this reference point were computed. Such a strategy, applied to both cases corresponding to the measurement with and without the fiber, allowed to subtract the unwanted group dispersion of the used optics from the overall group dispersion and obtain net differential group refraction index of the measured object (here the fiber cladding material) as a function of the equalization wavelength, provided that the sample length is known.

The proposed method was demonstrated on two samples of holey fibers. One of them was a pure silica fiber and the other one was made of SK222 multicomponent optical glass. Considering the silica fiber as a kind of "reference" sample, the determined differential group refractive index dispersion was compared with the results obtained using the dispersion equation of pure silica (as it is a well defined material), and good agreement confirmed that the method is suitable for the measurement of dispersion properties of optical fiber materials.

The usage of the method was then extended to the measurement of the group dispersion of fundamental mode of a holey fiber [IV]. By a proper choice of excitation conditions it is possible to couple the light to the fundamental mode as well as to the cladding modes propagating in its microstructured and solid parts. As it was shown in the literature [66], the modes propagating in the microstructured region exhibit very high attenuation, so most of the energy is transmitted by the modes propagating in the solid part of the cladding. These modes are well confined in the glass and so their group effective indices are equal to its group effective index. Thus, when the group dispersion of the holey fiber material is known, it is possible to properly identify the spectral signal related to the fundamental mode and to get its group effective index. The method is based on the assumption that the spectral fringes corresponding to the cladding modes, which can be distinguished in the vicinity of the equalization wavelength, can be obtained for a path

length that differs from the path length corresponding to the fundamental mode at the same equalization wavelength. When equations representing the zero conditions for the overall group OPD, and describing both situations are subtracted, the terms related to the dispersion of optical components cancel. So it is possible to obtain the expression for the group index of the fundamental mode at a given equalization wavelength written only in terms of group refractive index of glass and the appropriate path length difference. As usual, the length of the fiber has to be known, but that is no problem because the method is designed for short-length samples. The main limitation of this approach is that the path lengths has to be known for the same equalization wavelength set. A solution to this problem is to choose one specific value of equalization wavelength as a reference value and to rewrite all equations using appropriate differences. Thus the final relation for the fundamental mode group effective index contains only a single value of glass group index together with path length on the reference wavelength. The price is that the measurement is carried in two steps - with and without the fiber sample - as the knowledge of the path length differences related to coupling optics is necessary. Using the described strategy, the group index dispersion of pure silica fiber fundamental mode was determined and compared to the already computed data [I]. Good agreement between the experiment and theory was obtained.

The experimental method introduced in [III] was later improved and presented in paper [V]. The aim of the paper was to determine the group index dispersion when the differential group index is already known. This in fact means to determine one value of group index at a specific wavelength chosen as a reference point. Three possibilities how to choose the reference element were suggested: glass sample, reference fiber and the outer fiber cladding. As to the first case, the fiber under test was replaced by a suitable plate from a material transparent in the considered measurement range (for example glass or a crystal) whose thickness and group dispersion at the reference wavelength are well defined. The second technique utilized a reference fiber, whose group dispersion and length are known, to replace the tested one. The last technique used the change of excitation conditions in order to couple the light into the solid part of the sample cladding. The last technique is the easiest to implement, as the excitation conditions can be changed by mere defocusing of the input light beam.

The first and the last techniques were applied to two samples of holey fiber, already used in [IV]. In order to measure the group dispersion of polarization modes (the samples were pieces of polarization-maintaining fibers), the Mach-Zehnder interferometer was equipped with a linear polarizer inserted at its output. The polarizer was used for discrimination of spectral signals corresponding to both polarization modes, because the setup used and unpolarized source at its input. As the reference element, a polished birefringent crystal plate (quartz) of well defined thickness was used. The plate was cut in such a way that the optical axis was parallel to the polished surfaces and the collimated beam was incident on them perpendicularly. The reference group index then corresponds either to ordinary or to extraordinary wave propagating in the plate, depending on the polarizer orientation. The results, combined with the results obtained by the method already described in [III] finally yielded the group effective mode index. Thus, the methods described in all three mentioned papers form a versatile and powerful tool to characterize the group dispersion properties of short-length holey fiber samples and the materials used for their preparation. Alternatively, the methods can give some information about the dispersion properties of used cladding materials when a conventional optical fibers are considered. Such information are valuable especially for the laboratories oriented on the technology of optical fiber preparation, as it gives a complex feedback to the used technology processes. Besides the glass fibers, the polymer fibers can be tested as well.

5.3 Methods of absolute birefringence dispersion measurement

In beginning, it should be reminded that all suggested techniques of spectral interferometry discussed in previous two sections yield the dispersion of group quantities as group modal index or group birefringence. To determine the effective index or birefringence dispersion, the data obtained by these methods had to be combined with the results obtained by some other techniques. Considering the birefringence dispersion, the so called lateral force method was mentioned in section 5.1. Generally speaking, the method is based on the beat length measurement, as this quantity is directly related to the birefringence (see subsection 4.1.3). In order to observe the beat length, two polarization modes have to propagate in the tested fiber. The first one is excited on the entrance of the fiber using linearly polarized beam focused on the input face, and the other one appears as a result of some cross-polarization coupling process. The coupling results from the anisotropy of fiber material induced by externally applied stress, thus the technique is referred to as lateral force method. In its original variant [67], the stress-applying element (tip) was driven by a time harmonic signal and the result of interference of polarization modes was detected in the time domain using the heterodyne detection technique employing a lock-in amplifier. To measure the dispersion of the beat length, the setup utilized a fiber Raman laser as the light source and the detection chain was equipped with a bulk filter and monochromator in order to select individual wavelengths.

Later, a modification of the method was suggested in [65] to measure polarization mode dispersion in addition to modal birefringence measurement. This time, a constant point-like force was applied to the fiber and the result of the interference (fringes) was observed in the spatial domain using a CCD camera as a detector. The method was designed to obtain the birefringence value at a specific operation wavelength given by the used light source. Here a broad-band laser diode, operated below the lasing threshold was used. It is worth noting that both proposed methods did not yield the birefringence dispersion in really broad spectral range at once. In the first case the measurement had to be sequentially performed, whereas in the second case a set of different sources was needed. Nevertheless, to obtain the absolute birefringence dispersion, only one its value at a specific wavelength is need to combine with the spectral tandem interferometry results, as described in [I].

We focused our attention to this topic in paper [VI]. To solve the problem of birefringence dispersion, the measurement method was suggested that utilized the interference in the spectral domain. The method is based on the application of point-like force on the fiber sample in order to induce the cross-polarization coupling as in [65], but the response in the form of fringes is resolved in the spectral domain (sometimes the term "channeled spectrum" is used). Consider the light from a white-light source passing through the linear polarizer and launched to the fiber under test. The orientation of polarizer axis is parallel to one of the PMF axes in order to excite only one of two polarization modes. When a point-like force acts on the fiber, a part of the energy is transferred to the other polarization mode. As both polarizations are orthogonal, the analyzer oriented at 45° with respect to the polarization axes of the fiber has to be placed at the output end of the fiber to mix them and make them interfere. The position and shape of the spectral fringes is then given by the mutual phase difference related to the distance from the coupling point to the output face of the fiber. In response to the displacement of the coupling point along the fiber sample, a shift of the spectral fringes is observed. The beat length is directly related to the mentioned displacement and to the corresponding wavelength dependence of phase change reconstructed from two successive spectral interferograms.

It is clearly seen, that two problems have to be solved. One of them is to reconstruct the spectral phase of both interferograms to compute their difference. The other one is to remove the phase ambiguity. As to the first problem, there exist a large number of algorithms suitable for phase

retrieval from recorded channeled spectrum. In paper [VI] the method based on windowed Fourier transform applied in the wavelength domain was used. In contrast to standard Fourier transform, the convolution of spectral signal with the modified kernel (product of a window function with the exponential function) is computed. Next, the approach based on window Fourier filtering with modification (thresholding) is used to synthesize a new complex spectral signal used for spectral phase computation. We already applied this technique to the measurement of the effective thickness of cube beam splitters used for a Michelson interferometer [68]. The reconstructed spectral phase is obtained with $2\pi m$ ambiguity. To remove it, a simple procedure, similar to the approach described in subsection 4.3.2, can be applied. At first a maximum (or minimum) is chosen at one specific wavelength. Then the coupling point is shifted along the fiber until such a displacement is adjusted, for which another maximum at the same wavelength is resolved. Then we know that the phase was shifted by 2π at this wavelength. The beat length at this wavelength equals to the mentioned displacement. Consequently, the wavelength dependence of the beat length enables to determine the phase modal birefringence.

The method was applied to the elliptical-core fiber with the cut-off wavelength of 620 nm. As the measurement was carried out in $\langle 450, 850\rangle$ nm spectral range, a loop of the fiber was used to suppress the higher order modes. The results were compared with the data obtained using spectral tandem interferometry and good agreement of the results confirmed the suitability of the proposed method for modal birefringence dispersion measurement. Moreover, the technique is much simpler to implement than the method used in [65], and cost-effective in comparison to the periodic lateral force method.

The birefringence dispersion of an anisotropic sample can be obtained by an alternative technique described in paper [VII], not restricted to optical fibers only. General principle of the method is the same as in the case of point-like force method - the result of interference of polarization modes or eigenwaves is analyzed in the spectral domain, but this time no external agent used to excite the cross-polarization coupling is needed. The idea is quite simple: the fiber sample or a tested piece of a birefringent crystal is inserted between a pair of linear polarizers together with the launching optics (if necessary). The input polarizer is oriented in such a way, that two polarization modes or eigenwaves with equal amplitudes are excited. After the transmission through the measured object, both modes are mixed by the analyzer to obtain the interference. The resulting field is analyzed by a spectrometer, and the relative spectral phase is then retrieved from the recorded spectrum. The key point of the method is to obtain the absolute spectral phase directly related to the birefringence.

In previous papers, the polynomial representation of birefringence dispersion was used. Here, the approximation by a five-term, symmetric Cauchy-like dispersion function was used. The problem of $2\pi m$ ambiguity removal is now solved using the minimization of the introduced error (penalty) function which is the measure of difference between the retrieved and approximated spectral phase. The interference order m is now one of the unknown coefficients in the fitting process. The method consists of two steps. At first the spectral signal is constructed where the reference spectrum (acting as a "background") is removed from the recorded spectral interferogram. Then the relative spectral phase is retrieved using the method based on the windowed Fourier transform. In the second step, the unknown coefficients of used approximate dispersion function together with the interference order are estimated by trust-region algorithm. The value of retrieved interference order is then rounded to nearest integer and fixed in the following computations. Subsequently, the new values of the coefficients are computed using a Levenberg-Marquardt least-square algorithm. Finally, the birefringence is determined, provided that the length of the fiber sample or tested crystal is known.

The only limitation of the method is that the spectral fringes have to be resolved in the spectral

range, which leads to a constrain for the length of the analyzed object. This condition can be derived from the term describing the visibility of spectral fringes. The method was successfully tested on the sample of elliptical-core PMF and a birefringent crystal plate. In the case of the fiber, the results were compared with the data obtained from tandem interferometry in the spectral domain. The apparent mutual shift of birefringence dispersion curves was probably caused by the fact, that the fiber samples used in both measurements were not identical. The compared group birefringence data exhibited very good agreement. The results obtained for a birefringent crystal plate (quartz) exhibited very good agreement for birefringence and group birefringence dispersion compared with the results computed using appropriate Sellmeier-like dispersion relation. Thus the versatility of the technique was demonstrated. The measurement method can be further extended to the dispersion characteristics related to the interference of two spatial modes guided in the optical fiber.

5.4 Measurement of chromatic dispersion of polarization modes

The methods for a precise measurement of the group modal index can be used for the determination of chromatic dispersion too. The knowledge of this parameter is important for the design of various optical fiber systems as broad-band optical communications, high-speed transmission systems or generators of optical supercontinuum, as it is related to the distortion of propagating optical pulses. This optical fiber metrology task was the subject of paper [VIII]. As the chromatic dispersion coefficient can be determined simply by differentiation of the group index (see subsection 4.1.3), the already discussed method for differential group index determination can be exploited for this measurement too. The problem of reference choice is not relevant in this case, because when the group index is expressed as the sum of the differential group index and the group index value at the reference wavelength, the constant term related to the reference is removed in the process of differentiation. Thus, the measurement method suggested in paper [III] can be directly applied. The only modification of the Mach-Zehnder interferometer described in the mentioned paper is that a linear polarizer was placed at the output of the interferometer to distinguish the spectral signals corresponding to two polarization modes, because the method was applied to the fundamental mode of PMF samples. The idea of the method is to represent the obtained discrete set of differential group effective index data by a suitable approximate function which can be written in a closed form in order to be able to analytically express its first derivative, and subsequently obtain the chromatic dispersion coefficient.

In principle, this procedure can be applied to both polarization modes separately, but that is not necessary provided that the group birefringence dispersion is already known for the analyzed fiber. The group modal birefringence is defined as the difference between the group effective indices related to both polarization modes. Because the group modal effective indices are expressed using appropriate differential indices and the group modal birefringence is written in the same differential form, the process of differentiation removes the constant term and the chromatic dispersion difference can be introduced. Thus the chromatic dispersion of the other polarization mode can be expressed without performing the measurement, when the group modal birefringence of the tested sample was already obtained by some other method.

The method was used to determine the chromatic dispersion of polarization modes of two different PMFs. One of them was the pure silica holey fiber whose characteristics were already measured by tandem interferometry in the spectral domain, supporting higher-order modes for the wavelengths shorter than 1 μm, and the second one was an elliptical-core, highly birefringent fiber. This fiber supported the higher-order *even* LP_{11} mode for the wavelengths shorter than 630 nm and

the group modal birefringence of the fundamental mode was known too. Prior to the measurement itself, the proper alignment of optical component as well as the excitation conditions were checked using a laser diode used as the light source. Even if the short length of the samples allowed the propagation of higher-order modes, only the fundamental mode was excited in the fiber, as was revealed by the inspection of the far-field pattern in the test arm, and later confirmed by the shape of the spectral signal, which was not distorted by the presence of higher-order modes. The axis of the polarizer placed at the output of the interferometer was set to be parallel with the major or minor axis of the elliptical far-field pattern.

Considering the sample of holey silica fiber, an interesting behavior of spectral signal was observed. As the path length difference was adjusted in successive steps to resolve the equalization wavelength position, for values below some specific limit two positions of equalization wavelength appeared. Such behavior was revealed in the near-infrared part of the measured spectral interval. The mutual distance between the mentioned spectral positions decreased with the decreasing path length difference. Both values were used to obtain the differential group effective index until the mutual merging of the spectral fringes made the determination of equalization wavelength position impossible. This effect is caused by the non-monotonous behavior of the differential group effective index in a broad spectral interval. Thus, there can be a spectral range in the vicinity of the differential group effective index minimum where the method is not applicable.

As to the choice of the approximate function, the five-term power series (Laurent polynomial) was used for the representation of the differential group index dispersion. The group modal birefringence of a holey fiber sample was approximated by a relation obtained by differentiation of a heuristic power function used to approximate the phase modal birefringence of air-silica holey fibers [69]. By further differentiation of the group modal birefringence, the chromatic-dispersion difference was obtained in a closed form. The chromatic dispersion curve of the holey fiber was shifted toward the shorter wavelengths with respect to the chromatic dispersion curve of the fiber material. So its possible to optimize the dispersion behavior according to the requirements of a specific application just by the changes of fiber geometry. This design strategy is sometimes referred to as "dispersion engineering" and it is an important feature of PCF technology. To check the precision of the method, the chromatic dispersion values for both modes at specific wavelength were compared with the data specified by the manufacturer and very good agreement was obtained.

The proposed method is easy to implement and it offers sufficiently high measurement accuracy achieved with a simple and cost-effective instrumentation. Furthermore, it can be extended for dispersion characterization of other types of PMFs supporting the propagation of two polarization modes in a wide spectral range.

Besides the chromatic dispersion itself, the precise position of the wavelength where it equals to zero is often required. This parameter, referred to as the zero-dispersion wavelength (ZDW) plays an important role in design of specialty optical fibers used for the generation of supercontinuum. It is highly desirable, that the ZDW of such a fiber closely matches the wavelength of the laser used for optical pumping. The method how to measure the chromatic dispersion including the ZDW was presented in paper [IX]. In contrast to the technique based on equalization wavelength determination described in paper [VIII] where a series of spectral interferograms had to be recorded, only one spectral interferogram is needed. Moreover, the chromatic dispersion can be obtained even in the vicinity of the ZDW, where the previous method failed because of impossibility to properly resolve the equalization wavelength. At this point, the group modal effective index exhibits an extremum (minimum). As the extremum position is given by the zero of first derivative, it follows from the definition of chromatic dispersion that the ZDW is located at this very point.

In order to simplify the measurement procedure and increase the comfort, the experimental

setup was slightly modified to avoid the problem with the optical components used for coupling and decoupling of the optical beam into the fiber sample. This time, a dispersion balanced Mach-Zehnder interferometer was exploited, where a pair of identical optical components, as used in the tested arm, was inserted into the reference arm. Moreover, a supercontinuum source replaced the halogen lamp and this way, the signal-to-noise ratio was substantially improved. In addition to the linear polarizer used at the output of interferometer to discriminate between two orthogonal polarization modes, the other linear polarizer was placed between the source and interferometer. By proper adjusting of this polarizer only one polarization was excited and the fringe contrast was optimized to its maximum value.

The method itself is based on the processing of a single interferogram recorded in a spectral range as wide as possible containing the ZDW. Such an interval is framed by two points where the visibility reaches its maximum (the pattern characteristic for the equalization wavelength). Inside of the interval the positions of the fringe extrema (for example maxima) are resolved and numbered. The position of an interference maximum is given by a condition imposed on the spectral phase. Combining two such conditions related to the first and last maximum in the numbered set, it is possible to obtain an equation which couples together the path length difference in the air, effective index of the mode, sample length and unknown interference order. When the effective index dispersion is approximated by a suitable function, one obtains the equations, where coefficients of approximate functions and interference order are unknown parameters. By fitting this relation to the experimental data (fringe maximum number vs its wavelength), the unknown parameters are determined. Hence the second derivative of the approximate modal effective index leads directly to the expression for chromatic dispersion written in the closed form. The sample length is the only parameter which has to be known, as the constant containing path length difference in the air is removed by the differentiation.

As the successful use of the method depends on the representation of the modal effective index by an approximate function, the proper choice of such a function is quite important. The commonly used polynomial approximation, simple and easy to implement, would do the job but polynomials suffer from non-physical behavior in the vicinity of endpoints, where they tend to oscillate. So the modified Cauchy dispersion formula was used. Mathematically speaking, this type of function is referred to as a Laurent polynomial [70]. Considering the optical fiber metrology, such approximation was in the past successfully used for example in [71] to approximate the polarization dispersion, as it keeps the trends in the whole interval. To obtain a suitable representation of chromatic dispersion, the fourth-order symmetric Laurent approximation, containing only even orders, was used to represent the modal effective index dispersion. It should be mentioned that fitting to a Laurent polynomial has to be performed using some procedure applicable to non-linear fitting tasks, as for example Levenberg-Marquardt algorithm. This is because it leads to ill-condition matrix whose inversion can not be performed directly even for low-order approximation.

To demonstrate the feasibility of the described method, the measurement was performed with the pure silica holey fiber already characterized by other above described methods. Based on the already obtained results [VIII], the attention was paid to the NIR spectral range containing the ZDW, so only one spectrometer was used. The spectral interferograms corresponding to both polarization modes were recorded and processed using the above described procedure. The constants obtained from a least-square fit of modal effective indices to Laurent polynomial served as an estimate for the fit of spectral interferogram. The theoretical spectral signals agreed very well with the recorded ones, thus the accuracy of the method was clearly demonstrated. Besides the determination of the ZDW, the dispersion slope was computed as well. The values of both parameters were compared with those obtained by a broad spectral range measurement method [VIII] and good

agreement was confirmed. The small errors in ZDW were probably caused by poor resolution of used NIR spectrometer, so the precision could be improved using a spectrometer allowing denser sampling in the measurement range (for example optical spectrum analyzer). The method offers fast and accurate measurement of ZDW and dispersion slope together with the improvement of measurement comfort and if necessary, it can be extended to VIS spectral range.

5.5 Tandem configuration of birefringent fiber and birefringent crystal

Optical fibers are often used as sensors of various physical quantities. Especially the birefringent fibers in connection with the interferometric methods are an important part of optical sensing technology. The sensing concept based on the usage of a birefringent fiber, acting as sensing element, and birefringent crystal is presented in paper [X]. The idea is to utilize the interference of polarization modes depending on anisotropy induced in the sensing fiber by an external agent. The result is detected in the spectral domain where the required information is inscribed in the spectral fringes. The sensing capabilities of the proposed setup were demonstrated by the phase change of the spectral fringes induced by the change of fiber length. The sensor system comprised a tandem configuration of an elliptical-core fiber and uniaxial crystal inserted between a pair of linear polarizers including the coupling optics.

Whenever a system containing several polarization components has to be analyzed, the proper choice of the coordinate system is an important task. Here, the system connected with the directions of linearly polarized eigenwaves, propagating in the crystal, was used. The orientation of the other components was expressed using their azimuths with respect to the polarization direction of the crystal ordinary wave representing the horizontal axis. The setup is similar to the tandem configuration of a Michelson interferometer and a birefringent object (see subsection 4.3.3) used to demonstrate how to treat such systems. To keep the analysis general, the arbitrary orientation of polarizer, analyzer and sensing fiber was allowed, and the Jones formalism was used to express the spectral density at the output of the system. The knowledge of angle-dependent terms describing the influence of component orientation on the visibility of spectral fringes then helped to simplify the situation and optimize the fringe contrast. To obtain the closed-form expression for the theoretical spectral interferogram including the bandpass influence of a low-resolution spectrometer, the approach explained in section 4.2 was used. The model computation was performed for two cases concerning the combination of positive or negative birefringent crystal with elliptical-core fiber of known dispersion characteristics. The computation revealed that the visibility of the spectral fringes reaches its maximum when the group OPD in the fiber was compensated by the group OPD introduced by the crystal, as was later confirmed by experiment. The achieved results are important for the optimization of a birefringent crystal thickness to control the optimal shape of the interferogram with respect to the intended detection strategy and the spectral range of used spectrometer.

Considering the usage of the elliptical-core fibers as sensing elements, the knowledge of their spectral characteristics is essential for a proper design of fiber optic sensors operated in the spectral domain. The topic of determining the required dispersion parameters using experimental as well as theoretical methods was addressed in paper [XI]. The investigated fibers supported LP_{01} and *even* LP_{11} spatial modes in a broad spectral range. To obtain the phase and group modal birefringence, the measurement techniques already described in [III] and [VII] were utilized.

As the model computation is as important as the experimental methods, the choice of the appropriate theoretical approach is essential with respect to the analyzed fiber geometry. Based on

the results from the available literature [2], it can be concluded that the required high birefringence value corresponds to high eccentricity of the fiber core. Considering this fact, the approximate method based on perturbation approach (see subsection 2.3.1) can not handle the highly birefringent ECFs properly. Nevertheless, it gives a clear insight into the characteristics of propagating modes and to the LP-mode classification scheme widely used in the literature. The other method based on weakly guiding approximation can treat the waveguiding problem more precisely, but the core-cladding dielectric contrast has to be sufficiently low and the core eccentricity is limited as well. To quickly estimate some guiding properties, the approximation by equivalent rectangular core can be used (see subsection 2.3.3), especially when the fibers with high core eccentricity are considered. The other advantage of this method is the relatively simple mathematics compared to two above mentioned techniques, but the results obtained by this method can not explain the experimental results in detail. The computation of the propagation constants can be in principle performed using the exact theory of elliptical waveguides (see section 2.2), but the implementation of the method into computation practice is difficult because of the problem geometry inherently leads to infinity number of modes used for representation of the field components. Consequently, a proper truncation of appropriate matrices in needed. The other difficulty is related to the complex nature of Mathieu functions. In addition to this, the libraries for numerical computation of Mathieu function are not commonly available. Finally, the elliptical waveguide theory was not developed to handle the case of anisotropic materials. Nevertheless, the exact approach can serve as a starting point to various approximations used to handle special fiber configurations. To treat a complex fiber geometry as well as the material anisotropy, the FEM analysis was used in paper [XI]. The goal was to compute the propagation constants in case of highly elliptical fibers, where the side-effects of used producing technology led to some residual stress. Such a stress inevitably introduced the anisotropy of the fiber material. FEM allowed to treat the situation as a multi-physics problem, where various quantities are mutually coupled. At first, the distribution of residual thermal stress was modeled using plane-stress model based on the information about the technology, and consequently the relative permittivity tensor distribution was obtained in the fiber cross-section. Then the propagation constants for the ECF with included material anisotropy were computed using the same mesh.

As to the group modal birefringence measurement using the spectral-domain tandem interferometry, two guided modes were excited and two corresponding equalization wavelengths were detected. To avoid the situation when the corresponding interference signals overlaps, a sufficiently long fiber sample was used. For the phase modal birefringence measurement, the point-like force method in the spectral domain was utilized. Here it should be mentioned that the modal birefringence of higher-order mode (*even* LP_{11}) could not be obtained this way, as it was not possible to excite only this mode (the fundamental mode was always present). The experimental and theoretical values were compared and good agreement was confirmed. The small discrepancies in short-wavelength range were probably caused by lack of reliable material parameters and inaccuracy of the core dimensions used as input to computer models.

The concept based on tandem configuration fiber-crystal, demonstrated in [X], was used as a starting point for fiber optic temperature sensing described in paper [XII]. The main objective of the work was to realize a sensor using the available ECF whose characteristics were known, and test the applicability of the approach already introduced in [X]. At first, the theoretical spectral interferograms were computed. In principle, the fiber alone could be used, but the period of spectral modulation corresponding to a reasonable length of the fiber would be too short to be resolved by the considered spectrometer. So the tandem configuration of the birefringent crystal plate (quartz) and the fiber had to be used. The character of spectral fringes depends on the thickness of the plate. If the plate is thick enough, the interferogram contains the stationary phase point in the measuring

range. As the information is hidden in the spectral phase, it has to be retrieved, but the procedure is not simple [72]. When the plate thickness decreases, the stationary phase point shifts toward shorter wavelengths and the interferogram takes the form of channeled spectrum. Then the phase change corresponding to the measured temperature can be retrieved using much simpler procedure based on windowed Fourier transform. Moreover, the temperature change can be directly deduced from the shift of a position of a given interference extremum. This strategy was finally adopted. To evaluate the performance of the sensing scheme, the so-called polarization sensitivity [73] was determined. In the described case, the polarization change is induced by the change of the temperature. This parameter represents an increase of phase shift between two polarization modes of the sensing fiber induced by unit change of the temperature acting on the unit length of the fiber. It was revealed that it decreased with the increasing wavelength of the used spectral maximum. To check the temperature sensitivity of the system, different wavelengths were chosen and the shift of their maxima was traced as the temperature changed. In accordance with the obtained polarization sensitivity of the used fiber, the response to temperature was higher at the shorter wavelengths. The shift with the temperature was almost linear in the used temperature range. Thus it is possible to "tune" the sensitivity just by choice of the maxims located in different parts of used spectral range, provided that the phase change does not exceed 2π. However, it is possible extend the temperature measurement range, when the sequential measurement is performed with a step small enough to assure the phase unambiguity. The achieved results are important from a practical point of view, as the sensing is performed in VIS spectral range using a low-cost and accessible instrumentation.

Chapter 6

Summary and conclusion

The presented habilitation thesis deals with spectral interferometry of polarization maintaining fibers. As the progress in technology of preparation of such fibers has led to their availability at a reasonable cost, the number of possible applications utilizing their unique properties is perpetually growing. To be able to properly design various systems based on that kind of fibers, their dispersion characteristics have to be well known. Among various methods that are applicable to dispersion characteristics determination, the spectral interferometry offers high versatility and provides the dispersion data in a wide spectral range.

We focused our attention mainly on the spectral dependence of parameters related to the birefringence properties of studied fibers. At first the already developed techniques were successfully combined to obtain the phase and group modal birefringence of a holey fiber in a broad spectral range. Later, the method of tandem interferometry in the spectral domain was improved in order to determine the dispersion characteristics using this method only. Moreover, we proposed and experimentally tested the procedure how to specify a correct sign of the group modal birefringence.

Apart from the dispersion characteristics related to the guided modes, the dispersion of the fiber materials is important too as the knowledge of this information is essential to compute the parameters of fiber waveguides in a realistic way. We proposed a technique to measure the group differential index of material of holey fibers. Instead of tandem interferometry using a Michelson interferometer, the method utilizes an unbalanced Mach-Zehnder interferometer with the fiber sample inserted into its test arm. The method was successfully tested on the holey fiber samples made of different glasses. The results were then compared to the known material data computed using known dispersion formulae and good agreement confirmed the feasibility of the proposed method. The technique was subsequently applied to group modal dispersion determination. To obtain the mentioned parameter, the problem of reference element choice as well as the influence of used coupling optics was discussed and successfully solved.

As every measurement method based on the determination of equalization wavelength position leads to group quantities only, we developed a new simple method to measure the phase modal birefringence of polarization maintaining fibers directly. The method, utilizing the beat length, is based on already known lateral force technique, but in our variant the result of interference of polarized modes is observed in the spectral domain. It was applied on the sample of an elliptical-core fiber, and good compatibility with the results obtained by other methods was confirmed. Latter we proposed another technique which allows to treat not only the birefringence of fiber samples, but the birefringence of the bulk samples (for example birefringent crystals) too, as it does not rely on the beat length. This method was successfully tested on the previously studied fiber samples as well as on the quartz crystal sample. Both methods offer the possibility to determine the value of the

birefringence absolutely and so the results can be combined with our already proposed methods.

The problem of chromatic dispersion determination of optical fibers is considered to be an important task of optical fiber metrology, as chromatic dispersion can induce the distortion of propagating optical pulses. Based on our previous knowledge, we extended our spectral interferometry methods to be able to determine this parameter. The technique is based on a Mach-Zehnder interferometer used to measure the differential group effective index, fitted in the next step to a suitable approximate function. The chromatic dispersion is then obtained in a closed form by the differentiation of this function. The successful test of the method was performed using already tested samples of holey and elliptical-core fibers. Because the proposed method was limited by the equalization wavelength resolution in the vicinity of zero-dispersion wavelength, we proposed an alternative method. This new method, in contrast to the previous technique, uses only one recorded interferogram containing the zero-dispersion wavelength. The spectral fringes are properly located and numbered. The fringe number dependence on its position is then fitted to obtain the interference order and unknown coefficients of an approximate formula used to approximate the modal effective index dispersion. As in the case of the previous method, the second derivative of this function leads to the chromatic dispersion formula written in a closed form, allowing to compute the position of zero-dispersion wavelength. The results of this measurement were compared to the data determined by other methods and good agreement was obtained.

The knowledge of computational and experimental techniques allowed us to perform the analysis of a tandem configuration comprising the sample of a birefringent fiber and birefringent crystal. At first we theoretically showed the usage of such a setup in optical sensing utilizing the birefringent fibers and demonstrated the results using the change of the fiber sample length. Recently, we applied this concept to the problem of temperature sensing. Based on theoretical background, we demonstrated in practice the temperature measurement using the tandem configuration of elliptical-core fiber and quartz crystal plate serving here as a delay line. The information about the temperature was retrieved from the recorded channeled spectrum, where the fringe extrema were traced. The possibility to change the sensitivity to the temperature was shown too.

To conclude, we successfully demonstrated the feasibility of the spectral domain interferometry applied to the characterization of dispersion properties of polarization maintaining fibers. The proposed experimental methods together with the sophisticated computational techniques can serve as a powerful and versatile tool in optical fiber metrology as well as in the design of various applications.

It is worth mentioning that the application of spectral interferometry is not limited to the tasks of optical fiber metrology. Recently, the spectral interferometry has been successfully used in the detection of surface plasmon resonance (SPR) in the thin film systems. So we suggest that the future research can be oriented on the optical fibers containing some structures supporting surface plasmon waves. Such sensors based on the combination of SPR with mature optical fiber technology can utilize the interference of polarization modes. Optical sensors based on the single-mode fiber can offer higher sensitivity and detection accuracy in comparison with common sensing schemes utilizing multimode fibers.

Appendix A

List of discussed papers

[I] P. Hlubina, M. Szpulak, L. Knyblová, G. Statkiewicz, T. Martynkien, **D. Ciprian** and W. Urbanczyk, "Measurement and modelling of dispersion characteristics of a two-mode birefringent holey fibre," *Meas. Sci. Technol.*, **17**, 626-630 (2006)

[II] P. Hlubina, **D. Ciprian**, M. Kadulová, "Wide spectral range measurement of modal birefringence in polarization-maintaining fibres," *Meas. Sci. Technol.*, **20**, 025301 (2009)

[III] P. Hlubina, R. Chlebus, **D. Ciprian**, "Differential group refractive index dispersion of glasses of optical fibres measured by a white-light spectral interferometric technique," *Meas. Sci. Technol.*, **18**, 1547-1552 (2007)

[IV] P. Hlubina, M. Szpulak, **D. Ciprian**, T. Martynkien and W. Urbanczyk, "Measurement of the group dispersion of the fundamental mode of holey fiber by white-light spectral interferometry," *Opt. Express*, **15**, 11073-11081 (2007)

[V] P. Hlubina, **D. Ciprian**, R. Chlebus, "Group index dispersion of holey fibres measured by a white-light spectral interferometric technique," *Opt. Commun.*, **281**, 4008-4013 (2008)

[VI] P. Hlubina, **D. Ciprian**, "Spectral-domain measurement of phase modal birefringence in polarization-maintaining fiber," *Opt. Express*, **15**, 17019-17024 (2007)

[VII] P. Hlubina, **D. Ciprian**, "Absolute phase birefringence dispersion in polarization-maintaining fiber or birefringent crystal retrieved from a channeled spectrum," *Opt. Letters*, **35**, 1566-1568 (2010)

[VIII] P. Hlubina, **D. Ciprian**, M. Kadulová, "Measurement of chromatic dispersion of polarization modes in optical fibres using white-light spectral interferometry," *Meas. Sci. Technol.*, **21**, 045302 (2010)

[IX] P. Hlubina, M. Kadulová, **D. Ciprian**, "Spectral interferometry-based chromatic dispersion measurement of fibre including the zero-dispersion wavelength," *J. Europ. Opt. Soc. Rap. Public.*, **7**, 12017-12022 (2012)

[X] P. Hlubina, **D. Ciprian**, L. Knyblová, "Interference of white light in tandem configuration of birefringent crystal and sensing birefringent fiber," *Opt. Commun.*, **260**, 535-541 (2006)

[XI] P. Hlubina, T. Martynkien, **D. Ciprian**, J. Wójcik and W. Urbanczyk, "Broad spectral range measurements and modelling of birefringence dispersion in two-mode elliptical-core fibres" *J. Opt.*, **12**, 035405 (2010)

[XII] P. Hlubina, M. Kadulová, **D. Ciprian** and P. Mergo, "Temperature sensing using the spectral interference of polarization modes in highly birefringent fiber," *Opt. Las. Eng.*, **70**, 51-56 (2015)

Bibliography

[1] Stratton, J. A., [*Electromagnetic Theory*], McGraw-Hill (1941).

[2] Dyott, R. B., [*Elliptical Fiber Waveguides*], Artech House (1995).

[3] McLachlan, N., [*Theory and Application of Mathieu Functions*], Oxford University Press (1947).

[4] Gradshteyn, I. and Ryzhik, I., [*Table of Integrals, Series, and Products, 7th ed.*], Academic Press (2007).

[5] Yeh, C., "Elliptical dielectric waveguides," *J. Appl. Phys.* **33**, 3235–3243 (1962).

[6] Rengarajan, S. R. and Lewis, J. E., "Mathieu functions of integral order and real arguments," *IEEE Trans. Microwave Theory and Techniques* **38**, 276–277 (1980).

[7] Toyama, N. and Shogen, K., "Computation of the value of the even and odd Mathieu functions of order n for a given parameter s and an argument x," *IEEE Trans. on Antennas and Propagation* **32**, 537–539 (1984).

[8] Stamnes, J. J. and Spjelkavik, B., "New method for computing eigenfunctions (Mathieu functions) for scattering by elliptical cylinders," *J. Pure Appl. Opt.* **4**, 251–262 (1995).

[9] Kapany, H. S. and Burke, J. J., [*Optical Waveguides*], Academic Press (1972).

[10] Snyder, A. W., "Asymptotic expressions for eigenfunctions and eigenvalues of a dielectric or optical waveguide," *IEEE Trans. Microwave Theory and Techniques* **17**, 1130–1138 (1969).

[11] Gloge, D., "Weakly giuding fibers," *Appl. Opt.* **10**, 2252–2258 (1971).

[12] Snyder, A. W., "Modes of optical waveguides," *J. Opt. Soc. Am.* **68**, 297–309 (1978).

[13] Yeh, C., "Modes in weakly guiding elliptical optical fibres," *Opt. Quant. Electron.* **8**, 43–47 (1976).

[14] Shaw, J. K., Henry, W. M., and Winfrey, W. R., "Weakly guiding analysis of elliptical core step index waveguides based on the characteristic numbers of Mathieu's equation," *J. Lightwave Technol.* **13**, 2359–2371 (1995).

[15] Gomez-Castellanos, I. and Rodrigues-Dagnino, R. M., "Intensity distributions and cutoff frequencies of linearly polarized modes for a step-index elliptical optical fiber," *Opt. Eng.* **46**, 045003 (2007).

[16] Hu, X., South, R. B., and Rutter, M. J., "Analysis of linearly polarised modes in elliptical-core fibre," *IEE Proc.-Optoelectron.* **141**, 356–362 (1994).

[17] Citerne, J., "Comments on 'modes in weakly guiding elliptical optical fibres'," *Opt. Quant. Electron.* **12**, 529–532 (1980).

[18] Sodha, M. S. and Ghatak, A. K., [*Inhomogeneous Optical Waveguides*], Plenum Press, New York (1977).

[19] Kumar, A. K. and Varshney, R. K., "Propagation of highly elliptical core optical waveguides: a perturbation approach," *Opt. Quant. Electron.* **16**, 349–354 (1984).

[20] Yeh, C. and Shimabukuro, F. I., [*The Essence of Dielectric Waveguides*], Springer (2008).

[21] Birks, T. A., Knight, J. C., and Russell, P. S. J., "Endlessly single-mode photonic crystal fiber," *Opt. Lett.* **22**, 961–963 (1997).

[22] Joannopoulos, J. D., Winn, J. N., Johnson, S. G., and Meade, R. D., [*Photonic Crystals: Molding the Flow of Light*], Princeton University Press, Princeton (2008).

[23] Knight, J. C., Birks, T. A., Russell, P. S. J., and de Sandro, J. P., "Properties of photonic crystal fiber and the effective model," *J. Opt. Soc. Am. A* **15**, 748–752 (1998).

[24] Midrio, M., Singh, M. P., and Someda, C. G., "The space filling mode of holey fibers: An analytical vectorial solution," *J. Lightwave Technol.* **18**, 1031–1037 (2000).

[25] Li, Y., Wang, C., and Hu, M., "A fully vectorial effective index method for photonic crystal fibers: application to dispersion calculation," *Opt. Commun.* **238**, 29–33 (2004).

[26] Li, Y., Yao, Y., Hu, M., Chai, L., and Wang, C., "Improved fully vectorial effective index method for photonic crystal fibers: evaluation and enhancement," *J. Lightwave Technol.* **18**, 1031–1037 (2000).

[27] Brechet, F., Marcou, J., D.Pagnoux, and Roy, P., "Complete analysis of the characteristics of propagation in photonic crystal fibers by the finite element method," *Opt. Fiber Technol.* **6**, 181–191 (2000).

[28] Birks, T. A., Mogilvtsev, D., Knight, J. C., Russell, P. S., Broeng, J., Roberts, P. J., West, J. A., Allan, D. C., and Fajardo, J. C., "The analogy between photonic crystal fibers and step index fibers," *Proc. of OFC*, 114–116 (1999).

[29] Park, K. N. and Lee, K. S., "Improved effective-index method for analysis of photonic crystal fibers," *Opt. Lett.* **30**, 958–960 (2005).

[30] Zhao, X., Hou, L., Liu, Z., Zhou, G., and Hou, Z., "Improved fully vectorial effective index method in photonic crystal fibers," *Opt. Fiber Technol.* **6**, 181–191 (2000).

[31] Maradudin, A. A. and McGurn, A. R., "Out of plane propagation of electromagnetic waves in a two-dimensional periodic dielectric medium," *J. Mod. Opt.* **41**, 275–284 (1994).

[32] Pearce, G. J., Hedley, T. D., and Bird, D. M., "Adaptive curvilinear coordinates in a plane-wave solution of Maxwell's equations in photonic crystals," *Phys. Rev. B* **71**, 195108 (2005).

[33] Wang, Z., Ren, G., Lou, S., and Jian, S., "Supercell lattice method for photonic crystal fibers," *Opt. Express* **11**, 181–191 (2003).

[34] White, T. P., Kuhlmey, B. T., McPhedran, R. C., Maystre, D., Renversez, G., de Sterke, C. M., and Botten, L. C., "Multipole method for microstructured optical fibers. I. formulation," *J. Opt. Soc. Am. A* **19**, 2322–2330 (2002).

[35] Lo, K. M., McPhedran, R. C., Bassett, I. M., and Milton, G. W., "An electromagnetic theory of dielectric waveguides with multiple embedded cylinders," *J. Lightwave Technol.* **12**, 396–410 (1994).

[36] Wijngaard, W., "Guided normal modes in two parallel circular dielectric rods," *J. Opt. Soc. Am.* **63**, 944–950 (1973).

[37] Abramowitz, M. and Stegun, I., [*Handbook of Mathematical Functions*], Dover Publications, New York, NY (1970).

[38] Kuhlmey, B. T., White, T. P., Renversez, G., Maystre, D., Botten, L. C., de Sterke, C. M., and McPhedran, R. C., "Multipole method for microstructured optical fibers. II. implementation and results," *J. Opt. Soc. Am. B.* **19**, 2331–2339 (2002).

[39] Mikhlin, S. G., [*Variational Methods in Mathematical Physics*], Macmillan, New York, NY (1964).

[40] Finlayson, B. A., [*Method of Weighted Residuals and Variational Principles*], Academic Press, New York, NY (1972).

[41] Koshiba, M., [*Optical Waveguide Theory by the Finite Elements*], KTK Publishers (1993).

[42] Lee, J. F., Sun, D. K., and Cendes, Z. J., "Full-wave analysis of dielectric waveguide using tangential vector finite elements," *IEEE Trans. Microwave Theory Tech.* **39**, 1262–1271 (1991).

[43] Karp, S. N., "A convergent far-field expansion for two-dimensional radiation function," *Commin. Pure Appl. Math.* **14**, 427–434 (1961).

[44] Berenger, J. P., "Three-dimensional perfectly matched layer for the absorption of electromagnetic waves," *J. Comput. Phys.* **127**, 363–379 (1996).

[45] Chew, W. C., Jin, J. M., and Michielssen, E., "Complex coordinate stretching as a generalized absorbing boundary condition," *Microwave Opt. Tech. Lett.* **15**, 363–369 (1997).

[46] Teixeira, F. L. and Chew, W. C., "Systematic derivation of anisotropic PML absorbing media in cylindrical and spherical coordinated," *IEEE Microwave Guided Wave Lett.* **7**, 371–373 (1977).

[47] Malitson, I. H., "Interspecimen comparison of the refractive index of fused silica," *J. Opt. Soc. Am.* **55**, 1205–1209 (1965).

[48] Fleming, J. W., "Material dispersion in lightguide glasses," *Electron. Lett.* **14**, 326–328 (1978).

[49] Fleming, J. W., "Dispersion in GeO_2-SiO_2 glasses," *Appl. Opt.* **23**, 4486–4492 (1984).

[50] Melman, P. and Davies, R. W., "Application of the Clausius-Mossotti equation to dispersion calculations in optical fibers," *J. Lightwave Technol.* **3**, 1123–1124 (1985).

[51] Sunak, H. R. D. and Bastien, S. P., "Refractive index and material dispersion interpolation of doped silica in the $0.6 - 1.8\,\mu$m wavelength region," *IEEE Photon. Tech. Lett.* **1**, 142–145 (1989).

[52] Mandel, L. and Wolf, E., [*Optical Coherence and Quantum Optics*], Cambridge University Press (1995).

[53] Hlubina, P., "Dispersive spectral-domain two-beam interference analysed by a fiber-optic spectrometer," *J. Mod. Opt.* **51**, 537–547 (2004).

[54] Sainz, C., Jourdain, P., Escalona, R., and Calatroni, J., "Real time interferometric measurements of dispersion curves," *Opt. Commun.* **110**, 381–390 (1994).

[55] Hlubina, P., "White-light spectral interferometry with the uncompensated Michelson interferometer and the group refractive index dispersion in fused silica," *Opt. Commun.* **193**, 1–7 (2001).

[56] Hlubina, P., Gurov, I., and Chugunov, V., "White-light spectral interferometric technique to measure the wavelength dependence of the spectral bandpass of a fibre-optic spectrometer," *J. Mod. Opt.* **50**, 2067–2074 (2003).

[57] Gurov, I., Hlubina, P., and Chugunov, V., "Evaluation of spectral modulated interferograms using a Fourier transform and the iterative phase-locked loop method," *Meas. Sci. Technol.* **14**, 122–130 (2003).

[58] Reolon, D., Jacquot, M., Verrier, I., Brun, G., and Veillas, C., "High resolution group refractive index measurement by broadband supercontinuum interferometry and wavelet-transform analysis," *Opt. Express* **14**, 12744–12750 (2006).

[59] Hlubina, P., "Interference of white light analyzed at the output of a birefringent crystal by a fibre-optic spectrometer," *Opt. Commun.* **251**, 367–375 (2005).

[60] McIsaac, P. R. M., "Symmetry-induced modal characteristics of uniform waveguides, parts I and II," *IEEE Trans. Microwave Theory and Techniques* **23**, 421–433 (1975).

[61] Pottage, J. M., Bird, D. M., Hedley, T. D., Birks, T. A., J.C.Knight, J.Russell, P. S., and Roberts, P., "Robust photonic band gaps for hollow core guidance in PCF made from high index glass," *Opt. Express* **11**, 2854–2861 (2003).

[62] Li, L., "Use of Fourier series in the analysis of discontinuous periodic structures," *J. Opt. Soc. Am. A* **13**, 1870–1876 (1996).

[63] Norton, R. A. and Sheichl, R., "Planewave expansion methods for photonic crystal fibres," *Appl. Num. Math.* **63**, 88–1047 (2013).

[64] Felbacq, D., G.Tayeb, and Maystre, D., "Scattering by an random set of parallel cylinders," *J. Opt. Soc. Am. A* **11**, 2526–2538 (1994).

[65] Bock, W. J. and Urbanczyk, W., "Measurement of polarization mode dispersion and modal birefingence in highly birefringent fibers by means of electronically scanned shearing-type interferometry," *Appl. Opt.* **32**, 5841–5848 (1993).

[66] Yan, M. and Shum, P., "Antiguiding in microstructured optical fibers," *Opt. Express* **12**, 104–116 (2004).

[67] Takada, K., Noda, J., and Ulrich, R., "Precision measurement of modal birefringence of highly birefringent fibers by periodic lateral force," *Appl. Opt.* **24**, 4387–4391 (1985).

[68] Hlubina, P., Luňáček, J., Ciprian, D., and Chlebus, R., "Windowed Fourier transform applied in the wavelength domain to process the spectral interference signals," *Opt. Commun.* **281**, 2349–2354 (2008).

[69] Shibata, N., Nakazono, N., and Inoue, Y., "Interference between two orthogonally polarized modes traversing a highly birefringent air-silica fiber," *J. Lightwave Technol.* **23**, 1244–1252 (2005).

[70] Lang, S., [*Undergraduate Algebra, 2.ed.*], Springer Verlag, New York (1990).

[71] Tsubokawa, M., Shibata, N., Higashi, T., and Seikai, S., "Loss of longitudinal coherence as a result of the birefringence effect," *J. Opt. Soc. Am. A* **4**, 1895–1901 (1987).

[72] Hlubina, P., Olszewski, J., Martynkien, T., Mergo, P., Makara, M., Poturaj, K., and et. al., "Spectral-domain measurment of strain sensitivity of two-mode birefringent side-hole fiber," *Sensors* **12**, 12070–12081 (2012).

[73] Statkiewicz, G., Martynkien, T., and Urbanczyk, W., "Measurements of modal birefringence and polarimetric sensitivity of the birefringent holey fiber to hydrostatic pressure and strain," *Opt. Commun.* **241**, 339–348 (2004).

Part II

Discussed paper (fulltext)

Paper I.

INSTITUTE OF PHYSICS PUBLISHING MEASUREMENT SCIENCE AND TECHNOLOGY
Meas. Sci. Technol. **17** (2006) 626–630 doi:10.1088/0957-0233/17/4/003

Measurement and modelling of dispersion characteristics of a two-mode birefringent holey fibre

P Hlubina[1], M Szpulak[2], L Knyblová[1], G Statkiewicz[2], T Martynkien[2], D Ciprian[1] and W Urbańczyk[2]

[1] Department of Physics, Technical University Ostrava, 17 listopadu 15, 708 33 Ostrava-Poruba, Czech Republic
[2] Institute of Physics, Wrocław University of Technology, Wybrzeże Wyspiańskiego 27, 50-370 Wrocław, Poland

E-mail: petr.hlubina@vsb.cz

Received 10 October 2005, in final form 12 December 2005
Published 10 February 2006
Online at stacks.iop.org/MST/17/626

Abstract
Employing several interferometric methods, we measured in a broad spectral range the wavelength dependences of the phase modal birefringence and the polarization mode dispersion for the LP_{01} and *even* LP_{11} spatial modes supported by a birefringent holey fibre. We also determined the wavelength dependence of the intermodal dispersion between the *X*- and *Y*-polarized LP_{01} and *even* LP_{11} spatial modes. Furthermore, using a full-vector finite-element method, we modelled all the measured dispersion characteristics and demonstrated good agreement between experimental and theoretical results.

Keywords: fibre characterization, birefringent holey fibre, birefringence dispersion, intermodal dispersion

1. Introduction

Conventional birefringent two-mode optical fibres that support two stable spatial modes, i.e., the fundamental LP_{01} and the second-order *even* LP_{11} mode, have attracted considerable interest for a number of applications, such as interferometric modal/polarimetric sensors of strain, temperature or both at the same time [1–4]. A new class of birefringent holey fibres may also find metrological applications due to much higher flexibility in shaping propagation and sensing characteristics [5–8], including the possibility of operation in single-mode [9] and two-mode [10] regimes over a wide wavelength range.

Most of the birefringent holey fibres described in the literature so far are based on a hexagonal lattice. As shown in [5], high birefringence in these fibres can be induced by an asymmetrical cladding, in which one row of hexagonal cells has lower fill factor than the other cladding cells. Another type of cladding asymmetry was proposed in [11]. The birefringence in this structure is induced by two air holes adjacent to the fibre core and having diameters greater than the other cladding holes.

In this paper, we present the results of experimental and theoretical investigations of dispersion characteristics of a two-mode birefringent holey fibre. Different interferometric techniques were used to measure in a broad spectral range the wavelength dependences of the phase and the group modal birefringence for the LP_{01} and *even* LP_{11} spatial modes. We also measured the wavelength dependence of the intermodal dispersion for two orthogonal polarizations of the LP_{01} and *even* LP_{11} spatial modes employing a white-light spectral interferometric method. Furthermore, we modelled all the dispersion characteristics using a full-vector finite-element method and confirmed good agreement between experimental and theoretical results.

2. Dispersion characteristics of a birefringent fibre

Consider a birefringent holey fibre, which supports the *X*- and *Y*-polarized fundamental LP_{01} and second-order *even* LP_{11} spatial modes. If the wavelength-dependent propagation constants of the corresponding modes are denoted

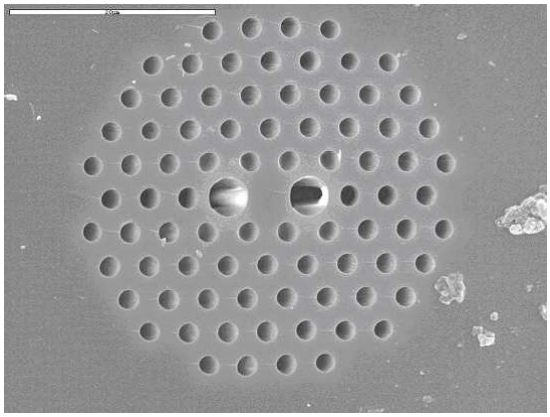

Figure 1. SEM photograph of the investigated holey fibre.

as $\beta_{01}^x(\lambda)$, $\beta_{01}^y(\lambda)$, $\beta_{11}^x(\lambda)$ and $\beta_{11}^y(\lambda)$, we can define the phase modal birefringences for the respective spatial modes in the following way:

$$\begin{aligned} \Delta n_{01}(\lambda) &= \frac{\lambda}{2\pi}\left[\beta_{01}^x(\lambda) - \beta_{01}^y(\lambda)\right], \\ \Delta n_{11}(\lambda) &= \frac{\lambda}{2\pi}\left[\beta_{11}^x(\lambda) - \beta_{11}^y(\lambda)\right]. \end{aligned} \tag{1}$$

The differences between the phase effective indices of the LP_{01} and *even* LP_{11} modes of the same polarization can be expressed, respectively, as

$$\begin{aligned} \Delta n_{\text{int}}^x(\lambda) &= \frac{\lambda}{2\pi}\left[\beta_{01}^x(\lambda) - \beta_{11}^x(\lambda)\right], \\ \Delta n_{\text{int}}^y(\lambda) &= \frac{\lambda}{2\pi}\left[\beta_{01}^y(\lambda) - \beta_{11}^y(\lambda)\right]. \end{aligned} \tag{2}$$

Furthermore, we can define the group modal birefringences $\Delta N_{01}(\lambda)$ and $\Delta N_{11}(\lambda)$ for the respective spatial modes and the differences between group effective indices $\Delta N_{\text{int}}^x(\lambda)$ and $\Delta N_{\text{int}}^y(\lambda)$ using the following general relation:

$$\Delta N(\lambda) = \Delta n(\lambda) - \lambda\frac{\mathrm{d}\Delta n(\lambda)}{\mathrm{d}\lambda} = -\lambda^2\frac{\mathrm{d}[\Delta n(\lambda)/\lambda]}{\mathrm{d}\lambda}. \tag{3}$$

It is clear from equation (3) that knowledge of the spectral dependence of $\Delta N(\lambda)$ can be used to obtain the relative wavelength dependence of $\Delta n(\lambda)$. It can be combined with the known value of Δn at one specific wavelength to obtain absolute values of $\Delta n(\lambda)$ [12].

3. Experimental methods

We investigated a birefringent holey fibre produced by Blaze Photonics Inc. Its cross section obtained by the scanning electron microscope (SEM) is shown in figure 1. The orientation of the polarization X and Y axes is as follows: X overlaps with the longer axis of the elliptical core, while Y overlaps with the shorter axis and crosses the two large holes adjacent to the fibre core. The average geometrical parameters of the holey fibre are as follows: pitch distance 4.30 μm, diameter of large holes 4.42 μm and diameter of the cladding holes 2.34 μm. This fibre supports the *even* LP_{11} spatial mode for wavelengths shorter than 1 μm.

The phase modal birefringences for the LP_{01} and *even* LP_{11} spatial modes, respectively, $\Delta n_{01}(\lambda)$ and $\Delta n_{11}(\lambda)$, were measured by a lateral force method [13], which was developed first for the characterization of conventional birefringent fibres. To perform the measurements of the phase modal birefringence over a wide wavelength range, we used different light sources such as YAG (533 nm), He–Ne laser (633 nm) and several laser diodes operating, respectively, at 680, 785, 830, 1314 and 1500 nm. In this method, a shift of interference fringes is observed in response to the displacement of the coupling point along the tested fibre. An accuracy better than 1% is easily achievable if the coupling point is displaced over a sufficiently long distance.

The group modal birefringences for the LP_{01} and *even* LP_{11} spatial modes, respectively, $\Delta N_{01}(\lambda)$ and $\Delta N_{11}(\lambda)$, were measured by two different interferometric methods: a method of spectral-domain tandem interferometry [12] and a wavelength-scanning method [14]. In both methods, a polarizer and an analyser were placed at the ends of the measured holey fibre and oriented at 45° relative to the fibre polarization axes. The method of spectral-domain tandem interferometry uses a white-light source (a halogen lamp) and is based on the fact that the optical path difference adjusted in the Michelson interferometer compensates for the group optical path difference introduced by the tested fibre at one specific wavelength, called the equalization wavelength. The equalization wavelength, in the vicinity of which the resolvable spectral interference fringes are localized, was measured in a wavelength range from 575 to 765 nm. Using this method, we measured the group birefringence for both spatial modes with a precision better than 1% [12].

In the wavelength-scanning method, we used four superluminescent diodes having broadband spectrum and the central wavelength 785, 840, 1300 and 1550 nm, respectively. This method, which is characterized by an accuracy better than 5%, is based on interference of both polarization modes that gives rise to the modulation of the output spectrum. The group birefringence is determined from the spectral separation of successive interference fringes [8].

The differences in group effective indices between the X- and Y-polarized LP_{01} and *even* LP_{11} spatial modes, respectively, $\Delta N_{\text{int}}^x(\lambda)$ and $\Delta N_{\text{int}}^y(\lambda)$, were measured in a wavelength range from 555 to 800 nm by the spectral-domain tandem interferometry method [15] with a precision better than 0.1%.

4. Numerical modelling

A full-vector mode solver based on a hybrid edge/nodal finite-element method (FEM) [16–18] was used to calculate the propagation constants and electric field distributions of guided modes. In this approach, the following eigenequation is solved:

$$\begin{bmatrix} -\nabla_\perp \times \nabla_\perp \times + k_0^2\varepsilon(\vec{r}) & 0 \\ 0 & 0 \end{bmatrix} \begin{bmatrix} \vec{E}_\perp \\ E_z \end{bmatrix} = \beta^2 \begin{bmatrix} 1 & \nabla_\perp \\ \nabla_\perp & \Delta + k_0^2\varepsilon(\vec{r}) \end{bmatrix} \begin{bmatrix} \vec{E}_\perp \\ E_z \end{bmatrix}, \tag{4}$$

where $(\vec{E}_\perp, E_z)$ is the electric field vector (eigenvector) and β is the propagation constant of the mode (eigenvalue). To

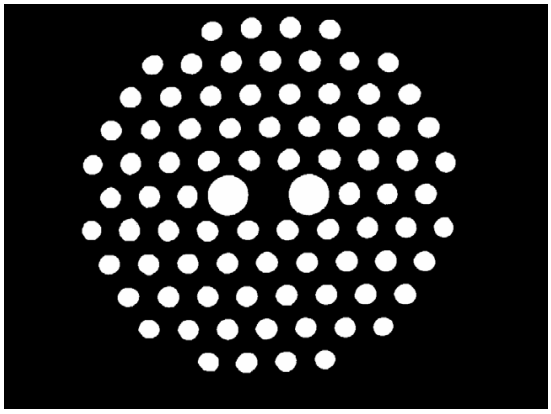

Figure 2. Binary mask used for mesh generation.

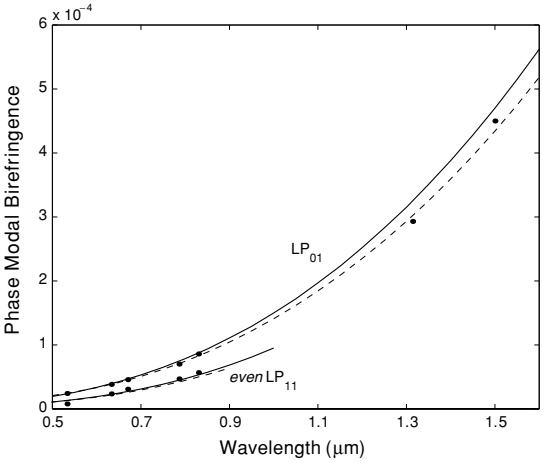

Figure 3. Calculated (solid lines) and measured (markers) phase modal birefringence as a function of wavelength.

find the eigenpairs of the above equation, we used the Arnoldi method as an eigensolver and an asymmetrical multifrontal method as a solver of a linear system of equations.

The calculations were carried out for the real geometry of the fibre. The edges of the holes in the cladding were automatically detected by special processing of the SEM image, which included modification of the histogram followed by thresholding and binarization. As a result, we obtained a binary image of the fibre cross section (figure 2) that was used as a mask to generate the mesh for FEM, which reflected the real shape and location of each hole. To assure high accuracy of numerical results, we applied a mesh composed of about 170 000 triangular elements and took into account the dispersion of the refractive index of the silica glass.

5. Results of the experiments and of the modelling

Figure 3 shows by the dots the measured values of the phase modal birefringence, respectively, $\Delta n_{01}(\lambda)$ and $\Delta n_{11}(\lambda)$, for the LP_{01} and *even* LP_{11} spatial modes. As already reported

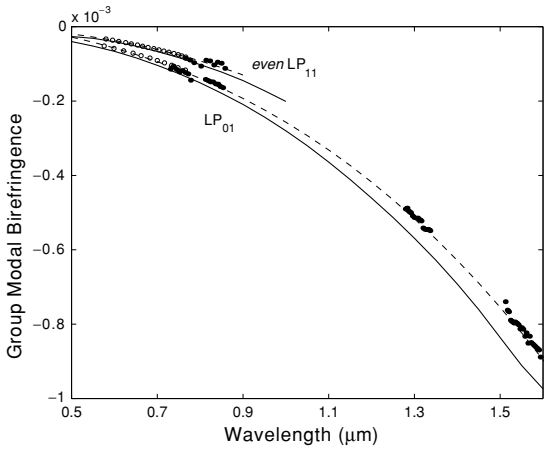

Figure 4. Calculated (solid lines) and measured (markers) group modal birefringence as a function of wavelength.

in earlier publications [5–8], Δn_{01} strongly increases against wavelength. The phase modal birefringence for the *even* LP_{11} spatial mode has similar wavelength dependence; however, its value is lower by about 30% compared to Δn_{01}. For the shorter wavelengths, the results of measurements for the fundamental mode agree well with theoretical ones. For the longer wavelengths, the experimental values are lower by about 10% than the theoretical ones. The discrepancy between the measured and calculated values of $\Delta n_{11}(\lambda)$ is even lower than in the case of the fundamental mode and does not exceed 2%.

Figure 4 shows by the markers the measured group modal birefringences ΔN_{01} and ΔN_{11} for the LP_{01} and *even* LP_{11} modes as a function of wavelength. Open circles correspond to the measurement results obtained by the method of spectral tandem interferometry whereas full circles are related to the wavelength-scanning method. The group modal birefringence for the LP_{01} mode is negative and strongly decreases against wavelength, which is in accordance with the results of numerical modelling. The group modal birefringence for the *even* LP_{11} spatial mode has similar wavelength dependence; however, the absolute value of ΔN_{11} is lower than ΔN_{01} by about 20%. The measured values of ΔN_{11} agree within 5% error with the results of numerical modelling. The difference between the experimental and theoretical values of the group birefringence for the LP_{01} mode increases against wavelength and reaches 10% at $\lambda = 1.5\ \mu$m. The measured values of ΔN_{01} and ΔN_{11} are fitted by polynomials shown in figure 4 by the dashed lines. Using a procedure presented in [12], we obtained the polynomial representations of the phase modal birefringences $\Delta n_{01}(\lambda)$ and $\Delta n_{11}(\lambda)$, which are indicated in figure 3 by the dashed lines. These lines fit well the experimental values which confirms the consistency of the phase and the group birefringence measurements.

Figure 5 shows the calculated differences in phase effective indices $\Delta n^x_{\mathrm{int}}(\lambda)$ and $\Delta n^y_{\mathrm{int}}(\lambda)$, respectively, for the *X*- and *Y*-polarized LP_{01} and *even* LP_{11} spatial modes. These calculation results show that $\Delta n^x_{\mathrm{int}}(\lambda)$ is higher than $\Delta n^y_{\mathrm{int}}(\lambda)$ in the whole analysed spectral range, indicating

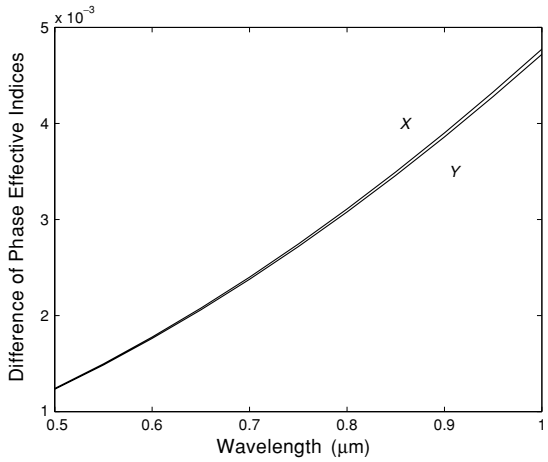

Figure 5. Calculated difference between phase effective indices of the LP_{01} and *even* LP_{11} modes of respective polarizations as a function of wavelength.

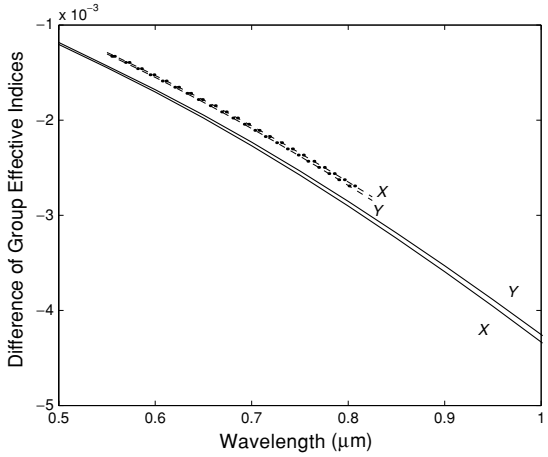

Figure 6. Calculated difference between group effective indices of the LP_{01} and *even* LP_{11} modes of respective polarizations as a function of wavelength. The measured values are indicated with dots.

noticeable discrimination between both polarizations for longer wavelengths. Figure 6 shows the differences in group effective indices $\Delta N^x_{\mathrm{int}}(\lambda)$ and $\Delta N^y_{\mathrm{int}}(\lambda)$ calculated as a function of wavelength using equation (3). The calculated values of $\Delta N^x_{\mathrm{int}}(\lambda)$ are lower than those of $\Delta N^y_{\mathrm{int}}(\lambda)$ in the whole analysed spectral range. Figure 6 also shows the measured values of $\Delta N^x_{\mathrm{int}}(\lambda)$ and $\Delta N^y_{\mathrm{int}}(\lambda)$ that differ from the calculated ones by about 10%. In contrast to the modelling results, the experimental values of $\Delta N^x_{\mathrm{int}}(\lambda)$ are greater than those of $\Delta N^y_{\mathrm{int}}(\lambda)$ by about 2%.

The small disagreements between experimental and calculated values observed in all measurements are most probably caused by the errors in reproducing the real structure geometry from the SEM image. When creating a binary mask used for mesh generation, we arbitrarily adjust the threshold level to discriminate between 0 and 1 values. As shown in figure 1, a SEM image of the fibre cross section contains halftones, which means that it is practically impossible to detect the location of the holes' edges with an accuracy better than 50 nm. Furthermore, every SEM image is charged with a scaling error that may reach up to 20%. We partially eliminated this problem by measuring the distance between the selected structural elements in the fibre cross section using an optical microscope. These measurements are later used to calibrate the magnification of the SEM image, which results in lowering of the scaling error to the level of about 2%. Finally, the accuracy of measurements of the holes' diameters is limited by the thickness of the conductive coating (carbon or gold) used to cover the fibre cleave before taking the SEM image, because such a coating partially shadows the holes' openings.

In conclusion, there are several experimental limitations causing the dimensions of the real fibre to be determined and transferred to the numerical model with limited precision. At the long wavelength limit, the modal field extends more deeply into the cladding and becomes more sensitive to inaccuracies of the numerical model. Therefore, one may expect an increasing difference between experimental and numerical results for longer wavelengths. As shown in figures 3 and 4, this effect is especially apparent for the fundamental mode.

It is also worth mentioning that the fibre characterized in this work is the same as that from [8]. The discrepancies in the fibre geometrical parameters presented in [8] and in the present work are caused by different methods of determining the fibre dimensions. In [8], we simply scaled the fibre image using the reference bar produced by the SEM, while in the present work we used a more accurate scaling procedure involving optical measurements. As a result, the fibre dimensions presented in [8] and in the present work differ by about 15%.

6. Conclusions

Using different interferometric methods, we measured in a wide spectral spectral range the wavelength dependences of both the phase and the group modal birefringence for two lowest order spatial modes supported by a birefringent holey fibre. We also determined the wavelength dependence of the difference in effective group indices for two orthogonal polarizations of the LP modes employing a white-light spectral interferometric method. Furthermore, all the measured dispersion characteristics were calculated for the real geometry of the fibre using a full-vector finite-element method. The discrepancy between theoretical and experimental values is low and in the worst case does not exceed 10%. The investigated dispersion characteristics may be of importance for applications of the holey fibres in optical interferometric systems and fibre optic sensors.

Acknowledgments

The research was partially supported by the Grant Agency of the Czech Republic, project no 102/06/0284, by the grant MSM6198910016, by an internal grant of TU Ostrava (IGS HGF VŠB-TUO) and by the Polish Committee for Scientific Research under grant no 3T10C 04228.

References

[1] Kim B Y, Blake J N, Huang S Y and Shaw H J 1987 Use of highly elliptical core fibers for two-mode fiber devices *Opt. Lett.* **12** 729–31

[2] Blake J N, Huang S Y, Kim B Y and Shaw H J 1987 Strain effects on highly elliptical core two-mode fibers *Opt. Lett.* **12** 732–4

[3] Murphy K A, Miller M S, Vengsarkar A M and Claus R O 1990 Elliptical-core two-mode optical-fiber sensor implementation methods *J. Lightwave Technol.* **8** 1688–96

[4] Vengsarkar A M, Michie W C, Jankovic L, Culshaw B and Claus R O 1994 Fiber-optic dual-technique sensor for simultaneous measurement of strain and temperature *J. Lightwave Technol.* **12** 170–7

[5] Ortigosa-Blanch A, Knight J C, Wadsworth W J, Arriaga J, Mangan B J, Birks T A and Russell P St J 2000 Highly birefringent photonic crystal fibers *Opt. Lett.* 1325–7

[6] Zhu Z and Brown T G 2003 Stress-induced birefringence in microstructured optical fibers *Opt. Express* **28** 2306–8

[7] Ritari T, Ludvigsen H, Wegmuller M, Legré M and Gisin N 2004 Experimental study of polarization properties of highly birefringent photonic crystal fibers *Opt. Express* **12** 5931–9

[8] Statkiewicz G, Martynkien T and Urbańczyk W 2004 Measurements of modal birefringence and polarimetric sensitivity of the birefringent holey fiber to hydrostatic pressure and strain *Opt. Commun.* **241** 339–48

[9] Birks T A, Knight J C and Russell P St J 1997 Endlessly single-mode photonic crystal fiber *Opt. Lett.* **22** 961–3

[10] Jin W, Wang Z and Ju J 2005 Two-mode photonic crystal fibers *Opt. Express* **13** 2082–8

[11] Suzuki K, Kubota H, Kawanishi S, Tanaka M and Fujita M 2001 Optical properties of a low-loss polarization-maintaining photonic crystal fiber *Opt. Express* **9** 676–80

[12] Hlubina P, Martynkien T and Urbańczyk W 2003 Dispersion of group and phase modal birefringence in elliptical-core fiber measured by white-light spectral interferometry *Opt. Express* **11** 2793–8

[13] Bock W J and Urbańczyk W 1993 Measurements of polarization mode dispersion and modal birefringence in highly birefringent fibers by means of electronically scanned shearing type interferometry *Appl. Opt.* **32** 5841–8

[14] Rashleigh S C 1982 Wavelength dependence of birefringence in highly birefringent fibers *Opt. Lett.* **7** 294–6

[15] Hlubina P 2003 White-light spectral interferometry to measure intermodal dispersion in two-mode elliptical-core optical fibers *Opt. Commun.* **218** 283–9

[16] Koshiba M, Maruyama S and Hirayama K 1994 A vector finite element method with the higher order mixed-interpolation-type triangular elements for optical waveguide problems *J. Lightwave Technol.* **12** 495–502

[17] Koshiba M and Saitoh K 2003 Finite-element analysis of birefringence and dispersion properties in actual and idealized holey-fiber structures *Appl. Opt.* **42** 6267–75

[18] Szpulak M *et al* 2005 Experimental and theoretical investigations of birefringent holey fiber with triple defect *Appl. Opt.* **44** 2652–8

Paper II.

IOP PUBLISHING MEASUREMENT SCIENCE AND TECHNOLOGY

Meas. Sci. Technol. **20** (2009) 025301 (5pp) doi:10.1088/0957-0233/20/2/025301

Wide spectral range measurement of modal birefringence in polarization-maintaining fibres

P Hlubina[1], **D Ciprian and M Kadulová**

Department of Physics, Technical University Ostrava, 17. listopadu 15, 708 33 Ostrava-Poruba, Czech Republic

E-mail: petr.hlubina@vsb.cz

Received 22 September 2008, in final form 22 October 2008
Published 17 December 2008
Online at stacks.iop.org/MST/20/025301

Abstract

We report on a substantially improved white-light spectral interferometric technique for measurement of the group and phase modal birefringence in polarization-maintaining fibres (PMFs) over a wide wavelength range (e.g. 480–1600 nm). The technique utilizes a tandem configuration of a Michelson interferometer and a PMF placed between Glan–Taylor polarizer and analyzer. Spectral signals are recorded by VIS–NIR and NIR fibre-optic spectrometers to measure the equalization wavelength as a function of the path length difference adjusted in the interferometer, or equivalently, the wavelength dependence of the group modal birefringence in the PMF. Moreover, a new procedure is used to specify the sign of the group modal birefringence. A polynomial fit is applied to the measured data to determine also the wavelength dependence of the phase modal birefringence in the PMF over a wide spectral range.

Keywords: spectral interferometry, fibre characterization, birefringent fibre, birefringence dispersion

1. Introduction

The phase and group modal birefringences and their wavelength dependences belong to the most important parameters and dispersion characteristics of polarization-maintaining fibres (PMFs). These have attracted considerable interest for a number of applications, including, e.g., polarization-sensitive optical devices and fibre-optic sensors of various physical quantities employing interferometric techniques. Several methods have been developed to measure the dispersion of birefringence in PMFs over a wide spectral range. A wavelength scanning technique can be applied to either short [1] or long fibres [2]. A standard technique of time-domain tandem interferometry [3] uses processing of either a single interferogram [4, 5] or a series of interferograms at different wavelengths [6–8] recorded in a tandem interferometer.

Recently, a white-light spectral interferometric technique employing a tandem configuration of a Michelson interferometer and an elliptical-core PMF has been used to measure the dispersion of group modal birefringence over a wide spectral range [9]. The technique utilizes a series of the recorded spectral interferograms to resolve the so-called equalization wavelength [9] at which the path length difference adjusted in the interferometer compensates the group delay between polarization modes of the fibre. Most recently, a lateral force method [10] applied in the spectral domain has been used for measuring the phase modal birefringence in an elliptical-core PMF [11]. Both techniques employed sheet polaroids as analyzer and polarizer with very bad extinction ratio in the infrared region and a fibre-optic spectrometer of limited spectral operation range (350–1000 nm).

In this paper, a substantially improved white-light spectral interferometric technique [9] is presented for measurement of the group and phase modal birefringence in PMFs over a wide spectral range (e.g. 480–1600 nm). The technique utilizes a Glan–Taylor polarizer and analyzer, and VIS–NIR

[1] Author to whom any correspondence should be addressed.

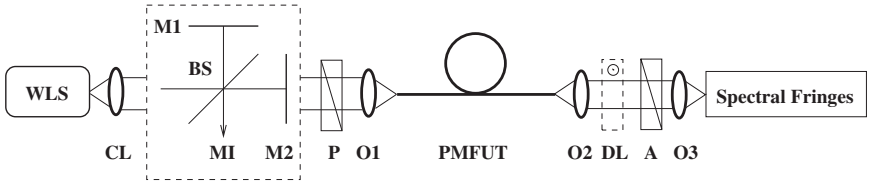

Figure 1. Experimental set-up for measuring the wavelength dependence of the group modal birefringence in a PM fibre under test.

and NIR fibre-optic spectrometers [12]. The spectral signals are recorded by the spectrometers in the transmission mode to measure precisely the equalization wavelength as a function of the path length difference adjusted in the interferometer, or equivalently, the wavelength dependence of the group modal birefringence in the PMF. The technique is used for two different fibres, including elliptical-core and holey PMFs. Moreover, a new procedure is used to specify the sign of the group modal birefringence. A polynomial fit is applied to the measured data to determine also the wavelength dependence of the phase modal birefringence in the PMF when one value is known precisely for a specific wavelength.

2. Experimental methods

Let us consider a PMF of length z supporting two polarization modes over a broad spectral range. The PMF is characterized by the wavelength-dependent differential propagation constant $\Delta\beta(\lambda) = \beta_x(\lambda) - \beta_y(\lambda)$, where $\beta_x(\lambda)$ and $\beta_y(\lambda)$ are propagation constants for the respective polarization modes. We define the beat length $L_B(\lambda)$ as

$$L_B(\lambda) = 2\pi/\Delta\beta(\lambda), \tag{1}$$

the phase modal birefringence $B(\lambda)$ as

$$B(\lambda) = \lambda/L_B(\lambda), \tag{2}$$

and the group modal birefringence $G(\lambda)$ as

$$G(\lambda) = B(\lambda) - \lambda\frac{\mathrm{d}B(\lambda)}{\mathrm{d}\lambda} = -\lambda^2\frac{\mathrm{d}\,[B(\lambda)/\lambda]}{\mathrm{d}\lambda}. \tag{3}$$

The beat length $L_B(\lambda)$ can be measured by a spectral-domain method [11] based on the application of a lateral point-like force on the fibre. The force causes strong coupling between polarization modes whose interference is resolved as the spectral fringes (channelled spectrum). In response to the displacement ΔL of the coupling point along the tested fibre, a phase shift of the channelled spectrum is observed, from which the beat length can be determined according to the relation

$$L_B(\lambda) = 2\pi\,\Delta L/\Delta\phi(\lambda), \tag{4}$$

where $\Delta\phi(\lambda)$ is the phase change reconstructed from two successive channelled spectra.

Figure 1 illustrates a simple experimental set-up based on spectral-domain tandem interferometry [9] used for measuring the wavelength dependence of the group modal birefringence $G(\lambda)$ in a PMF. Light from white-light source WLS (a 20 W quartz-tungsten-halogen lamp) passes through collimator CL and enters bulk-optic Michelson interferometer MI in which the path length difference Δ_M is adjusted with a micropositioner. The light from the output of the interferometer passes though Glan–Taylor calcite polarizer P (Thorlabs) and is focused by microscope objective O1 (15×/0.30) into the PMF under test. The PMF under test is either an elliptical-core fibre with the cutoff wavelength of 620 nm or pure silica holey PMF (PM-1550-01, Thorlabs) [13, 14]. The transmission azimuth of the polarizer is adjusted 45° with respect to the polarization axes of the PMF so that both polarization modes are excited in the tested fibre. Using another microscope objective O2 (10×/0.30) at the output of the tested fibre, a collimated light beam is generated that passes through Glan–Taylor calcite analyzer A (Thorlabs) and is focused by the next objective O3 (10×/0.30) into the read fibre of a spectrometer (S2000, NIR-512, Ocean Optics) which resolves the interference of polarization modes as a spectral signal. The transmission azimuth of the analyzer is adjusted at 45° with respect to the polarization axes of the PMF. The spectral signal is recorded by the spectrometer in the transmission mode after a dark spectrum and a reference one (without the interference) is stored.

The spectrometers S2000 and NIR-516 [12] have a spectral operation ranging from 350 to 1000 nm and from 850 to 1700 nm, respectively. For both spectrometers we used the read optical fibre with a 50 μm core diameter which results in a Gaussian response function. If the PMF is with $G(\lambda)z \gg 0$ and the path length difference adjusted in the Michelson interferometer is similarly $\Delta_M \gg 0$, the spectral signal recoded in the set-up by a spectrometer can be represented in the form [9]

$$S(\lambda) = 1 + 0.5V(\lambda)\exp\{-(\pi^2/2)[(G(\lambda)z - \Delta_M)\Delta\lambda_R/\lambda^2]^2\} \times \cos[(2\pi/\lambda)(B(\lambda)z - \Delta_M)], \tag{5}$$

where $V(\lambda)$ is a visibility term, and λ_R is the width of the spectrometer response function.

To resolve the spectral interference fringes in the vicinity of the so-called equalization wavelength λ_0 [9], the path length difference governed by the relation $\Delta_M = G(\lambda_0)z$ needs to be adjusted in the Michelson interferometer. Thus, the path length difference Δ_M adjusted in the interferometer and measured as a function of the equalization wavelength λ_0 gives directly the spectral dependence of the group modal birefringence $G(\lambda_0) = \Delta_M/z$ in the PMF under test. Because the group modal birefringence $G(\lambda)$ is related to the phase modal birefringence $B(\lambda)$ via equation (3), we can obtain the relative wavelength dependence of the phase modal birefringence. It can be combined with the known value at one specific wavelength to obtain absolute values of the wavelength dependence of the phase modal birefringence $B(\lambda)$ [11].

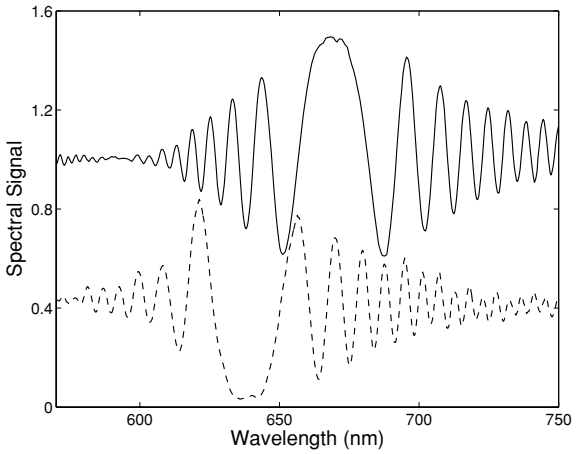

Figure 2. Two spectral signals recorded for $\Delta_M = 952$ μm without (solid) and with the effect of a delay line (dashed).

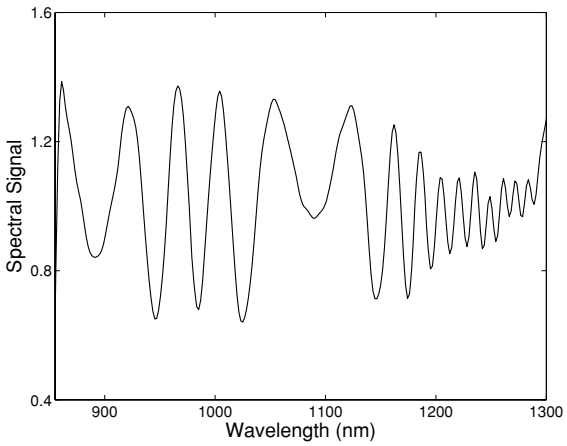

Figure 3. Spectral signal recorded for $\Delta_M = 1172$ μm.

3. Experimental results and discussion

After optimizing excitation and detection conditions to assure the highest visibility of spectral interference fringes, the spectral signals were recorded for the path length differences Δ_M adjusted in the Michelson interferometer with a step of 10 μm. We revealed for the elliptical-core fibre having length $z = 7.460$ m that the equalization wavelengths increase approximately from 555 to 910 nm with Δ_M increasing from 812 to 1182 μm. An example of the spectral signal recorded by the first spectrometer for the adjusted $\Delta_M = 952$ μm is shown in figure 2 by the solid curve. We can clearly resolve the spectral interference fringes in the vicinity of the equalization wavelength $\lambda_0 = 669.08$ nm to which $G(\lambda_0) = 1.28 \times 10^{-4}$ corresponds. The positive sign of the group modal birefringence was also determined in the set-up shown in figure 1. We placed a delay line (see DL in figure 1), represented by the quartz crystal of suitable thickness and orientation, in tandem with the PMF under test and used a procedure similar to that presented in [8]. If the extraordinary axis of the crystal, which has the positive group birefringence ($N_e > N_o$), is parallel to the major axis of the fibre elliptical core (along the X polarization mode), the group birefringence of the fibre is positive or negative, if the equalization wavelength shifts to shorter or longer wavelengths. Figure 2 shows by the dashed curve the effect of the quartz crystal having a thickness of 4 mm and it demonstrates that the group modal birefringence of the elliptical-core fibre is positive. Moreover, figure 3 shows an example of the spectral signal recorded by the second spectrometer for $\Delta_M = 1172$ μm. We can clearly resolve the spectral interference fringes in the vicinities of two different equalization wavelengths $\lambda_{01} = 891.93$ and $\lambda_{02} = 1090.92$ nm to which $G(\lambda_{01}) = G(\lambda_{02}) = 1.57 \times 10^{-4}$ corresponds. This is due to the maximum in $G(\lambda)$ located between λ_{01} and λ_{02} as is demonstrated in figure 4 which shows by the full and open circles the measured group modal birefringence $G(\lambda_0)$ in the elliptical-core optical fibre

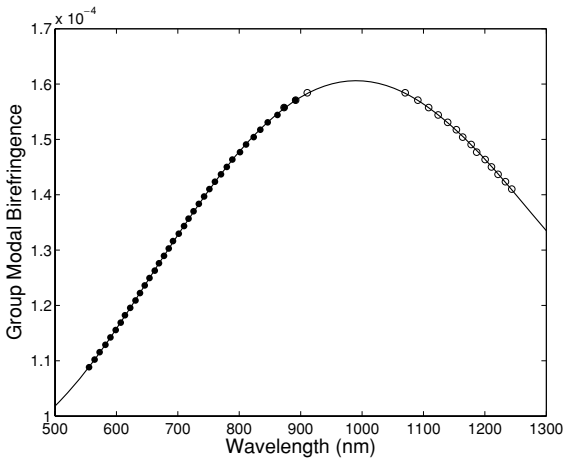

Figure 4. Group modal birefringence measured as a function of wavelength for the elliptical-core PMF (solid curve corresponds to a polynomial fit).

determined for respective equalization wavelengths λ_0. The full circles correspond to the values obtained by the first spectrometer whereas the open ones were obtained by the second spectrometer. The solid line in the same figure represents the group modal birefringence $G(\lambda)$ obtained from the values $-G(\lambda_0)/\lambda_0^2$ fitted to a fourth-order polynomial. The polynomial order is sufficiently high because the fit is characterized by a correlation factor as high as 0.99998.

The fit is used to determine the corresponding phase modal birefringence $B(\lambda)$ versus wavelength λ, with $B(\lambda)/\lambda$ represented by a fifth-order polynomial, shown in figure 5. It was obtained by combining the relative phase modal birefringence with one value $B = 8.55 \times 10^{-5}$ measured at a wavelength of 637.08 nm. This value was obtained by using equations (2) and (4) for the displacement $\Delta L = 7450$ μm of the coupling point when the phase change $\Delta\phi(\lambda) \approx 2\pi$ [11]. It should be noted here that the phase modal birefringence

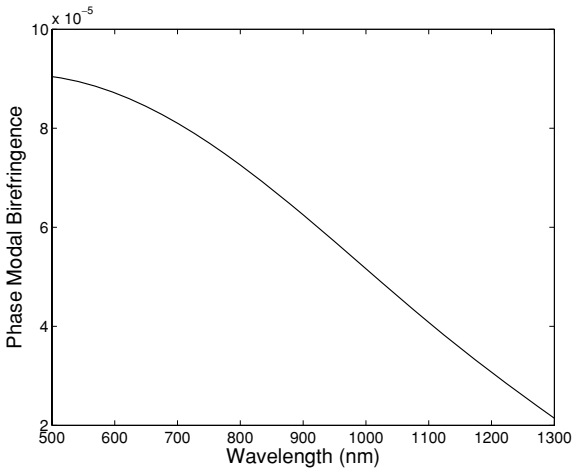

Figure 5. Phase modal birefringence as a function of wavelength for the elliptical-core PMF.

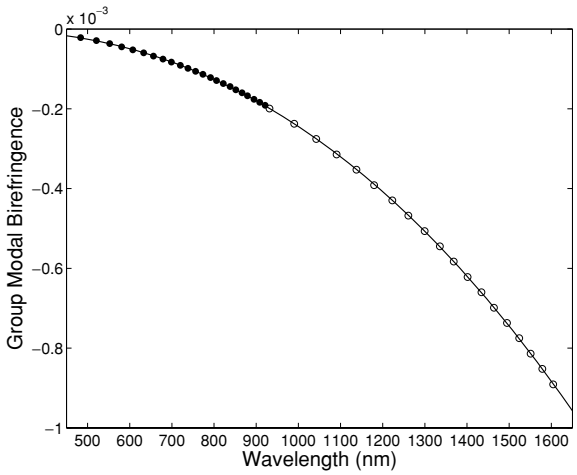

Figure 6. Group modal birefringence measured as a function of wavelength for the holey PMF (solid curve corresponds to a polynomial fit).

decreases with increasing wavelength and that its positive sign is the same as the sign of the group modal birefringence.

We can estimate the precision of the group modal birefringence measurement. If the equalization wavelength is determined with an error of $\delta(\lambda_0)$, the path length difference Δ_M adjusted in the interferometer is known with a precision of $\delta(\Delta_M)$ and the length of the PM fibre is known with a precision of $\delta(z)$, the group modal birefringence G is obtained with a precision given by the following formula:

$$\frac{\delta(G)}{G} = \sqrt{\left[\frac{1}{G}\frac{\mathrm{d}G(\lambda_0)}{\mathrm{d}\lambda_0}\delta(\lambda_0)\right]^2 + \left[\frac{\delta(\Delta_M)}{\Delta_M}\right]^2 + \left[\frac{\delta(z)}{z}\right]^2}. \quad (6)$$

In our case, the error $\delta(\lambda_0)$ is 0.3 nm or 1.8 nm and it corresponds to the wavelength difference of adjacent pixels of the detector of the first or second spectrometer, the precision $\delta(\Delta_M)$ is 1 μm and the precision $\delta(z)$ is 1 mm so that the precision $\delta(G)$ in obtaining the group modal birefringence is better than 0.1%.

Next, we measured the group modal birefringence for the holey fibre [13, 14] having the length $z = 2.603$ m when the spectral signals were recorded for the path length differences Δ_M adjusted in the Michelson interferometer with a step of 20 μm or 100 μm. We revealed that the equalization wavelengths increase approximately from 480 to 1600 nm with Δ_M increasing from 56 to 2318 μm. Figure 6 shows by the full and open circles the measured group modal birefringence $G(\lambda_0)$ in the holey fibre determined for respective equalization wavelengths λ_0. The solid line in the same figure represents the group modal birefringence $G(\lambda)$ obtained from the values $-G(\lambda_0)/\lambda_0^2$ fitted to a fourth-order polynomial. The fit is used to determine the corresponding phase modal birefringence $B(\lambda)$ versus wavelength λ, with $B(\lambda)/\lambda$ represented by a fifth-order polynomial, shown in figure 7. It was obtained by combining the relative phase modal birefringence with one value $B = 3.84 \times 10^{-5}$ measured at a wavelength of 632.8 nm [13] by a lateral force method applied in the time domain [6]. The phase modal birefringence increases with increasing wavelength but its sign is opposite to the sign of the group modal birefringence.

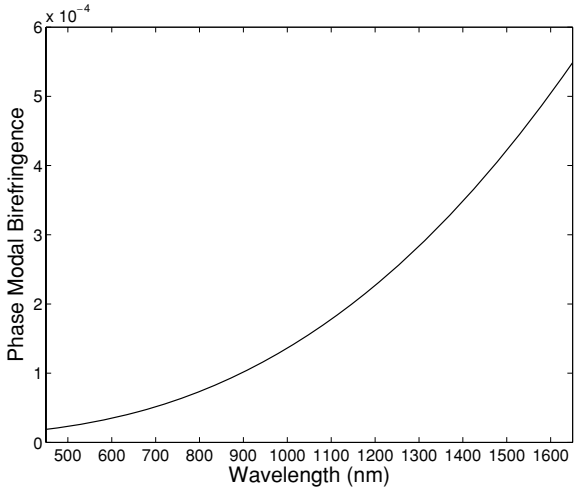

Figure 7. Phase modal birefringence as a function of wavelength for the holey PMF.

4. Conclusions

We used the substantially improved white-light spectral interferometric technique to measure the wavelength dependence of the phase and group modal birefringence in PMFs over a wide spectral range (e.g. 480–1600 nm). The technique utilized a tandem configuration of a Michelson interferometer and a PMF placed between Glan–Taylor polarizer and analyzer, and VIS–NIR and NIR fibre-optic spectrometers to increase the spectral range of the measurements. A new recording mode of the spectrometers (the transmission mode) was used to record the spectral

signals and to measure precisely the equalization wavelength as a function of the path length difference adjusted in the interferometer, or equivalently, the wavelength dependence of the group modal birefringence in the PMF. Moreover, a new procedure was used to specify the sign of the group modal birefringence. We applied a polynomial fit to the measured data to obtain also the wavelength dependence of the phase modal birefringence when one value was known precisely for a specific wavelength. We demonstrated the applicability of the white-light spectral interferometric technique for dispersion characterizing of two different fibres (elliptical-core and holey PMFs) over a wide spectral range.

The described method offers high measurement precision of 0.1% achieved with simple and cost-effective instrumentation. It allows for simultaneous measurements of the group and phase modal birefringence that can be extended for dispersion characterizing of other fibres guiding two polarization modes over a wide spectral range (Panda and bow-tie fibres, PCFs).

Acknowledgments

The research was partially supported by the Grant Agency of the Czech Republic (project no 102/06/0284), by grant MSM6198910016 and by the COST Action 299.

References

[1] Rashleigh S C 1982 Wavelength dependence of birefringence in highly birefringent fibres *Opt. Lett.* **7** 294–6
[2] Shlyagin M G, Khomenko A V and Tentori D 1995 Birefringence dispersion measurement in optical fibres by wavelength scanning *Opt. Lett.* **20** 869–71
[3] Rao Y J and Jackson D A 1996 Recent progress in fibre optic low-coherence interferometry *Meas. Sci. Technol.* **7** 981–99
[4] Flavin D A, McBride R and Jones J D C 2002 Dispersion of birefringence and differential group delay in polarizarion maintaining fibres *Opt. Lett.* **27** 1010–2
[5] Tang F, Wang X Z, Zhang Y and Jing W 2006 Distributed measurement of birefringence dispersion in polarization-maintaining fibres *Opt. Lett.* **31** 3411–3
[6] Bock W J and Urbańczyk W 1993 Measurement of polarization mode dispersion and modal birefringence in highly birefringent fibres by means of electronically scanned shearing-type interferometry *Appl. Opt.* **32** 5841–8
[7] Urbańczyk W, Martynkien T and Bock W J 2001 Dispersion effects in elliptical-core highly birefringent fibres *Appl. Opt.* **40** 1911–20
[8] Statkiewicz G, Martynkien T and Urbańczyk W 2004 Measurements of modal birefringence and polarimetric sensitivity of the birefringent holey fibre to hydrostatic pressure and strain *Opt. Commun.* **241** 339–48
[9] Hlubina P, Martynkien T and Urbańczyk W 2003 Dispersion of group and phase modal birefringence in elliptical-core fibre measured by white-light spectral interferometry *Opt. Express* **11** 2793–8
[10] Takada K, Noda J and Ulrich R 1985 Precision measurement of modal birefringence of highly birefringent fibres by periodic lateral force *Appl. Opt.* **24** 4387–91
[11] Hlubina P and Ciprian D 2007 Spectral-domain measurement of phase modal birefringence in polarization-maintaining fibre *Opt. Express* **15** 17019–24
[12] Ocean Optics Inc. 2007 Spectrometers *Catalog 07* 11–32
[13] Hlubina P, Szpulak M, Knyblová L, Statkiewicz G, Martynkien T, Ciprian D and Urbańczyk W 2006 Measurement and modelling of dispersion characteristics of two-mode birefringent holey fibre *Meas. Sci. Technol.* **17** 626–30
[14] Hlubina P, Szpulak M, Ciprian D, Martynkien T and Urbańczyk W 2007 Measurement of the group dispersion of the fundamental mode of holey fibre by white-light spectral interferometry *Opt. Express* **15** 11073–81

Paper III.

IOP Publishing Measurement Science and Technology
Meas. Sci. Technol. **18** (2007) 1547–1552 doi:10.1088/0957-0233/18/5/046

Differential group refractive index dispersion of glasses of optical fibres measured by a white-light spectral interferometric technique

Petr Hlubina, Radek Chlebus and Dalibor Ciprian

Department of Physics, Technical University Ostrava, 17. listopadu 15, 708 33 Ostrava-Poruba, Czech Republic

E-mail: petr.hlubina@vsb.cz

Received 22 January 2007, in final form 9 February 2007
Published 27 March 2007
Online at stacks.iop.org/MST/18/1547

Abstract
We report on a white-light interferometric technique employing a low-resolution spectrometer to measure the differential group refractive index of glasses of optical fibres over a wide wavelength range. The technique utilizes an unbalanced Mach–Zehnder interferometer with a fibre under test of known length inserted in one of the interferometer arms and the other arm with adjustable path length. We record a series of spectral interferograms to measure the equalization wavelength as a function of the path length difference, or equivalently the group dispersion. Subtracting the group dispersion of the optical components present in the interferometer along with the fibre, we measure the wavelength dependence of differential group refractive index for pure silica and SK222 glasses. We confirm that the differential group dispersion measured for pure silica glass agrees well with that described by the dispersion equation.

Keywords: spectral interferometry, white-light source, low-resolution spectrometer, Mach–Zehnder interferometer, group refractive index, dispersion, pure silica glass, SK222 glass

1. Introduction

A precise measurement of the group dispersion of optical components over a broad spectral range is important in various research areas including applications of femtosecond lasers, material characterization and broadband optical communications. White-light interferometry based on the use of a broadband source in combination with a standard Michelson or a Mach–Zehnder interferometer is considered as one of the best tools for dispersion characterization of optical guiding media such as optical fibres.

White-light interferometry usually utilizes a temporal method or a spectral method. The temporal method involves measurement of the time of flight of optical pulses through a sample. A method for measuring the group delay introduced by an optical material consists in placing the sample in one of the interferometer arms and evaluating the temporal shift of the peak of the cross-correlation interferogram. As the central wavelength is varied, the relative group delay of the different frequency components is observed directly [1]. Alternatively, the spectral phase over the full bandwidth of the white-light source can be obtained in a single measurement by a Fourier transform of the cross-correlation interferogram [2–5]. The group dispersion of the sample under study can be obtained by simply differentiating the measured spectral phase.

The spectral method is based on the observation of spectrally resolved interference fringes (channelled spectrum) in the vicinity [6, 7] of a stationary-phase point or far from it [8–11] and involves measurement of the phase or period of the spectral fringes. The group dispersion of the sample under study can be obtained by simply differentiating the spectral phase retrieved from a single interferogram. The

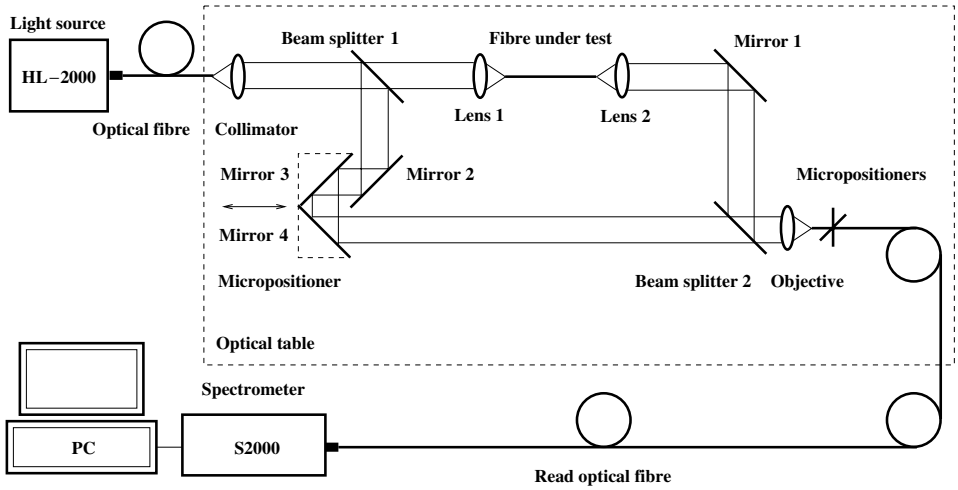

Figure 1. Experimental set-up with an unbalanced Mach–Zehnder interferometer to measure the differential group refractive index dispersion of glasses of optical fibres.

stationary-phase point [6] appears in the recorded spectral interferogram when the group optical path difference (OPD) between two beams in the interferometer is close to zero. The main limitation of the method is reached for thick or strongly dispersive materials because under such conditions the spectral interference fringes that are far from the stationary-phase point become difficult to resolve. Using a low-resolution spectrometer [12], the measurement of the group refractive index dispersion of a given material is still possible in the vicinity of the stationary-phase point if one moves it in successive steps to different wavelengths and repeats the measurement. We measured in this way the dispersion of differential group refractive index of a pure silica beam splitter present in a Michelson interferometer [12]. The modification of the technique with a tandem configuration of a Michelson interferometer and an optical fibre has been used in measurement of the group dispersion in standard [13] and birefringent [14, 15] fibres of a known length. Recently, the use of the method with a Mach–Zehnder interferometer was extended to two-dimensional spectral interferometry [16] or for dispersion characterization of tapered fibres [17].

The aim of this paper is to present a white-light interferometric technique employing a low-resolution spectrometer for measurement of the differential group refractive index of glasses of optical fibres over a wide wavelength range. The technique utilizes an unbalanced Mach–Zehnder interferometer with a fibre under test of known length inserted in one of the interferometer arms and the other arm with adjustable path length. We record a series of spectral interferograms to measure the equalization wavelength as a function of the path length difference, or equivalently the group dispersion over the wavelength range approximately from 500 to 910 nm. Subtracting the group dispersion of a microscope objective in front and a lens behind the fibre present in the interferometer, we measure the wavelength dependence of the differential group refractive index for pure silica and SK222 glasses with a precision of 2×10^{-5}. The group dispersion measured for pure silica glass agrees well with that described by the dispersion equation.

2. Experimental method

First, let us consider an unbalanced Mach–Zehnder interferometer (see figure 1) with a fibre under test of length z and refractive index $n(\lambda)$ and optical components (lens 1 and lens 2) to which the effective thickness d and refractive index $n_c(\lambda)$ correspond. The fibre is inserted into the first (test) arm of the interferometer and the other (reference) arm has adjustable path length L in air so that the group OPD $\Delta^{\mathrm{g}}_{\mathrm{MZ}}(\lambda)$ between the beams in the interferometer is given by

$$\Delta^{\mathrm{g}}_{\mathrm{MZ}}(\lambda) = L - l - N(\lambda)z - N_c(\lambda)d, \tag{1}$$

where l is the path length in the air in the test arm and $N(\lambda)$ and $N_c(\lambda)$ are the group refractive indices satisfying the relation

$$N(\lambda) = n(\lambda) - \lambda \frac{\mathrm{d}n(\lambda)}{\mathrm{d}\lambda}. \tag{2}$$

Let us consider now that the spectral interference fringes recorded in the set-up have the largest period in the vicinity of a stationary-phase point for which the group OPD is zero at one specific wavelength λ_0, referred to as the equalization wavelength [12]. The condition $\Delta^{\mathrm{g}}_{\mathrm{MZ}}(\lambda_0) = 0$ gives for the overall path length $L = L_o = L_o(\lambda_0)$ for which the equalization wavelength λ_0 is resolved in the recorded spectrum the relation

$$L_o(\lambda_0) = N(\lambda_0)z + N_c(\lambda_0)d + l. \tag{3}$$

If we choose one of the equalization wavelengths, λ_{0r}, as the reference one, we can introduce the overall path length difference $\Delta L_o(\lambda_0) = L_o(\lambda_0) - L_o(\lambda_{0r})$ given by

$$\Delta L_o(\lambda_0) = \Delta N(\lambda_0)z + \Delta N_c(\lambda_0)d, \tag{4}$$

where $\Delta N(\lambda_0) = N(\lambda_0) - N(\lambda_{0r})$ and $\Delta N_c(\lambda_0) = N_c(\lambda_0) - N_c(\lambda_{0r})$ are the corresponding differential group refractive indices.

Second, let us consider the unbalanced Mach–Zehnder interferometer in which the fibre is removed and which is used for measuring the group dispersion of the optical components. This group dispersion has to be subtracted from the overall group dispersion to determine the group dispersion of the fibre alone. The corresponding path length difference is denoted as $\Delta L_c(\lambda_0) = L_c(\lambda_0) - L_c(\lambda_{0r})$ and is given by

$$\Delta L_c(\lambda_0) = \Delta N_c(\lambda_0) d. \tag{5}$$

Using equations (4) and (5), we obtain the relation

$$\Delta N(\lambda_0) = [\Delta L_o(\lambda_0) - \Delta L_c(\lambda_0)]/z, \tag{6}$$

which means that the differential group refractive index $\Delta N(\lambda_0)$ of the fibre can be measured directly as a function of the equalization wavelength λ_0 if the fibre length z is known.

3. Experimental set-up

The experimental set-up used in the application of spectral-domain white-light interferometry for measuring the differential group refractive index dispersion of glasses of optical fibres is shown in figure 1. It consists of a white-light source: a quartz–tungsten–halogen lamp (HL-2000HP, Ocean Optics, Inc.) with launching optics, optical fibre of cut-off wavelength as short as possible, a collimating lens, a bulk-optic Mach–Zehnder interferometer with plate beam splitters (BSW07, Thorlabs), a micropositioner connected to mirrors 3 and 4 of the interferometer, a microscope objective, micropositioners, a fibre-optic spectrometer (S2000, Ocean Optics, Inc.), an A/D converter and a personal computer. The spectrometer resolution is given by a 50 μm core diameter of the read optical fibre to which a Gaussian response function with the width of about 3 nm corresponds [18].

In the test arm of the interferometer is inserted a combination of components (shown schematically in figure 1 as lens 1, fibre under test and lens 2) represented by a microscope objective (10×/0.30, Meopta), a fibre sample and an achromatic lens (74-ACR, Ocean Optics, Inc.). We measured two different fibre samples. The first sample is pure silica holey fibre (PM-1550-01, Thorlabs) of length $z = 50\,650$ μm and the second sample is a holey fibre of length $z = 54\,200$ μm made of SK222 optical glass [19]. The fibre lengths were measured by a micrometer with an accuracy of ± 10 μm.

4. Experimental results and discussion

First, the overall group dispersion of a combination of the first fibre sample and optical components was measured in the set-up shown in figure 1. Prior to the measurement we utilized the main advantage of the set-up, which is in fibre connection of a light source (that can be varied) with the interferometer. We used a laser diode instead of the halogen lamp to check the precise placement and alignment of the optical components in the test arm by observing the interference fringes. The ring-shape optical field was revealed at the output of the test arm indicating that the light was guided by the outer cladding of the fibre [15]. It should also be noted here that the alignment of the components is much simpler in the interferometer with a single pass of light through the test arm than in a Michelson interferometer with two passes [20].

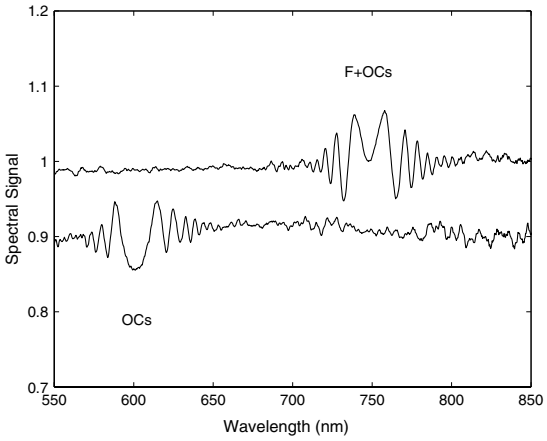

Figure 2. Examples of the spectral signals recorded for two cases: pure silica fibre plus optical components (F+OCs) and optical components (OCs).

In the dispersion measurement, such a path length in the reference arm of the interferometer was adjusted to resolve spectral interference fringes. Figure 2 shows an example of the recorded normalized spectral signal (denoted as F+OCs) obtained by subtracting the reference signal (without the interference) from the interferogram. It clearly shows the effect of the limiting resolving power of the spectrometer on the visibility of the spectral interference fringes identified only in the vicinity of the equalization wavelength $\lambda_0 = 748.23$ nm, which was chosen as the reference one λ_{0r}. The equalization wavelength was determined with an error of 0.32 nm corresponding to the wavelength difference for adjacent pixels of the spectrometer linear CCD-array detector [18].

Second, the group dispersion of the optical components for which the equalization wavelength cannot be resolved with the unbalanced Mach–Zehnder interferometer was measured by a method of tandem interferometry [14]. The method utilizes a Michelson interferometer placed in between the source and the unbalanced Mach–Zehnder interferometer and the adjustment of such an OPD in the Michelson interferometer to resolve the spectral interference fringes at the output of the Mach–Zehnder interferometer. We checked the precise placement and alignment of the microscope objective and the achromatic lens in the test arm by observing the interference fringes when a laser diode was used instead of the halogen lamp. Figure 2 shows an example of the recorded spectral signal (denoted as OCs) with the spectral interference fringes identified only in the vicinity of the equalization wavelength $\lambda_0 = 601.35$ nm.

We measured the dependence of the adjusted path length difference on the equalization wavelength for both cases. We displaced the stage with mirrors 3 and 4 manually by using the micropositioner with a constant step of 10 μm and performed recording of the corresponding spectral signals. The spectral signals recorded for the first case revealed that the equalization wavelength λ_0 can be resolved in the spectral range from 508 to 910 nm and that the path length difference ΔL_o varies from 1480 to -340 μm. The measured values are shown in figure 3

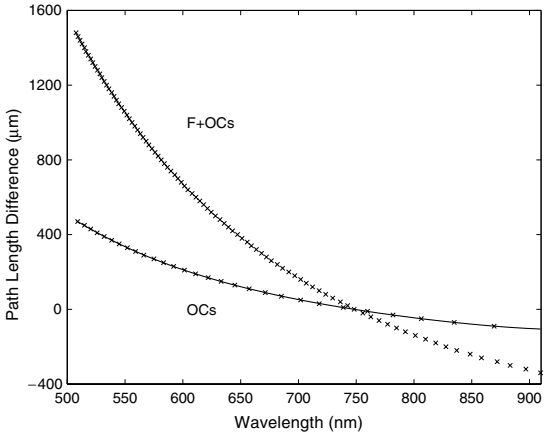

Figure 3. Path length difference measured as a function of wavelength for two cases: pure silica fibre plus optical components (F+OCs) and optical components (OCs). The solid line is a polynomial fit.

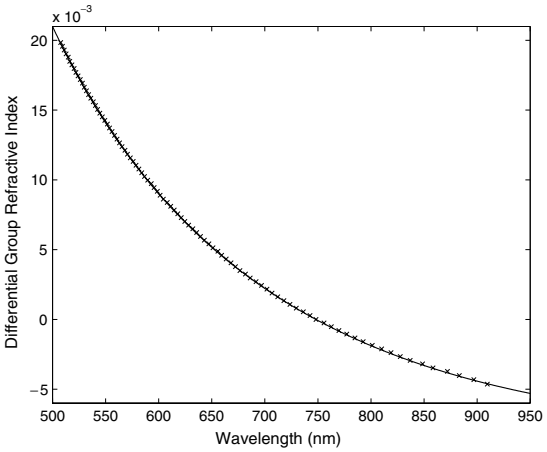

Figure 4. Differential group refractive index of pure silica measured as a function of wavelength. The solid line corresponds to theory.

by the crosses. Similarly, the spectral signals recorded for the second case revealed that the equalization wavelength λ_0 can be resolved in the spectral range from 509 to 869 nm and that the path length difference ΔL_c varies from 470 to -90 μm. The measured values are shown in figure 3 by the crosses together with the polynomial fit. Knowledge of the measured dependences and the fibre length z of the first sample enables us to evaluate directly the differential group refractive index $\Delta N(\lambda_0)$ as a function of the equalization wavelength λ_0. The function is represented in figure 4 by the crosses, and it is shown together with the theoretical function resulting from the Sellmeier formula for pure silica [12]. This figure confirms very good agreement between theory and experiment.

We can estimate the precision of the differential group refractive index measurement. If the path length difference $\Delta L = \Delta L_o - \Delta L_c$ is adjusted with a precision of $\delta(\Delta L)$ and the length z of the fibre is known with a precision of $\delta(z)$,

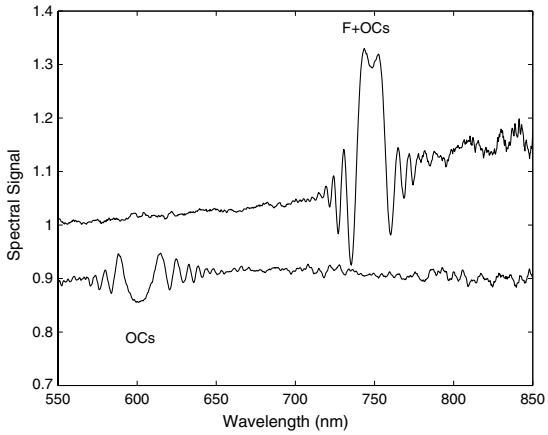

Figure 5. Examples of the spectral signals recorded for two cases: fibre made of SK222 glass plus optical components (F+OCs) and optical components (OCs).

the differential group refractive index ΔN is obtained with a precision given by the following formula:

$$\delta(\Delta N) = \sqrt{\left[\frac{\delta(\Delta L)}{z}\right]^2 + \left[\Delta L \frac{\delta(z)}{z^2}\right]^2}. \tag{7}$$

In our case, the precision $\delta(\Delta L)$ is 1 μm and the precision $\delta(z)$ is 10 μm so that the precision $\delta(\Delta N)$ in determining the differential group refractive index is 2×10^{-5}. Higher measurement precision can be achieved, for example, using a longer fibre. However, there exists a maximum length of the fibre given by the limited resolving power of the spectrometer.

Finally we measured the group dispersion of the second fibre sample made of SK222 glass, which is a multicomponent glass that exhibits a higher nonlinearity (up to a factor of 2) than pure silica [19]. Figure 5 shows an example of the recorded spectral signal (denoted as F+OCs) with the spectral interference fringes identified only in the vicinity of the equalization wavelength $\lambda_0 = 747.91$ nm, chosen as the reference one λ_{0r}. Figure 5 also shows an example of the spectral signal (denoted as OCs) recorded for optical components. The dependence of the overall path length difference on the equalization wavelength was once again measured when the stage with mirrors 3 and 4 was displaced manually by using the micropositioner with a constant step of 10 μm. The spectral signals recorded revealed that the equalization wavelength λ_0 can be resolved in the spectral range from 497 to 907 nm and that the path length difference ΔL_o varies from 2160 to -480 μm. The measured values are shown in figure 6 by the crosses and in comparison with the values from figure 3 are greater. In the same figure are shown the measured values regarding the group dispersion of the microscope objective and the achromatic lens. They are represented by the crosses and are shown together with the polynomial fit. Knowledge of the measured dependences and the fibre length z of the second sample enables us to evaluate directly the wavelength dependence of the differential group refractive index $\Delta N(\lambda_0)$. The function is represented in figure 7 by the crosses, and it is shown together with a

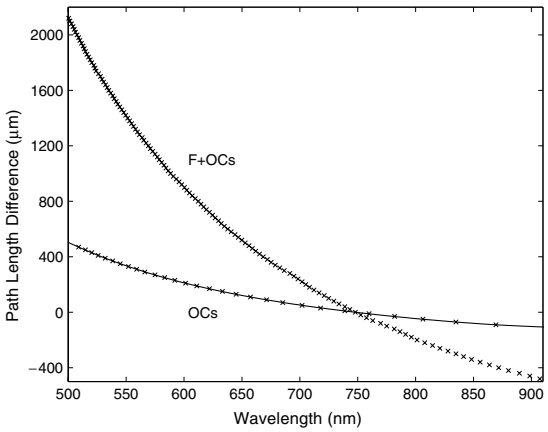

Figure 6. Path length difference measured as a function of wavelength for two cases: fibre made of SK222 glass plus optical components (F+OCs) and optical components (OCs). The solid line is a polynomial fit.

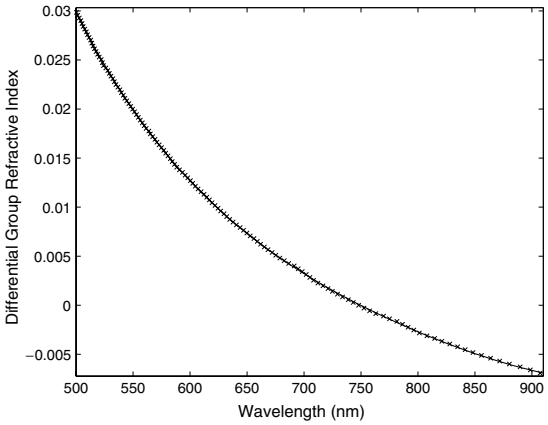

Figure 7. Differential group refractive index of SK222 glass measured as a function of wavelength. The solid line is a polynomial fit.

polynomial fit. The differential group refractive index ΔN of SK222 glass is obtained with a precision of 2×10^{-5}.

5. Conclusions

We used a white-light interferometric technique employing a low-resolution spectrometer for measurement of the differential group refractive index of glasses of optical fibres over a wide spectral range (500 to 910 nm). The technique utilized an unbalanced Mach–Zehnder interferometer with a fibre under test of known length inserted in one of the interferometer arms and the other arm with adjustable path length. From a series of recorded spectral signals we measured the equalization wavelength as a function of the path length difference, or equivalently the group dispersion. Subtracting the group dispersion of a microscope objective in front and a lens behind the fibre present in the interferometer arm, we measured the wavelength dependence of the differential group refractive index for pure silica and SK222 glasses with a precision of 2×10^{-5}. We confirmed that the differential group dispersion measured for pure silica glass agrees well with that described by the dispersion equation.

The use of the method, whose main advantage is in easy inspection of the optical field at the output of the test arm, can be extended for measuring the group dispersion of core or cladding parts of fibres composed of different glasses. Moreover, suitable excitation of an optical fibre, for example by means of a supercontinuum source [20], will enable measurement of the group dispersion for modes guided by the fibre. Experimental results regarding the group dispersion of both the glass and guided modes of the optical fibre are crucial for comparison with theoretical results in order to verify the reliability of numerical modelling.

Acknowledgments

The research was partially supported by the Grant Agency of the Czech Republic (project no 102/06/0284), MSM6198910016, MŠMT grant (OC142) within the COST Action P11 and internal grant of TU Ostrava (IGS HGF VŠ B-TUO).

References

[1] Knox W H, Pearson N M, Li K D and Hirlimann C A 1988 Interferometric measurements of femtosecond group delay in optical components *Opt. Lett.* **13** 574–6
[2] Beck M and Walmsley I A 1990 Measurement of group delay with high temporal and spectral resolution *Opt. Lett.* **15** 492–4
[3] Naganuma K, Mogi K and Yamada 1990 Group-delay measurements using the Fourier transform of an interferometric cross correlation generated by white light *Opt. Lett.* **15** 393–5
[4] Diddams S and Diels J C 1996 Dispersion measurements with white-light interferometry *J. Opt. Soc. Am.* B **13** 1120–8
[5] Galli M, Marabelli F and Gizzetti G 2003 Direct measurement of refractive-index dispersion of transparent media by white-light interferometry *Appl. Opt.* **42** 3910–4
[6] Sáinz C, Jourdain P, Escalona R and Calatroni J 1994 Real time interferometric measurements of dispersion curves *Opt. Commun.* **110** 381–90
[7] Kumar V N and Rao D N 1995 Using interference in the frequency domain for precise determination of the thickness and refractive indices of normal dispersive materials *J. Opt. Soc. Am.* B **55** 1559–63
[8] Liang Y and Grover C H 1998 Modified white-light Mach–Zehnder interferometer for direct group-delay measurements *Appl. Opt.* **37** 4105–11
[9] El-Zaiat S Y 2004 Group refractive index measurements by fringes of equal chromatic order *Opt. Laser Technol.* **37** 181–6
[10] Lee J Y and Kim D Y 2006 Versatile chromatic dispersion measurement of a single mode fiber using spectral white light interferometry *Opt. Express* **14** 11608–15
[11] Reolon D, Jacquot M, Verrier I, Brun G and Veillas C 2006 High resolution group refractive index measurement by broadband supercontinuum interferometry and wavelet-transform analysis *Opt. Express* **14** 12744–50
[12] Hlubina P 2001 White-light spectral interferometry with the uncompensated Michelson interferometer and the group refractive index dispersion in fused silica *Opt. Commun.* **193** 1–7

[13] Hlubina P, Martynkien T and Urbańczyk W 2003 Measurements of intermodal dispersion in few-mode optical fibres using a spectral-domain white-light interferometric method *Meas. Sci. Technol.* **14** 784–9
[14] Hlubina P, Martynkien T and Urbańczyk W 2003 Dispersion of group and phase modal birefringence in elliptical-core fiber measured by white-light spectral interferometry *Opt. Express* **11** 2793–8
[15] Hlubina P, Szpulak M, Knyblová L, Statkiewicz G, Martynkien T, Ciprian D and Urbańczyk W 2006 Measurement and modelling of dispersion characteristics of two-mode birefringent holey fibre *Meas. Sci. Technol.* **17** 626–30
[16] Kovács A P, Osvay K, Kurdi G, Gobre M, Klebniczki J and Bor Z 2005 Dispersion control of a pulse stretcher–compressor system with two-dimensional spectral interferometry *Appl. Phys.* B **80** 165–70
[17] Lu P, Ding H and Mihailov S J 2005 Direct measurement of the zero-dispersion wavelength of tapered fibres using broadband-light interferometry *Meas. Sci. Technol.* **16** 1631–6
[18] Hlubina P, Gurov I and Chugunov V 2003 White-light spectral interferometric technique to measure the wavelength dependence of the spectral bandpass of a fibre-optic spectrometer *J. Mod. Opt.* **50** 2067–74
[19] Mitrofanov A V, Linik Y M, Buczynski R, Pysz D, Lorenc D, Bugar I, Ivanov A A, Alfimov M V, Fedotov A B and Zheltikov A M 2006 Highly birefringent silicate glass photonic-crystal fiber with polarization-controlled frequency shifted output: a promising fiber light source for nonlinear Raman microspectroscopy *Opt. Express* **14** 10645–51
[20] Labonté L, Roy P, Pagnoux F, Louradour F, Restoin C, Mélin G and Burov E 2006 Experimental and numerical analysis of the chromatic dispersion dependence upon the actual profile of small core microstructured fibres *J. Opt. A: Pure Appl. Opt.* **8** 933–8

Paper IV.

Measurement of the group dispersion of the fundamental mode of holey fiber by white-light spectral interferometry

P. Hlubina[1], M. Szpulak[2], D. Ciprian[1], T. Martynkien[2], and W. Urbańczyk[2]

[1]*Department of Physics, Technical University Ostrava, 17. listopadu 15, 708 33 Ostrava-Poruba, Czech Republic*
petr.hlubina@vsb.cz

[2]*Institute of Physics, Wroclaw University of Technology, Wybrzeże Wyspiańskiego 27, 50-370 Wroclaw, Poland*
marcin.szpulak@pwr.wroc.pl

Abstract: We present a new method for measuring the group dispersion of the fundamental mode of a holey fiber over a wide wavelength range by white-light interferometry employing a low-resolution spectrometer. The method utilizes an unbalanced Mach-Zehnder interferometer with a fiber under test placed in one arm and the other arm with adjustable path length. A series of spectral signals are recorded to measure the equalization wavelength as a function of the path length, or equivalently the group dispersion. We reveal that some of the spectral signals are due to the fundamental mode supported by the fiber and some are due to light guided by the outer cladding of the fiber. Knowing the group dispersion of the cladding made of pure silica, we measure the wavelength dependence of the group effective index of the fundamental mode of the holey fiber. Furthermore, using a full-vector finite element method, we model the group dispersion and demonstrate good agreement between experiment and theory.

OCIS codes: (060.2270) Fiber characterization; (060.2300) Fiber measurements; (120.3180) Interferometry; (999.999) Photonic crystal fiber;

References and links

1. L.G. Cohen, "Comparison of single-mode fiber dispersion measurement techniques," J. Lightwave Technol. **3**, 958–966 (1985).
2. S. Diddams and J.C. Diels, "Dispersion measurements with white-light interferometry," J. Opt. Soc. Am. B **13**, 1120–1128 (1995).
3. M. Tateda, N. Shibata, and S. Seikai, "Interferometric method for chromatic dispersion measurement in a single-mode optical fiber," IEEE J. Quantum Electron. **17**, 404–407 (1981).
4. M.J. Saunders and W.B. Gardner, "Interferometric determination of dispersion variations in single-mode fibers," J. Lightwave Technol. **5**, 1701–1705 (1987).
5. P. Merritt, R.P. Tatam, and D.A. Jackson, "Interferometric chromatic dispersion measurements on short lengths of monomode optical fiber," J. Lightwave Technol. **7**, 703-716 (1989).
6. P. Lu, H. Ding, and S.J. Mihailov, "Direct measurement of the zero-dispersion wavelength of tapered fibres using broadband-light interferometry," Meas. Sci. Technol. **16**, 1631–1636 (2005).
7. J.Y. Lee and D.Y. Kim, "Versatile chromatic dispersion measurement of a single mode fiber using spectral white light interferometry," Opt. Express **14**, 11608–11614 (2006).

#81784 - $15.00 USD Received 3 Apr 2007; revised 25 Jun 2007; accepted 26 Jul 2007; published 20 Aug 2007

8. F. Koch, S.V. Chernikov, and J.R. Taylor, "Dispersion measurement in optical fibres over the entire spectral range from 1.1 μmm to 1.7 μmm," Opt. Commun. **175**, 209–213 (2001).
9. D. Ouzounov, D. Homoelle, W. Zipfel, W.W. Webb, A.L. Gaeta, J.A. West, J.C. Fajardo, and K.W. Koch, "Dispersion measurements of microstructure fibers using femtosecond laser pulses," Opt. Commun. **192**, 219–223 (2001).
10. Q. Ye, C. Xu, X. Liu, W.H. Knox, M.F. Yan, R.S. Windeler, and B. Eggleton,"Dispersion measurement of tapered airsilica microstructure fiber by white-light interferometry," Appl. Opt. **41**, 4467–4470 (2002).
11. L. Labonté, P. Roy, F. Pagnoux, F. Louradour, C. Restoin, G. Mélin, and E. Burov, "Experimental and numerical analysis of the chromatic dispersion dependence upon the actual profile of small core microstructured fibres," J. Opt. A: Pure App. Opt. **8**, 933–938 (2006).
12. P. Hlubina, "White-light spectral interferometry with the uncompensated Michelson interferometer and the group refractive index dispersion in fused silica," Opt. Commun. **193**, 1–7 (2001).
13. M. Yan and P. Shum, "Antiguiding in microstructured optical fibers," Opt. Express **12**, 104–116 (2004).
14. P. Hlubina, R. Chlebus, and D. Ciprian, "Differential group refractive index dispersion of glasses of optical fibres measured by a white-light spectral interferometric technique," Meas. Sci. Technol. **18**, 1547–1552 (2007).
15. Q. Li, P.Z. Dashti, I.V. Tomov, and H.P. Lee, "Measurement of modal dispersion in optical fiber by means of acousto-optic coupling," Opt. Lett. **28**, 75–77 (2003).
16. M. Koshiba, S. Maruyama, and K. Hirayama, "A vector finite element method with the higher order mixed-interpolation-type triangular elements for optical waveguide problems," J. Lightwave Technol. **12**, 495–502 (1994).
17. P. Hlubina, M. Szpulak, L. Knyblová, G. Statkiewicz, T. Martynkien, D. Ciprian, and W. Urbańczyk, "Measurement and modelling of dispersion characteristics of two-mode birefringent holey fibre," Meas. Sci. Technol. **17**, 626–630 (2006).
18. P. Hlubina and I. Gurov, "Spectral interferograms including the equalization wavelengths processed by autoconvolution method," Proc. SPIE **5064**, 198–205 (2003).
19. P. Hlubina, T. Martynkien, and W. Urbańczyk, "Dispersion of group and phase modal birefringence in elliptical-core fiber measured by white-light spectral interferometry," Opt. Express **11**, 2793–2798 (2003).

1. Introduction

The group dispersion, that is, the wavelength dependence of the group index, belongs to one of the fundamental dispersion characteristics of optical fibers. The chromatic dispersion, which can be obtained by simply differentiating the measured relative group index, is a significant characteristic that affects the bandwidth of a high speed optical transmission system through pulse broadening and nonlinear optical distortion. Chromatic dispersion of long length optical fibers is determined by two widely used methods [1]: the time-of-flight method which measures relative temporal delays for pulses at different wavelengths, and the modulation phase shift technique which measures the phase delay of a modulated signal as a function of wavelength.

White-light interferometry based on the use of a broadband source in combination with a standard Michelson or a Mach-Zehnder interferometer [2] is considered as one of the best tools for dispersion characterization of short length optical fibers. White-light interferometry usually utilizes a temporal method or a spectral method. The temporal method involves measurement of the group delay introduced by an optical fiber which is placed in one of the interferometer arms and evaluating the temporal shift of the peak of the cross-correlation interferogram. As the central wavelength is varied, the relative group delay of different frequency components is observed directly [3]. Alternatively, the spectral distribution of the phase delay over the full bandwidth of the white-light source is obtained in a single measurement by a Fourier transform of the cross-correlation interferogram [4]. The dispersion characteristics of the fiber sample under study can be obtained by simply differentiating the measured phase delay.

The spectral method is based on the observation of channeled spectrum [5, 6, 7, 8] and involves measurement of the period of the spectral fringes in the vicinity of a stationary-phase point in the recorded spectral interferogram [5, 6]. The main limitation of this method is related to the fact that the spectral interference fringes far from the stationary-phase point [7] are difficult to resolve. Fortunately, the measurement of the chromatic dispersion of a fiber sample is still possible in the vicinity of the stationary-phase point if one shifts it in successive steps

#81784 - $15.00 USD Received 3 Apr 2007; revised 25 Jun 2007; accepted 26 Jul 2007; published 20 Aug 2007

to different wavelengths [8]. The feasibility of the interferometric techniques has been demonstrated in measuring the dispersion in microstructured and holey fibers [9, 10, 11]. To the best of our knowledge, non of these methods directly measure the dispersion of group effective index.

In this paper, a new technique, based on white-light interferometry and employing a low-resolution spectrometer, is used for measuring the group effective index dispersion of the fundamental mode of a holey fiber over a wide wavelength range. The technique utilizes an unbalanced Mach-Zehnder interferometer with a fiber under test placed in one arm while the other arm has adjustable path length to record a series of spectral signals and to measure the equalization wavelength as a function of the path length. We revealed that there is an apparent path length discrimination between the spectral signals associated with the fundamental mode supported by the fiber and light guided by the outer cladding of the fiber. Using the fact that the group dispersion of the cladding, which is made of pure silica, is known, we were able to identify the spectral signal related to the fundamental mode and to measure the dispersion of the group effective index. Furthermore, using a full-vector finite element method, we modelled the dispersion of the group effective index and demonstrated good agreement between experiment and theory.

2. Experimental method

Let us consider an unbalanced Mach-Zehnder interferometer as shown in Fig. 1 with a fiber under test of length z supporting the guided mode of the phase effective index $n_{eff}(\lambda)$. The fiber is placed in the first (test) arm of the interferometer that comprises optical components (lens 1 and lens 2) to which the effective thickness d and refractive index $n_c(\lambda)$ correspond. The other (reference) arm of the interferometer has the adjustable path length L in the air so that the group OPD $\Delta^{g}_{MZ}(\lambda)$ between the beams in the interferometer is given by:

$$\Delta^{g}_{MZ}(\lambda) = L - l - N_{eff}(\lambda)z - N_c(\lambda)d, \tag{1}$$

where l is the path length in the air in the test arm, and $N_{eff}(\lambda)$ and $N_c(\lambda)$ are the group (refractive) indices satisfying the relation:

$$N(\lambda) = n(\lambda) - \lambda \frac{dn(\lambda)}{d\lambda}. \tag{2}$$

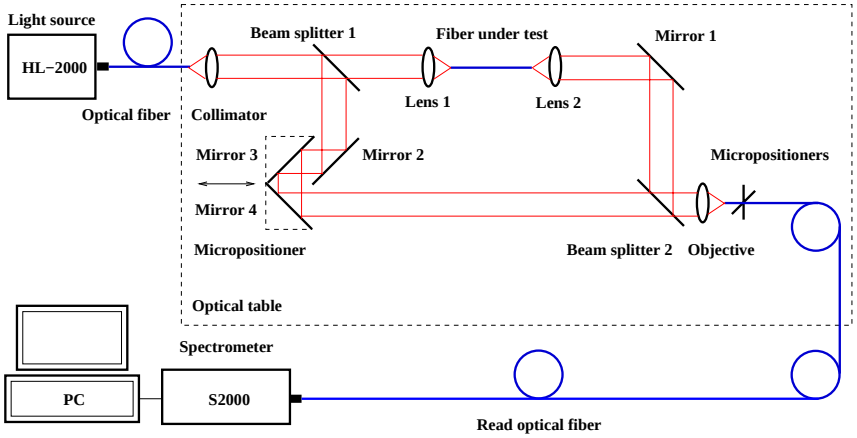

Fig. 1. Experimental setup with an unbalanced Mach-Zehnder interferometer to measure the group dispersion of the mode supported by a fiber under test.

#81784 - $15.00 USD Received 3 Apr 2007; revised 25 Jun 2007; accepted 26 Jul 2007; published 20 Aug 2007

Let us consider now that the spectral interference fringes recorded in the setup have the largest period in the vicinity of a stationary-phase point for which the group optical path difference is zero at one specific wavelength λ_0, referred to as the equalization wavelength [12]. The condition $\Delta^{g}_{MZ}(\lambda_0) = 0$ gives for the overall path length $L = L_o = L_o(\lambda_0)$ for which the equalization wavelength λ_0 is resolved in the recorded spectrum the relation:

$$L_o(\lambda_0) = N_{eff}(\lambda_0)z + N_c(\lambda_0)d + l. \tag{3}$$

The light is also guided in the gallery of the cladding modes arising in the microstructured and solid parts of the cladding. As shown in [13], attenuation of the modes propagating in the microstructured region is very high and reaches 1-5 $dB\,cm^{-1}$, depending on wavelength range. Therefore, most of the energy is transmitted through the modes propagating in the solid part of the cladding. These modes are very well confined in the glass (except the ones close to the cut-off), which justifies the assumption that their group effective index is equal to the group index of the glass $N_g(\lambda)$. It is worth mentioning that correctness of this simplifying assumption was recently confirmed experimentally in [14] by direct interferometric measurements of the group index of light transmitted through the solid part of the cladding in the holey fiber. Furthermore, such an assumption was also used in earlier works [15] devoted to dispersion measurements in conventional fibers. In consequence, the spectral interference fringes associated to the cladding modes, which arise in the vicinity of the equalization wavelength λ_0 but for the different path lengths $L = L_g = L_g(\lambda_0)$, may be represented by the following equation:

$$L_g(\lambda_0) = N_g(\lambda_0)z + N_c(\lambda_0)d + l, \tag{4}$$

where $N_g(\lambda_0)$ is the group index of the glass at the equalization wavelength λ_0. Using Eqs. (3) and (4), we obtain the simple relation:

$$N_{eff}(\lambda_0) = N_g(\lambda_0) + [L_o(\lambda_0) - L_g(\lambda_0)]/z, \tag{5}$$

which means that the group effective index $N_{eff}(\lambda_0)$ of the mode supported by the fiber can be measured directly as a function of the equalization wavelength λ_0 if the fiber length z and the dispersion of the group index $N_g(\lambda)$ of the glass (pure silica) are known. The main limitation of the method is in the measured wavelength dependences of the path lengths $L_o(\lambda_0)$ and $L_g(\lambda_0)$ that must be known for the same equalization wavelengths λ_0.

Another possibility for measuring the group effective index $N_{eff}(\lambda_0)$ as a function of the equalization wavelength λ_0 is based on the knowledge of only a single value of the path length $L_g(\lambda_{0r})$ at one specific equalization wavelength, λ_{0r}, the reference one. In this case, we need to know the group dispersion of the optical components, which is measured in the unbalanced Mach-Zehnder interferometer with the fiber removed. If the corresponding path length is denoted as $L_c = L_c(\lambda_0)$, we can measure the path length difference $\Delta L_c(\lambda_0) = L_c(\lambda_0) - L_c(\lambda_{0r})$ given by

$$\Delta L_c(\lambda_0) = \Delta N_c(\lambda_0)d, \tag{6}$$

where $\Delta N_c(\lambda_0) = N_c(\lambda_0) - N_c(\lambda_{0r})$ is the differential group index of the optical components. Equation (4) can be rewritten as

$$L_g(\lambda_0) = L_g(\lambda_{0r}) + \Delta N_g(\lambda_0)z + \Delta N_c(\lambda_0)d, \tag{7}$$

where $\Delta N_g(\lambda_0) = N_g(\lambda_0) - N_g(\lambda_{0r})$ is the differential group index of the glass. On substituting Eq. (7) into Eq. (5) and using Eq. (6), we obtain the final relation for the group effective index $N_{eff}(\lambda_0)$:

$$N_{eff}(\lambda_0) = N_g(\lambda_{0r}) + [L_o(\lambda_0) - L_g(\lambda_{0r}) - \Delta L_c(\lambda_0)]/z, \tag{8}$$

which is easy to use if the group index $N_g(\lambda_{0r})$ of the fiber glass is known at the reference equalization wavelength λ_{0r}.

#81784 - $15.00 USD Received 3 Apr 2007; revised 25 Jun 2007; accepted 26 Jul 2007; published 20 Aug 2007

3. Experimental setup

The setup for measuring the dispersion of the group effective index of the mode supported by the fiber using spectral-domain white-light interferometry is shown in Fig. 1. It consists of a white-light source: a quartz-tungsten-halogen lamp (HL-2000HP, Ocean Optics, Inc.) with launching optics, a single-mode optical fiber (FS-SN-3224, 3M), a collimating lens, a bulk-optic Mach-Zehnder interferometer with plate beam splitters (BSW07, Thorlabs), a micropositioner connected to mirrors 3 and 4 of the interferometer, a microscope objective, micropositioners, a fiber-optic spectrometer (S2000, Ocean Optics, Inc.), an A/D converter and a personal computer. In the test arm of the interferometer is inserted a combination of a fiber sample and optical components (shown schematically in Fig. 1 as lens 1 and lens 2) represented by a microscope objective (10×/0.30, Meopta), and an achromatic lens (74-ACR, Ocean Optics, Inc.). The fiber sample is pure silica holey fiber (PM-1550-01, Thorlabs) [17] of length $z = (50650 \pm 10)\,\mu$m.

4. Numerical modelling

Prior to the measurements, we model the dispersion of the modes supported by the investigated holey fiber. Its cross-section obtained by the scanning electron microscope (SEM) is shown in Fig. 2(a). A full-vector mode solver based on hybrid edge/nodal finite-element method (FEM) [16] was used to calculate the propagation constants of guided modes. In this approach, the following eigenequation is solved

$$\begin{bmatrix} -\nabla_\perp \times \nabla_\perp \times + k_0^2 \varepsilon(\vec{r}) & 0 \\ 0 & 0 \end{bmatrix} \begin{bmatrix} \vec{E_\perp} \\ E_z \end{bmatrix} = \beta^2 \begin{bmatrix} 1 & \nabla_\perp \\ \nabla_\perp & \Delta + k_0^2 \varepsilon(\vec{r}) \end{bmatrix} \begin{bmatrix} \vec{E_\perp} \\ E_z \end{bmatrix}, \quad (9)$$

where $(\vec{E}_\perp, E_z)$ is the electric field vector (eigenvector) and β is the propagation constant of the mode (eigenvalue). To find the eigenpairs of the above equation, we used the Arnoldi method as an eigensolver and an unsymmetrical multifrontal method as a solver of linear system of equations. The calculations were carried out for the real geometry of the fiber [17]. The binary image of the fiber cross section shown in Fig. 2(b) was used as a mask to generate the mesh for FEM, which reflected the real shape and location of each hole. To assure high accuracy of numerical results, we applied a mesh composed of about 170 000 triangular elements and took into account the dispersion of the refractive index of the pure silica glass.

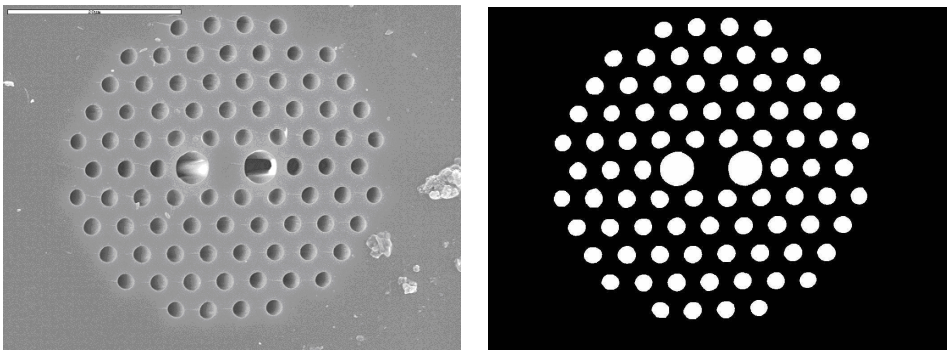

(a) (b)

Fig. 2. (a) SEM photograph of the investigated holey fiber and (b) binary mask used for mesh generation.

#81784 - $15.00 USD Received 3 Apr 2007; revised 25 Jun 2007; accepted 26 Jul 2007; published 20 Aug 2007

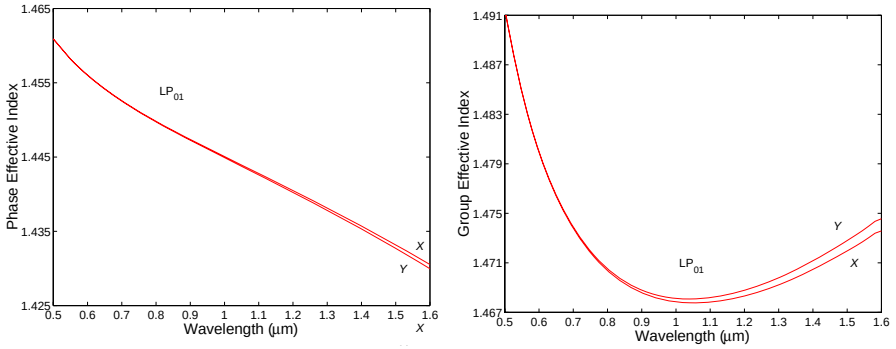

(a) (b)

Fig. 3. Calculated phase (a) and group (b) effective indices of the LP_{01} mode of respective polarizations as a function of wavelength.

Figure 3(a) shows the wavelength dependence of the phase effective index $n_{eff}(\lambda) = \beta(\lambda)/(2\pi/\lambda)$ for the fundamental (LP_{01}) mode supported by the fiber. Figure 3(b) then shows the wavelength dependence of the group effective index $N_{eff}(\lambda)$ calculated by means of Eq. (2) for the LP_{01} mode. It should be noted that there is a minimum in the group effective index. In Figs. 3(a) and 3(b) are shown the effective indices for two orthogonal polarizations and the apparent discrimination between them is demonstrated.

5. Experimental results and discussion

First, the measurement was performed on a combination of the fiber sample and optical components in the setup shown in Fig. 1. Prior to the measurement we utilized the main advantage of the setup, which is in fiber connection of a light source (that can be exchanged) with the interferometer. We used a laser diode instead of the halogen lamp to check the right excitation of the modes supported the fiber, and the precise placement and alignment of the optical components in the test arm by observing the interference fringes. The optical field corresponding to the fundamental mode was revealed at the output of the test arm together with some patterns indicating that the light was also guided by the outer cladding of the fiber [14].

During the dispersion measurement we adjusted such a path length in the reference arm of the interferometer that allows to resolve spectral interference fringes. Figure 4(a) shows an example of the recorded normalized spectral signal (denoted as F+OCs) obtained by subtracting the reference signal (without the interference) from the interferogram. It clearly shows that the spectral interference fringes can be identified only in the vicinity of the equalization wavelength $\lambda_0 = 664.54$ nm. To reveal the dependence of the equalization wavelength λ_0 on the adjusted path length $L_o = L_o(\lambda_0)$, we displaced manually the stage with mirrors 3 and 4 by using the micropositioner with a constant step of 10 μm and recorded the corresponding spectral signals. Using this method, we revealed that the equalization wavelength λ_0 can be resolved in two different spectral ranges from 515 to 807 nm and from 769 to 882 nm. Figure 4(b) shows an example of the normalized spectral signal (denoted as G+OCs) recorded in the second spectral range with the spectral interference fringes arising in the vicinity of the equalization wavelength $\lambda_0 = 816.42$ nm. The spectral signal was preprocessed to remove the noise and the equalization wavelength was determined precisely by an autoconvolution method [18]. It is clearly seen that the spectral signal from Fig. 4(b) has substantially lower visibility in comparison with that

#81784 - $15.00 USD Received 3 Apr 2007; revised 25 Jun 2007; accepted 26 Jul 2007; published 20 Aug 2007

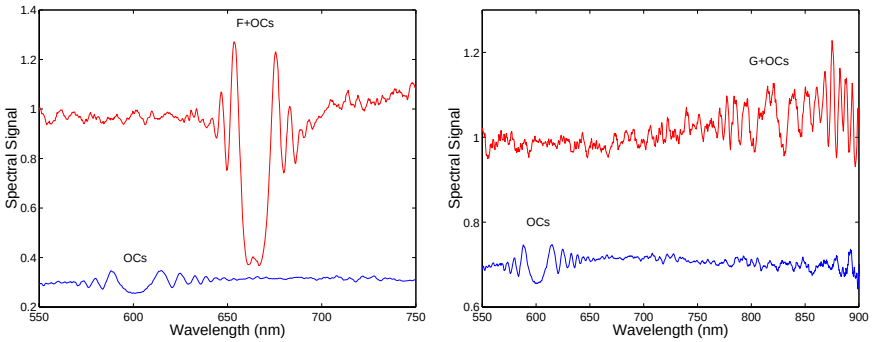

(a) (b)

Fig. 4. Examples of the recorded spectral signals: (a) optical components (OCs), fiber plus optical components (F+OCs); (b) optical components (OCs), glass plus optical components (G+OCs).

from Fig. 4(a). This is due to the fact that the light is guided by the outer cladding so that in this spectral signal the group dispersion of the fiber glass is encoded [14]. Moreover, the measured path lengths $L_o(\lambda_0)$ and $L_g(\lambda_0)$ are with the same equalization wavelengths λ_0 in too narrow spectral range from 769 to 807 nm to use Eq. (5). Better is to utilize Eq. (8) when only a single value of the path length $L_g(\lambda_{0r})$ at the reference equalization wavelength λ_{0r} needs to be known.

In the second step, the measurement was performed for the optical components for which the equalization wavelength cannot be resolved with the unbalanced Mach-Zehnder interferometer alone. A method of tandem interferometry [19] was used, which utilizes a Michelson interferometer placed in between the source and the unbalanced Mach-Zehnder interferometer and an appropriate OPD in the Michelson interferometer was introduced to resolve the spectral interference fringes at the output of the Mach-Zehnder interferometer. We checked the precise placement and alignment of the microscope objective and the achromatic lens in the test arm by observing the interference fringes when a laser diode was used instead of the halogen lamp. Figures 4(a) and 4(b) show an example of the recorded spectral signal (denoted as OCs) with the spectral interference fringes arising only in the vicinity of the equalization wavelength $\lambda_0 = 601.35$ nm.

From the two measurements described above, the wavelength dependences of the adjusted path length were obtained. In the first case we revealed that the overall path length difference $L_o(\lambda_0) - L_g(\lambda_{0r})$ varies from 1840 to -120 μm, when the reference equalization wavelength $\lambda_{0r} = 816.42$ nm was chosen. The measured values are shown in Fig. 5(a) by the crosses and there is an apparent discrimination between the values that can be attributed to the fundamental mode guided by the fiber (denoted as F+OCs) and to the light guided by the solid part of the cladding (denoted as G+OCs). Similarly, the spectral signals recorded for the second case revealed that the equalization wavelength λ_0 can be resolved in the spectral range from 509 to 869 nm and that the path length difference $\Delta L_c(\lambda_0)$ varies from 470 to -90 μm. The measured values are shown in Fig. 5(a) by the crosses together with the polynomial fit.

Knowledge of the measured dependences and the fiber length z enabled us to calculate the group effective index $N_{eff}(\lambda_0)$ of the fundamental mode as a function of the equalization wavelength λ_0. The function, which was obtained by means of Eq. (8) and the known group index $N_g(\lambda_{0r})$ of the pure silica glass [12], is represented in Fig. 5(b) by the crosses and it is shown together with the calculated functions also shown in Fig. 3(b). This figure confirms very good

#81784 - $15.00 USD Received 3 Apr 2007; revised 25 Jun 2007; accepted 26 Jul 2007; published 20 Aug 2007

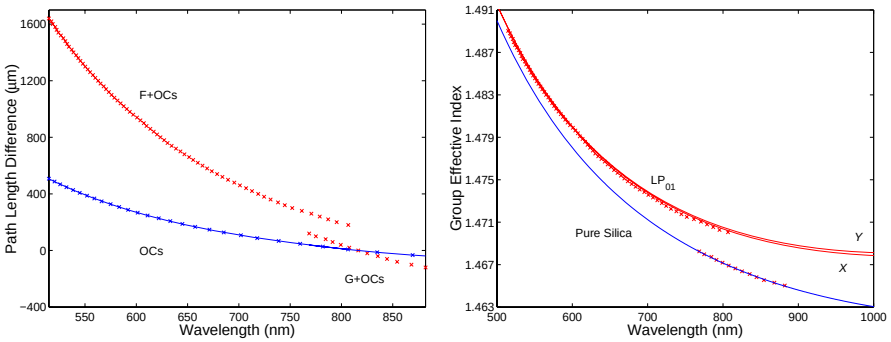

(a) (b)

Fig. 5. Path length difference (a) and group effective index (b) measured as a function of wavelength: optical components (OCs), fiber plus optical components (F+OCs), glass plus optical components (G+OCs); LP_{01} mode, pure silica (solid lines are theoretical functions).

agreement between theory and experiment, and also shows that the group effective index of the fundamental mode is substantially higher than the group index of the pure silica glass. Furthermore, no apparent discrimination between the group effective indices for the orthogonal polarizations was revealed in the measured spectral range. This is owing to short length of optical fiber used in the experiment.

We can estimate a precision of the group effective index measurement. If the reference equalization wavelength is determined with an error of $\delta(\lambda_{0r})$, the path length difference $\Delta L = L_o(\lambda_0) - L_g(\lambda_{0r}) - \Delta L_c(\lambda_0)$ is adjusted with a precision of $\delta(\Delta L)$ and the length z of the fiber is known with a precision of $\delta(z)$, the group effective index N_{eff} is obtained with a precision given by the following formula:

$$\delta(N_{eff}) = \sqrt{\left[\frac{\mathrm{d}N_g(\lambda_{0r})}{\mathrm{d}\lambda_{0r}}\delta(\lambda_{0r})\right]^2 + \left[\frac{\delta(\Delta L)}{z}\right]^2 + \left[\Delta L\frac{\delta(z)}{z^2}\right]^2}. \tag{10}$$

In our case, the error $\delta(\lambda_{0r})$ is 0.32 nm (the wavelength difference corresponding to adjacent pixels of the spectrometer linear CCD-array detector), the precision $\delta(\Delta L)$ is 1 μm and the precision $\delta(z)$ is 10 μm so that the precision $\delta(N_{eff})$ in determining the group effective index is 2×10^{-5}. Higher measurement precision can be achieved, for example, using a longer fiber. However, the maximum length of the investigated fiber is limited by resolving power of the spectrometer.

6. Conclusions

We proposed a new technique for measuring the dispersion of group effective index in the fundamental mode of a holey fiber over a wide wavelength range. The technique, which is based on white-light interferometry employing a low-resolution spectrometer, utilizes an unbalanced Mach-Zehnder interferometer with a fiber under test placed in one arm and the other arm with adjustable path length. A series of the spectral interferograms were recorded to measure the equalization wavelength as a function of the path length, or equivalently the dispersion of the effective index. We revealed that there is an apparent path length discrimination between the spectral signals associated with the fundamental mode supported by the fiber and light guided by the outer cladding of the fiber. Using the fact that the group dispersion of the pure-silica

#81784 - $15.00 USD Received 3 Apr 2007; revised 25 Jun 2007; accepted 26 Jul 2007; published 20 Aug 2007

cladding is known, we measured the wavelength dependence of the group effective index of the fundamental mode of the holey fiber. Furthermore, we modelled the group dispersion using a full-vector finite element method and demonstrated good agreement between experiment and theory. The use of the method, whose main advantage is in easy inspection of the optical field at the output of the test arm, can be extended for measuring the group dispersion of the spatial and/or polarization modes supported by a fiber under study.

Acknowledgements

The research was partially supported by the Grant Agency of the Czech Republic (project No. 102/06/0284), by the grant MSM6198910016, by the COST Action P11, and by the Grant for Bilateral Scientific Cooperation between Poland and Czech Republic.

#81784 - $15.00 USD Received 3 Apr 2007; revised 25 Jun 2007; accepted 26 Jul 2007; published 20 Aug 2007

Paper V.

Optics Communications 281 (2008) 4008–4013

Contents lists available at ScienceDirect

Optics Communications

journal homepage: www.elsevier.com/locate/optcom

Group index dispersion of holey fibres measured by a white-light spectral interferometric technique

P. Hlubina *, D. Ciprian, R. Chlebus

Department of Physics, Technical University Ostrava, 17. Listopadu 15, 708 33 Ostrava-Poruba, Czech Republic

ARTICLE INFO

Article history:
Received 16 January 2008
Received in revised form 7 April 2008
Accepted 7 April 2008

PACS:
07.60.Ly
42.25.Hz
42.70.Ce
42.81.Cn
78.20.Ci

Keywords:
Spectral interferometry
White-light source
Mach–Zehnder interferometer
Holey fibre
Group index
Dispersion
Pure silica glass
SK222 glass

ABSTRACT

We present a new white-light interferometric technique to measure the group index of holey fibres over a wide wavelength range. The technique utilizes an unbalanced Mach–Zehnder interferometer with a fibre under test of known length placed in one of the interferometer arms and the other arm with adjustable path length. In a first step, the differential group index of the fibre is measured over a wide wavelength range. In a second step, the fibre is replaced by the reference sample of known thickness and group dispersion to determine precisely the group index of the fibre at one specific wavelength. The group index as a function of wavelength is measured for two different holey fibres, one made of pure silica glass and the other made of SK222 glass. For both fibres, the wavelength dependence of the group index of the outer cladding and modes supported by the fibre is measured.

1. Introduction

A precise measurement of the wavelength dependence of the group refractive index (group index dispersion) of optical fibres over a broad spectral range is important in various research areas including high-speed optical transmission systems and broadband optical communications. The chromatic dispersion, which can be obtained by simply differentiating the differential group index in the spectral domain, is a significant characteristic that affects the bandwidth of a high-speed optical transmission system through pulse broadening and nonlinear optical distortion. Chromatic dispersion of long length optical fibres is determined by two widely used methods [1]: the time-of-flight method, which measures relative temporal delays for pulses at different wavelengths, and the modulation phase shift technique, which measures the phase delay of a modulated signal as a function of wavelength.

White-light interferometry based on the use of a broadband source in combination with a standard Michelson or Mach–Zehnder interferometer [2] is considered as one of the best tools for dispersion characterization of short length optical fibres. White-light interferometry usually utilizes a temporal method or a spectral method. The temporal method involves measurement of the group delay introduced by an optical fibre which is placed in one of the interferometer arms and evaluating the temporal shift of the peak of the cross-correlation interferogram. As the central wavelength is varied, the relative group delay of different frequency components is observed directly [3]. Alternatively, the spectral distribution of the phase delay over the full bandwidth of the white-light source is obtained in a single measurement by a Fourier transform of the cross-correlation interferogram [4]. The dispersion characteristics of the fiber sample under study can be obtained by simply differentiating the measured phase delay.

The spectral method is based on the observation of spectrally resolved interference fringes (channelled spectrum) in the vicinity [5–7] of a stationary phase point or far from it [8] and involves measurement of the phase or period of the spectral fringes. The

* Corresponding author. Tel.: +420 597 323 134; fax: +420 597 323 139.
E-mail address: petr.hlubina@vsb.cz (P. Hlubina).

0030-4018/$ - see front matter © 2008 Elsevier B.V. All rights reserved.
doi:10.1016/j.optcom.2008.04.015

group dispersion of a fibre sample can be obtained by simply differentiating the spectral phase retrieved from a single interferogram. The stationary phase point appears in the recorded spectral interferogram when the overall group optical path difference (OPD) between two beams in the interferometer is close to zero. The main limitation of this method is related to the fact that the spectral interference fringes far from the stationary phase point [8] are difficult to resolve. Using a low-resolution spectrometer [9], the measurement of the group refractive index dispersion of a given fibre is still possible in the vicinity of the stationary phase point if one moves it in successive steps to different wavelengths and repeats the measurement. The modification of the technique with a tandem configuration of a Michelson interferometer and an optical fibre has been used in measurement of the group dispersion in birefringent fibres [10–12] of known lengths. Recently, the use of the method with a Mach–Zehnder interferometer was extended for dispersion characterization of tapered fibres [7] or glasses of optical fibres [13].

The feasibility of the interferometric techniques has been demonstrated in measuring the dispersion in microstructured and holey fibres [14–17]. Both fibre-optic [15] and bulk-optic [16,17] implementations of a Michelson [15,16] or Mach–Zehnder [17] interferometer were utilized. The dispersion parameters were obtained either by fitting the measured channelled spectrum to wavelength when the location of the stationary phase point was adjusted by the path length in the air [15] or by measuring the location of the stationary phase point (the equalization wavelength [17]) as a function of the path length difference [16,17]. The most recent paper [17] describes a new method of measuring the group dispersion of a holey fibre based on an apparent path length discrimination between the spectral interference fringes associated with the fundamental mode supported by the fibre and light guided by the fibre cladding the group dispersion of which is known.

The aim of this paper is to present a new white-light interferometric technique for measurement of the group index of holey fibres over a wide wavelength range. The technique utilizes an unbalanced Mach–Zehnder interferometer with a fibre under test of known length placed in one of the interferometer arms and the other arm with adjustable path length. A series of spectral interferograms is recorded to measure the equalization wavelength as a function of the path length difference. First, the differential group index of the fibre is measured over a wide wavelength range. Second, the fibre is replaced by the reference sample of known thickness and group dispersion to determine precisely the group index of the fibre under test at one specific wavelength. The group index as a function of the wavelength is measured for two different holey fibres, one made of pure silica glass and the other made of SK222 glass. For both cases, the wavelength dependence of the group index of the outer cladding and modes supported by the fibre is measured with a precision of 13×10^{-5}.

2. Experimental method

First, let us consider a technique presented in a previous paper [13] that has been used for measuring the differential group index $\Delta N(\lambda)$ of a fibre under test of length z and refractive index $n(\lambda)$. The technique utilizes an unbalanced Mach–Zehnder interferometer (see Fig. 1) with optical components (lens 1 and lens 2) to which the effective thickness d and refractive index $n_c(\lambda)$ correspond. The fibre under test is placed in the first (test) arm of the interferometer and the other (reference) arm is with the adjustable path length L in the air so that the group OPD $\Delta^{g}_{MZ}(\lambda)$ between the beams in the interferometer is given by

$$\Delta^{g}_{MZ}(\lambda) = L - l - N(\lambda)z - N_c(\lambda)d, \tag{1}$$

where l is the path length in the air in the test arm, and $N(\lambda)$ and $N_c(\lambda)$ are the group refractive indices satisfying the relation

$$N(\lambda) = n(\lambda) - \lambda \frac{dn(\lambda)}{d\lambda}. \tag{2}$$

The spectral interference fringes recorded in the set-up have the largest period in the vicinity of a stationary phase point for which the group OPD is zero at one specific wavelength, the equalization wavelength λ_0. To measure the differential group index $\Delta N(\lambda_0) = N(\lambda_0) - N(\lambda_{0r})$ of the fiber [13], the overall path length $L = L_o = L_o(\lambda_0)$ has to be adjusted for which the equalization wavelength λ_0 is resolved in the recorded spectrum. If we choose one of

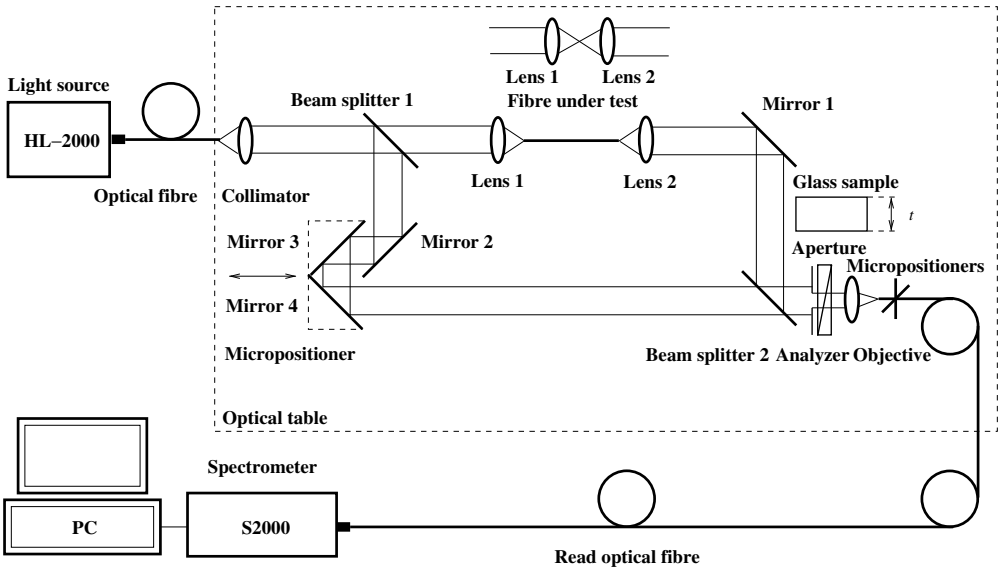

Fig. 1. Experimental set-up with an unbalanced Mach–Zehnder interferometer to measure the group index dispersion of a fibre under test.

the equalization wavelengths, λ_{0r}, as the reference one, the overall path length $L_o(\lambda_{0r})$ that results from the condition $\Delta^g_{MZ}(\lambda_{0r}) = 0$ is given by

$$L_o(\lambda_{0r}) = N(\lambda_{0r})z + N_c(\lambda_{0r})d + l. \quad (3)$$

The path length is the basis of the measurement of the fibre group dispersion $N = N(\lambda_0)$ from the measured differential group index dispersion $\Delta N(\lambda_0) = N(\lambda_0) - N(\lambda_{0r})$ [13] and the group index $N(\lambda_{0r})$ determined precisely by another technique.

Let us consider three different techniques with three different reference elements that can be used for measuring the fibre group index $N(\lambda_{0r})$.

2.1. First reference element: glass sample

In this technique we consider a set-up of the unbalanced Mach–Zehnder interferometer in which the fibre under test is replaced by a glass sample of known thickness t and group refractive index $N_r(\lambda_{0r})$ (see Fig. 1). To resolve the reference equalization wavelength λ_{0r} in the recorded spectrum, the reference path length $L = L_r = L_r(\lambda_{0r})$ have to be adjusted which satisfies the relation

$$L_r(\lambda_{0r}) = N_r(\lambda_{0r})t + N_c(\lambda_{0r})d + l - t + z. \quad (4)$$

By combining Eq. (3) with Eq. (4), we obtain for the group refractive index $N(\lambda_{0r})$ of the fiber the relation

$$N(\lambda_{0r}) = 1 + [N_r(\lambda_{0r}) - 1]t/z + [L_o(\lambda_{0r}) - L_r(\lambda_{0r})]/z. \quad (5)$$

2.2. Second reference element: fibre

In this technique we consider a set-up of the unbalanced Mach–Zehnder interferometer (see Fig. 1) in which the fibre under test is replaced by the reference fibre of length t and known group refractive index $N_r(\lambda_{0r})$. If the reference equalization wavelength λ_{0r} is resolved in the recorded spectrum for the reference path length $L_r(\lambda_{0r})$, the group refractive index $N(\lambda_{0r})$ of the fiber under test is given by Eq. (5).

2.3. Third reference element: outer fibre cladding

In this technique we consider a set-up of the unbalanced Mach–Zehnder interferometer (see Fig. 1) with the fibre under test of length z. If the fibre is excited in such a way that light is guided by the outer fibre cladding of known group index $N_r(\lambda_{0r})$ and if the reference equalization wavelength λ_{0r} is resolved in the recorded spectrum for the reference path length $L_r(\lambda_{0r})$, the group index $N(\lambda_{0r})$ of the fiber under test is given by

$$N(\lambda_{0r}) = N_r(\lambda_{0r}) + [L_o(\lambda_{0r}) - L_r(\lambda_{0r})]/z. \quad (6)$$

To summarize the implementation merits of the above methods, the simplest is the third one. However in this case we need to know the group dispersion of the outer fibre cladding. In the opposite case, the second method is simpler than the first one if the fibre of known dispersion is available.

3. Experimental set-ups

The experimental set-up used in the application of spectral-domain white-light interferometry for measuring the differential group index dispersion $\Delta N = \Delta N(\lambda_0)$ of optical fibres is shown in Fig. 1. It consists of a white-light source: a quartz–tungsten–halogen lamp (HL-2000HP, Ocean Optics, Inc.) with launching optics, a single-mode optical fibre (FS-SN-3224, 3M), a collimating lens, a bulk-optic Mach–Zehnder interferometer with plate beam splitters (BSW07, Thorlabs), a micropositioner connected to mirrors three and four of the interferometer, an aperture, a Glan–Taylor polarizer (Thorlabs), a microscope objective, micropositioners, a fibre-optic spectrometer (S2000, Ocean Optics, Inc.), an A/D converter and a personal computer. The spectrometer resolution is given by a 50 μm core diameter of the read optical fibre to which a Gaussian response function with the width of about 3 nm corresponds [9]. In the test arm of the interferometer is placed a combination of a fiber under test (fibre sample) and optical components (shown schematically in Fig. 1 as lens 1 and lens 2) represented by a microscope objective (10×/0.30, Meopta) and an achromatic lens (74-ACR, Ocean Optics, Inc.). We measured two different fibre samples. The first sample is pure silica holey fibre of length $z = 50650$ μm (PM-1550-01, Thorlabs, see its SEM photograph in [12]). The second sample is a rectangular-shape highly birefringent holey fibre of length $z = 54200$ μm made of SK222 optical glass with rectangular lattice and circular holes (see a similar fibre of IEMT with elliptical holes in [18]). The fibre lengths were measured by a micrometer with an accuracy of ±10 μm.

The experimental set-up used in the application of spectral-domain white-light interferometry for measuring the group index $N(\lambda_{0r})$ with the reference element is also shown in Fig. 1. The reference element is represented by a birefringent quartz plate of thickness $t = (25750 \pm 10)$ μm. The quartz plate consists of two polished surfaces, parallel to the optical axis of the crystal with a precision of 15 arcmin. The plate is inserted into the test arm of the interferometer in such a way that the collimated beam is incident on the surfaces perpendicularly. The reference group index $N_r(\lambda_{0r})$ is either $N_o(\lambda_{0r})$ or $N_e(\lambda_{0r})$ depending on the orientation of the polarizer in the set-up and subscripts o and e stand for the ordinary and extraordinary waves propagating in the crystal.

4. Experimental results and discussion

Prior to the group dispersion measurements we utilized the main advantage of the set-ups, which is in fibre connection of a light source (that can be varied) with the interferometer. We used a laser diode instead of the halogen lamp to check the precise placement and alignment of the optical components in the test arm by observing the interference fringes. Moreover, the excitation of the outer fibre cladding or core was easily inspected at the output of the test arm. In the case of the first fibre sample, the ring-shape optical field indicated that the light was guided by the outer fibre cladding [13]. Similarly, the elliptical-shape optical field indicated that the light was guided by the fiber core and the fundamental mode was supported. The orientation of the polarizer was along the longer or shorter axis of the elliptical core so that the group dispersion in the X or Y polarization [12] was measured.

In the dispersion measurement of the outer cladding and the fibre mode, such a path length in the reference arm of the interferometer was adjusted to resolve spectral interference fringes. Fig. 2 shows an example of the recorded normalized spectral signal [13] corresponding to the excitation of the outer fibre cladding (denoted as F + OCs). It clearly shows the effect of the limiting resolving power of the spectrometer on the visibility of the spectral interference fringes identified only in the vicinity of the equalization wavelength $\lambda_0 = 748.23$ nm. Fig. 2 also shows an example of the recorded spectral signal corresponding to the excitation of the fundamental mode (denoted as M + OCs) in the X polarization with the spectral interference fringes identified only in the vicinity of the equalization wavelength $\lambda_0 = 664.54$ nm.

We measured the dependence of the adjusted path length difference on the equalization wavelength for both cases. We displaced the stage with mirrors 3 and 4 manually by using the micropositioner with a constant step of 10 μm and performed recording of the corresponding spectral signals. The spectral signals recorded for the outer fibre cladding revealed that the equalization wavelength

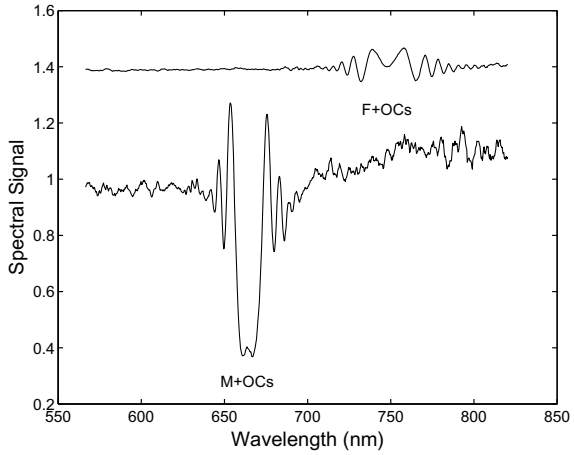

Fig. 2. Examples of the spectral signals recorded for two cases: outer fibre cladding plus optical components (F + OCs), fibre mode plus optical components (M + OCs).

λ_0 can be resolved in the spectral range from 508 to 910 nm [13]. Similarly, the spectral signals recorded for the fundamental mode revealed that the equalization wavelength λ_0 can be resolved in the spectral range from 515 to 807 nm. Knowledge of the measured dependences and the fibre length z enables us to evaluate directly the differential group index $\Delta N(\lambda_0)$ as a function of the equalization wavelength λ_0 [13]. Fig. 3 shows the function for the outer cladding by the crosses (denoted as pure silica) together with the theoretical function resulting from the Sellmeier formula for pure silica [19]. This figure confirms very good agreement between theory and experiment. Similarly, Fig. 3 shows the function for the fundamental mode by the crosses (denoted as mode) and demonstrates different dispersion slope for the mode in the comparison with that for the pure silica. It should be noted here that no apparent discrimination between the spectral signals for the orthogonal polarizations of the mode was revealed in the measured spectral range. This is owing to short length of the optical fibre used in the experiment.

To measure the fibre group index $N(\lambda_{0r})$ at the reference equalization wavelength λ_{0r}, first, the procedure presented in Section 2.1 was used. It is important to insert the quartz crystal into the test arm of the interferometer (see Fig. 1) in order not to shift the interference pattern with respect to the centre of the aperture. Similar procedure needs to be applied in the alignment of the optical components after removing the fibre from the test arm of the interferometer. Then, such a path length $L_r(\lambda_{0r})$ in the reference arm of the interferometer was adjusted to resolve spectral interference fringes at the reference equalization wavelength λ_{0r}. In our case, when $\lambda_{0r} = 693.62$ nm was chosen, we adjusted $\Delta L(\lambda_{0r}) = L_o(\lambda_{0r}) - L_r(\lambda_{0r}) = 9348$ μm. Using $N_r(\lambda_{0r}) = N_e(\lambda_{0r}) = 1.56904$ resulting from dispersion relation for the birefringent quartz [20] and Eq. (5), we obtain $N_x(\lambda_{0r}) = 1.47386$. From the value and the measured values of the differential group index $\Delta N_x(\lambda_0)$, the group index $N_x(\lambda_0)$ of the fundamental mode as a function of the equalization wavelength λ_0 was determined. The function is represented in Fig. 4 by the crosses and is shown together with the function for the pure silica (crosses with the solid line). This figure shows that the group index of the fundamental mode is substantially higher than that of the pure silica.

We can estimate a precision of the group index measurement. If the reference equalization wavelength λ_{0r} is determined with an error of $\delta(\lambda_{0r})$, the path length difference ΔL is adjusted with a precision of $\delta(\Delta L)$ and the lengths z and t of the fibre and crystal are known with precisions of $\delta(z)$ and $\delta(t)$, respectively, the group index N is obtained with a precision given by the following formula

$$\delta^2(N) = \left[\frac{dN_r(\lambda_{0r})}{d\lambda_{0r}}\frac{t}{z}\delta(\lambda_{0r})\right]^2 + \left[(N_r-1)\frac{\delta(t)}{z}\right]^2 + \left[(N_r-1)t\frac{\delta(z)}{z^2}\right]^2 + \left[\frac{\delta(\Delta L)}{z}\right]^2 + \left[\Delta L\frac{\delta(z)}{z^2}\right]^2. \quad (7)$$

In our case, the error $\delta(\lambda_{0r})$ is given by the wavelength difference corresponding to adjacent pixels of the spectrometer linear CCD-array detector and is 0.32 nm, the precision $\delta(\Delta L)$ is 1 μm and the precisions $\delta(z)$ and $\delta(t)$ are 10 μm so that the precision $\delta(N)$ in determining the group index is 13×10^{-5}. Higher measurement precision can be achieved using more precisely determined lengths and/or a longer fibre sample. However, there exists maximum length of the fibre given by the limited resolving power of the spectrometer.

The group index $N(\lambda_{0r})$ of the fundamental mode at the reference equalization wavelength λ_{0r} was also measured by the procedure presented in Section 2.3. In this case, the excitation of the fundamental mode was changed to that of the outer cladding,

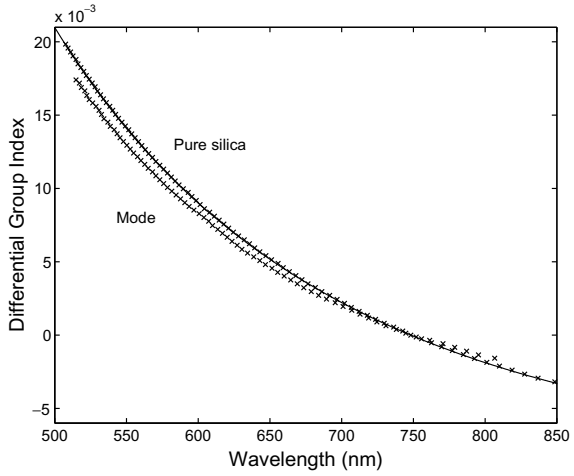

Fig. 3. Differential group index of outer fibre cladding (pure silica) and fibre mode measured as a function of wavelength. The solid line corresponds to theory.

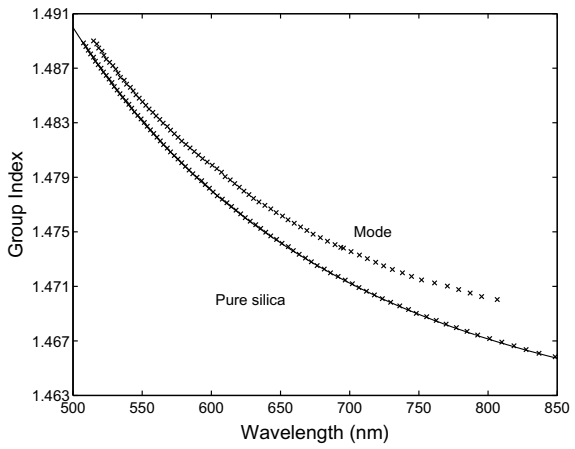

Fig. 4. Group index of outer fibre cladding (pure silica) and fibre mode measured as a function of wavelength. The solid line corresponds to theory.

the group index $N_r(\lambda_{0r})$ of which is known. Simultaneously, path length $L_o(\lambda_{0r})$ in the reference arm of the interferometer was changed to $L_r(\lambda_{0r})$ and spectral interference fringes were resolved at the same reference equalization wavelength λ_{0r}. In our case, when $\lambda_{0r} = 693.62$ nm was chosen, $\Delta L(\lambda_{0r}) = 118$ μm was adjusted. Using $N_r(\lambda_{0r}) = 1.47158$ resulting from dispersion relation for the pure silica [19] and Eq. (6), we obtain $N_x(\lambda_{0r}) = 1.47391$. This value is in very good agreement with that obtained by a previous procedure. Also in this case we can estimate a precision of the group index measurement, which is given by the following formula

$$\delta^2(N) = \left[\frac{dN_r(\lambda_{0r})}{d\lambda_{0r}}\delta(\lambda_{0r})\right]^2 + \left[\frac{\delta(\Delta L)}{z}\right]^2 + \left[\Delta L\frac{\delta(z)}{z^2}\right]^2. \quad (8)$$

The precision $\delta(N)$ in determining the group index by the procedure is 3×10^{-5} and is higher than that of the previous procedure.

Finally we measured the group dispersion of the second fibre sample. The excitation of the outer fibre cladding or core was once again easily inspected at the output of the test arm. The rectangular-shape optical field indicated that the light was guided by the outer fibre cladding. Similarly, the elliptical-shape optical field indicated that the light was guided by the fiber core and the fibre mode was supported. The orientation of the polarizer was along the longer or shorter axis of the elliptical core so that the group dispersion in the *X* or *Y* polarization was measured. Fig. 5 shows an example of the recorded spectral signal (denoted as F + OCs), which corresponds to the excitation of the outer fibre cladding with the spectral interference fringes identified only in the vicinity of the equalization wavelength $\lambda_0 = 747.91$ nm [13]. Fig. 5 also shows an example of the spectral signal (denoted as *X*M + OCs), which corresponds to the excitation of the fibre mode in the *X* polarization with the spectral interference fringes identified only in the vicinity of the equalization wavelength $\lambda_0 = 607.34$ nm. Moreover, Fig. 5 shows an example of the spectral signal (denoted as *Y*M + OCs) corresponding to the excitation of the fibre mode in the *Y* polarization with the spectral interference fringes identified only in the vicinity of the equalization wavelength $\lambda_0 = 608.01$ nm. The two spectral signals demonstrate discrimination of both polarization modes resolved for a given length of the fibre sample. From the different values of the equalization wavelengths resolved for the same path length difference adjusted in the interferometer we can conclude that the sign of the group birefringence $G = N_x - N_y$ is negative.

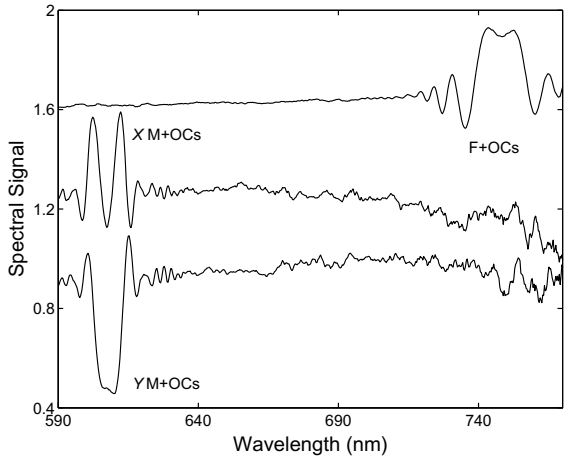

Fig. 5. Examples of the spectral signals recorded for two cases: outer fibre cladding plus optical components (F + OCs), fibre modes plus optical components (*X*M + OCs, *Y*M + OCs).

The spectral signals recorded for the outer fibre cladding revealed that the equalization wavelength λ_0 can be resolved in the spectral range from 497 to 907 nm [13]. Similarly, the spectral signals recorded for the polarization modes revealed that the equalization wavelength λ_0 can be resolved in the spectral range from 536 to 766 nm. In these spectral ranges, the wavelength dependence of the differential group index $\Delta N(\lambda_0)$ was measured. The measured values related to the outer cladding are shown in Fig. 6 by the crosses (denoted as SK222 glass) together with a polynomial fit. Similarly, the measured values related to the fundamental mode in the *X* and *Y* polarizations are shown by the crosses (denoted as *X* mode and *Y* mode) and demonstrates different dispersion slope for the polarization modes in the comparison with that for the SK222 glass. It should be noted here that an apparent discrimination between the spectral signals for the orthogonal polarizations was revealed in the measured spectral range, which indicates that the second holey fibre has higher group birefringence than the first one.

To measure the fibre group index $N(\lambda_{0r})$ at the reference equalization wavelength λ_{0r}, the procedure presented in Section 2.1. was

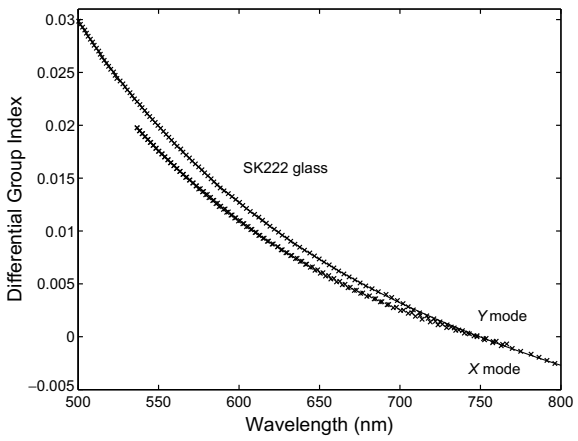

Fig. 6. Differential group index of outer fibre cladding (SK222 glass) and fibre modes measured as a function of wavelength. The solid line is a polynomial fit.

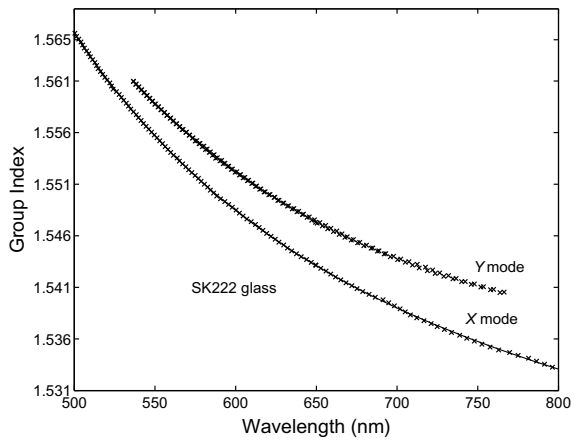

Fig. 7. Group index of outer fibre cladding (SK222 glass) and fibre modes measured as a function of wavelength. The solid line is a polynomial fit.

used. For the outer fibre cladding, when $\lambda_{0r} = 649.54$ nm was chosen, we adjusted $\Delta L(\lambda_{0r}) = 14956\ \mu$m. Using $N_r(\lambda_{0r}) = N_o(\lambda_{0r}) = 1.56247$ and Eq. (5), we obtain $N_g(\lambda_{0r}) = 1.54317$. Similarly, for the mode in the X polarization, when $\lambda_{0r} = 649.54$ nm was chosen, we adjusted $\Delta L(\lambda_{0r}) = 15180\ \mu$m. Using $N_r(\lambda_{0r}) = 1.56247$ and Eq. (5), we obtain $N_x(\lambda_{0r}) = 1.54730$. Moreover, using the procedure presented in Section 2.3, this value gives for the measured $\Delta L(\lambda_{0r}) = 214\ \mu$m the cladding group index $N_g(\lambda_{0r}) = 1.54335$. From the values and the measured values of the differential group indices $\Delta N_g(\lambda_0)$, $\Delta N_x(\lambda_0)$, $\Delta N_y(\lambda_0)$, the group index $N_g(\lambda_0)$ of the outer fibre cladding and the group indices $N_x(\lambda_0)$, $N_y(\lambda_0)$ of the polarization modes as a function of the equalization wavelength λ_0 were determined. The functions are represented in Fig. 7 by the crosses and are shown together with the polynomial fit for the cladding. This figure shows that the group indices of the polarization modes are substantially higher than the group index of the SK222 glass. According to Eq. (7), the group indices were measured with a precision of 13×10^{-5}.

5. Conclusions

We used a new white-light interferometric technique for measurement of the group index of holey fibres over a wide spectral range (in one case from 515 to 807 nm). The technique utilized an unbalanced Mach–Zehnder interferometer with a fibre under test of known length placed in one of the interferometer arms and the other arm with adjustable path length. First, from a series of recorded spectral signals we measured the equalization wavelength as a function of the path length difference, or equivalently the differential group index dispersion of the fibre. Second, the fibre was replaced by the reference sample of known thickness and group dispersion and the group index of the fibre at one specific wavelength was determined precisely. The group index as a function of wavelength was measured for two different holey fibres, one made of pure silica glass and the other made of SK222 glass, and a precision was 13×10^{-5}.

The use of the method, whose main advantage is in the absolute group dispersion determination, can be extended for measuring cladding modes of holey fibres. Moreover, the sign of the group birefringence in highly birefringent holey fibres can be specified by the method. The method allows for the dispersion measurement in a wider spectral band, which can be further extended by applying the CCD array operating in another spectral range.

Acknowledgement

The research was partially supported by the Grant Agency of the Czech Republic (Project No. 102/06/0284), grant MSM6198910016, the COST Action 299 and internal grant of TU Ostrava (IGS HGF VŠB-TUO).

References

[1] L.G. Cohen, J. Lightwave Technol. 3 (1985) 958.
[2] S. Diddams, J.C. Diels, J. Opt. Soc. Amer. B 13 (1996) 1120.
[3] M. Tateda, N. Shibata, S. Seikai, J. Quantum Electron. 17 (1981) 404.
[4] M.J. Saunders, W.G. Gardner, J. Lightwave Technol. 5 (1987) 1701.
[5] P. Merritt, R.P. Tatam, D.A. Jackson, J. Lightwave Technol. 7 (1989) 703.
[6] F. Koch, S.V. Chernikov, J.R. Taylor, Opt. Commun. 175 (2001) 209.
[7] P. Lu, H. Ding, S.J. Mihailov, Meas. Sci. Technol. 16 (2005) 1631.
[8] J.Y. Lee, D.Y. Kim, Opt. Express 14 (2006) 11608.
[9] P. Hlubina, I. Gurov, V. Chugunov, J. Mod. Opt. 50 (2003) 2067.
[10] P. Hlubina, Opt. Commun. 218 (2003) 283.
[11] P. Hlubina, T. Martynkien, W. Urbańczyk, Opt. Express 11 (2003) 2793.
[12] P. Hlubina, M. Szpulak, L. Knyblová, G. Statkiewicz, T. Martynkien, D. Ciprian, W. Urbańczyk, Meas. Sci. Technol. 17 (2006) 626.
[13] P. Hlubina, R. Chlebus, D. Ciprian, Meas. Sci. Technol. 18 (2007) 1547.
[14] D. Ouzounov, D. Homoelle, W. Zipfel, W.W. Webb, A.L. Gaeta, J.A. West, J.C. Fajardo, K.W. Koch, Opt. Commun. 192 (2001) 219.
[15] Q. Ye, C. Xu, X. Liu, W.H. Knox, M.F. Yan, R.S. Windeler, B. Eggleton, Appl. Opt. 41 (2002) 4467.
[16] L. Labonté, P. Roy, F. Pagnoux, F. Louradour, C. Restoin, G. Mélin, E. Burov, J. Opt. A: Pure Appl. Opt. 8 (2006) 933.
[17] P. Hlubina, M. Szpulak, D. Ciprian, T. Martynkien, W. Urbańczyk, Opt. Express 15 (2007) 11073.
[18] R. Buczynski, Acta Phys. Pol. 106 (2004) 141.
[19] P. Hlubina, Opt. Commun. 193 (2001) 1.
[20] P. Hlubina, D. Ciprian, L. Knyblová, Opt. Commun. 269 (2007) 8.

Paper VI.

Spectral-domain measurement of phase modal birefringence in polarization-maintaining fiber

Petr Hlubina and Dalibor Ciprian

Department of Physics, Technical University Ostrava, 17. listopadu 15, 708 33 Ostrava-Poruba, Czech Republic

petr.hlubina@vsb.cz

Abstract: We report on a new and simple method for measuring the wavelength dependence of phase modal birefringence in a polarization-maintaining fiber. The method is based on application of a lateral pointlike force on the fiber that causes strong coupling between polarization modes and utilizes their interference resolved as the channeled spectrum. The change of the phase retrieved from two recorded channeled spectra that are associated with the known displacement of coupling point is used to determine the phase modal birefringence as a function of wavelength. A windowed Fourier transform is applied to reconstruct precisely the phase change and the phase ambiguity is removed provided that we know the phase change of the spectral fringes at one specific wavelength. The measured wavelength dependence of phase modal birefringence is compared with that resulting from the group modal birefringence measurement.

OCIS codes: (060.2270) Fiber characterization; (060.2300) Fiber measurements; (120.3180) Interferometry; (260.1440) Birefringence;

References and links

1. S. C. Rashleigh, "Wavelength dependence of birefringence in highly birefringent fibers," Opt. Lett. **7**, 294–296 (1982).
2. M. G. Shlyagin, A. V. Khomenko, and D. Tentori, "Birefringence dispersion measurement in optical fibers by wavelength scanning," Opt. Lett. **20**, 869–871 (1995).
3. Y. J. Rao and D. A. Jackson, "Recent progress in fiber optic low-coherence interferometry," Meas. Sci. Technol. **7**, 981–999 (1996).
4. D. A. Flavin, R. McBride, and J. D. C. Jones, "Dispersion of birefringence and differential group delay in polarization-maintaining fiber," Opt. Lett. **27**, 1010–1012 (2002).
5. F. Tang, X.-Z. Wang, Y. Zhang, and W. Jing, "Distributed measurement of birefringence dispersion in polarization-maintaining fibers," Opt. Lett. **31**, 3411–3413 (2006).
6. W. J. Bock and W. Urbańczyk, "Measurements of polarization mode dispersion and modal birefringence in highly birefringent fibers by means of ellectronically scanned shearing type interferometry," Appl. Opt. **32**, 5841–5848 (1993).
7. W. Urbańczyk, T. Martynkien, and W. J. Bock, "Dispersion effects in elliptical-core highly birefringent fibers," Appl. Opt. **40**, 1911–1920 (2001).
8. G. Statkiewicz, T. Martynkien, and W. Urbańczyk, "Measurement of birefringence and its sensitivity to hydrostatic pressure and elongation in photonic bandgap hollow core fiber with residual core ellipticity," Opt. Commun. **255**, 175–183 (2005).
9. K. Takada, J. Noda, and R. Ulrich, "Precision measurement of modal birefringence of highly birefringent fibers by periodic lateral force," Appl. Opt. **24**, 4387–4391 (1985).
10. P. Hlubina, "White-light spectral interferometry to measure intermodal dispersion in two-mode elliptical-core optical fibers," Opt. Commun. **218**, 283–289 (2003).

#88299 - $15.00 USD Received 5 Oct 2007; revised 30 Oct 2007; accepted 16 Nov 2007; published 5 Dec 2007

11. P. Hlubina, T. Martynkien, and W. Urbańczyk, "Dispersion of group and phase modal birefringence in elliptical-core fiber measured by white-light spectral interferometry," Opt. Express **11**, 2793–2798 (2003).
12. P. Hlubina, J. Luňáček, D. Ciprian, and R. Chlebus, "Windowed Fourier transform applied in the wavelength domain to process the spectral interference signals," submitted.
13. I. Gurov, P. Hlubina, and V. Chugunov, "Evaluation of the spectral modulated interferograms using a Fourier transform and the iterative phase locked loop method," Meas. Sci. Technol. **14**, 122–130 (2003).

1. Introduction

Polarization-maintaining fibers (PMFs) have attracted considerable interest for a number of applications, including e.g. polarization-sensitive optical devices and fiber-optic sensors of various physical quantities employing interferometric techniques. For these applications, it is important to know the dispersion, i.e. the wavelength dependence, of the phase and group modal birefringence in the PMFs. Several methods have been developed to measure the dispersion of birefringence in PMFs over a wide spectral range. A wavelength scanning technique can be applied to either short [1] or long fibers [2]. A standard technique of time-domain tandem interferometry [3] uses processing of either a single interferogram [4, 5] or a series of interferograms at different wavelengths [6, 7, 8] recorded in a tandem interferometer. The latter technique is a modification of a lateral force method proposed and demonstrated for precisely measuring the phase modal birefringence in PMFs [9].

Recently, a new measurement technique employing a low-resolution spectrometer at the output of a tandem configuration of a Michelson interferometer and an elliptical-core PMF [10, 11] has been used to measure the dispersion of group modal birefringence over a wide spectral range [11]. In comparison with the standard time-domain tandem interferometry, the technique of spectral-domain tandem interferometry uses a series of the recorded spectral interferograms to resolve the so-called equalization wavelengths [10, 11] at which the overall group optical path difference (OPD) is zero. Measuring the equalization wavelengths as a function of the OPD adjusted in a Michelson interferometer, the wavelength dependence of the group modal birefringence in the PMF is obtained [11].

In this paper, a new and simple method to measure the wavelength dependence of phase modal birefringence in an elliptical-core PMF is presented using spectral-domain white-light interferometry. The method is based on application of a lateral pointlike force on the fiber that causes strong coupling between polarization modes and utilizes their interference resolved as the spectral fringes (channeled spectrum). The phase modal birefringence as a function of wavelength is determined from the change of the phase retrieved from two recorded channeled spectra that are associated with the known displacement of coupling point. A windowed Fourier transform is applied to reconstruct precisely the phase change and the phase ambiguity is removed provided that we know the phase change of the spectral fringes at one specific wavelength. The wavelength dependence of phase modal birefringence measured over a broad spectral range is compared with that resulting from the group modal birefringence measurement and good compatibility of the results is confirmed.

2. Experimental method

Consider a PMF of length z supporting two polarization modes over a broad spectral range. We can introduce the wavelength-dependent differential propagation constant $\Delta\beta(\lambda) = \beta_x(\lambda) - \beta_y(\lambda)$, where $\beta_x(\lambda)$ and $\beta_y(\lambda)$ are propagation constants for the respective polarization modes. We define the beat length $L_B(\lambda)$ as

$$L_B(\lambda) = 2\pi/\Delta\beta(\lambda), \tag{1}$$

#88299 - $15.00 USD Received 5 Oct 2007; revised 30 Oct 2007; accepted 16 Nov 2007; published 5 Dec 2007

the phase modal birefringence $B(\lambda)$ as

$$B(\lambda) = \lambda / L_B(\lambda), \tag{2}$$

and the group modal birefringence $G(\lambda)$ as

$$G(\lambda) = B(\lambda) - \lambda \frac{\mathrm{d}B(\lambda)}{\mathrm{d}\lambda} = -\lambda^2 \frac{\mathrm{d}[B(\lambda)/\lambda]}{\mathrm{d}\lambda}. \tag{3}$$

Figure 1 illustrates a simple experimental setup we propose for measuring the wavelength dependence of phase modal birefringence $B(\lambda)$ in a PMF. Light from a white-light source passes through a polarizer and is focused by a microscope objective into the PMF under test. The transmission azimuth of the polarizer is adjusted parallel to the symmetry axis of the PMF so that only one polarization mode is excited in the tested fiber. A pointlike force is applied to the tested fiber causing polarization coupling so that a fraction of light is coupled into the polarization mode that is not excited at the input of the tested fiber. The two polarization modes are propagating through the fiber of length L, which is given by the distance of the coupling point from the fiber end. The two polarization modes are mixed with an analyzer and their interference is resolved by a spectrometer as channeled spectrum. The transmission azimuth of the analyzer is adjusted at 45° with respect to the polarization axes of the PMF. The spectrum recoded by the spectrometer of a Gaussian response function can be represented in the form [10, 11]

$$I(\lambda) = I_0(\lambda)\{1 + V(\lambda)\exp\{-(\pi^2/2)[G(\lambda)L\Delta\lambda_{\mathrm{R}}/\lambda^2]^2\}\cos[(2\pi/\lambda)B(\lambda)L]\}, \tag{4}$$

where $I_0(\lambda)$ is the reference (unmodulated) spectrum, $V(\lambda)$ is a visibility term, and λ_{R} is the width of the spectrometer response function.

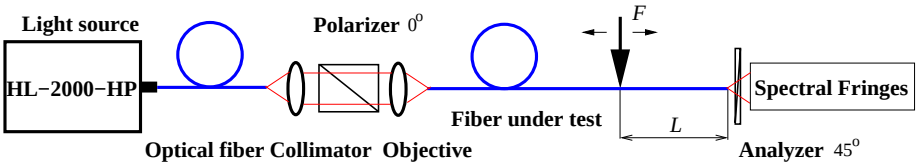

Fig. 1. Experimental setup for measuring the wavelength dependence of phase modal birefringence in fiber under test.

In response to the displacement $\Delta L = L_2 - L_1$ of the coupling point along the tested fiber, a phase shift of channeled spectrum (spectral interference fringes) is observed, from which the beat length can be determined according to the relation

$$L_B(\lambda) = 2\pi\Delta L / \Delta\phi(\lambda), \tag{5}$$

where $\Delta\phi(\lambda) = \phi_2(\lambda) - \phi_1(\lambda)$ is the wavelength-dependent phase change corresponding to two phase functions $\phi_2(\lambda)$ and $\phi_2(\lambda)$ reconstructed from two successive channeled spectra. The ambiguity of $2m\pi$, where m is an integer, in the phase retrieval from the two recorded channeled spectra can be removed by a simple procedure. In the first step we choose in the recorded spectrum interference maximum (minimum) which is resolved at one specific wavelength λ'. Next, the phase shift of the channeled spectrum with the displacement of the coupling point is inspected and in the second step we adjust such a displacement ΔL for which another maximum (minimum) is resolved in the recorded spectrum at the same wavelength λ' and the phase change $\Delta\phi(\lambda') = 2\pi$. Similarly, successive phase changes $\Delta\phi(\lambda') = 4\pi, 6\pi, \ldots$, can be adjusted at the wavelength λ'. The fiber beat length $L_B(\lambda)$ determined from Eq. (5) enables us to calculate the phase modal birefringence $B(\lambda)$ from Eq. (2).

#88299 - $15.00 USD Received 5 Oct 2007; revised 30 Oct 2007; accepted 16 Nov 2007; published 5 Dec 2007

3. Experimental configuration

The setup used for measuring the wavelength dependence of the phase modal birefringence in a PMF by spectral-domain white-light interferometry is shown in Fig. 1. It consists of a white-light source: a quartz-tungsten-halogen lamp (HL-2000-HP, Ocean Optics, Inc.) with launching optics, an optical fiber, a collimating lens, Glan Taylor calcite polarizer (Thorlabs), a microscope objective (10×/0.30), a PM fiber under test, a tip connected with a micropotioner, an analyzer (Polaroid), micropositioners, a fiber-optic spectrometer (S2000, Ocean Optics, Inc.), an A/D converter and a personal computer. The PMF under test is an elliptical-core fiber with the cutoff wavelength of 620 nm. A loop of the fiber was used to strip off the higher-order modes and to smooth the reference spectrum as much as possible. The spectrometer has a spectral operation range from 350 to 1000 nm and its spectral resolution is limited by the effective width of the light beam from the read optical fiber. We used the read optical fiber with a 50 μm core diameter which results in a Gaussian response function with the width $\Delta\lambda_{\mathrm{R}} = 2.7$ nm.

4. Experimental results and discussion

After optimizing excitation conditions to assure that only one polarization mode is excited in the tested PMF, a pointlike force was applied. Similarly, after optimizing detection conditions to assure the highest visibility of spectral interference fringes, the channeled spectrum was recorded for the first distance L_1 of the coupling point from the fiber end. Figure 2(a) shows the corresponding recorded spectrum by the blue curve. Next, the displacement $\Delta L = L_2 - L_1 = 7450$ μm of the coupling point along the tested PMF was adjusted provided that the phase change $\Delta\phi(\lambda')$ at chosen wavelength $\lambda' = 637.08$ nm is approximately 2π. Figure 2(a) shows the corresponding recorded spectrum by the red curve and illustrates the wavelength-dependent phase change, which is larger then 2π for the wavelengths shorter then λ' (see the shift to the right) and smaller then 2π for the wavelengths longer then λ' (see the shift to the left).

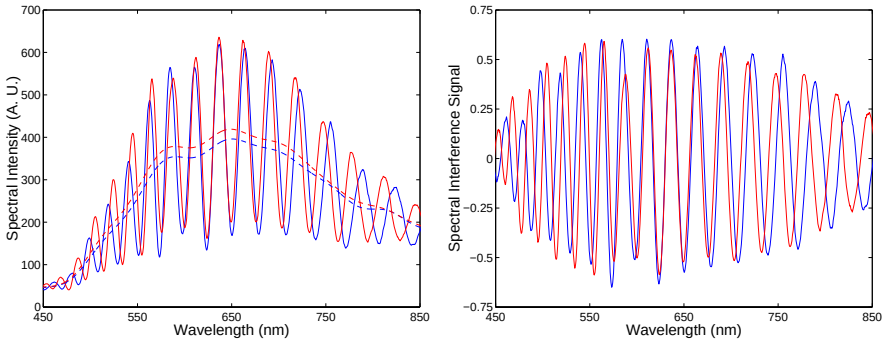

(a) (b)

Fig. 2. (a) Two recorded channeled spectra with the corresponding unmodulated spectra. (b) Two spectral interference signals constructed from the spectra shown in Fig 2(a).

To reconstruct precisely the spectral phase functions $\phi_1(\lambda)$ and $\phi_2(\lambda)$ from the two recorded channeled spectra, a new procedure of the phase retrieval in the wavelength domain was applied [12]. It is based on the processing of the spectral interference signal $S(\lambda)$ defined as

$$S(\lambda) = I(\lambda)/I_0(\lambda) - 1. \tag{6}$$

In the first step, the unmodulated spectrum $I_0(\lambda)$ needs to be reconstructed from the recorded channeled spectrum. It is obtained as the inverse Fourier transform of the zero-order com-

#88299 - $15.00 USD Received 5 Oct 2007; revised 30 Oct 2007; accepted 16 Nov 2007; published 5 Dec 2007

ponent of the Fourier spectrum of the recorded channeled signal [13]. Figure 2(a) shows the unmodulated spectra corresponding to the two recorded channeled spectra by the dashed lines. Figure 2(b) then shows the corresponding spectral interference signals that clearly illustrate the wavelength-dependent phase change. In the second step, the spectral phase functions $\phi_1(\lambda)$ and $\phi_2(\lambda)$ were retrieved from the spectral signal $S_1(\lambda)$ and $S_2(\lambda)$ using a procedure based on a windowed Fourier transform applied in the wavelength domain [12]. From the retrieved spectral phase functions, the signals $\cos[\phi_1(\lambda)]$ and $\cos[\phi_2(\lambda)]$ were constructed as shown in Fig. 3(a). Figure 3(a) once again clearly demonstrates the wavelength-dependent phase change with $\Delta\phi(\lambda^{'}) \approx 2\pi$ at $\lambda^{'} = 637.08$ nm. This fact is also confirmed in Fig. 3(b) which shows the retrieved phase difference $\Delta\phi(\lambda)$ that decreases with increasing wavelength.

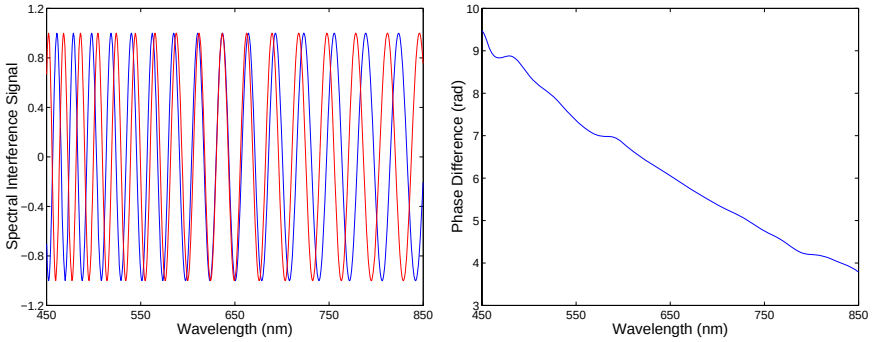

(a) (b)

Fig. 3. (a) Two spectral interference signals constructed from the retrieved phase functions $\phi_1(\lambda)$ and $\phi_2(\lambda)$ and the corresponding phase difference (b) as a function of wavelength.

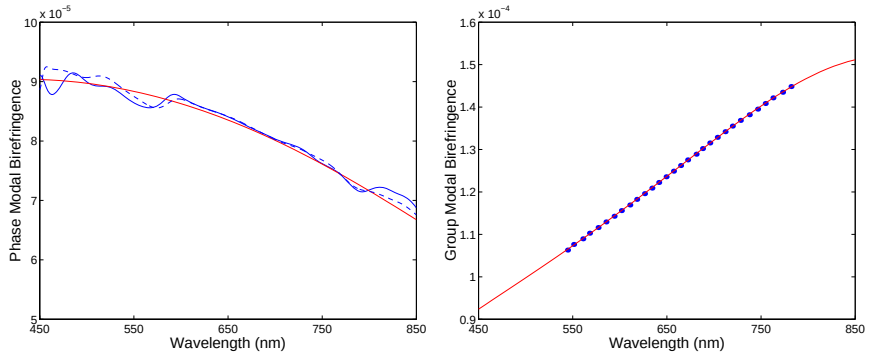

(a) (b)

Fig. 4. Phase (a) and group (b) modal birefringences measured as a function of wavelength (red curves correspond to a polynomial fit).

Figure 4(a) finally shows by the blue curve the wavelength dependence of the phase modal birefringence $B(\lambda)$ determined from Eqs. (2) and (5). These equations can be used to estimate the precision $\delta B = B\sqrt{[\delta(\Delta\phi)]^2/\Delta\phi^2 + [\delta(\Delta L)]^2/\Delta L^2}$ of the phase modal birefringence measurement, which is affected by the precision $\delta(\Delta\phi)$ with which the phase difference is known and by the precision $\delta(\Delta L)$ of adjusting the displacement. In our case we estimate $\delta(\Delta\phi) = 2\pi/100$ and $\delta(\Delta L) = 1$ μm, so that $B(\lambda^{'}) = 8.55 \times 10^{-5}$ at $\lambda^{'} = 637.08$ nm is known with precision $\delta B(\lambda^{'}) = 8.55 \times 10^{-7}$. We can also estimate the minimum B_{min} and

#88299 - $15.00 USD Received 5 Oct 2007; revised 30 Oct 2007; accepted 16 Nov 2007; published 5 Dec 2007

maximum B_{max} birefringences that can be measured by the technique. The minimum birefringence is given by $B_{min}(\lambda) = \lambda\Delta\phi/(2\pi\Delta L_{max})$, where ΔL_{max} is the maximum displacement adjustable in the setup. For $\Delta L_{max} = 2.5$ cm (travel of the micropositioner) and $\Delta\phi = 2\pi$ we obtain $B_{min}(\lambda) = 2.6\times10^{-5}$ at $\lambda = 650$ nm. The maximum birefringence is limited by the resolution of the channeled spectra [see the overall visibility in Eq. (4)] and is given on the assumption $B(\lambda) = G(\lambda)$ by $B_{max}(\lambda) = [\lambda^2/(\pi\Delta\lambda_{\mathrm{R}}L)]\sqrt{\ln 2/V_{\mathrm{R}min}}$, where $V_{\mathrm{R}min}$ is the minimum visibility. For $L = 1$ cm and $V_{\mathrm{R}min} = 0.5$, we obtain $B_{max}(\lambda) = 5.9\times10^{-3}$ at $\lambda = 650$ nm.

The measured phase modal birefringence $B(\lambda)$ in the elliptical-core PMF can be compared with that resulting from the group modal birefringence $G(\lambda)$ measured by a method of spectral-domain tandem interferometry [11]. Figure 4(b) shows by markers the group modal birefringence $G(\lambda_0)$ determined for respective wavelengths λ_0. The red line in the same figure represents the group modal birefringence $G(\lambda)$ obtained from the values $-G(\lambda_0)/\lambda_0^2$ fitted to a fourth-order polynomial. The polynomial order is sufficiently high because the fit is characterized by a correlation factor as high as 0.99998. The corresponding absolute phase modal birefringence $B(\lambda)$, with $B(\lambda)/\lambda$ represented by a fifth-order polynomial, is shown in Fig. 4(a) by the red curve. It was obtained by combining the relative phase modal birefringence $B(\lambda)$ with the measured one [blue curve in Fig. 4(a)] to reach minimal deviation between them. The difference between the determined values is approximately within $\pm2.6\times10^{-6}$. In order to reduce the deviation, the larger displacement ΔL of the coupling point along the tested PMF has to be adjusted. In our case we adjusted $\Delta L = 14900$ μm with $\Delta\phi(\lambda') \approx 4\pi$ at $\lambda' = 637.08$ nm. The corresponding phase modal birefringence $B(\lambda)$ is shown by the dashed curve and the above difference is approximately within $\pm2\times10^{-6}$. The difference can be attributed to the distortions of the channeled spectra and thus the retrieved phase difference [see Fig. 3(b)] due to the wavelength-dependent polarization coupling and/or the presence of the residual higher-order modes supported by the fiber.

5. Conclusions

We used a new and simple spectral-domain method to measure the wavelength dependence of the phase modal birefringence in an elliptical-core PMF over a wide spectral range (450 to 850 nm). The method is based on a lateral pointlike force applied on the fiber that causes strong coupling between polarization modes and resolving the channeled spectrum arising due to interference of the modes. The change of the phase retrieved from two recorded channeled spectra that are associated with the known displacement of coupling point was used for determining the phase modal birefringence as a function of wavelength. The phase change was reconstructed precisely by a windowed Fourier transform and the phase ambiguity was removed provided that the phase change of the spectral fringes at one specific wavelength is known. The measured wavelength dependence of phase modal birefringence was compared with that resulting from the group modal birefringence measurement. Good compatibility of the results was confirmed.

We demonstrated the applicability of the spectral-domain white-light interferometric technique that can be extended for dispersion characterizing of other fibers guiding two polarization modes over a wide spectral range (Panda and bow-tie fibers, PCFs). Moreover, if the proposed technique is combined with the data from group modal birefringence dispersion measurement, then the obtaining of phase modal birefringence dispersion can be substantially simplified because the measurement can be performed at one specific wavelength (e. g., λ') only.

Acknowledgements

The research was partially supported by the Grant Agency of the Czech Republic (project No. 102/06/0284), by the grant MSM6198910016, and by the COST Action P11.

#88299 - $15.00 USD Received 5 Oct 2007; revised 30 Oct 2007; accepted 16 Nov 2007; published 5 Dec 2007

Paper VII.

Absolute phase birefringence dispersion in polarization-maintaining fiber or birefringent crystal retrieved from a channeled spectrum

Petr Hlubina* and Dalibor Ciprian

Department of Physics, Technical University Ostrava, 17. listopadu 15, 708 33 Ostrava-Poruba, Czech Republic
**Corresponding author: petr.hlubina@vsb.cz*

Received February 5, 2010; revised March 22, 2010; accepted March 30, 2010;
posted April 6, 2010 (Doc. ID 123892); published May 5, 2010

We report on a simple method for retrieving the wavelength dependence of the phase birefringence in a polarization-maintaining fiber or a birefringent crystal from a channeled spectrum. The method utilizes interference of polarized modes or waves resolved as the channeled spectrum and its processing by a windowed Fourier transform to reconstruct precisely the phase as a function of wavelength. The ambiguity of the phase is removed provided that we know both the approximative function for the birefringence dispersion and the length of the fiber or the thickness of the crystal. The method is used in measuring the wavelength dependence of the phase birefringence in an elliptical-core fiber or in a quartz crystal in a range from 500 to 900 nm. The dependences are compared with those resulting from the available data, and very good agreement is confirmed.

OCIS codes: 060.2300, 060.2420, 120.3180, 260.1180, 260.1440, 260.2030.

Highly birefringent, polarization-maintaining fibers (PMFs) have attracted considerable interest for a number of applications, including, e.g., polarization-sensitive optical devices and fiber-optic sensors of various physical quantities employing interferometric techniques. For these applications, it is important to know the birefringence dispersion, i.e., the wavelength dependence of the phase and group birefringence in the PMFs. Several methods have been developed to measure the phase birefringence in PMFs over a wide spectral range. A wavelength scanning technique can be applied to either short [1] or long [2] fibers.

It is well known that scanning the wavelength alone (a channeled spectrum) gives only a relative measure of the phase birefringence, and it inherently measures the group birefringence. The absolute phase birefringence is obtained by both scanning the wavelength and absolutely measuring the birefringence at one particular wavelength. To measure this quantity, a precision electromagnetic modulation technique [1] or a lateral force method [3] applied in the time [4] or wavelength [5] domain can be used. Similarly, the birefringence dispersion is of fundamental importance for anisotropic materials used in optical devices such as wave plates, compensators, retarders, and polarizers. Measurement of the phase birefringence of a prescribed dispersion function can be performed by spectral interferometric techniques based on either determining the positions of the maxima in a channeled spectrum [6] or fitting the measured spectrum to the theoretical one [7].

In this Letter, a simple method for retrieving the wavelength dependence of the phase birefringence in a PMF of known length is presented. The technique, which is based on processing of a channeled spectrum to retrieve the phase function, utilizes the approximative function of the phase birefringence dispersion. We extended the use of the technique for measuring the phase birefringence in a quartz crystal of known thickness.

Consider a PMF supporting two polarization modes over a broad spectral range. We can introduce the wavelength-dependent phase birefringence $B(\lambda) = n_x(\lambda) - n_y(\lambda)$, where $n_x(\lambda)$ and $n_y(\lambda)$ are the effective phase refractive indices for the respective polarization modes. Figure 1 illustrates a simple experimental setup we use for recording of a channeled spectrum from which we retrieve the wavelength dependence of $B(\lambda)$ in a PMF, if its length L is known precisely. Light from white-light source WLS passes through collimator CL and polarizer P and is launched by microscope objective O1 into the PMF under test. The transmission azimuth of the polarizer is adjusted at 45° with respect to the polarization axes of the PMF so both polarization modes are excited equally in the tested fiber. The two polarization modes are mixed with analyzer A, which is placed between microscope objectives O2 and O3, and their interference is resolved by spectrometer S as a channeled spectrum. The transmission azimuth of the analyzer is adjusted at 45° with respect to the polarization axes of the PMF. The spectral intensity recoded by the spectrometer of a Gaussian response function can be represented in the form [8]

$$I(\lambda) = I_0(\lambda)\{1 + V_R(\lambda)\cos[(2\pi/\lambda)B(\lambda)L]\}, \qquad (1)$$

where $I_0(\lambda)$ is the reference (unmodulated) spectrum and $V_R(\lambda) = \exp\{-(\pi^2/2)[G(\lambda)L\Delta\lambda_R/\lambda^2]^2\}$ is a visibility

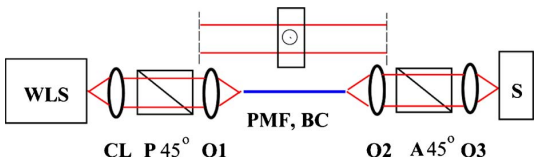

Fig. 1. (Color online) Experimental setup to record a channeled spectrum for a PMF or a birefringent crystal.

0146-9592/10/101566-3/$15.00

term dependent on both the group birefringence $G(\lambda)=-\lambda^2 d[B(\lambda)/\lambda]/d\lambda$ and the width $\Delta\lambda_R$ of the spectrometer response function. To resolve a channeled spectrum (spectral fringes) in a spectral range from λ_1 to λ_2, the fiber length must satisfy the condition $L<\lambda_1^2/[G(\lambda_1)\Delta\lambda_R]$.

From the recorded channeled spectrum, a relative spectral phase $\Phi_r(\lambda)$ can be retrieved with the ambiguity of $m2\pi$, where m is an integer. To remove the phase ambiguity, we assume that the phase birefringence dispersion is given by the relation [9]

$$B(\lambda)=A_1\lambda^{-4}+A_2\lambda^{-2}+A_3+A_4\lambda^2+A_5\lambda^4, \qquad (2)$$

where A_i are the coefficients. The difference between the retrieved phase function and the absolute phase function is the phase error function

$$e(\lambda)=\Phi_r(\lambda)+m2\pi-(2\pi/\lambda)B(\lambda)L, \qquad (3)$$

which is a measure of the correct determination of the coefficients A_i and the interference order m. In an ideal case $e(\lambda)=0$.

The experimental setup used for measurement of the phase birefringence $B(\lambda)$ in a PMF is shown schematically in Fig. 1, and it consists of a halogen lamp HL-2000 (Ocean Optics), a collimating lens, microscope objectives ($10\times/0.30$), a Glan–Taylor calcite polarizer and analyzer (Thorlabs), an elliptical-core PMF of length $L=(356.5\pm0.5)$ mm, a fiber-optic spectrometer S2000 (Ocean Optics), and other components. The PMF has a core made of GeO_2-doped silica glass (19.3 mol. %) and a cladding made of pure silica. The dimensions of the fiber elliptical core are approximately $3.2\ \mu m\times1.2\ \mu m$. The spectrometer, with $\Delta\lambda_R\approx3$ nm, has a spectral operation range from 350 to 1000 nm.

We demonstrate the ability of our method in measuring the phase birefringence $B(\lambda)$ in the PMF for which the channeled spectrum shown in Fig. 2 was recorded. It is clearly seen that a large number of the spectral interference fringes of sufficiently high visibility are resolved. The procedure used to retrieve a relative spectral phase $\Phi_r(\lambda)$ from the recorded channeled spectrum comprises two steps. In the first step, the reference spectrum $I_0(\lambda)$ is retrieved from the channeled spectrum $I(\lambda)$. It is obtained as the inverse Fourier transform of the zero-order component of the Fourier spectrum of the recorded channeled spectrum. In the second step, the spectral phase function $\Phi_r(\lambda)$ is retrieved from the spectral signal $S(\lambda)=I(\lambda)/I_0(\lambda)-1$ using a procedure based on a windowed Fourier transform [10].

The procedure used in the determining the coefficients A_i in Eq. (2) consists of two steps. In the first step, a trust-region algorithm [11] is used for the retrieved $\Phi_r(\lambda)$ to estimate m and A_i, which give the absolute phase function. The integer value of m is used in the second step when the coefficients A_i are obtained by using the Levenberg–Marquardt least-squares algorithm, which minimizes the function $\chi^2=\sum_{i=1}^{N}e^2(\lambda_i)$, where λ_i are wavelengths at which the spectrum was recorded. The procedure gives the phase error function $e(\lambda)$ shown in Fig. 2. Note that this function consists of the artifacts (due to the phase retrieval procedure [10]) that oscillate around the zero value. Using the coefficients A_i and Eq. (2), the absolute phase birefringence $B(\lambda)$ shown in Fig. 3 was determined. For an error of ±0.5 mm in the length of the PMF a relative error in the birefringence is about 0.1%. The contribution of the phase error $e(\lambda)=\pm0.1$ rad to the relative error is even smaller. In Fig. 3 is also shown the birefringence $B(\lambda)$ measured over a broader wavelength range. It was retrieved from the group birefringence $G(\lambda)$ measured by a technique of tandem interferometry [12] and using $B(\lambda_0)=8.55\times10^{-5}$ at $\lambda_0=637.08$ nm measured by a lateral force method applied in the wavelength domain [5]. There is a nearly constant shift between these dependences, and our method gives $B(\lambda_0)=7.32\times10^{-5}$, which represents a 14% difference between the measurement results. The discrepancy is probably caused by different birefringences of fiber samples used in the experiments. Figure 3 demonstrates very good agreement between the group birefringences $G(\lambda)$ measured by both techniques.

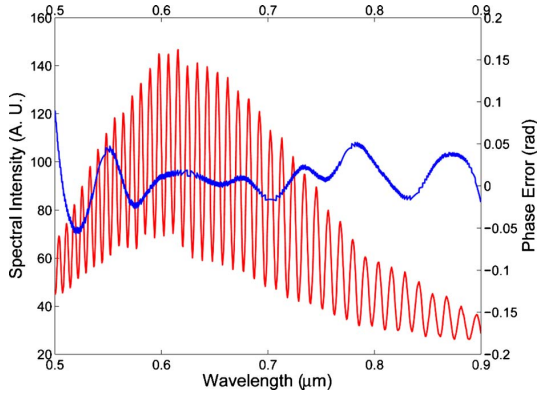

Fig. 2. (Color online) Channeled spectrum recorded for a PMF and the phase error function $e(\lambda)$ obtained by our procedure.

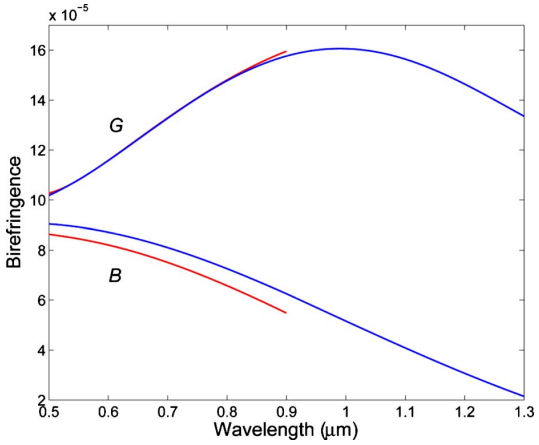

Fig. 3. (Color online) Retrieved phase and group birefringences, $B(\lambda)$ and $G(\lambda)$, for a PMF compared with those measured over a broader spectral range.

We extended the use of our method in determining the phase birefringence $B_f(\lambda)=n_e(\lambda)-n_o(\lambda)$ in a quartz crystal, where $n_e(\lambda)$ and $n_o(\lambda)$ are the phase refractive indices of the extraordinary and ordinary eigenwaves, respectively. Our setup was modified (see the upper part of Fig. 1), and for the crystal of thickness $t=(4010\pm1)$ μm and the orientation of the optic axis shown in Fig. 1 we recorded the channeled spectrum shown in Fig. 4. It is clearly seen that a large number of the spectral interference fringes of sufficiently high visibility are resolved. The number of the spectral fringes in the wavelength range from 500 to 900 nm is given by the group path difference $G_f(\lambda)t$ in the crystal. Using the same procedure as presented above, we retrieved the absolute birefringence $B_f(\lambda)$ shown in Fig. 5. For the phase error $e(\lambda)\approx0.03$ rad a relative error in the birefringence is about 0.03%. The contribution of the thickness uncertainty to the relative error is even smaller. The same figure shows the birefringence $B_f(\lambda)$ resulting from the Sellmeier-like form of the dispersion relation for the quartz crystal [8]. We clearly see that there is very good agreement between these dependences, which have slightly different dispersion slopes. This is illustrated in Fig. 5 that shows the dispersion functions for the group birefringence $G_f(\lambda)=-\lambda^2 d[B_f(\lambda)/\lambda]/d\lambda$. The difference between them, which is in general dependent on the fitting function, is in part caused by the approximation (2) of the phase birefringence dispersion $B_f(\lambda)$ we used.

In conclusion, a simple technique for retrieving the absolute phase birefringence from a channeled spectrum has been presented. It utilizes the approximative function of the birefringence dispersion and the phase retrieval using a windowed Fourier transform.

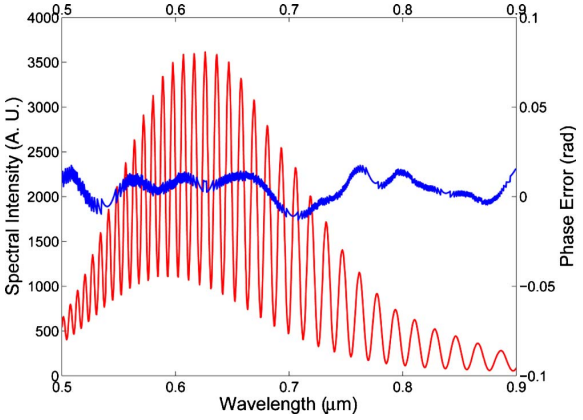

Fig. 4. (Color online) Channeled spectrum recorded for a birefringent quartz and the phase error function $e(\lambda)$ obtained by our procedure.

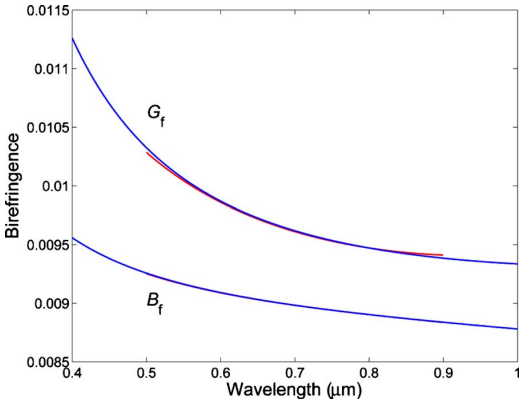

Fig. 5. (Color online) Retrieved phase and group birefringences, $B_f(\lambda)$ and $G_f(\lambda)$, for a birefringent quartz compared with those given by the dispersion relation.

The feasibility of the technique has been demonstrated in measuring the phase birefringence in a PMF or in a quartz crystal. We confirmed very good agreement with the available data. The use of the technique can be extended, e.g., for retrieving the dispersion of the differential phase refractive index from a channeled spectrum originated from interference of two spatial modes guided in a fiber.

The research has been partially supported by the Ministry of Education, Youth and Sports of the Czech Republic through grant MSM6198910016 and by the regional grant CZ.1.05/2.1.00/01.0040.

References

1. S. C. Rashleigh, Opt. Lett. **7**, 294 (1982).
2. M. G. Shlyagin, A. V. Khomenko, and D. Tentori, Opt. Lett. **20**, 869 (1995).
3. K. Takada, J. Noda, and R. Ulrich, Appl. Opt. **24**, 4387 (1985).
4. W. J. Bock and W. Urbanczyk, Appl. Opt. **32**, 5841 (1993).
5. P. Hlubina and D. Ciprian, Opt. Express **15**, 17019 (2007).
6. M. Medhat and S. Y. El-Zaiat, Opt. Commun. **141**, 145 (1997).
7. H. Delbarre, M. Przygodzki, C. Tassou, and D. Boucher, Appl. Phys. B **70**, 45 (2000).
8. P. Hlubina, D. Ciprian, and L. Knyblova, Opt. Commun. **260**, 535 (2006).
9. M. Tsubokawa, N. Shibata, T. Higashi, and S. Seikai, J. Opt. Soc. Am. A **4**, 1895 (1987).
10. P. Hlubina, J. Lunacek, D. Ciprian, and R. Chlebus, Opt. Commun. **281**, 2349 (2008).
11. *Curve Fitting Toolbox for Use with MATLAB* (MathWorks, 2000).
12. P. Hlubina, D. Ciprian, and M. Kadulova, Meas. Sci. Technol. **20**, 025301 (2009).

Paper VIII.

IOP PUBLISHING MEASUREMENT SCIENCE AND TECHNOLOGY

Meas. Sci. Technol. **21** (2010) 045302 (7pp) doi:10.1088/0957-0233/21/4/045302

Measurement of chromatic dispersion of polarization modes in optical fibres using white-light spectral interferometry

P Hlubina[1], **D Ciprian and M Kadulová**

Department of Physics, Technical University Ostrava, 17. listopadu 15, 708 33 Ostrava-Poruba, Czech Republic

E-mail: petr.hlubina@vsb.cz

Received 16 October 2009, in final form 8 January 2010
Published 3 March 2010
Online at stacks.iop.org/MST/21/045302

Abstract

We report on a white-light interferometric technique for a broad spectral range measurement (e.g. 500–1600 nm) of chromatic dispersion of polarization modes in short-length optical fibres. The technique utilizes an unbalanced Mach–Zehnder interferometer with a fibre under test of known length inserted in one of the interferometer arms and the other arm with adjustable path length. We record a series of spectral interferograms by VIS–NIR and NIR fibre-optic spectrometers to measure the equalization wavelength as a function of the path length difference, or equivalently the differential group index dispersion of one polarization mode. The differential group dispersion of the other polarization mode is obtained from measurement of the group modal birefringence dispersion. We verify the applicability of the method by measuring the chromatic dispersion of polarization modes in a birefringent holey fibre. We apply a five-term power series fit to the measured data and confirm by its differentiation that the chromatic dispersion agrees well with that specified by the manufacturer. We also measure by this technique the chromatic dispersion of polarization modes in an elliptical-core fibre.

Keywords: spectral interferometry, white-light source, Mach–Zehnder interferometer, group refractive index, chromatic dispersion, holey fibre, elliptical-core fibre

1. Introduction

A precise measurement of the group index dispersion of optical fibres over a broad spectral range is important in various research areas including high-speed optical transmission systems, broadband optical communications and supercontinuum generation. The chromatic dispersion, which can be obtained by simply differentiating the group index, is a significant characteristic that affects the bandwidth of a high-speed optical transmission system through pulse broadening and nonlinear optical distortion. Chromatic dispersion of long-length optical fibres is determined by two widely used methods [1]: the time-of-flight method, which measures relative temporal delays for pulses at different wavelengths, and the modulation phase shift technique [2], which measures the phase delay of a modulated signal as a function of wavelength.

White-light interferometry based on the use of a broadband source in combination with a standard Michelson or a Mach–Zehnder interferometer [3] is considered as one of the best tools for dispersion characterization of short-length optical fibres. White-light interferometry usually utilizes a temporal method or a spectral method. The temporal method involves measurement of the group delay introduced by an optical fibre which is placed in one of the interferometer arms and evaluating the temporal shift of the peak of the cross-correlation interferogram. As the central wavelength is varied, the relative group delay of different frequency components is observed directly [4]. Alternatively, the spectral distribution of the phase delay over the full bandwidth of the white-light source is obtained in a single measurement by a Fourier transform of the cross-correlation interferogram [5]. The dispersion characteristics of the fibre sample under study

[1] Author to whom any correspondence should be addressed.

can be obtained by simply differentiating the measured phase delay.

The spectral method is based on the observation of spectrally resolved interference fringes (channelled spectrum) in the vicinity [6–11] of a stationary-phase point or far from it [12] and involves measurement of the phase or period of the spectral fringes. The stationary-phase point appears in the recorded spectral interferogram when the overall group optical path difference (OPD) between two beams in the interferometer is close to zero. The main limitation of this method is related to the fact that the spectral interference fringes far from the stationary-phase point [12] become difficult to resolve. The measurement of the group refractive index dispersion of a given fibre is still possible in the vicinity of the stationary-phase point if one moves it in successive steps to different wavelengths and repeats the measurement.

The feasibility of the interferometric techniques has been demonstrated in measuring the dispersion in microstructured and holey fibres [13–19]. Recently, the dispersion of birefringent microstructured fibres useful in generating controllable supercontinuum has been investigated [20]. Both fibre-optic [14, 17] and bulk-optic [15, 16, 18–20] implementations of a Michelson [14, 15, 17] or a Mach–Zehnder [16, 18, 20] interferometer were utilized. The dispersion parameters were obtained either by fitting the measured spectrum to the theoretical one when the location of the stationary-phase point was adjusted by the path length in air [14, 19] or by measuring the location of the stationary-phase point (the equalization wavelength [16]) as a function of the path length difference [15, 16, 18].

The aim of this paper is to present a technique based on white-light spectral interferometry for measuring the chromatic dispersion of polarization modes in short-length optical fibres over a broad wavelength range (e.g. 500–1600 nm). The technique comprises the recording of a series of spectral interferograms in a Mach–Zehnder interferometer with the fibre of known length placed in one of the interferometer arms and the other arm with adjustable path length. We measure the equalization wavelength as a function of the path length difference, or equivalently the differential group index dispersion of one polarization mode. The differential group dispersion of the other polarization mode is obtained from measurement of the group modal birefringence dispersion. First, we verify the applicability of the method by measuring the chromatic dispersion of polarization modes in a birefringent holey fibre. We confirm very good agreement with data specified by the manufacturer. Second, we measure the chromatic dispersion of polarization modes in an elliptical-core fibre.

2. Experimental method

Let us consider an unbalanced Mach–Zehnder interferometer (see figure 1) with a fibre under test of length z that supports two polarization modes over a broad wavelength range with the effective refractive indices $n_x(\lambda)$ and $n_y(\lambda)$. The interferometer includes optical components (lens 1 and lens 2) to which the effective thickness d and refractive index $n_c(\lambda)$ correspond. The fibre is inserted into the first (test) arm of the interferometer and the other (reference) arm has the adjustable path length L in air. If the polarizer at the output of the interferometer discriminates the x polarization only, the OPD $\Delta_{MZ}(\lambda)$ and the group OPD $\Delta^{g}_{MZ}(\lambda)$ between the beams in the interferometer are given by

$$\Delta_{MZ}(\lambda) = L - l - n_x(\lambda)z - n_c(\lambda)d, \tag{1}$$

and

$$\Delta^{g}_{MZ}(\lambda) = L - l - N_x(\lambda)z - N_c(\lambda)d, \tag{2}$$

where l is the path length in the air in the test arm and $N_x(\lambda)$ and $N_c(\lambda)$ are the group refractive indices satisfying the relation

$$N(\lambda) = n(\lambda) - \lambda\frac{\mathrm{d}n(\lambda)}{\mathrm{d}\lambda}. \tag{3}$$

Let us consider now that the spectral interference fringes can be resolved by a spectrometer used at the output of the Mach–Zehnder interferometer. The spectral signal (interference fringes) recorded by the spectrometer of a Gaussian response function is given by [26]

$$S_{MZ}(\lambda) = 1 + V(\lambda)\exp\left\{-(\pi^2/2)\left[\Delta^{g}_{MZ}(\lambda)\Delta\lambda_R/\lambda^2\right]^2\right\} \times \cos[(2\pi/\lambda)\Delta_{MZ}(\lambda)], \tag{4}$$

where $V(\lambda)$ is a visibility term dependent on the overlap of the beams from the test and the reference arms, and $\Delta\lambda_R$ is the width of the spectrometer response function, which affects the number of fringes resolved.

The spectral interference fringes recorded in the set-up have the highest visibility and the largest period in the vicinity of a stationary-phase point for which the group OPD $\Delta^{g}_{MZ}(\lambda)$ is zero at one specific wavelength λ_0, referred to as the equalization wavelength [22]. The condition $\Delta^{g}_{MZ}(\lambda_0) = 0$ gives for the overall path length $L = L_o = L_o(\lambda_0)$ for which the equalization wavelength λ_0 is resolved in the recorded spectrum the relation

$$L_o(\lambda_0) = N_x(\lambda_0)z + N_c(\lambda_0)d + l. \tag{5}$$

If we choose one of the equalization wavelengths, λ_{0r}, as the reference one, we can introduce the overall path length difference $\Delta L_o(\lambda_0) = L_o(\lambda_0) - L_o(\lambda_{0r})$ given by

$$\Delta L_o(\lambda_0) = \Delta N_x(\lambda_0)z + \Delta N_c(\lambda_0)d, \tag{6}$$

where $\Delta N_x(\lambda_0) = N_x(\lambda_0) - N_x(\lambda_{0r})$ and $\Delta N_c(\lambda_0) = N_c(\lambda_0) - N_c(\lambda_{0r})$ are the corresponding differential group refractive indices.

Next, let us consider the unbalanced Mach–Zehnder interferometer in which the fibre is removed and which is used for measuring the differential group dispersion of the optical components [22]. This differential group dispersion has to be subtracted from the overall group dispersion to determine the group dispersion of the fibre polarization mode alone. The corresponding path length difference is denoted as $\Delta L_c(\lambda_0) = L_c(\lambda_0) - L_c(\lambda_{0r})$ and is given by

$$\Delta L_c(\lambda_0) = \Delta N_c(\lambda_0)d. \tag{7}$$

Using equations (6) and (7), we obtain the relation

$$\Delta N_x(\lambda_0) = [\Delta L_o(\lambda_0) - \Delta L_c(\lambda_0)]/z, \tag{8}$$

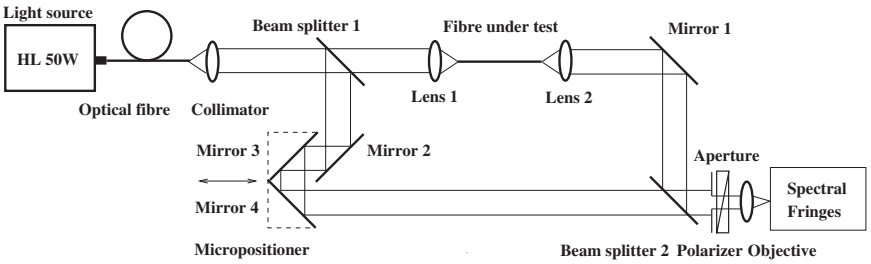

Figure 1. Experimental set-up with an unbalanced Mach–Zehnder interferometer to measure the chromatic dispersion of polarization modes in optical fibres.

which means that the differential group index $\Delta N_x(\lambda_0)$ of the x-polarization mode in the fibre can be measured directly as a function of the equalization wavelength λ_0.

The measured wavelength dependence of the differential group refractive index can be fitted to a function $\Delta N_x(\lambda)$ from which the chromatic dispersion $D_x(\lambda)$ can be evaluated by using the relation

$$D_x(\lambda) = \frac{1}{c}\frac{\mathrm{d}[\Delta N_x(\lambda)]}{\mathrm{d}\lambda}, \tag{9}$$

where c is the velocity of light in vacuum. Similarly, if the polarizer at the output of the interferometer discriminates the y polarization only, both the differential group index $\Delta N_y(\lambda_0)$ and chromatic dispersion $D_y(\lambda)$ of the y-polarization mode in the fibre can also be measured.

For highly birefringent fibres supporting two polarization modes a simple white-light spectral interferometric technique employing a Michelson interferometer [23] is also available that can be used for measuring the group modal birefringence $G(\lambda)$ defined as

$$G(\lambda) = N_x(\lambda) - N_y(\lambda). \tag{10}$$

From the group modal birefringence $G(\lambda)$ we can deduce the chromatic-dispersion difference $D_p(\lambda)$ defined as

$$D_p(\lambda) = D_x(\lambda) - D_y(\lambda) = \frac{1}{c}\frac{\mathrm{d}[G(\lambda)]}{\mathrm{d}\lambda}, \tag{11}$$

or the chromatic dispersion $D_y(\lambda)$ of the y-polarization mode if the chromatic dispersion $D_x(\lambda)$ of the x-polarization mode is known.

3. Experimental set-up

The experimental set-up used in the application of spectral-domain white-light interferometry for measuring the chromatic dispersion of polarization modes in optical fibres is shown in figure 1. It consists of a white-light source: a quartz–tungsten–halogen lamp (50 W) with launching optics, optical fibre of cut-off wavelength as short as possible, a collimating lens, a bulk-optic Mach–Zehnder interferometer with plate beam splitters (BSW07, Thorlabs), a micropositioner connected to mirrors 3 and 4 of the interferometer, an aperture, a Glan–Taylor polarizer (Thorlabs), a microscope objective, micropositioners, a fibre-optic spectrometer (S2000, NIR-512, Ocean Optics), an A/D converter and a personal computer. The spectral signal is recorded by the spectrometer in the transmission mode after a dark spectrum and a reference one (without the interference) are stored. The spectrometers S2000 and NIR-516 have a spectral operation range from 350 to 1000 nm and from 850 to 1700 nm, respectively. For both spectrometers we used the read optical fibre with a 50 μm core diameter which results in a Gaussian response function with $\Delta\lambda_R \approx 3$ nm for the first one [26]. In the test arm of the interferometer a combination of a fibre under test (fibre sample) and optical components (shown schematically in figure 1 as lens 1 and lens 2) represented by a microscope objective (10×/0.30, Meopta) and an achromatic lens (74-ACR, Ocean Optics) is placed.

We measured the chromatic dispersion of polarization modes for two different samples of birefringent fibres. The first sample is pure silica highly birefringent holey fibre of length $z = 48\,850$ μm (PM-1550-01, Thorlabs, see its SEM photograph in [21]). The geometrical parameters of the holey fibre are as follows: pitch distance 4.30 μm, diameter of large holes 4.42 μm and diameter of the cladding holes 2.34 μm. This fibre supports the *even* LP_{11} spatial mode for wavelengths shorter than 1 μm. The second sample is an elliptical-core highly birefringent fibre of length $z = 60\,500$ μm with the core made of GeO_2-doped silica glass (19.3 mol%) and the cladding made of pure silica. The dimensions of the fibre elliptical core are approximately 3.2 μm × 1.2 μm. The fibre supports the *even* LP_{11} spatial mode for wavelengths shorter than 630 nm. The fibre lengths were measured by a micrometer with an accuracy of ±10 μm. The wavelength dependence of the group modal birefringence $G(\lambda)$ in fibres under test was measured by a technique of spectral-domain tandem interferometry [23].

4. Experimental results and discussion

Prior to the measurement we utilized the main advantage of the set-up, which is in fibre connection of a light source (that can be varied) with the interferometer. We used a laser diode ($\lambda \approx 670$ nm) instead of the halogen lamp to check the precise placement and alignment of the optical components in the test arm by observing the interference pattern. Moreover, the proper excitation of the fibre core by a microscope objective was easily inspected at the output of the test arm. Even if we used short-length fibres in which higher order modes can

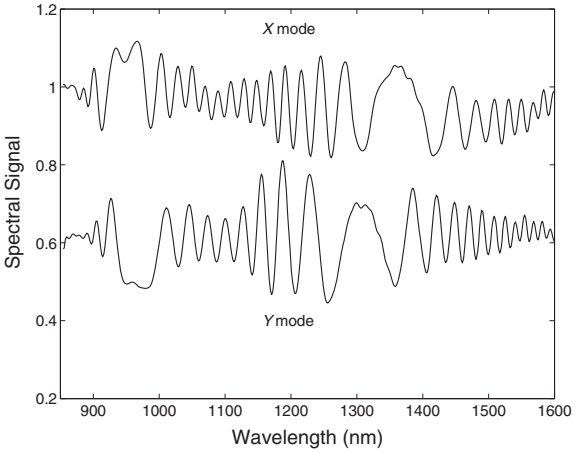

Figure 2. Examples of the spectral signals recorded for two polarization modes and the same path length difference adjusted in the interferometer.

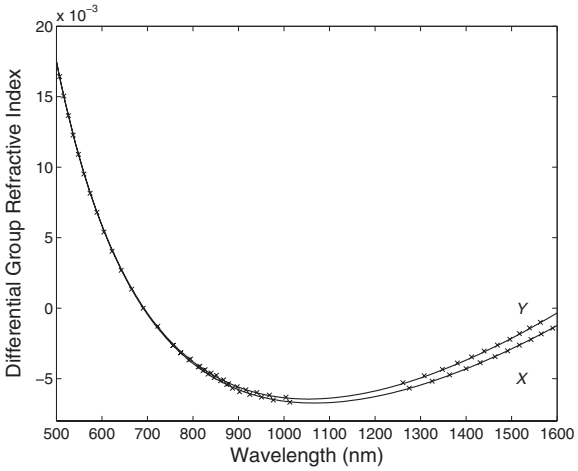

Figure 3. Measured differential group refractive indices (crosses) for two polarization modes as a function of the wavelength with the corresponding fits (solid lines).

propagate, the excitation of only the fundamental mode was reached. This was indicated by the elliptical-shape far-field pattern of the fundamental mode (with the laser diode) and by the spectral signals (with the halogen lamp) not distorted by the higher order modes. Note that the long axis of the far-field pattern is along the short axis of the elliptical core of the fibre. In order to measure the chromatic dispersion of the x- or y-polarization mode, the polarizer needs to be oriented along the short or the long axis of the far-field pattern.

In the dispersion measurement, such a path length in the reference arm of the interferometer was adjusted to resolve spectral interference fringes and to determine the equalization wavelength. We displaced the stage with mirrors 3 and 4 manually by using the micropositioner with a constant step ranging from 10 to 50 μm and performed recording of the corresponding spectral signals. The spectral signals recorded by the first spectrometer (S2000) revealed that the equalization wavelength λ_0 can be resolved in the spectral range from 509 to 888 nm. Similarly, the spectral signals recorded by the second spectrometer (NIR-516) revealed that the equalization wavelength λ_0 can be resolved in the spectral range from 902 to 1591 nm. Figure 2 shows an example of the spectral signal recorded by the second spectrometer when the polarizer was oriented along the longer axis of the elliptical core of the first fibre sample. It clearly shows the effect of the limiting resolving power of the spectrometer on the visibility of the spectral interference fringes (see equation (4)) in the vicinities of two different equalization wavelengths $\lambda_{01} = 950.57$ nm and $\lambda_{02} = 1363.52$ nm. This is due to the minimum in the group index $N_x(\lambda)$ or in the differential group index $\Delta N_x(\lambda)$ located between the wavelengths λ_{01} and λ_{02}. In figure 2 is also shown an example of the spectral signal recorded for the same path length adjusted in the reference arm of the interferometer and for the y-polarization mode when the spectral interference fringes are resolved in the vicinities of two different equalization wavelengths $\lambda_{01} = 967.86$ nm and $\lambda_{02} = 1308.06$ nm.

In our case, when the differential group index $\Delta N_y(\lambda_0)$ is higher than $\Delta N_x(\lambda_0)$, two orientations of the polarizer enable the apparent discrimination between the spectral signals corresponding to the two polarization modes. This is illustrated in figure 3 which shows by the crosses the measured differential group indices $\Delta N_x(\lambda_0)$ and $\Delta N_y(\lambda_0)$ for the first fibre sample determined for respective equalization wavelengths λ_0 when the group dispersion of the optical components was subtracted [22]. Note that some experimental data are missed due to the superimposed interference fringes for which the equalization wavelengths cannot be resolved. The equalization wavelengths were determined by the autoconvolution method [27] with errors of 0.3 or 1.7 nm corresponding to the wavelength difference for adjacent pixels of the linear array detectors of the spectrometers. The measured differential group index $\Delta N_x(\lambda_0)$ is shown in figure 3 by the lower crosses, together with a five-term power series fit [17]

$$\Delta N_x(\lambda) = \frac{a_1}{\lambda^4} + \frac{a_2}{\lambda^2} + a_3 + a_4\lambda^2 + a_5\lambda^4. \tag{12}$$

For the same fibre we measured by a technique of white-light spectral interferometry (see a previous paper [22]) the group modal birefringence $G(\lambda)$ as a function of the wavelength λ. It is shown in figure 4 by the crosses together with a fit using the relation

$$G(\lambda) = (1 - m)\xi\lambda^m, \tag{13}$$

where ξ and m are constants. This relation results from the works [24, 25] treating air–silica birefringent holey fibres in such a way that the phase modal birefringence $B(\lambda) = n_x(\lambda) - n_y(\lambda)$ can be approximated as

$$B(\lambda) = \xi\lambda^m. \tag{14}$$

The chromatic-dispersion difference $D_p(\lambda)$ is given by

$$D_p(\lambda) = m(1 - m)\xi\lambda^{m-1}/c. \tag{15}$$

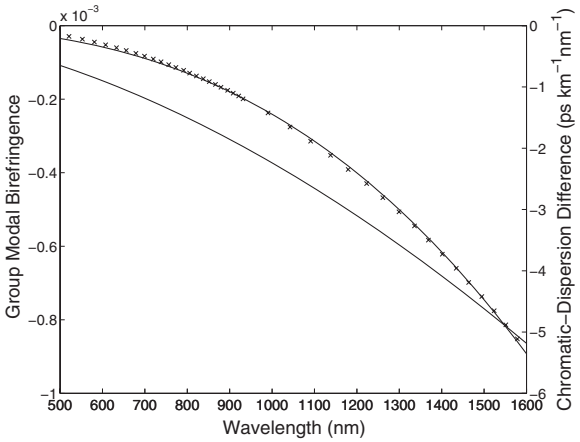

Figure 4. Measured group modal birefringence (crosses) in a holey fibre with a fit (solid line) and the chromatic-dispersion difference as a function of the wavelength.

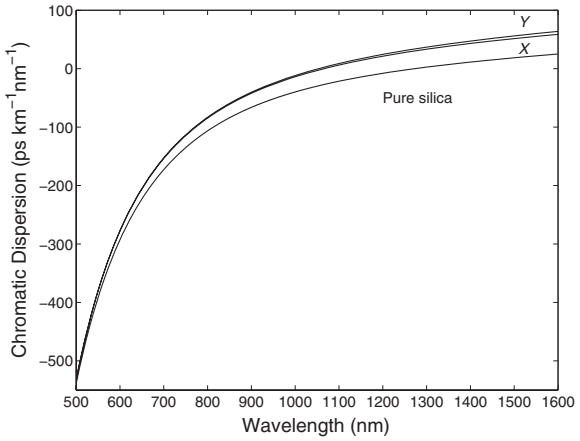

Figure 5. Chromatic dispersion of two polarization modes in a holey fibre and pure silica as a function of the wavelength.

A least-squares fit of $G(\lambda)$ to the experimental data, which is shown in figure 4 by the solid line, gives $m = 2.786$. In the same figure is shown the chromatic-dispersion difference $D_p(\lambda)$ as a function of wavelength λ evaluated by using equation (15). The fit according to equation (13) was used to deduce the wavelength dependence of $\Delta N_y(\lambda)$ from the wavelength dependence of $\Delta N_x(\lambda)$. It is shown in figure 3 by the upper solid line and it demonstrates very good agreement with experimental values shown by the crosses. Similarly, the chromatic-dispersion difference is negative and it decreases with increasing wavelength which causes, as illustrated in figure 5, the chromatic dispersion $D_y(\lambda)$ to be higher than $D_x(\lambda)$ with greater separation at longer wavelengths. The chromatic dispersion $D_x(\lambda)$ corresponding to the fit given by equation (12) is shown in figure 5 together with the material dispersion of pure silica. It is clearly seen that the chromatic dispersion for the polarization modes of the fibre is higher than that for pure silica so that the fibre acts nearly as dispersion-

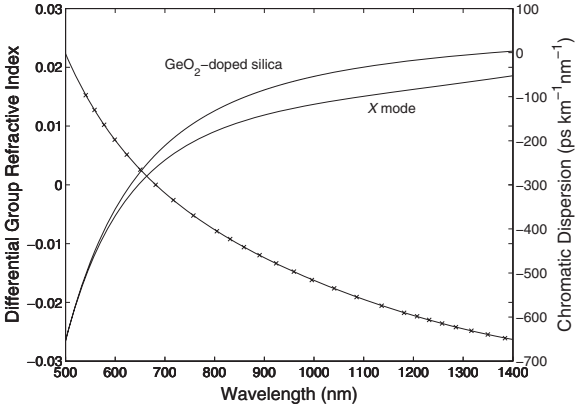

Figure 6. Measured differential group refractive index (crosses) for the x-polarization mode with a fit (solid line) and the chromatic dispersion of the x-polarization mode and doped silica as a function of the wavelength.

shifted fibre. The difference between these dispersions can be attributed to the waveguide dispersion that is higher for longer wavelengths than for shorter ones. This behaviour is expected due to the well-known fact that the contribution from waveguide dispersion increases with wavelength. Physically, this is because the mode is well confined to the core for short wavelengths, and the light therefore primarily interacts with the bulk material; as the mode size increases with wavelength, the light will increase its interaction with the surrounding air holes of the fibre. The values $D_x = 55$ ps km^{-1} nm^{-1} and $D_y = 60$ ps km^{-1} nm^{-1} measured at a wavelength of 1550 nm with a relative error of a few tenths of a per cent are in very good agreement with values $D_x = 54$ ps km^{-1} nm^{-1} and $D_y = 59$ ps km^{-1} nm^{-1} specified by the manufacturer.

For the second fibre sample, we revealed from the spectral signals recorded by both spectrometers that the equalization wavelength λ_0 can be resolved in the spectral range from 540 to 1380 nm. Figure 6 shows by the crosses the measured differential group index $\Delta N_x(\lambda_0)$ determined for respective equalization wavelengths λ_0 when the polarizer was oriented along the longer axis of the elliptical core of the fibre sample and when the group dispersion of the optical components was subtracted. The solid line in figure 6 corresponds to a five-term power series fit (12) and in the same figure is shown the chromatic dispersion $D_x(\lambda)$ together with the material dispersion of doped silica. It is clearly seen that in contrast to the first fibre sample the chromatic dispersion for the x-polarization mode of the second fibre sample is lower than that for the GeO_2-doped silica glass (19.3 mol%) [28]. This is caused by the contribution of the negative waveguide dispersion in the elliptical-core fibre. It should be noted here that no apparent discrimination between the spectral signals corresponding to the x- and y-polarization modes was revealed in the measured spectral range. This is owing to a low-group modal birefringence and short length of the optical fibre used in the experiment.

The group modal birefringence $G(\lambda)$ measured as a function of the wavelength λ for the second fibre sample is

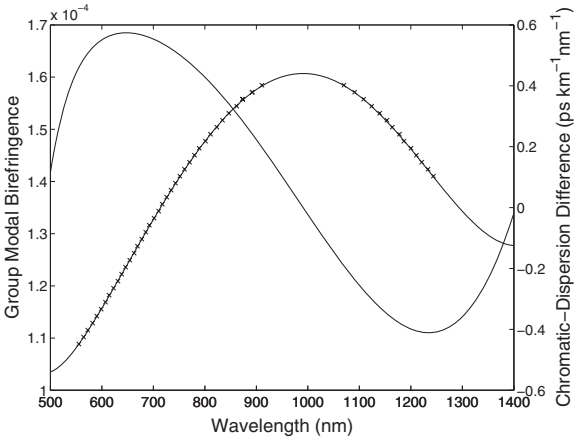

Figure 7. Measured group modal birefringence (crosses) in an elliptical-core fibre with a fit (solid line) and the chromatic-dispersion difference as a function of the wavelength.

shown in figure 7 by the crosses together with a seven-term power series fit. In contrast to the first fibre sample for which the group modal birefringence is negative and its absolute value increases with increasing wavelength, the one for the second fibre sample is positive with maximum at a wavelength of about 991 nm. At the same wavelength the chromatic-dispersion difference reaches the zero value as figure 7 illustrates, which shows $D_p(\lambda)$ as a function of the wavelength λ evaluated by using equation (11). It is supposed that the wavelength of the zero chromatic-dispersion difference can be tuned by the fibre geometry and fibre glass composition.

5. Conclusions

We used a white-light spectral interferometric technique for measuring the chromatic dispersion of polarization modes supported by short-length optical fibres over a broad spectral range (e.g. 500–1600 nm). The technique utilized an unbalanced Mach–Zehnder interferometer with a fibre under test of known length inserted into one of the interferometer arms and the other arm with adjustable path length. From a series of spectral signals recorded by VIS-NIR and NIR fibre-optic spectrometers we measured the equalization wavelength as a function of the path length difference, or equivalently the differential group index dispersion of one polarization mode. The differential group dispersion of the other polarization mode was obtained from measurement of the group modal birefringence dispersion. We verified the applicability of the method by differentiating the measured data to retrieve the chromatic dispersion of polarization modes in a birefringent holey fibre. The results obtained were in very good agreement with those specified by the manufacturer. We also measured the chromatic dispersion of polarization modes in an elliptical-core fibre. The characteristics that include chromatic, group modal birefringence and chromatic-difference dispersions substantially differ from those for the holey fibre. As an example, the chromatic-dispersion difference of the elliptical-core fibre reaches the zero value at a specified wavelength.

The described method, whose main advantage is in inspection of the optical field at the output of the test arm, is easy to implement and it offers sufficiently high measurement precision achieved with simple and cost-effective instrumentation. The method can be used for example to measure the chromatic dispersion in birefringent microstructured fibres that are useful for the supercontinuum generation. The method can be extended for dispersion characterization of other fibres guiding two polarization modes over a broad spectral range (PCFs, Panda and bow-tie fibres).

Acknowledgments

The research was partially supported by the COST Action 299 (project OC09020), by grant MSM6198910016, and by internal grant of TU Ostrava (IGS HGF VŠB-TUO).

References

[1] Cohen L G 1985 Comparison of single-mode fiber dispersion measurement techniques *J. Lightwave Technol.* **3** 958–66
[2] Costa B, Mazzoni D, Puleo M and Vezzoni E 1982 Phase shift technique for the measurement of chromatic dispersion in optical fibers using LEDs *IEEE J. Quantum Electron.* **118** 1509–15
[3] Diddams S and Diels J C 1996 Dispersion measurements with white-light interferometry 1996 *J. Opt. Soc. Am.* B **13** 1120–8
[4] Tateda M, Shibata N and Seikai S 1981 Interferometric method for chromatic dispersion measurement in a single-mode optical fiber *IEEE J. Quantum Electron.* **17** 404–7
[5] Saunders M J and Gardner W B 1987 Interferometric determination of dispersion variations in single-mode fibers *J. Lightwave Technol.* **5** 1701–5
[6] Pelayo J, Paniello J and Villuendas F 1988 Chromatic dispersion characterization in short single-mode fibers by spectral scanning of phase difference in a Michelson interferometer *J. Lightwave Technol.* **6** 1861–5
[7] Merritt P, Tatam R P and Jackson D A 1989 Interferometric chromatic dispersion measurements on short lengths of monomode optical fiber *J. Lightwave Technol.* **7** 703–16
[8] Koch F, Chernikov S V and Taylor J R 2001 Dispersion measurement in optical fibres over the entire spectral range from 1.1 μm to 1.7 μm *Opt. Commun.* **175** 209–13
[9] Zhao Y C and Fleming S 2005 Direct measurement for second-order dispersion using multi-section interference fringes in spectral domain *Meas. Sci. Technol.* **16** 1628–30
[10] Lu P, Ding H and Mihailov S J 2005 Direct measurement of the zero-dispersion wavelength of tapered fibres using broadband-light interferometry *Meas. Sci. Technol.* **16** 1631–6
[11] Galle M A, Mohammed W, Qian L and Smith P W E 2007 Single-arm three-wave interferometer for measuring dispersion of short lengths of fiber *Opt. Express* **16** 16896–908
[12] Lee J Y and Kim D Y 2006 Versatile chromatic dispersion measurement of a single mode fiber using spectral white light interferometry *Opt. Express* **14** 11608–15
[13] Ouzounov D, Homoelle D, Zipfel W, Webb W W, Gaeta A L, West J A, Fajardo J C and Koch K W 2001 Dispersion measurements of microstructure fibers using femtosecond laser pulses *Opt. Commun.* **192** 219–23
[14] Ye Q, Xu C, Liu X, Knox W H, Yan M F, Windeler R S and Eggleton B 2002 Dispersion measurement of tapered air–silica microstructure fiber by white-light interferometry *Appl. Opt.* **41** 4467–70

[15] Labonté L, Roy P, Pagnoux F, Louradour F, Restoin C, Mélin G and Burov E 2006 Experimental and numerical analysis of the chromatic dispersion dependence upon the actual profile of small core microstructured fibres *J. Opt. A: Pure Appl. Opt.* **8** 933–8

[16] Hlubina P, Szpulak M, Ciprian D, Martynkien T and Urbańczyk W 2007 Measurement of the group dispersion of the fundamental mode of holey fiber by white-light spectral interferometry *Opt. Express* **15** 11073–81

[17] Peterka P, Kaňka J, Honzátko P and Káčik D 2008 Measurement of chromatic dispersion of microstructure optical fibers using interferometric method *Opt. Appl.* **38** 295–303

[18] Hlubina P, Ciprian D, Frosz M H and Nielsen K 2009 Measurement of chromatic dispersion of microstructured polymer fibers by white-light spectral interferometry *Proc. SPIE* **7389** 73890J

[19] Kardaś T M and Radzewicz C 2009 Broadband near-infrared fibers dispersion measurement using white-light spectral interferometry *Opt. Commun.* **282** 4361–5

[20] Choi H G, Kee C S, Hong K H, Sung J H, Kim S, Ko D K, Lee J, Kim J U and Park H Y 2007 Dispersion and birefringence of irregularly microstructured fiber with an elliptic core *Appl. Opt.* **41** 8493–8

[21] Hlubina P, Szpulak M, Knyblová L, Statkiewicz G, Martynkien T, Ciprian D and Urbańczyk W 2006 Measurement and modelling of dispersion characteristics of two-mode birefringent holey fibre *Meas. Sci. Technol.* **17** 626–30

[22] Hlubina P, Chlebus R and Ciprian D 2007 Differential group refractive index dispersion of glasses of optical fibres measured by a white-light spectral interferometric technique *Meas. Sci. Technol.* **18** 1547–52

[23] Hlubina P, Ciprian D and Kadulová M 2009 Wide spectral range measurement of modal birefringence in polarization-maintaining fibres *Meas. Sci. Technol.* **20** 025301

[24] Ortigosa-Blanch A, Knight J C, Wadsworth W J, Arriaga J, Mangan B J, Birks T A and Russell P St J 2000 Highly birefringent photonic crystal fibers *Opt. Lett.* **25** 1325–7

[25] Shibata N, Nakazono A and Inoue Y 2005 Interference between two orthogonally polarized modes traversing a highly birefringent air–silica microstructure fiber *J. Lightwave Technol.* **23** 1244–52

[26] Hlubina P, Gurov I and Chugunov V 2003 White-light spectral interferometric technique to measure the wavelength dependence of the spectral bandpass of a fibre-optic spectrometer *J. Mod. Opt.* **50** 2067–74

[27] Hlubina P and Gurov I 2003 Spectral interferograms including the equalization wavelengths processed by autoconvolution method *Proc. SPIE* **5064** 198–205

[28] Fleming J W 1984 Dispersion in GeO_2–SiO_2 glasses *Appl. Opt.* **23** 4486–93

Paper IX.

J. Europ. Opt. Soc. Rap. Public. 7, 12017 (2012) www.jeos.org

Spectral interferometry-based chromatic dispersion measurement of fibre including the zero-dispersion wavelength

P. Hlubina
petr.hlubina@vsb.cz
Department of Physics, Technical University Ostrava, 17. listopadu 15, 708 33 Ostrava-Poruba, Czech Republic

M. Kadulová
Department of Physics, Technical University Ostrava, 17. listopadu 15, 708 33 Ostrava-Poruba, Czech Republic

D. Ciprian
Department of Physics, Technical University Ostrava, 17. listopadu 15, 708 33 Ostrava-Poruba, Czech Republic

We report on a simple spectral interferometric technique for chromatic dispersion measurement of a short length optical fibre including the zero-dispersion wavelength. The method utilizes a supercontinuum source, a dispersion balanced Mach-Zehnder interferometer and a fibre under test of known length inserted in one of the interferometer arms and the other arm with adjustable path length. The method is based on resolving one spectral interferogram (spectral fringes) by a low-resolution NIR spectrometer. The fringe order versus the precise wavelength position of the interference extreme in the recorded spectral signal is fitted to the approximate function from which the chromatic dispersion is obtained. We verify the applicability of the method by measuring the chromatic dispersion of two polarization modes in a birefringent holey fibre. The measurement results are compared with those obtained by a broad spectral range (500–1600 nm) measurement method, and good agreement is confirmed.
[DOI: http://dx.doi.org/10.2971/jeos.2012.12017]

Keywords: spectral interferometry, Mach-Zehnder interferometer, holey fibre, chromatic dispersion, zero-dispersion wavelength

1 INTRODUCTION

The chromatic dispersion, which is a significant characteristic of optical fibre, affects the bandwidth of a high speed optical transmission system through pulse broadening and nonlinear optical distortion. Chromatic dispersion of long length optical fibres is determined by two widely used methods [1]: the time-of-flight method which measures relative temporal delays for pulses at different wavelengths, and the modulation phase shift technique which measures the phase delay of a modulated signal as a function of wavelength. Recently, a rapid and accurate spectral interferometry-based measurement method using an asymmetric Sagnac interferometer has been presented [2].

White-light interferometry based on the use of a broadband source in combination with a standard Michelson or a Mach-Zehnder interferometer [3] is considered as one of the best tools for dispersion characterization of short length optical fibres. White-light interferometry usually utilizes a temporal method [4] or a spectral method [5]–[13]. The spectral method is based on the observation of spectral fringes in the vicinity of a stationary-phase point [5]–[12] or far from it [13]. The feasibility of the interferometric techniques has been demonstrated in measuring the dispersion of holey fibres [14]–[16] usable for supercontinuum generation [17]. However, an accurate control of the chromatic dispersion is required for the application [18]. As an example, a highly-birefringent holey fibre [19] has been designed and fabricated with the zero-dispersion wavelength (ZDW) close to a 1064 nm of a microchip laser, enabling savings in size and cost of a supercontinuum source. Moreover, these broadband and high-power sources have enabled to increase the comfort of dispersion measurement [16].

In this paper, a simple technique, based on spectral interferometry and employing a NIR low-resolution spectrometer, is used for chromatic dispersion measurement of a short length optical fibre including the ZDW. The method utilizes a supercontinuum source, a dispersion balanced Mach-Zehnder interferometer and a fibre under test of known length placed in one arm of the interferometer while the other arm has adjustable path length. The method is based on resolving one spectral interferogram from which the fringe order versus the precise wavelength position of the interference extreme is obtained [20]. This dependence is fitted to the approximate function enabling to obtain the chromatic dispersion. We verify the applicability of the method by measuring the chromatic dispersion of two polarization modes in a birefringent holey fibre. Good agreement between the measurement results and those obtained by a broad spectral range (500–1600 nm) measurement method is confirmed.

2 EXPERIMENTAL METHOD

Consider a dispersion balanced Mach-Zehnder interferometer (see Figure 1) and a fibre under test of length z that supports two polarization modes over a broad wavelength range. The

Received March 14, 2012; revised ms. received April 23, 2012; published May 30, 2012 ISSN 1990-2573

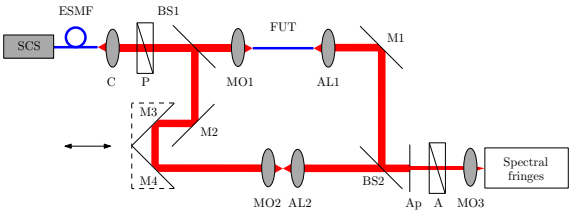

FIG. 1 Experimental set-up for measuring the chromatic dispersion of a fibre under test.

fibre, which is characterized by the effective indices $n_x(\lambda)$ and $n_y(\lambda)$, is inserted into the first (test) arm of the interferometer and the other (reference) arm has the adjustable path length L in the air. If the analyser at the output interferometer discriminates the x polarization only, the optical path difference (OPD) $\Delta_{MZ}(\lambda)$ between the beams in the interferometer is given by

$$\Delta_{MZ}(\lambda) = L - l - n_x(\lambda)z, \tag{1}$$

where l is the path length in the air in the test arm. The group OPD $\Delta^g_{MZ}(\lambda)$ is similar to Eq. (1), in which $n_x(\lambda)$ is replaced by the group effective index $N_x(\lambda)$ given by the relation

$$N_x(\lambda) = n_x(\lambda) - \lambda \frac{dn_x(\lambda)}{d\lambda}. \tag{2}$$

Next, consider that the spectral interference fringes can be resolved by a spectrometer used at the output of the Mach-Zehnder interferometer. The spectral signal (interference fringes) recorded by the spectrometer of a Gaussian response function can be expressed as [12]

$$\begin{aligned} S_{MZ}(\lambda) =& 1 + V \exp\{-(\pi^2/2)[\Delta^g_{MZ}(\lambda)\Delta\lambda_R/\lambda^2]^2\} \\ & \times \cos[(2\pi/\lambda)\Delta_{MZ}(\lambda)], \end{aligned} \tag{3}$$

where V is a visibility term and $\Delta\lambda_R$ is the width of the spectrometer response function.

To resolve spectral fringes in a spectral range from λ_1 to λ_2, the group OPD $\Delta^g_{MZ}(\lambda)$ must satisfy the condition $\Delta^g_{MZ}(\lambda) < \lambda_1^2/\Delta\lambda_R$. We can resolve in the recorded spectral interferogram a suitable number of spectral fringes. The interference maximum (a bright fringe) satisfies the relation

$$L - l - n_x(\lambda)z = m\lambda, \tag{4}$$

where m is the order of interference of the fringes. After counting i bright spectral fringes in the direction of shorter wavelengths, Eq. (4) can be written as

$$[L - l - n_x(\lambda)z]/\lambda = m + i. \tag{5}$$

The wavelength dependence of the effective index $n_x(\lambda)$ can be well approximated by a modified Cauchy dispersion formula [21]

$$n_x(\lambda) = A_1\lambda^{-4} + A_2\lambda^{-2} + A_3 + A_4\lambda^2 + A_5\lambda^4, \tag{6}$$

where A_i are the coefficients. On substituting from Eq. (5) into Eq. (6), we obtain

$$a_1\lambda^{-5} + a_2\lambda^{-3} + a_3\lambda^{-1} + a_4\lambda + a_5\lambda^3 = m + i, \tag{7}$$

where $a_1 = -A_1z$, $a_2 = -A_2z$, $a_3 = L - l - A_3z$, $a_4 = -A_4z$, and $a_5 = -A_5z$. By a least-squares fitting of Eq. (7), the constants a_i and m are determined, and knowing the fibre length z, the wavelength dependence of the group effective index $N_x(\lambda)$ can be deduced from Eqs. (2) and (6). The chromatic dispersion $D_x(\lambda)$ can be evaluated as

$$\begin{aligned} D_x(\lambda) &= \frac{1}{c}\frac{dN_x(\lambda)}{d\lambda} \\ &= \frac{1}{c}(-20A_1\lambda^{-5} - 6A_2\lambda^{-3} - 2A_4\lambda - 12A_5\lambda^3), \end{aligned} \tag{8}$$

where c is the velocity of light in vacuum. The ZDW λ_0^x is given by $D_x(\lambda_0^x) = 0$. Similarly, the dispersion slope $S_x(\lambda) = dN_x(\lambda)/d\lambda$ and its value $S_x(\lambda_0^x)$ at the ZDW λ_0^x can be determined. If the analyser at the output of the interferometer discriminates the y polarization only, the chromatic dispersion $D_y(\lambda)$, the ZDW λ_0^y given by $D_y(\lambda_0^y) = 0$ and the dispersion slope $S_y(\lambda_0^y)$ of the y-polarization mode can also be measured.

The method can also be applied for fibres with two ZDWs provided that a sufficient number of spectral fringes can be resolved in a measured spectral range. In addition, the degree of Laurent polynomial (a modified Cauchy dispersion formula) used in the data evaluation has to be chosen with respect to this fact.

3 EXPERIMENTAL CONFIGURATION

The set-up for spectral interferometry-based measurement of the chromatic dispersion of the polarization modes supported by a fibre under test, including the ZDW, is shown in Figure 1. It consists of supercontinuum source SCS (SC450-4, Fianium) with a splitter (Splitter-900, Fianium) and endlessly single-mode fibre ESMF (FDS-PCF, Fianium), collimator C, polarizer P and analyser A (LPVIS050, Thorlabs), a bulk-optic Mach-Zehnder interferometer with plate beam splitters BS (BSW07, Thorlabs), a micropositioner connected to mirrors M3 and M4 of the interferometer, three microscope objectives MO (10×/0.30, Meopta), two achromatic lenses AL (74-ACR, Ocean Optics), aperture Ap, a fibre-optic spectrometer (NIR-512, Ocean Optics) and a personal computer.

The spectral signal is recorded by the spectrometer in the transmission mode after a dark spectrum and a reference spectrum (without the interference) are stored. The spectrometer has a spectral operation range from 850 to 1700 nm and its read optical fibre with a 50 μm core diameter results in a Gaussian response function of $\Delta\lambda_R \approx 9$ nm. In the test arm of the interferometer, a fibre sample of length $z = (77640 \pm 10)$ μm is placed. The fibre sample is a pure silica birefringent holey fibre similar to that analysed in a previous paper [9].

4 EXPERIMENTAL RESULTS AND DISCUSSION

Prior to the measurement we utilized the main advantage of the set-up, which is in fibre connection of a light source (that can be varied) with the interferometer. We used a laser diode

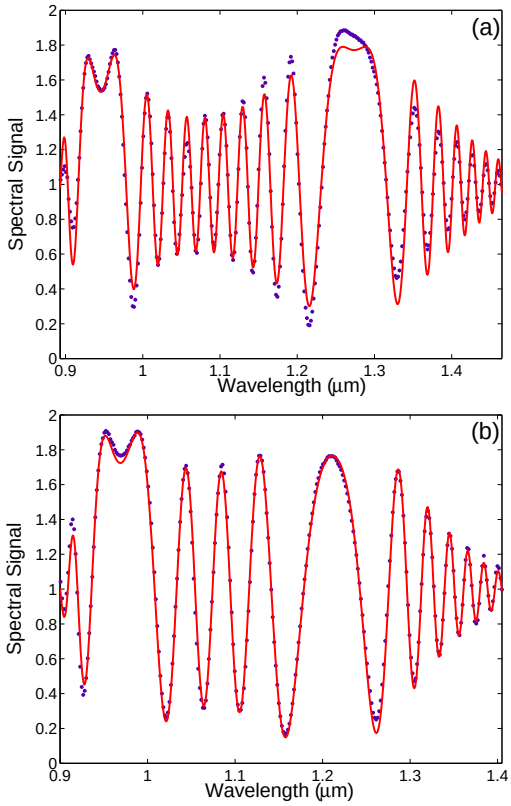

FIG. 2 Example of the recorded spectral signal (markers) together with a fit (solid curve): (a) x-polarization mode, (b) y-polarization mode.

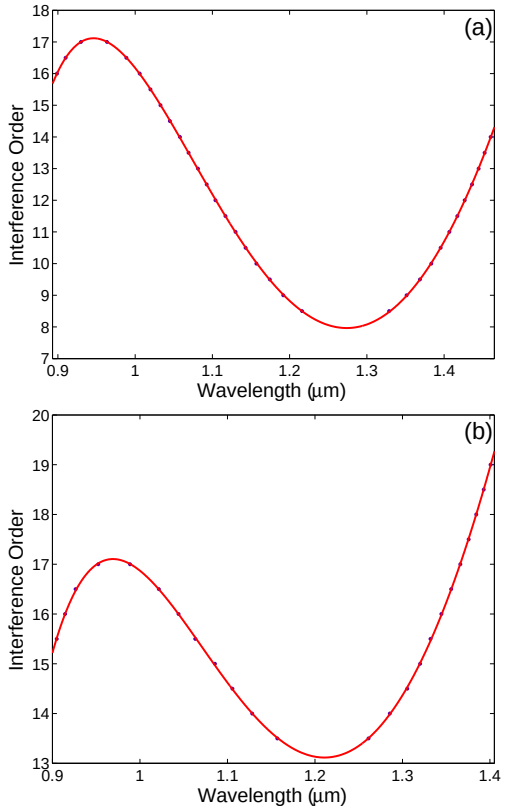

FIG. 3 Fringe order (markers) as a function of wavelength retrieved from the recorded spectral signal shown in Figure 2: (a) x-polarization mode, (b) y-polarization mode. The solid lines correspond to the fit of Eq. (7).

($\lambda \approx 670$ nm) instead of the supercontinuum source to check the precise placement and alignment of the optical components in both arms of the interferometer by observing the interference pattern. The proper excitation of the fibre was also inspected [9], and in order to measure the chromatic dispersion of the x- or y-polarization mode, the polarizer and analyser need to be oriented along the short or the long axis of the far-field pattern [12].

In the chromatic dispersion measurement, such a path length in the reference arm of the interferometer was adjusted to resolve interference fringes in a spectral range as wide as possible. Figure 2(a) shows an example of the spectral signal recorded by the spectrometer for the x-polarization mode. It clearly shows the effect of the limiting resolving power of the spectrometer on the visibility of the spectral interference fringes [see Eq. (3)]. The visibility is the highest in the vicinities of two different equalization wavelengths at which the group OPD in the interferometer is zero. Between the two equalization wavelengths the minimum in the group effective index $N_x(\lambda)$ or equivalently the ZDW is located.

The procedure used to retrieve the chromatic dispersion $D_x(\lambda)$ from the recorded spectral signal consists of two steps. In the first step, the wavelengths of interference maxima and minima are determined for the recorded signal. The spectral interference fringes are numbered in such a way that the fringe order increases in the direction of longer wavelengths to the first equalization wavelength (≈ 0.95 μm), decreases to the second equalization wavelength (≈ 1.28 μm) and from it once again increases in the direction of longer wavelengths. Figure 3(a) shows by the markers the dependence of the fringe order on the wavelength obtained from the spectrum shown in Figure 2(a). In the second step, a least-squares fit of Eq. (7) is used to the dependence which gives the constants a_i and m. Figure 3(a) shows the results of the fit by the solid line. Then the constants a_i and the known fibre length z give the constants A_i needed in the determination of the chromatic dispersion $D_x(\lambda)$ according to Eq. (8). It is shown in Figure 4(a) together with $D_x(\lambda)$ measured in the same set-up by a broad spectral range (500–1600 nm) measurement technique presented in a previous paper [12]. It is clearly seen that both functions agree well in the vicinity of the ZDW. Their different courses, especially in a short-wavelength range, are caused by the approximation (6) used in this narrower spectral range.

The constants a_i obtained from a least-squares fit of Eq. (7) can serve as the first estimate in a least-squares fit of Eq. (3) to the recorded spectral signal. The result of the fit is shown in Figure 2(a) by the solid curve and it illustrates very good agreement. The corresponding ZDWs λ_0^x and the dispersion slopes $S_x(\lambda_0^x)$ are listed in Table 1. We estimate the error of determin-

	λ_0^x (nm)	$S_x(\lambda_0^x)$ (ps km^{-1}nm^{-2})	λ_0^y (nm)	$S_y(\lambda_0^y)$ (ps km^{-1}nm^{-2})
Fit of Eq. (3)	1097.4	0.161	1083.6	0.172
Fit of Eq. (7)	1097.7	0.162	1083.3	0.172
Method [12]	1097.4	0.168	1084.0	0.178

TABLE 1 The ZDW λ_0 and the dispersion slope $S(\lambda_0)$ for x- and y-polarization modes.

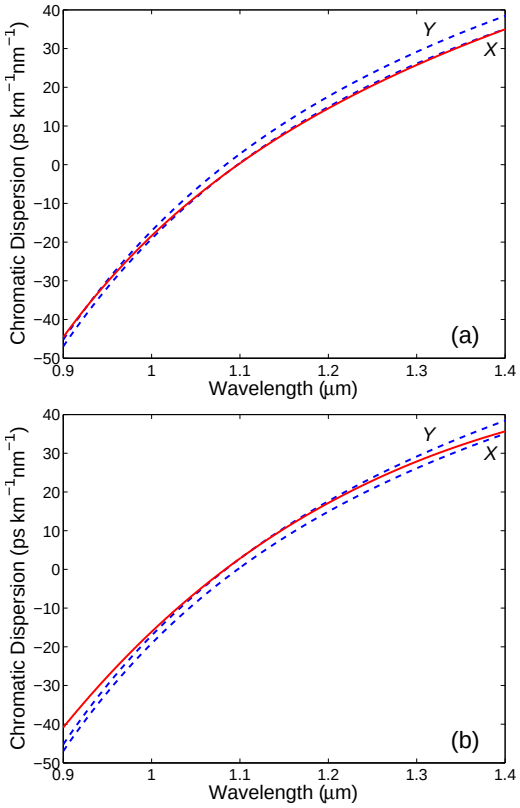

FIG. 4 Chromatic dispersion obtained from the fit shown in Figure 3: (a) x-polarization mode, (b) y-polarization mode. The dashed lines are the result of a broad spectral range measurement.

ing the ZDW, which is affected by the wavelength sampling of a low-resolution spectrometer [12], below 1 nm and the error of the dispersion slope below 10 fs km^{-1}nm^{-2}. It is supposed that the smaller error in determining the ZDW can be attained using an optical spectrum analyser with a denser wavelength sampling. Similar procedure with all the mentioned steps was used for the spectral signal shown in Figure 2(b), i.e., for the y-polarization mode. Figure 4(b) shows the chromatic dispersion $D_y(\lambda)$ which is shifted to shorter wavelengths in comparison with $D_x(\lambda)$. Table 1 then lists the ZDWs λ_0^y and the dispersion slopes $S_y(\lambda_0^y)$.

5 CONCLUSIONS

In this paper, a simple technique for chromatic dispersion measurement of short length optical fibres, including the ZDW, is presented. The technique, which is based on spectral interferometry employing a low-resolution NIR spectrometer, utilizes a supercontinuum source, a dispersion balanced Mach-Zehnder interferometer and a fibre under test placed in one arm of the interferometer and the other arm with adjustable path length. Within the method, the precise wavelength positions of the interference maxima and minima in one spectral interferogram are determined. These are used to retrieve the fringe order versus the wavelength which is fitted to the approximate function enabling to obtain the chromatic dispersion. We verify the applicability of the method by measuring the chromatic dispersion of two polarization modes in a birefringent holey fibre. The measurement results are compared with those obtained by a broad spectral range measurement method [12], and good agreement is confirmed. The use of the method, whose main advantage is in the measurement comfort, i.e. in rapid and accurate measurements of the ZDW and the dispersion slope, can be extended for fibres with the ZDW in the VIS spectral range. Moreover, in comparison with fibre-optic implementations of measuring setups the presented one is dispersion balanced and it enables an easy inspection of the optical field at the output of the test arm of the interferometer.

6 ACKNOWLEDGEMENTS

The research was partially supported by the Grant Agency of the Czech Republic through grant P102/11/0675 and by the regional grant CZ.1.05/2.1.00/01.0040.

References

[1] L. G. Cohen, "Comparison of single-mode fibre dispersion measurement techniques," J. Lightwave Technol. **3**, 958–966 (1985).

[2] L. Zong, F. Luo, S. Cui, and X. Cao, "Rapid and accurate chromatic dispersion measurement of fibre using asymmetric Sagnac interferometer," Opt. Lett. **36**, 660–662 (2011).

[3] S. Diddams, and J. C. Diels, "Dispersion measurements with white-light interferometry," J. Opt. Soc. Am. B **13**, 1120–1128 (1995).

[4] M. Tateda, N. Shibata, and S. Seikai, "Interferometric method for chromatic dispersion measurement in a single-mode optical fibre," J. Quantum Electr. **17**, 404–407 (1981).

[5] P. Merritt, R. P. Tatam, and D. A. Jackson, "Interferometric chromatic dispersion measurements on short lengths of monomode optical fibre," J. Lightwave Technol. **7**, 703–716 (1989).

[6] F. Koch, S. V. Chernikov, and J. R. Taylor, "Dispersion measurement in optical fibres over the entire spectral range from 1.1 μm to 1.7 μm," Opt. Commun. **175**, 209–213 (2001).

[7] P. Lu, H. Ding, and S. J. Mihailov, "Direct measurement of the zero-dispersion wavelength of tapered fibres using broadband-light in-

terferometry," Meas. Sci. Technol. **16**, 1631–1636 (2005).

[8] M. A. Galle, W. Mohammed, L. Qian, P. W. E. Smith, "Single-arm three-wave interferometer for measuring dispersion of short lengths of fiber," Opt. Express **16**, 16896–16908 (2007).

[9] P. Hlubina, M. Szpulak, D. Ciprian, T. Martynkien, and W. Urbańczyk, "Measurement of the group dispersion of the fundamental mode of holey fibre by white-light spectral interferometry," Opt. Express **15**, 11073–11081 (2007).

[10] T. Zhang, Z. Yang, W. Zhao, Y. Wang, P. Fang, and C. Li, "Dispersion measurement of Yb-doped fiber by a spectral interferometric technique," Chin. Opt. Lett. **8**, 262–265 (2008).

[11] T. M. Kardaś, and C. Radzewicz, "Broadband near-infrared fibres dispersion measurement using white-light spectral interferometry," Opt. Commun. **282**, 4361–4365 (2009).

[12] P. Hlubina, D. Ciprian, and M. Kadulová, "Measurement of chromatic dispersion of polarization modes in optical fibres using white-light spectral interferometry," Meas. Sci. Technol. **21**, 045302 (2010).

[13] J. Y. Lee, and D. Y. Kim, "Versatile chromatic dispersion measurement of a single mode fibre using spectral white light interferometry," Opt. Express **14**, 11608–11614 (2006).

[14] D. Ouzounov, D. Homoelle, W. Zipfel, W. W. Webb, A. L. Gaeta, J. A. West, J. C. Fajardo, and K. W. Koch, "Dispersion measurements of microstructure fibres using femtosecond laser pulses," Opt. Commun. **192**, 219–223 (2001).

[15] Q. Ye, C. Xu, X. Liu, W. H. Knox, M. F. Yan, R. S. Windeler, and B. Eggleton, "Dispersion measurement of tapered air-silica microstructure fibre by white-light interferometry," Appl. Optics **41**, 4467–4470 (2002).

[16] L. Labonté, P. Roy, F. Pagnoux, F. Louradour, C. Restoin, G. Mélin, and E. Burov, "Experimental and numerical analysis of the chromatic dispersion dependence upon the actual profile of small core microstructured fibres," J. Opt. A-Pure App. Op. **8**, 933–938 (2006).

[17] J. M. Dudley, G. Genty, and S. Coen, "Supercontinuum generation in photonic crystal fibre," Rev. Mod. Phys. **78**, 1135–1185 (2006).

[18] R. Buczynski, D. Pysz, R. Stepien, R Kasztelanic, I. Kujawa, M. Franczyk, A. Filipkowski, A. J. Waddie, and M. R. Taghizadeh, "Dispersion management in nonlinear photonic crystal fibres with nanostructured core," J. Eur. Opt. Soc. Rap. Public. **6**, 11038 (2011).

[19] C. Xiong, and W. J. Wadsworth, "Polarized supercontinuum in birefringent photonic crystal fibre pumped at 1064 nm and application to tuneable visible/UV generation," Opt. Express **16**, 2438–2445 (2008).

[20] P. Hlubina, and D. Ciprian, "Birefringence dispersion in a quartz crystal retrieved from a channelled spectrum resolved by a fibre-optic spectrometer," Opt. Commun. **284**, 2683–2686 (2011).

[21] P. Hlubina, and D. Ciprian, "Absolute phase birefringence dispersion in polarization-maintaining fibre or birefringent crystal retrieved from a channeled spectrum," Opt. Lett. **35**, 1566–1568 (2010).

Paper X.

Available online at www.sciencedirect.com
SCIENCE DIRECT®
Optics Communications 260 (2006) 535–541
OPTICS COMMUNICATIONS
www.elsevier.com/locate/optcom

Interference of white light in tandem configuration of birefringent crystal and sensing birefringent fiber

Petr Hlubina *, Dalibor Ciprian, Lenka Knyblová

Department of Physics, Technical University Ostrava, 17. Listopadu 15, 708 33 Ostrava-Poruba, Czech Republic

Received 12 September 2005; accepted 31 October 2005

Abstract

Spectral interference of white-light beams propagating through a tandem configuration of birefringent crystal and sensing birefringent fiber is analyzed theoretically and experimentally. The spectral interference law is expressed analytically under the condition of a Gaussian response function of a spectrometer taking into account the dispersion of birefringence in the crystal and in the fiber. Two types of spectral interferograms are modeled knowing dispersion characteristics of the sensing fiber and using a quartz crystal of the positive or a calcite crystal of the negative birefringence. The theoretical analysis is accompanied by two experiments employing a highly birefringent fiber and a birefringent quartz crystal of two suitable thicknesses. Within both experiments the spectral interference fringes are resolved in accordance with the theory with phases dependent on the fiber length.

PACS: 42.25.Hz; 42.25.Lc; 42.81.Gs; 78.20.Fm

Keywords: White light; Spectral interference; Birefringent crystal; Birefringent fiber; Dispersion; Spectrometer; Fiber sensor

1. Introduction

Fiber optic white-light interferometry [1] has attracted much interest in recent years and has become an important technique for measuring physical quantities, such as displacement, temperature, pressure, strain and refractive index. The main advantages of white-light interferometric systems are the possibility of absolute measurements, a significant reduction in the noise level, an insensitivity to optical power fluctuations and the possibility of multiplexing a large number of sensors in a measuring system. Numerous applications of fiber optic white-light interferometric sensors have been reported [2–6].

A typical, simple example of a fiber optic white-light interferometric system is a setup comprising a white-light source, a sensor interferometer made of a birefringent optical fiber, a receiving interferometer, e.g., another birefringent fiber or Wollaston prism [7,8]. The sensor element is subjected to the measured quantity and introduces a phase shift between two eigenwaves of propagated light. This phase shift can be detected on the receiving interferometer, in which controlled introduced changes of phase shift must be possible. Because of the different group delays introduced by the sensor and by the receiving interferometer, many of the interference patterns can be raised and detected only if the resultant group delay, responsible for the detected pattern, is smaller than the group delay of the broadband source. Pattern contrasts depend on the alignment of all elements of the setup. The technique is an extension of time-domain method used to measure phase and group modal birefringence in optical fibers [9]. Most recently, we have proposed and realized a new spectral-domain white-light interferometric method to measure the group birefringence in a fiber sample [10] and in a calcite crystal

* Corresponding author. Tel.: +420 597 323 134; fax: +420 597 323 139.
E-mail address: petr.hlubina@vsb.cz (P. Hlubina).

0030-4018/$ - see front matter © 2005 Elsevier B.V. All rights reserved.
doi:10.1016/j.optcom.2005.10.078

[11,12]. The technique of tandem interferometry, which uses a Michelson interferometer as an element with adjustable compensating optical path difference (OPD), can be modified to realize a new spectral-domain sensor configuration.

In this paper, we analyse theoretically and experimentally spectral interference of white-light beams propagating through a tandem configuration of birefringent crystal and sensing birefringent fiber. We express the spectral interference law analytically under the condition of a Gaussian response function of a spectrometer taking into account the dispersion of birefringence in the crystal and in the fiber. We reveal that the visibility of spectral interference fringes is highest for the group OPD in the crystal compensating the group OPD in the fiber. We model two types of spectral interferograms knowing dispersion characteristics of the sensing fiber and using a quartz crystal of the positive or a calcite crystal of the negative birefringence. Sensing capabilities of the configuration are demonstrated by the change of the phase of spectral fringes due to the change of fiber length. We perform two experiments with a highly birefringent fiber and a birefringent quartz crystal of two suitable thicknesses. We confirm in accordance with the theory that the wavelength-dependent phases of spectral interference fringes vary with the fiber length.

2. Theoretical background

In this section, first the spectral intensity in the frequency domain will be expressed for a tandem configuration of uniaxial birefringent crystal and birefringent fiber. Then, the wavelength-domain spectral intensity will be specified for two cases of a uniaxial crystal with the positive or the negative birefringence.

2.1. The spectral intensity in the frequency domain

First, let us consider the experimental setup shown in Fig. 1 that consists of a white-light source (WLS), a collimating lens (L1), a polarizer (P), a uniaxial birefringent crystal (BC) of thickness d, a microscope objective lens (L2), a sensing highly birefringent optical fiber (SHBOF) of length L, an analyzer (A) and a spectrometer. The crystal is characterized by the spectrally dependent birefringence $B_f(\omega)$ defined as

$$B_f(\omega) = n_e(\omega) - n_o(\omega), \tag{1}$$

where $n_e(\omega)$ and $n_o(\omega)$ are refractive indices of the extraordinary and ordinary eigenwaves, respectively. Similarly, the highly birefringent fiber is characterized by the spectrally dependent phase modal birefringence $B(\omega)$ defined as

$$B(\omega) = (c/\omega)[\beta_x(\omega) - \beta_y(\omega)], \tag{2}$$

where $\beta_x(\omega)$ and $\beta_y(\omega)$ are the propagation constants of the orthogonally polarized eigenmodes guided by the optical fiber and c is the velocity of light in the vacuum. For convenience, the longitudinal z-axis of the optical fiber is chosen along the propagation direction of the beam through the birefringent crystal, which is perpendicular to the optic axis of the birefringent crystal. As shown in Fig. 2, let the transmission axis of the polarizer P be α with respect to the polarization direction of the ordinary eigenwave in the birefringent crystal. Similarly, let the x-axis of the highly birefringent fiber, oriented for example along the major axis of an elliptical core of the fiber, be β with respect to the polarization direction of the ordinary eigenwave in the birefringent crystal. Finally, let the transmission axis of the analyzer A be γ with respect to the x-axis of the highly birefringent fiber.

Let us consider now a random scalar field, represented by a statistical ensemble $\{E(\alpha,\beta,\gamma;\omega)\}$, where $E(\alpha,\beta,\gamma;\omega)$ is the complex representation of a linearly polarized optical field at the output of the analyzer A at the angular frequency ω, propagating through the whole setup shown in Fig. 1. The measurable quantity, the spectral density $S(\alpha,\beta,\gamma;\omega)$, is defined as [13]

$$S(\alpha,\beta,\gamma;\omega) = \langle |E(\alpha,\beta,\gamma;\omega)|^2 \rangle, \tag{3}$$

where the angular brackets denote the ensemble average and the brackets || represent the modulus. If we introduce $P(\omega)$, $C(\omega)$, $F(\omega)$ and $A(\omega)$ as the spectrally dependent transmittances of the polarizer, the crystal, the fiber and the analyzer, respectively, $G(\omega) = \langle |E_0(\omega)|^2 s \rangle$ as the source spectral density expressed by means of the source field $E_0(\omega)$, $\Phi_f(d;\omega) = (\omega/c)B_f(\omega)d$ and $\Phi(L;\omega) = (\omega/c)B(\omega)L$ as the retardances, the spectral density $S(\alpha,\beta,\gamma;\omega)$ is given by

$$\begin{aligned} S(\alpha,\beta,\gamma;\omega) &= S_0(\omega)\{V_1(\alpha,\beta,\gamma) + V_2(\alpha,\beta,\gamma)\mathrm{Re}\{\exp\{-i[\Phi_f(d;\omega)]\}\} \\ &+ V_3(\alpha,\beta,\gamma)\mathrm{Re}\{\exp\{-i[\Phi_f(d;\omega) - \Phi(L;\omega)]\}\} \\ &+ V_4(\alpha,\beta,\gamma)\mathrm{Re}\{\exp\{-i[-\Phi(L;\omega)]\}\} \\ &+ V_5(\alpha,\beta,\gamma)\mathrm{Re}\{\exp\{-i[-\Phi_f(d;\omega) - \Phi(L;\omega)]\}\} \\ &+ V_6(\alpha,\beta,\gamma)\mathrm{Re}\{\exp\{-i[-\Phi_f(d;\omega)]\}\}\}, \end{aligned} \tag{4}$$

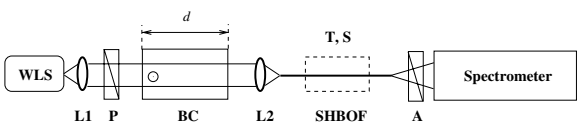

Fig. 1. Experimental setup with a birefringent crystal (BC) and a sensing highly birefringent optical fiber (SHBOF) to record spectral interferograms.

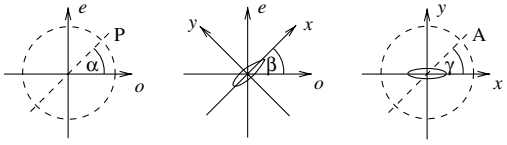

Fig. 2. Orientations of the transmission axes of the polarizer P and the analyzer A and the x-axis of the optical fiber.

where

$$S_0(\omega) = A(\omega)F(\omega)C(\omega)P(\omega)G(\omega) \tag{5}$$

and the angle-dependent functions $V_i(\alpha,\beta,\gamma)$ with $i = 1,\ldots,6$ are as follows:

$$V_1(\alpha,\beta,\gamma) = \cos^2\alpha(\cos^2\beta\cos^2\gamma + \sin^2\beta\sin^2\gamma) + \sin^2\alpha(\sin^2\beta\cos^2\gamma + \cos^2\beta\sin^2\gamma), \tag{6}$$

$$V_2(\alpha,\beta,\gamma) = (1/2)\sin 2\alpha \sin 2\beta\cos^2\gamma, \tag{7}$$

$$V_3(\alpha,\beta,\gamma) = (1/2)\sin 2\alpha\cos^2\beta \sin 2\gamma, \tag{8}$$

$$V_4(\alpha,\beta,\gamma) = -(1/2)\cos 2\alpha \sin 2\beta \sin 2\gamma, \tag{9}$$

$$V_5(\alpha,\beta,\gamma) = -(1/2)\sin 2\alpha\sin^2\beta \sin 2\gamma, \tag{10}$$

$$V_6(\alpha,\beta,\gamma) = -(1/2)\sin 2\alpha \sin 2\beta\sin^2\gamma. \tag{11}$$

We can now resolve two important cases: one case with $\beta = 0°$ to which the non-zero terms $V_1(\alpha,\beta = 0°,\gamma)$ and $V_3(\alpha,\beta = 0°,\gamma)$ correspond and the spectral density $S^+(\alpha,\gamma;\omega) = S(\alpha,\beta = 0°,\gamma;\omega)$ is given by

$$S^+(\alpha,\gamma;\omega) = S_0(\omega)\{\sin^2\alpha\sin^2\gamma + \cos^2\alpha\cos^2\gamma + (1/2)\sin 2\alpha \sin 2\gamma\,\mathrm{Re}\{\exp\{-\mathrm{i}[\Phi^+(\omega)]\}\}\}, \tag{12}$$

where

$$\Phi^+(\omega) = \Phi_\mathrm{f}(d;\omega) - \Phi(L;\omega) = (\omega/c)[B_\mathrm{f}(\omega)d - B(\omega)L]. \tag{13}$$

The other case is with $\beta = 90°$ to which the non-zero terms $V_1(\alpha,\beta = 90°,\gamma)$ and $V_5(\alpha,\beta = 90°,\gamma)$ correspond and the spectral density $S^-(\alpha,\gamma;\omega) = S(\alpha,\beta = 90°,\gamma;\omega)$ is given by

$$S^-(\alpha,\gamma;\omega) = S_0(\omega)\{\sin^2\alpha\cos^2\gamma + \cos^2\alpha\sin^2\gamma - (1/2)\sin 2\alpha \sin 2\gamma\,\mathrm{Re}\{\exp\{+\mathrm{i}[\Phi^-(\omega)]\}\}\}, \tag{14}$$

where

$$\Phi^-(\omega) = \Phi_\mathrm{f}(d;\omega) + \Phi(L;\omega) = (\omega/c)[B_\mathrm{f}(\omega)d + B(\omega)L]. \tag{15}$$

Next, let us consider that the optical field at the output of the sensing optical fiber, including the effect of the polarizer, the birefringent crystal and the analyzer, is analyzed by a spectrometer characterized by both the spectrally dependent transmittance $F_\mathrm{R}(\omega)$ of the read optical fiber [12] and the response function $R(\omega-\omega')$ of a given spectral bandpass. The spectral intensity $I^\pm(\alpha,\gamma;\omega)$ as a function of the angular frequency ω adjusted by the spectrometer can be expressed by the convolution relation:

$$I^\pm(\alpha,\gamma;\omega) = \int_0^\infty S^\pm(\alpha,\gamma;\omega')R(\omega-\omega')\,\mathrm{d}\omega'. \tag{16}$$

On substituting from Eqs. (12) and (14) into Eq. (16), and assuming that the spectral density $I_0(\omega) = F_\mathrm{R}(\omega)S_0(\omega)$ is slowly varying function of ω, or equivalently, that it is constant within the spectrometer bandpass, we obtain for the spectral intensity at the output of the setup shown in Fig. 1:

$$I^\pm(\alpha,\gamma;\omega) = I_0^\pm(\alpha,\gamma;\omega)\{1 + V^\pm(\alpha,\gamma)\mathrm{Re}\{\Gamma^\pm(\omega)\}\}, \tag{17}$$

where for example

$$I_0^+(\alpha,\gamma;\omega) = I_0(\omega)(\sin^2\alpha\cos^2\gamma + \cos^2\alpha\sin^2\gamma) \tag{18}$$

is the reference spectral intensity,

$$V^+(\alpha,\gamma) = \frac{1}{2}\frac{\sin 2\alpha \sin 2\gamma}{\sin^2\alpha\cos^2\gamma + \cos^2\alpha\sin^2\gamma} \tag{19}$$

is a visibility term and $\Gamma^\pm(\omega)$ is given by

$$\Gamma^\pm(\omega) = \int_0^\infty R(\omega-\omega')\exp\{\mp\mathrm{i}[\Phi^\pm(\omega')]\}\,\mathrm{d}\omega'. \tag{20}$$

Let us assume now that the spectrometer response function is a Gaussian function with half-width Γ_R:

$$R(\omega-\omega') = (1/\pi\Gamma_\mathrm{R})\exp\left[-(\omega-\omega')^2/\Gamma_\mathrm{R}^2\right]. \tag{21}$$

Similarly, let us assume that the retardances $\Phi^\pm(\omega')$ can be expanded in a Taylor series around the frequency ω so that it is truncated only to the two terms (higher-order dispersion effects are negligible):

$$\Phi^\pm(\omega') \approx \Phi^\pm(\omega) + \Phi^{\pm\prime}(\omega)(\omega'-\omega), \tag{22}$$

where $\Phi^\pm(\omega)$ and $\Phi^{\pm\prime}(\omega)$ are the retardances and the first derivatives of the retardances, respectively, at the frequency ω. On substituting Eqs. (21) and (22) into Eq. (20) we obtain [14]:

$$\Gamma^\pm(\omega) = \exp\left[-(\pi/2)\Delta\tau^{\pm2}(\omega)/\tau_\mathrm{c}^2\right]\exp\{\mp\mathrm{i}[\Phi^\pm(\omega)]\}, \tag{23}$$

where

$$\Delta\tau^\pm(\omega) = \Phi^{\pm\prime}(\omega) \tag{24}$$

are the overall differential group delays between the orthogonally polarized eigenwaves in the setup shown in Fig. 1 and $\tau_\mathrm{c} = (2\pi)^{1/2}/\Gamma_\mathrm{R}$ is the modified coherence time [13].

2.2. The spectral intensity in the wavelength domain

Let a birefringent crystal and optical fiber are characterized by the wavelength-dependent birefringences $B_\mathrm{f}(\lambda)$ and $B(\lambda)$. The spectral intensity recorded at the output of the setup shown in Fig. 1 is given by

$$I^\pm(\alpha,\gamma;\lambda) = I_0^\pm(\alpha,\gamma;\lambda)\left\{1 + V^\pm(\alpha,\gamma)V_R^\pm(\lambda)\cos[\Phi^\pm(\lambda)]\right\}, \tag{25}$$

where

$$V_R^\pm(\lambda) = \exp\left[-(\pi/2)\Delta\tau^{\pm2}(\lambda)/\tau_\mathrm{c}^2\right] \tag{26}$$

is a visibility term due to the effect of the spectrometer. Using Eq. (24) we can express the wavelength-dependent differential group OPD $\Delta^{\mathrm{g}\pm}(\lambda)$ between eigenwaves in the setup as

$$\Delta^{g\pm}(\lambda) = -\frac{\lambda^2}{2\pi}\frac{d[B_f(\lambda)d \mp B(\lambda)L]}{d\lambda} = G_f(\lambda)d \mp G(\lambda)L, \quad (27)$$

where $G_f(\lambda)$ and $G(\lambda)$ are the wavelength-dependent group birefringences given by

$$G_f(\lambda) = B_f(\lambda) - \lambda\frac{dB_f(\lambda)}{d\lambda}, \quad G(\lambda) = B(\lambda) - \lambda\frac{dB(\lambda)}{d\lambda}. \quad (28)$$

Denoting $\Delta\lambda_R = \Delta\lambda'_R\sqrt{2}$ the width of the spectrometer response function $R(\lambda)$ in the wavelength domain [12] with $\Delta\lambda'_R = \lambda^2\Gamma_R/(2\pi c)$, we can express the wavelength-dependent visibility term $V_R^{\pm}(\lambda)$ as:

$$V_R^{\pm}(\lambda) = \exp\{-(\pi^2/2)[(G_f(\lambda)d \mp G(\lambda)L)\Delta\lambda_R/\lambda^2]^2\}. \quad (29)$$

2.2.1. The positive birefringence of a uniaxial crystal

Let us consider a uniaxial birefringent crystal, such as quartz, which has the positive birefringence, that is, $B_f(\lambda) > 0$ over the wavelength range of the visible spectrum. In this case, the recorded spectrum can be represented in the form

$$\begin{aligned} I^+(\alpha,\gamma;\lambda) = I_0^+(\alpha,\gamma;\lambda)\{1 + V^+(\alpha,\gamma) \\ \times \exp\{-(\pi^2/2)[(G_f(\lambda)d - G(\lambda)L)\Delta\lambda_R/\lambda^2]^2\} \\ \times \cos\{(2\pi/\lambda)[B_f(\lambda)d - B(\lambda)L]\}\}, \end{aligned} \quad (30)$$

from which it results that the spectral interference fringes have the highest visibility at the equalization wavelength λ_0^+ that fulfills the relation

$$G(\lambda_0^+)L = G_f(\lambda_0^+)d. \quad (31)$$

2.2.2. The negative birefringence of a uniaxial crystal

Let us consider a uniaxial birefringent crystal, such as calcite, which has the negative birefringence, that is, $B_f(\lambda) < 0$ over the wavelength range of the visible spectrum. In this case, the recorded spectrum can be represented in the form

$$\begin{aligned} I^-(\alpha,\gamma;\lambda) = I_0^-(\alpha,\gamma;\lambda)\{1 + V^-(\alpha,\gamma) \\ \times \exp\{-(\pi^2/2)[(G_f(\lambda)d + G(\lambda)L)\Delta\lambda_R/\lambda^2]^2\} \\ \times \cos\{(2\pi/\lambda)[B_f(\lambda)d + B(\lambda)L]\}\}, \end{aligned} \quad (32)$$

from which it results that the spectral interference fringes have the highest visibility at the equalization wavelength λ_0^- that fulfills the relation

$$G(\lambda_0^-)L = -G_f(\lambda_0^-)d. \quad (33)$$

3. Modeling spectral interferograms

In this section, the wavelength-domain spectral intensity will be modeled for two cases of a uniaxial crystal having opposite sign of birefringence and a highly birefringent optical fiber of known dispersion characteristics.

3.1. Quartz crystal

First, we consider a uniaxial crystal of the positive birefringence, a quartz crystal, the dispersion of which can be represented in the Sellmeier-like form [15]:

$$B_f(\lambda) = H + \frac{I\lambda^2}{\lambda^2 - G} + \frac{J\lambda^2}{\lambda^2 - K}, \quad (34)$$

where λ is wavelength in microns and the dispersion coefficients at room temperature are as follows: $G = 1.37254429\times10^{-2}$, $H = 0.78890253\times10^{-3}$, $I = 8.04095323\times10^{-3}$, $J = 10.1933186\times10^{-3}$ and $K = 64$. Using Eq. (28), the group birefringence dispersion can be represented as

$$G_f(\lambda) = B_f(\lambda) + \frac{2IG\lambda^2}{(\lambda^2 - G)^2} + \frac{2JK\lambda^2}{(\lambda^2 - K)^2}. \quad (35)$$

We will model the spectral intensity $I^+(\alpha,\gamma;\lambda)$ given by Eq. (30) for a highly birefringent fiber, the phase and group modal birefringences $B(\lambda)$ and $G(\lambda)$ of which are known from previous measurements [10]. The phase birefringence $B(\lambda)$ decreases from 2.615×10^{-4} to 2.353×10^{-4} and the group birefringence $G(\lambda)$ increases from 2.685×10^{-4} to 3.883×10^{-4} in the wavelength range from 550 to 800 nm. Fig. 3 shows the group OPD $G(\lambda)L$ between the polarization modes as a function of the wavelength λ for the length $L = 1$ m of the optical fiber. In the same figure, the group OPD $G_f(\lambda)d$ between the polarization eigenwaves in the quartz crystal is shown by the bold line as a function of the wavelength λ for the crystal thickness $d = 3.2$ cm. Both lines cross at the equalization wavelength $\lambda_0^+ = 646.50$ nm fulfilling Eq. (31).

Fig. 4 then shows by the solid curve the corresponding spectral intensity $I^+(\alpha,\gamma;\lambda)$ given by Eq. (30) when $I_0^+(\alpha,\gamma;\lambda)$ is represented by a Gaussian spectrum, $V^+(\alpha,\gamma) = 0.5$ and $\Delta\lambda_R = 3$ nm. The dashed curve in the

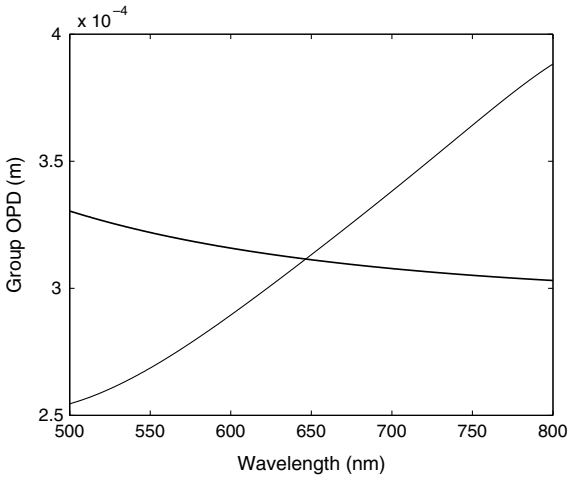

Fig. 3. Wavelength dependence of the group OPD $G_f(\lambda)d$ in the quartz crystal of thickness $d = 3.2$ cm (bold line) and $G(\lambda)L$ in the birefringent fiber of length $L = 1$ m.

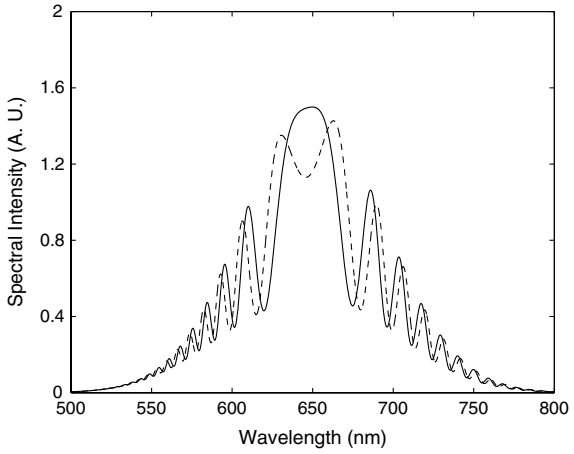

Fig. 4. Theoretical spectral interferograms corresponding to two different fiber lengths L of 1 and 1.0005 m.

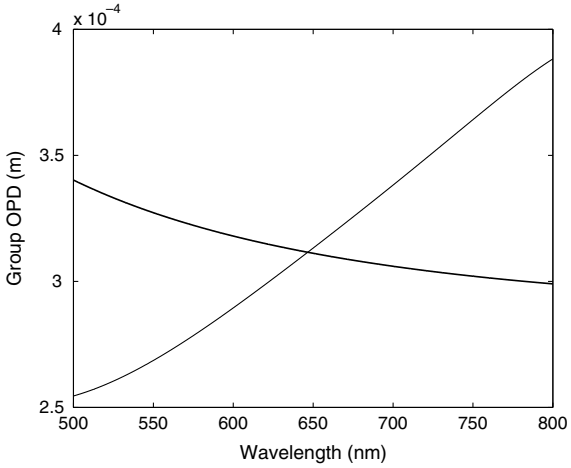

Fig. 5. Wavelength dependence of the group OPD $-G_{\mathrm{f}}(\lambda)d$ in the calcite crystal of thickness $d = 1.65$ mm (bold line) and $G(\lambda)L$ in the birefringent fiber of length $L = 1$ m.

same figure shows the spectral intensity $I^{+}(\alpha,\gamma;\lambda)$ when the length of the fiber is $L = 1.0005$ m. This figure clearly demonstrates the sensitivity of the phase of the spectral interference fringes to the change of the fiber length. We may introduce the polarimetric sensitivity [8]

$$S_L(\lambda) = \frac{1}{L}\frac{\mathrm{d}[\Phi(L;\lambda)]}{\mathrm{d}L} = \frac{1}{L}\frac{\mathrm{d}}{\mathrm{d}L}\left[\frac{2\pi}{\lambda}B(\lambda)L\right] = \frac{2\pi}{\lambda}\frac{B(\lambda)}{L}, \qquad (36)$$

which decreases in the 550–800 nm wavelength range from 2.99 to 1.85 rad mm^{-1} m^{-1}. These values mean that for the fiber length $L = 1$ m the phase changes of 2π at 550 and 800 nm, respectively, are associated with the fiber length changes of 2.1 and 3.4 mm.

3.2. Calcite crystal

Next, we consider a uniaxial crystal of the negative birefringence, a calcite crystal, the dispersion of which can be represented in the Sellmeier-like form given by Eqs. (34) and (35) with the dispersion coefficients at room temperature as follows [15]: $G = 2.17641576 \times 10^{-2}$, $H = -29.435688 \times 10^{-3}$, $I = -134.804456 \times 10^{-3}$, $J = -294.96110 \times 10^{-3}$ and $K = 80$.

We will model the spectral intensity $I^{-}(\alpha,\gamma;\lambda)$ given by Eq. (32) for the same highly birefringent fiber as in the previous section. Fig. 5 shows the group OPD $G(\lambda)L$ between the polarization modes as a function of the wavelength λ for the length $L = 1$ m of the optical fiber. In the same figure, the group OPD $-G_{\mathrm{f}}(\lambda)d$ between the polarization eigenwaves in the calcite crystal is shown by the bold line as a function of the wavelength λ for the crystal thickness $d = 1.65$ mm. Both lines cross at the equalization wavelength $\lambda_0^{-} = 646.60$ nm fulfilling Eq. (33).

Fig. 6 then shows by the solid curve the corresponding spectral intensity $I^{-}(\alpha,\gamma;\lambda)$ given by Eq. (32) when $I_0^{-}(\alpha,\gamma;\lambda)$ is represented by a Gaussian spectrum, $V^{-}(\alpha,\gamma) = 0.5$ and $\Delta\lambda_{\mathrm{R}} = 3$ nm. The dashed curve in the

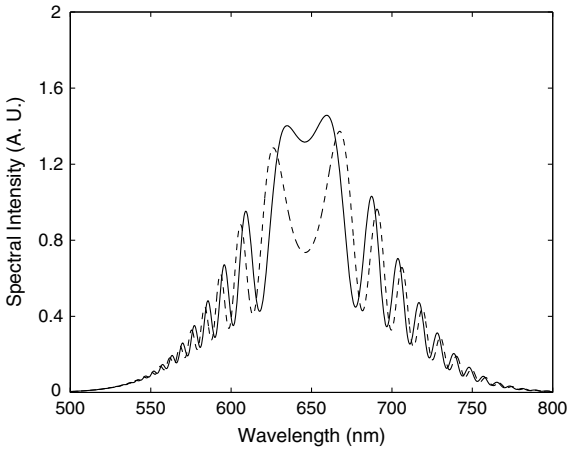

Fig. 6. Theoretical spectral interferograms corresponding to two different fiber lengths L of 1 and 1.0005 m.

same figure shows the spectral intensity $I^{-}(\alpha,\gamma;\lambda)$ when the length of the fiber is $L = 1.0005$ m. This figure once again clearly demonstrates the sensitivity of the phase of the spectral interference fringes to the change of the fiber length. The polarimetric sensitivities in the 550–800 nm wavelength range are the same as stated in the previous section.

4. Experimental setup, results and discussion

The experimental setup used in the application of spectral-domain interferometry to resolve spectral interference fringes in a tandem configuration of birefringent crystal and birefringent fiber is shown in Fig. 1. It consists of a white-light source, a 20 W quartz tungsten halogen (QTH) lamp with a collimating lens, a polarizer, a quartz

parallel plate, a microscope objective, a birefringent optical fiber, an analyzer, a fiber optic spectrometer S2000, an A/D converter and a personal computer. The quartz plate consists of four polished surfaces, parallel to the optical axis of the crystal with a precision of 15″. The plate is placed in the setup in such a way that the collimated beam from the halogen lamp is incident on the two polished surfaces perpendicularly. The thickness of the plate is in the direction of the z-axis $d_1 = (20{,}950 \pm 10)$ μm and in the direction of the x-axis $d_2 = (25{,}750 \pm 10)$ μm.

The birefringent fiber with the elliptical core has length $L = 0.69$ m, a cutoff wavelength for the *even* LP_{11} mode is equal to 780 nm, a core-cladding refractive index difference of 0.026 at a wavelength of 630 nm (the core is doped with GeO_2 of 18 mol% concentration and the cladding is made of fused silica) and core dimensions of 3.26×1.14 μm. The fiber optic spectrometer S2000 has the spectral operation range from 350 to 1000 nm and the resolution given by the effective width of the light beam from a core of the read optical fiber. We used the read optical fiber of a 50 μm core diameter to which a Gaussian response function corresponds [16] with the width $\Delta\lambda_R = 3.0$ nm.

We used the first orientation of the quartz plate with the corresponding thickness d_1 and adjusted the transmission axes of the polarizer and analyzer to be $\alpha, \gamma = 45°$ so that $V^+(\alpha, \gamma) = 1$. We recorded two spectral interferograms, one for the original length and the other one for slightly changed length of the optical fiber. These interferograms are shown in Fig. 7 by the solid and dashed curves. Both interferograms are characterized by the equalization wavelength λ_0^+, which is close to the theoretical value $\lambda_0^+ = 618.20$ nm given by Eq. (31).

Next, we used the second orientation of the quartz plate with the corresponding thickness d_2. We recorded two spectral interferograms, one for the original length and the other one for slightly changed length of the optical fiber. These interferograms are shown in Fig. 8 by the solid and dashed curves. Both interferograms are characterized by the equalization wavelength λ_0^+, which is close to the theoretical value $\lambda_0^+ = 723.70$ nm given by Eq. (31). The interferograms demonstrate qualitatively sensing abilities of the birefringent fiber in the setup with the birefringent crystal. From the point of the practical implementation of the sensing configuration, the use of longer fiber and consequently the birefringent crystal of the greater thickness are needed. Moreover, to detect phase changes at one specific wavelength that are related to the sensing of a measurand, a specialized interrogation procedure has to be proposed and applied.

5. Conclusions

We analyzed theoretically and experimentally spectral interference of white-light beams propagating through a tandem configuration of birefringent crystal and sensing birefringent fiber. The spectral interference law was expressed analytically under the condition of a Gaussian response function of a spectrometer taking into account the dispersion of birefringence in the crystal and in the fiber. We revealed that the visibility of spectral interference fringes is highest for the group OPD in the crystal compensating the group OPD in the fiber. We modeled two types of spectral interferograms knowing dispersion characteristics of the sensing fiber and using a quartz crystal of the positive or a calcite crystal of the negative birefringence. A highly birefringent fiber and a birefringent quartz crystal of two suitable thicknesses were employed in two experiments. We resolved spectral interference fringes and confirmed in accordance with the theory that the wavelength-dependent phases of spectral interference fringes vary with the fiber length. The results obtained are important from the point of view of an optimal adjustment of thickness of a birefringent crystal in this new fiber optic white-light interferometric sensor configuration. We

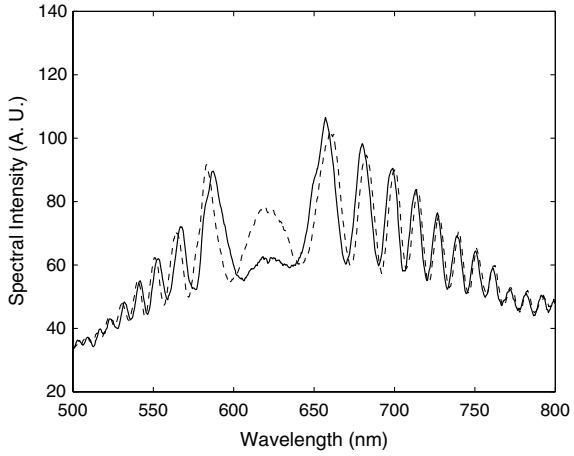

Fig. 7. Spectral interferograms recorded for two different fiber lengths. The thickness of the quartz crystal is $d_1 = (20{,}950 \pm 10)$ μm.

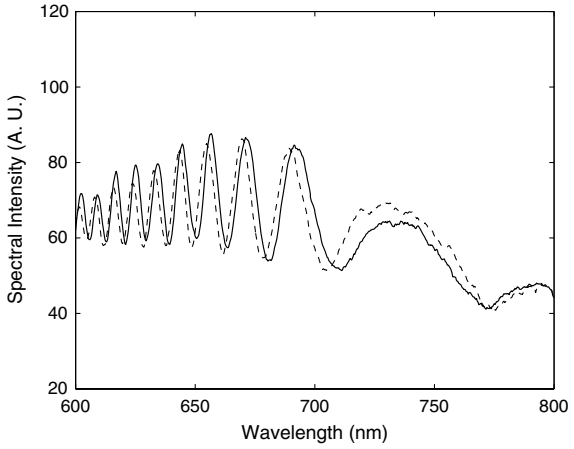

Fig. 8. Spectral interferograms recorded for two different fiber lengths. The thickness of the quartz crystal is $d_2 = (25{,}750 \pm 10)$ μm.

are going to use the fiber sensor to resolve spectral fringes and to measure temperature, strain, pressure, etc.

Acknowledgements

This research was partially supported by the Grant Agency of the Czech Republic (Project No. 202/03/0776), by the Grant MSM6198910016, and by an internal grant of TU Ostrava (IGS HGF VŠB-TUO).

References

[1] Y.J. Rao, D.A. Jackson, Meas. Sci. Technol. 7 (1996) 981.
[2] F. Farahi, T.P. Newson, J.D.C. Jones, D.A. Jackson, Opt. Commun. 65 (1988) 319.
[3] K. Takada, K. Chida, J. Noda, Appl. Opt. 26 (1987) 2979.
[4] A.S. Gerges, T.P. Newson, D.A. Jackson, Appl. Opt. 29 (1990) 4473.
[5] K. Bohnert, G. de Wit, J. Nehring, Opt. Lett. 17 (1992) 694.
[6] D.A. Flavin, R. McBride, J.D.C. Jones, Opt. Commun. 156 (1998) 367.
[7] W. Urbańczyk, T. Martynkien, W.J. Bock, Appl. Opt. 40 (2001) 1911.
[8] G. Statkiewicz, T. Martynkien, W. Urbańczyk, Opt. Commun. 241 (2004) 339.
[9] W.J. Bock, W. Urbańczyk, Appl. Opt. 32 (1993) 5841.
[10] P. Hlubina, T. Martynkien, W. Urbańczyk, Opt. Express. 11 (2003) 2793.
[11] P. Hlubina, W. Urbańczyk, Meas. Sci. Technol. 16 (2005) 1267.
[12] P. Hlubina, Opt. Commun. 251 (2005) 367.
[13] L. Mandel, E. Wolf, Optical Coherence and Quantum Optics, Cambridge University Press, Cambridge, 1995, Section 5.8.
[14] I.S. Gradsteyn, I.M. Ryzhik, Table of Integrals, Series, and Products, Academic Press, New York, 1980.
[15] G. Ghosh, Opt. Commun. 163 (1999) 95.
[16] P. Hlubina, I. Gurov, V. Chugunov, J. Mod. Opt. 50 (2003) 2067.

Paper XI.

IOP Publishing Journal of Optics
J. Opt. **12** (2010) 035405 (8pp) doi:10.1088/2040-8978/12/3/035405

Broad spectral range measurements and modelling of birefringence dispersion in two-mode elliptical-core fibres

P Hlubina[1,4], T Martynkien[2], D Ciprian[1], J Wójcik[3] and W Urbańczyk[2]

[1] Department of Physics, Technical University Ostrava, 17. listopadu 15, 708 33 Ostrava-Poruba, Czech Republic
[2] Institute of Physics, Wroclaw University of Technology, Wybrzeże, Wyspiańskiego 27, 50-370 Wroclaw, Poland
[3] Laboratory of Optical Fibre Technology, Maria Curie-Sklodowska University, Pl. M Curie-Sklodowskiej 3, 20-031 Lublin, Poland

E-mail: petr.hlubina@vsb.cz

Received 18 November 2009, accepted for publication 1 February 2010
Published 8 March 2010
Online at stacks.iop.org/JOpt/12/035405

Abstract
We present the results of measurement and modelling of the birefringence dispersion in elliptical-core fibres (ECFs). The measurement is performed over a broad wavelength range (e.g. 450–1450 nm) by two spectral interferometric techniques. First, a technique employing a tandem configuration of a Michelson interferometer and an ECF under test is used for a broad spectral range measurement of the group modal birefringence for two spatial modes supported by the fibre. Second, a method with a lateral point-like force acting on the fibre and based on spectral interferometry is used for measuring the phase modal birefringence at one wavelength for the fundamental mode only. The measured value is combined with the dispersion of the group modal birefringence to obtain the phase modal birefringence over a broad wavelength range. We also modelled the dispersion characteristics taking into account contributions of both the elliptical shape of the core and the residual thermal stress. The dispersion characteristics measured for the three ECFs show very good agreement with the results of numerical modelling.

Keywords: spectral interferometry, birefringent fibre, elliptical core, birefringence, dispersion, numerical modelling

1. Introduction

Two-mode optical fibres have found numerous applications in the field of speciality optical devices and sensors. They are frequently used as active elements of interferometric sensors in which polarization modes must be controlled to assure a high-contrast interference signal. To overcome the problem of interference contrast fading, which degrades operation of optical devices and sensors based on conventional circular-core fibres, elliptical-core fibres (ECFs) [1] with nondegenerate polarization modes have been proposed and fabricated. The ECFs are capable of maintaining the state of polarization of propagating light over long distances. As a result, the ECFs have attracted considerable interest for a number of applications in which polarization control plays an essential role, such as interferometric modal/polarimetric sensors for measuring strain, temperature, pressure or several parameters simultaneously [2–5].

For the sensing of various physical quantities employing interferometric techniques [6], it is important to know the dispersion characteristics such as the phase and group modal birefringence versus wavelength. So far, the dispersion of the orthogonally polarized fundamental modes and the dispersion of the second-order even LP_{11} mode near cut-off have been

[4] Author to whom any correspondence should be addressed.

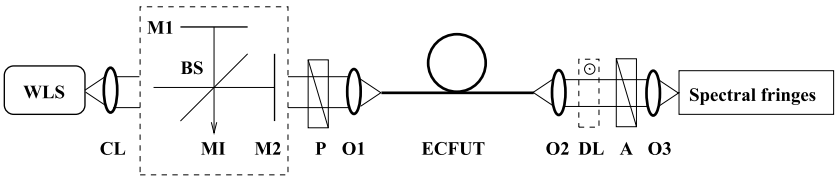

Figure 1. Experimental set-up for measuring the wavelength dependence of the group modal birefringence in the elliptical-core fibre (ECF) under test.

analysed theoretically and experimentally. Time domain low-coherence interferometry and spectral domain white-light interferometry with channelled spectrum detection have been used for measuring dispersion characteristics of birefringent optical fibres [7–16]. Time domain interferometry has been used to measure the polarization-mode dispersion [7] and dispersion of modal birefringence in highly birefringent optical fibres [8–10]. Spectral domain interferometry has been used to measure birefringence dispersion in polarization-maintaining optical fibres [11–16]. Recently, the dispersion in a two-mode birefringent ECF has been analysed theoretically [17]. However, to the best of our knowledge, comprehensive experimental and theoretical analysis of dispersion properties of two-mode birefringent ECFs has not been carried out.

In this paper, two spectral interferometric techniques are used for measuring the birefringence dispersion in three ECFs. We measured the phase and group modal birefringence for the LP_{01} and even LP_{11} spatial modes over a broad wavelength range. The group modal birefringence was measured by a spectral interferometric technique [15, 18] employing a tandem configuration of a Michelson interferometer and an ECF under test. The phase modal birefringence was measured at one wavelength for the fundamental mode only by a method with a lateral point-like force acting on the fibre [19]. The method was applied in the spectral domain and the measured value of the phase modal birefringence was combined with the dispersion of the group modal birefringence to determine the phase modal birefringence over a broad wavelength range. The dispersion characteristics were also calculated numerically using an approach that takes into account contributions of both the elliptical shape of the core and the residual thermal stress. We confirmed for all three ECFs good agreement between modelling and experiment.

2. Experimental methods

Let us consider an ECF, which supports the x- and y-polarized LP_{01} and even LP_{11} spatial modes. If the wavelength-dependent propagation constants of the corresponding modes are denoted as $\beta_{01}^x(\lambda)$, $\beta_{01}^y(\lambda)$, $\beta_{11}^x(\lambda)$, and $\beta_{11}^y(\lambda)$, we can define the phase modal birefringences for the respective spatial modes in the following way:

$$B_{01}(\lambda) = \frac{\lambda}{2\pi}[\beta_{01}^x(\lambda) - \beta_{01}^y(\lambda)] \tag{1}$$

and

$$B_{11}(\lambda) = \frac{\lambda}{2\pi}[\beta_{11}^x(\lambda) - \beta_{11}^y(\lambda)]. \tag{2}$$

Furthermore, using the following relation for the group modal birefringence $G(\lambda)$:

$$G(\lambda) = B(\lambda) - \lambda\frac{\mathrm{d}B(\lambda)}{\mathrm{d}\lambda} = -\lambda^2\frac{\mathrm{d}[B(\lambda)/\lambda]}{\mathrm{d}\lambda}, \tag{3}$$

we can determine the group modal birefringences $G_{01}(\lambda)$ and $G_{11}(\lambda)$ for the respective spatial modes.

2.1. Measurement of group modal birefringence

The group modal birefringences $G_{01}(\lambda)$ and $G_{11}(\lambda)$ for the LP_{01} and the even LP_{11} spatial modes, respectively, were measured by a method of spectral domain tandem interferometry [15, 18] in the set-up shown in figure 1. Light from a white-light source WLS (a 20 W quartz–tungsten–halogen lamp) passes through collimator CL and enters Michelson interferometer MI in which the path length difference Δ_M is adjusted. The light from the output of the interferometer passes though Glan–Taylor calcite polarizer P (Thorlabs) and is introduced by microscope objective O1 ($15\times$ /0.30) into an ECF under test. The transmission azimuth of the polarizer is adjusted at 45° with respect to the polarization axes of the ECF so that both polarization modes are excited in the tested fibre. Using microscope objective O2 ($10\times$ /0.30) at the output of the tested fibre, a collimated light beam is generated that passes through Glan–Taylor calcite analyser A (Thorlabs) and is introduced by the next objective O3 ($10\times$ /0.30) into the read fibre of a spectrometer (S2000, NIR-512, Ocean Optics) which resolves the interference of polarization modes as a spectral signal. The transmission azimuth of the analyser is adjusted at 45° with respect to the polarization axes of the ECF. The orientations of the fibre polarization axes were first determined at the fibre input and output by rotating the analyser A and the polarizer P until light at the fibre output is extinguished. For a white-light illumination, a complete light extinction can only be achieved for the polarizer and analyser aligned in parallel with the fibre axes of orthogonal polarization.

The spectrometers S2000 and NIR-516 have a spectral operation range from 350 to 1000 nm and from 850 to 1700 nm, respectively. The spectral signal is recorded by the spectrometer in the transmission mode after dark and reference (without the interference) spectra are stored. If the two-mode ECF of length z investigated has $G_{01}(\lambda)z \gg 0$ and $G_{11}(\lambda)z \gg 0$, and the path length difference adjusted in the Michelson interferometer is similarly $\Delta_M \gg 0$, the spectral signal recoded

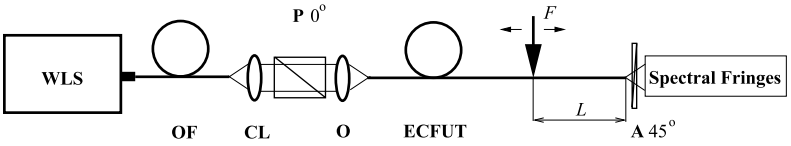

Figure 2. Experimental set-up for measuring the phase modal birefringence at a specific wavelength in the ECF under test.

by a spectrometer of a Gaussian response function can be represented in the following form [15, 18]:

$$\begin{aligned} S(\lambda) &= 1 + 0.5V_0(\lambda) \\ &\times \exp\{-(\pi^2/2)[(G_{01}(\lambda)z - \Delta_M)\Delta\lambda_R/\lambda^2]^2\} \\ &\times \cos[(2\pi/\lambda)(B_{01}(\lambda)z - \Delta_M)] \\ &+ 0.5V_1(\lambda)\exp\{-(\pi^2/2)[(G_{11}(\lambda)z - \Delta_M)\Delta\lambda_R/\lambda^2]^2\} \\ &\times \cos[(2\pi/\lambda)(B_{11}(\lambda)z - \Delta_M)], \end{aligned} \quad (4)$$

where $V_0(\lambda)$ and $V_1(\lambda)$ are visibility terms, and $\Delta\lambda_R$ is the width of the spectrometer response function. Generally speaking, at the output of the spectrometer we observe two separated interference signals associated with LP_{01} and even LP_{11} modes respectively. The first one corresponds to the LP_{01} spatial mode and arises in the vicinity of the so-called equalization wavelength λ_{eq}^{01} [15]. The second one corresponds to the even LP_{11} spatial mode and arises in the vicinity of the equalization wavelength λ_{eq}^{11}.

To resolve the spectral fringes in one of the interference signals or in both signals, the path length difference governed by the relations $\Delta_M^{01} = G_{01}(\lambda_{eq}^{01})z$ and $\Delta_M^{11} = G_{11}(\lambda_{eq}^{11})z$ needs to be adjusted in the Michelson interferometer. Thus, the path length difference Δ_M adjusted in the interferometer and measured as a function of the equalization wavelengths λ_{eq}^{01} and λ_{eq}^{11} gives directly the wavelength dependence of the group modal birefringences $G_{01}(\lambda_{eq}^{01}) = \Delta_M^{01}/z$ and $G_{11}(\lambda_{eq}^{11}) = \Delta_M^{11}/z$ in the ECF under test. To avoid overlapping of interference signals corresponding to the LP_{01} and even LP_{11} modes, one needs to use sufficiently long fibre.

The sign of the group modal birefringence can also be determined in the set-up shown in figure 1. We place delay line DL, represented by a quartz crystal of suitable thickness and orientation, in tandem with the ECF under test and use a simple procedure [18]. If the extraordinary axis of the crystal, which has the positive group birefringence ($N_e > N_o$), is parallel to the major axis of the elliptical core (along the x polarization mode), and the group birefringence of the fibre is positive, the equalization wavelength shifts to shorter wavelengths after inserting the delay plate. In the opposite case the group birefringence is negative.

2.2. Measurement of phase modal birefringence

The phase modal birefringence $B_{01}(\lambda)$ for the LP_{01} spatial mode was measured by a lateral force method applied in the spectral domain [19]. Figure 2 illustrates the corresponding experimental set-up in which light from the white-light source WLS is launched into optical fibre OF with collimator CL, passes through polarizer P and is introduced by microscope objective O into an ECF under test. The transmission azimuth of the polarizer is adjusted in parallel with the symmetry axis of the ECF so that only one polarization mode is excited in the tested fibre. Point-like force F is applied to the tested fibre causing polarization coupling so that a fraction of light is coupled into the polarization mode that is not excited at the input of the test fibre. The two polarization modes are propagating through the fibre of length L, which is given by the distance of the coupling point from the fibre end. The two polarization modes are mixed with analyser A (Polaroid) and their interference is resolved by a spectrometer as the interferogram. The transmission azimuth of the analyser is adjusted to 45° with respect to the polarization axes of the ECF under test. A loop of the ECF was used to strip off the higher-order modes and to smooth the reference spectrum as much as possible.

In response to the displacement $\Delta L = L_2 - L_1$ of the coupling point along the tested fibre, we measure the phase change $\Delta\phi(\lambda_0)$ of the spectral interference fringes (e.g. 2π), from which the beat length can be determined according to

$$L_B(\lambda_0) = 2\pi\,\Delta L/\Delta\phi(\lambda_0), \quad (5)$$

where λ_0 is the wavelength at which the phase change $\Delta\phi(\lambda_0)$ has been determined [19]. If the fibre beat length $L_B(\lambda_0)$ is known, the phase modal birefringence $B(\lambda_0)$ can be easily calculated by means of the following relation:

$$B(\lambda_0) = \lambda/L_B(\lambda_0). \quad (6)$$

Because the group modal birefringence $G_{01}(\lambda)$ measured by the first method is related to the phase modal birefringence $B_{01}(\lambda)$ via equation (3), we are able to obtain the relative wavelength dependence of the phase modal birefringence. It can be combined with the known value $B(\lambda_0)$ at the wavelength λ_0 to obtain the absolute values of the wavelength dependence of the phase modal birefringence $B_{01}(\lambda)$ [15, 18]. The phase modal birefringence $B_{11}(\lambda)$ could not be measured in this way because it was impossible to excite purely the even LP_{11} spatial mode.

3. ECFs investigated

We investigated three ECFs: the first one was PMF-38 fibre from Corning (ECF 1) and the remaining two fibres were manufactured by Fibre Optic Technology Group, MCS University, Lublin, Poland (ECF 2 and 3). We performed a microanalysis of the fibres using a scanning electron microscope (type JSM 5800LV). The photographs of the fibre cross-sections are shown in figure 3. The corresponding

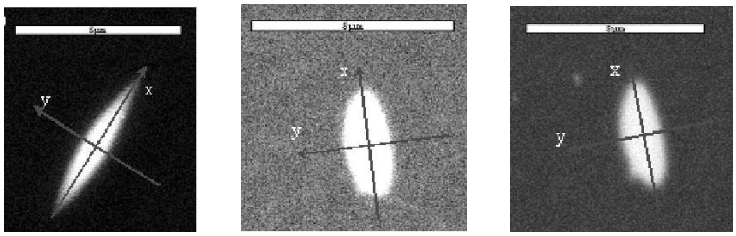

Figure 3. SEM photographs of the fibres investigated: (a) ECF 1, (b) ECF 2, (c) ECF 3.

Table 1. Core and cladding parameters of the ECFs used in calculations.

	ECF 1		ECF 2		ECF 3	
	Core	Cladding	Core	Cladding	Core	Cladding
Dimensions (μm)	3.74×0.74	80	2.5×1	76	3.42×1.2	96
Dopant concentration	18.5 mol% GeO_2	SiO_2	16.7 mol% GeO_2	SiO_2	16.7 mol% GeO_2	SiO_2
$\alpha \times 10^{-7}$ (K^{-1})	24.71	5.5	23.7	5.5	23.7	5.5
E (GPa)	62.00	72.45	62.6	72.5	62.6	72.5
ν	0.17	0.165	0.17	0.165	0.17	0.165
T_g (°C)			930			
$C_1 \times 10^{-13}$ (Pa^{-1})			−6.9			
$C_2 \times 10^{-13}$ (Pa^{-1})			−41.8			

dimensions of the fibre cores and the levels of GeO_2 concentrations in the cores are presented in table 1. The wavelength dependence of the refractive indices $n_{co}(\lambda)$ and $n_{cl}(\lambda)$ in fibre core and cladding, respectively, was taken into account in numerical simulations using the Sellmeier formulae for pure silica and GeO_2-doped silica glass [1]. To calculate the stress distribution in the fibre cross-section induced by different thermal expansion coefficients of pure and doped silica, the knowledge of several material constants is required. These are: the thermal expansion coefficient α, Young modulus E, Poisson ratio ν, glass transition temperature T_g, and stress–optical coefficients C_1, C_2. The values of these constants for pure SiO_2 glass are well known [20]. Unfortunately, there are no comprehensive data on the dependence of E, ν, C_1, C_2 upon the GeO_2 concentration in SiO_2/GeO_2; therefore we estimated these parameters for the fibre cores taking into account assumptions described in detail in the previous paper [8]. The values of all parameters used in the calculations are presented in table 1.

4. Numerical modelling

Because of the complex nature of the modal birefringence in ECFs, the calculations of the propagation constants $\beta_{01}^x(\lambda)$, $\beta_{01}^y(\lambda)$, $\beta_{11}^x(\lambda)$, and $\beta_{11}^y(\lambda)$ as a function of wavelength were divided into two steps. First, we determined the changes in refractive index that are induced by the thermal stress arising due to the fibre cooling during the drawing process as a consequence of mismatch between the thermal expansion coefficients of core and cladding glasses. In the second step, we calculated the propagation constants $\beta_{01}^x(\lambda)$, $\beta_{01}^y(\lambda)$, $\beta_{11}^x(\lambda)$, and $\beta_{11}^y(\lambda)$ of the polarization modes, taking into account the material birefringence induced by the thermal stress.

The stress calculations were carried out by means of the finite-element method FEM (software package Comsol Multiphysics). We applied the plane-stress model to calculate thermal stress distribution in the fibre cross-section [8, 21–27]. From knowledge of the distributions of the normal stress components $\sigma_x(x, y)$, $\sigma_y(x, y)$, $\sigma_z(x, y)$, and $\tau_{xy}(x, y)$ at room temperature ($T_0 = 20\,°C$), the relative permittivity tensor in the cross-section of the elliptical-core fibre under stress is determined using the following relation [26]:

$$[\varepsilon] = \begin{bmatrix} [n_0 - C_1\sigma_{xx} - C_2(\sigma_{yy} + \sigma_{zz})]^2 & 2n(C_2 - C_1)\tau_{xy} & 0 \\ 2n(C_2 - C_1)\tau_{xy} & [n_0 - C_1\sigma_{yy} - C_2(\sigma_{xx} + \sigma_{zz})]^2 & 0 \\ 0 & 0 & [n_0 - C_1\sigma_{zz} - C_2(\sigma_{xx} + \sigma_{yy})]^2 \end{bmatrix}, \tag{7}$$

where n_0 is the refractive index in the glass without stress.

The spatial distribution of the relative permittivity tensor represented by equation (7) provides the necessary information for the electromagnetic calculations by means of the FEM method. An advantage of the above approach is that mechanical and electromagnetic calculations are carried out using the same numerical technique (FEM). This makes possible easy transfer of the meshes between the mechanical and electromagnetic software modules and simplifies data-exchange procedures. As soon as the phase modal birefringence $B(\lambda)$ was determined for a given set of wavelengths, we numerically calculated the group modal birefringence $G(\lambda)$ according to equation (3).

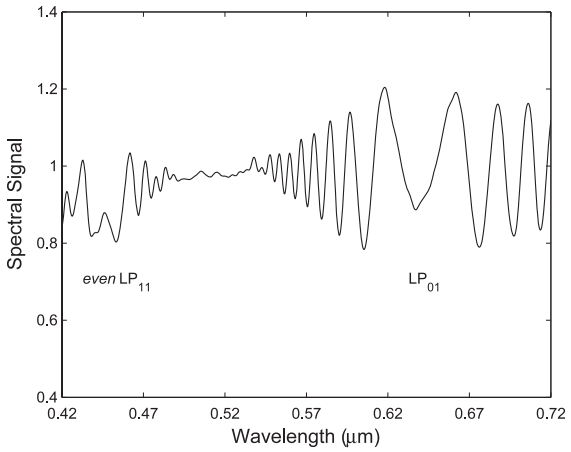

Figure 4. Example of a spectral signal recorded for ECF 1 for the path length difference in the interferometer $\Delta_M = 648\ \mu$m.

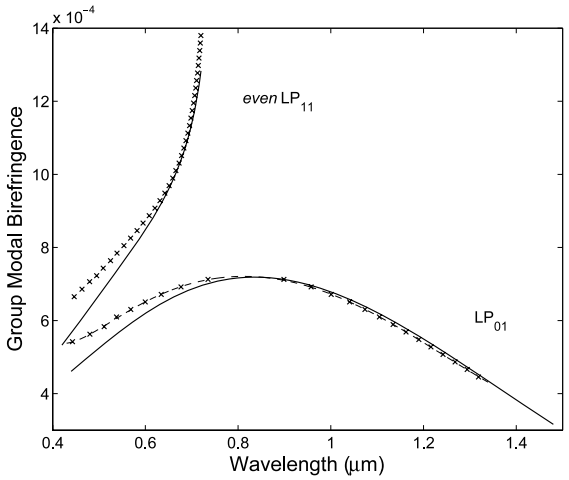

Figure 5. Group modal birefringence measured as a function of wavelength for two spatial modes of ECF 1 (the dashed line represents a power series fit) and the simulation results (the solid lines).

5. Measurement and simulation results

After optimizing the excitation and detection conditions to ensure the highest visibility of spectral interference fringes, the spectral signals were recorded for ECF 1 of length $z = 0.974$ m, for the path length differences Δ_M adjusted in the Michelson interferometer with a step of 20 μm. We revealed for the LP_{01} spatial mode that the equalization wavelength increases approximately from 443 to 735 nm (measured using an S2000 spectrometer) and from 899 to 1318 nm (measured using an NIR-512 spectrometer) with Δ_M increasing from 528 to 698 μm and decreasing from 698 to 438 μm, respectively. Similarly, we revealed for the even LP_{11} spatial mode that the equalization wavelength increases approximately from 448 to 584 nm with Δ_M increasing from 448 to 1388 μm. Figure 4 shows an example of the spectral signal recorded using the first spectrometer for $\Delta_M = 648\ \mu$m. We can clearly resolve the spectral interference fringes in the vicinities of two equalization wavelengths $\lambda_{eq}^{11} = 446.55$ and $\lambda_{eq}^{01} = 639.05$ nm. The first one corresponds to the even LP_{11} spatial mode and the second one to the LP_{01} spatial mode. It should be noted here that the visibility of the spectral fringes for the fundamental mode is higher than that for the even LP_{11} mode.

The group modal birefringences corresponding to the spatial modes are both positive. Figure 5 shows, as crosses, the measured group modal birefringences $G_{01}(\lambda_{eq})$ and $G_{11}(\lambda_{eq})$ in ECF 1 determined for the respective equalization wavelengths λ_{eq}. The precision in measuring the group modal birefringences is better than 0.1% [18]. We clearly see from figure 5 that the LP_{01} spatial mode shows a lower group modal birefringence than the even LP_{11} mode. The dashed line in the same figure represents the approximation of the measured group modal birefringence $G_{01}(\lambda)$ by a seven-term power series

$$G_{01}(\lambda) = A_1\lambda^{-6} + A_2\lambda^{-4} + A_3\lambda^{-2} + A_4 + A_5\lambda^2 + A_6\lambda^4 + A_7\lambda^6, \quad (8)$$

where the A_i are the coefficients. The shape of the measured wavelength dependence of the group modal birefringence $G_{01}(\lambda)$ is similar to that obtained by numerical modelling. Greater differences are observed for wavelengths at which $G_{01}(\lambda)$ reaches a maximum (near 812 nm) and for a short wavelength region. The difference between the experimental and calculated values increases in this region and reaches 12% at $\lambda = 0.46\ \mu$m. The group modal birefringence $G_{11}(\lambda)$ for the even LP_{11} spatial mode strongly increases against wavelength near the cut-off (approximately at 0.725 μm), which is in accordance with the results of numerical modelling. The difference between the experimental and calculated values increases with decreasing wavelength and reaches 13% at $\lambda = 0.46\ \mu$m.

The approximation of $G_{01}(\lambda)$ according to equation (8) is used to determine the corresponding wavelength dependence of the phase modal birefringence $B_{01}(\lambda)$, shown in figure 6 by the dashed line. It was obtained by combining the relative phase modal birefringence with one value $B_{01} = 3.90 \times 10^{-4}$ measured at 628.3 nm. This value is obtained from equations (5) and (6) for the measured displacement $\Delta L = 1623\ \mu$m of the coupling point producing the phase change $\Delta\phi(\lambda) = 2\pi$. The phase modal birefringence for the LP_{01} spatial mode has positive sign, similarly to the group modal birefringence. It decreases strongly against wavelength, which is in very good agreement with the results of numerical modelling. The difference between the experimental and calculated values is greater in a short wavelength region and reaches 3% at $\lambda = 0.46\ \mu$m. The calculated phase modal birefringence $B_{11}(\lambda)$ for the even LP_{11} spatial mode decreases much more steeply against wavelength compared to $B_{01}(\lambda)$ calculated for the LP_{01} spatial mode. It is interesting to note that there is a specific wavelength (approximately 0.46 μm) at which the two phase birefringences are the same.

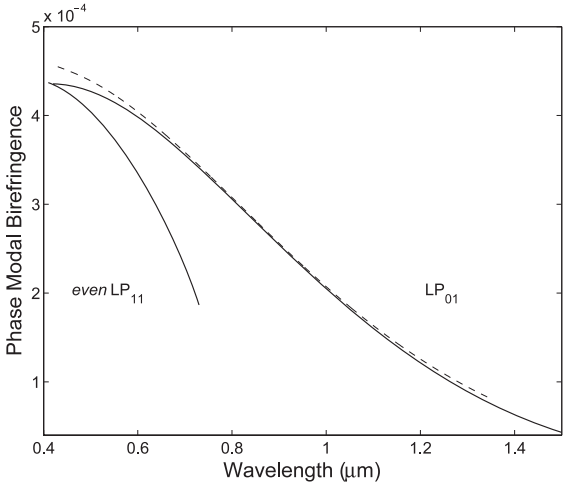

Figure 6. Calculated phase modal birefringence as a function of wavelength for two spatial modes of ECF 1 (solid lines). The dashed line represents the phase modal birefringence obtained from the experimental data.

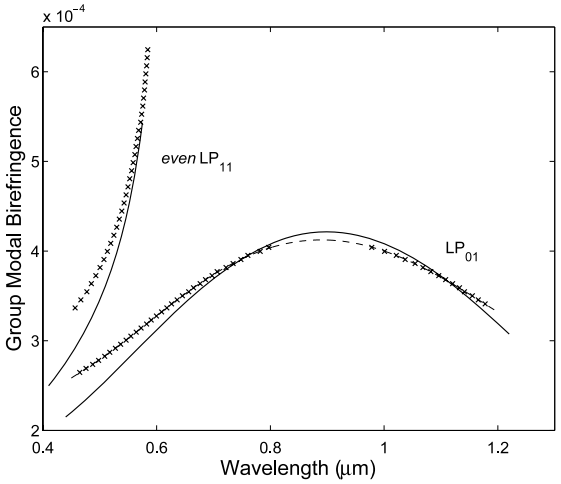

Figure 7. Group modal birefringence measured as a function of wavelength for two spatial modes of ECF 2 (the dashed line represents a power series fit) and the simulation results (solid lines).

Figure 7 shows, as crosses, the measured group modal birefringences $G_{01}(\lambda_{eq})$ and $G_{11}(\lambda_{eq})$ in ECF 2 determined for the respective equalization wavelengths λ_{eq}. The dashed line in the same figure represents the approximation $G_{01}(\lambda)$ of measured results obtained by a seven-term power series according to equation (8). We clearly see from figure 7 that the wavelength at which $G_{01}(\lambda)$ reaches a maximum (approximately at 0.89 μm) is shifted towards the infrared compared with that for the first ECF. The shape of the wavelength dependence of the group modal birefringence $G_{01}(\lambda)$ is similar to that obtained by numerical modelling. The difference between the experimental and calculated values for the LP_{01} spatial mode is greater in a short wavelength region and reaches 14% at $\lambda = 0.46$ μm. The group modal birefringence $G_{11}(\lambda_{eq})$ for the even LP_{11} spatial mode strongly increases against wavelength near the cut-off (approximately at 0.59 μm), which is in accordance with the results of numerical modelling. The difference between the experimental and calculated values increases for shorter wavelengths and reaches 13% at $\lambda = 0.46$ μm.

The approximation of $G_{01}(\lambda)$ according to equation (8) gives the corresponding wavelength dependence of the phase modal birefringence $B_{01}(\lambda)$, shown in figure 8 by the dashed line. It was obtained by combining the relative phase modal birefringence with one value $B_{01} = 2.20 \times 10^{-4}$ measured at 621.92 nm. The phase modal birefringence for the LP_{01} spatial mode decreases against wavelength. The LP_{01} birefringence has positive sign, similarly to the group modal birefringence, which is in accordance with the results of numerical modelling. The difference between the experimental and calculated values is positive and nearly constant over a broad wavelength range. This difference increases in a short wavelength region and reaches 4% at $\lambda = 0.46$ μm. The calculated phase modal birefringence $B_{11}(\lambda)$ for the even LP_{11} spatial mode has similar

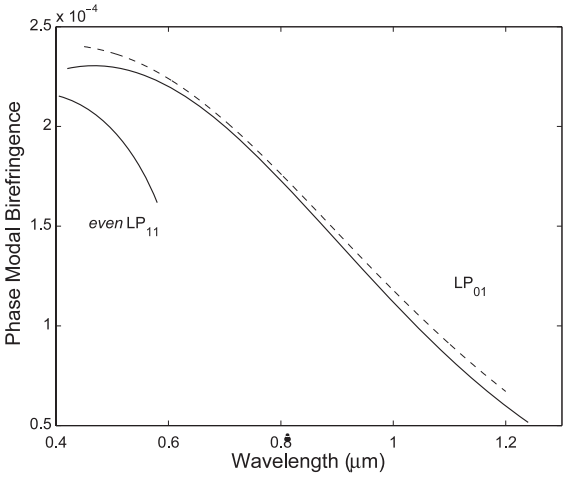

Figure 8. Calculated phase modal birefringence as a function of wavelength for two spatial modes of ECF 2 (solid lines). The dashed line represents the phase modal birefringence obtained from the experimental data.

wavelength dependence; however, its value is lower by about 25% compared to that of $B_{01}(\lambda)$.

Figure 9 shows, as crosses, the measured group modal birefringences $G_{01}(\lambda_{eq})$ and $G_{11}(\lambda_{eq})$ in ECF 3 determined for the respective equalization wavelengths λ_{eq}. The dashed line represents the approximation $G_{01}(\lambda)$ of measured results obtained using a seven-term power series. We clearly see from figure 9 that the wavelength at which $G_{01}(\lambda)$ reaches a maximum (approximately at 1.122 μm) is shifted towards longer wavelengths compared with that for ECF 2. The shape of the wavelength dependence of the group modal birefringence $G_{01}(\lambda)$ is similar to that obtained by numerical modelling. The group modal birefringence $G_{11}(\lambda_{eq})$ for the

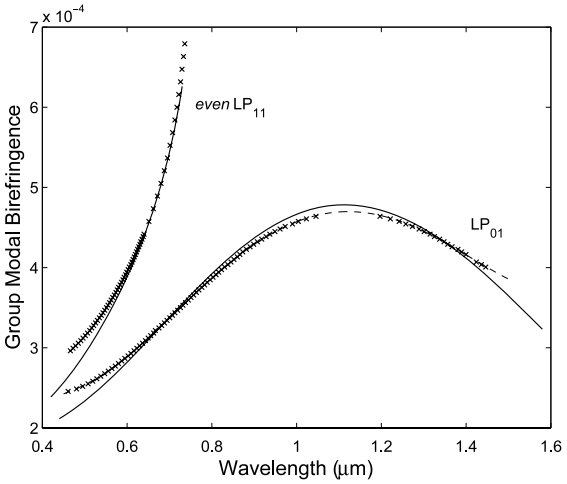

Figure 9. Group modal birefringence measured as a function of wavelength for two spatial modes of ECF 3 (the dashed line represents a power series fit) and the simulation results (solid lines).

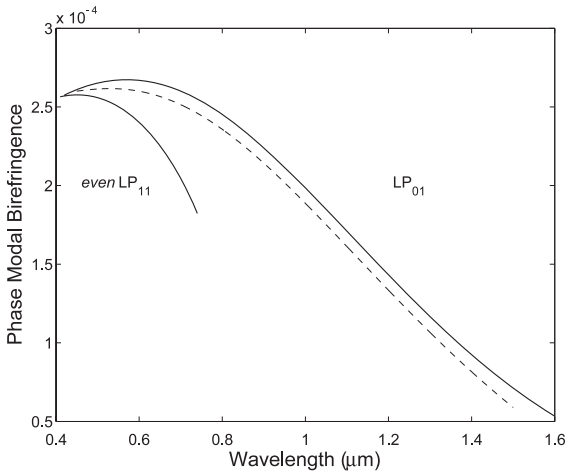

Figure 10. Calculated phase modal birefringence as a function of wavelength for two spatial modes of ECF 3 (solid lines). The dashed line represents the phase modal birefringence obtained from the experimental data.

even LP_{11} spatial mode strongly increases against wavelength near the cut-off (approximately at 0.740 μm), which is in agreement with the results of numerical modelling. The differences between the experimental and theoretical values of the group modal birefringences for the LP_{01} and even LP_{11} spatial modes are the greatest in a short wavelength region and reach 7% and 9% ($\lambda = 0.46$ μm), respectively.

The wavelength dependence of the phase modal birefringence $B_{01}(\lambda)$ corresponding to the approximation of $G_{01}(\lambda)$ according to equation (8) is shown in figure 10 by the dashed line. This dependence was obtained by combining the relative phase modal birefringence with one value $B_{01} = 2.58 \times 10^{-4}$ measured at 632.8 nm. The phase modal birefringence measured for the LP_{01} spatial mode is very similar to the results of numerical modelling. There is a constant negative shift of measured values compared to the calculated ones over a broad wavelength range that reaches 5%. The calculated phase modal birefringence $B_{11}(\lambda)$ for the even LP_{11} spatial mode is strongly decreasing against wavelength. Its decrease at longer wavelengths is much steeper compared to that of the fundamental mode. Moreover, a specific wavelength (approximately 0.42 μm) can be resolved at which the phase birefringences of both spatial modes are the same.

Our experimental results show that greater ellipticity of the ECF core results in higher maximum values of the group and phase modal birefringences for the LP_{01} spatial mode. Moreover, the spectral position of the maximum of group modal birefringence depends on the core size. Similarly, a higher group modal birefringence of the even LP_{11} spatial mode near the cut-off wavelength was observed in fibres with greater core ellipticity.

6. Conclusions

We have presented the results of measurement and modelling of birefringence dispersion in ECFs over a broad spectral range. We have used two different interferometric techniques for measuring the birefringence dispersion in three ECFs, including Corning PMF-38 highly birefringent fibre. By a white-light spectral interferometric technique employing a tandem configuration of a Michelson interferometer and an ECF under test, we measured the dispersion of the group modal birefringence. The technique is based on recording spectral interference signals and resolving the equalization wavelengths. Measuring the path length difference adjusted in the interferometer as a function of the equalization wavelength has served to provide dispersion characterization of the optical fibre guiding two spatial modes of orthogonal polarizations. We measured the dispersion of the group modal birefringence for both the LP_{01} and the even LP_{11} spatial modes over a broad wavelength range (e.g. 450–1450 nm). Using a method of a lateral point-like force acting on the fibre and based on spectral interferometry, we also measured the phase modal birefringence at one wavelength for the fundamental mode only. The measured value was combined with the dispersion of the group modal birefringence to obtain the phase modal birefringence over a broad wavelength range.

We also modelled the dispersion characteristics taking into account contributions of both the elliptical shape of the core and the residual thermal stress. We confirmed for all the fibres investigated good agreement between simulations and measurements. Small discrepancies reaching at most 15% are observed in the short wavelength range. This is most probably caused by a lack of reliable data on the spectral dependence of material constants (C_1, C_2) in SiO_2/GeO_2 glass and by the inaccuracy of determining the core dimensions.

The results obtained are important from the point of view of the development of ECFs with desirable birefringence dispersions. Our results show that the maximum values of the group and phase modal birefringences for the LP_{01} spatial mode are higher for ECFs with greater core ellipticities.

Similarly, the maximum of the group modal birefringence for the LP_{01} can be shifted to a desired wavelength by tuning the core geometry. Moreover, we demonstrate experimentally that the group modal birefringence for the even LP_{11} mode rapidly increases near the cut-off wavelength.

Acknowledgments

The research was partially supported by the COST Action 299 (project OC09020), by grant MSM6198910016, and by grant of the Czech–Polish collaboration (project MEB050809). T Martynkien and W Urbańczyk acknowledge support from the Statutory Grant.

References

[1] Dyott R B 1995 *Elliptical Fiber Waveguides* (Boston, MA: Artech House Publishers)
[2] Blake J N, Huang S Y, Kim B Y and Shaw H J 1987 Strain effects on highly elliptical core two-mode fibers *Opt. Lett.* **12** 732–4
[3] Murphy K A, Miller M S, Vengsarkar A M and Claus R O 1990 Elliptical-core two-mode optical-fiber sensor implementation methods *J. Lightwave Technol.* **8** 1688–96
[4] Vengsarkar A M, Michie W C, Jankovic L, Culshaw B and Claus R O 1994 Fiber-optic dual-technique sensor for simultaneous measurement of strain and temperature *J. Lightwave Technol.* **12** 170–7
[5] Sinha P G, Kolltveit E and Bløtekjær K 1995 Two-mode fiber-optic time-delay scanner for white-light interferometry *Opt. Lett.* **20** 94–6
[6] Jackson D A and Jones J D C 1989 *Optical Fibre Sensors* ed J P Dakin and B Culshaw (London: Artech House) p 329
[7] Bock W J and Urbańczyk W 1993 Measurement of polarization mode dispersion and modal birefringence in highly birefringent fibers by means of electronically scanned shearing-type interferometry *Appl. Opt.* **32** 5841–8
[8] Urbańczyk W, Martynkien T and Bock W J 2001 Dispersion effects in elliptical-core highly birefringent fibers *Appl. Opt.* **40** 1911–20
[9] Flavin D A, McBride R and Jones J D C 2002 Dispersion of birefringence and differential group delay in polarization maintaining fibers *Opt. Lett.* **27** 1010–2
[10] Tang F, Wang X Z, Zhang Y and Jing W 2006 Distributed measurement of birefringence dispersion in polarization-maintaining fibers *Opt. Lett.* **31** 3411–3
[11] Rashleigh S C 1982 Wavelength dependence of birefringence in highly birefringent fibers *Opt. Lett.* **7** 294–6
[12] Shlyagin M G, Khomenko A V and Tentori D 1995 Birefringence dispersion measurement in optical fibers by wavelength scanning *Opt. Lett.* **20** 869–71
[13] Posey R, Phillips L, Diggs D and Sharma A 1996 LP_{01}–LP_{11} interference using a spectrally extended light source: measurement of the non-step-refractive-index profile of optical fibers *Opt. Lett.* **21** 1357–9
[14] Hlubina P 2003 White-light spectral interferometry to measure intermodal dispersion in two-mode elliptical-core optical fibres *Opt. Commun.* **218** 283–9
[15] Hlubina P, Martynkien T and Urbańczyk W 2003 Dispersion of group and phase modal birefringence in elliptical-core fiber measured by white-light spectral interferometry *Opt. Express* **11** 2793–8
[16] Hlubina P, Urbańczyk W and Martynkien T 2004 Spectral-domain interferometric techniques used to measure the intermodal group dispersion in a two-mode bow-tie optical fibre *Opt. Commun.* **328** 313–21
[17] Wang Z, Ju J and Jin W 2005 Properties of elliptical-core two-mode fiber *Opt. Express* **13** 4350–7
[18] Hlubina P, Ciprian D and Kadulová M 2009 Wide spectral range measurement of modal birefringence in polarization-maintaining fibres *Meas. Sci. Technol.* **20** 025301
[19] Hlubina P and Ciprian D 2007 Spectral-domain measurement of phase modal birefringence in polarization-maintaining fiber *Opt. Express* **15** 17019–24
[20] Bansal N P and Doremus R H 1986 *Handbook of Glass Properties* (London: Academic)
[21] Shibata N, Tateda M, Seikei S and Uchida N 1983 Birefringence and polarization mode dispersion caused by thermal stress in single-mode fibers with various core ellipticities *IEEE J. Quantum Electron.* **19** 1223–7
[22] Okamoto K, Hosaka T and Edahiro T 1981 Stress analysis of optical fibres by a finite element method *IEEE J. Quantum Electron.* **17** 2123–9
[23] Noda J, Okamoto K and Sakai Y 1986 Polarization-maintaining fibers and their applications *J. Lightwave Technol.* **4** 1071–89
[24] Eguchi M and Koshiba M 1994 Accurate finite-element analysis of dual-mode highly elliptical-core fibers *J. Lightwave Technol.* **12** 607–13
[25] Fontaine M, Wu B, Tzolov V P, Bock W J and Urbańczyk W 1996 Theoretical and experimental analysis of thermal stress effects on modal polarization properties of highly birefringent optical fibers *J. Lightwave Technol.* **14** 585–91
[26] Okamoto K 2000 *Fundamentals of Optical Waveguides* (New York: Academic) chapter 3
[27] Ward B G 2008 Finite element analysis of photonic crystal rods with inhomogeneous anisotropic refractive index tensor *IEEE J. Quantum Electron.* **44** 150–6

Paper XII.

Optics and Lasers in Engineering 70 (2015) 51–56

Contents lists available at ScienceDirect

Optics and Lasers in Engineering

journal homepage: www.elsevier.com/locate/optlaseng

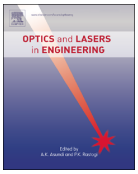

Temperature sensing using the spectral interference of polarization modes in a highly birefringent fiber

P. Hlubina [a,*], M. Kadulova [a], D. Ciprian [a], P. Mergo [b]

[a] Department of Physics, Technical University Ostrava, 17. listopadu 15, 708 33 Ostrava-Poruba, Czech Republic
[b] Laboratory of Optical Fibre Technology, Maria Curie-Sklodowska University, Pl. M. Curie-Sklodowskiej 3, 20-031 Lublin, Poland

ARTICLE INFO

Article history:
Received 27 October 2014
Received in revised form
13 February 2015
Accepted 2 March 2015
Available online 19 March 2015

Keywords:
Spectral interferometry
Birefringent fiber
Polarimetric sensitivity
Temperature sensing
Wavelength interrogation

ABSTRACT

The spectral interference of polarization modes in a highly birefringent (HB) fiber to measure temperature is analyzed theoretically and experimentally. A tandem configuration of a birefringent delay line and a sensing HB fiber is considered and the spectral interferograms are modelled for the known birefringence dispersion of the HB fiber under test. As the delay line, a birefringent quartz crystal of a suitable thickness is employed to resolve a channeled spectrum. The channeled spectra are recorded for different temperatures and the polarimetric sensitivity to temperature, determined in the spectral range from 500 to 850 nm, is decreasing with wavelength. It is demonstrated that the temperature sensing is possible using the wavelength interrogation, i.e., the position of a given interference maximum is temperature dependent. The temperature sensitivity of the HB fiber under test is −0.25 nm/K and the resolution is better than 0.5 K.

1. Introduction

Optical fibers are of great importance in sensing different physical parameters with high sensitivity, wide dynamic range and high resolution [1]. Moreover, fiber optic sensors possess advantages such as small size, low weight and electromagnetic immunity. Among the fiber optic sensors, temperature sensors with different structures and principles of operation have been extensively investigated [2–11]. As an example, the sensors were realized by using a special microstructure in a single-mode fiber such as Bragg gratings [2,3], long period gratings [4], an in-fiber Fabry–Perot [5] or Mach–Zehnder [6] interferometer, a tapered fiber [7], and a D-shaped fiber [8]. Included are also sensors enabling high-temperature measurements [9] and simultaneous measurements of temperature and strain [10], and sensors based on the in-line reflection principle of operation [11]. The microstructures are post-fabricated and require complicated processes employing techniques such as UV-laser writing, laser machining, fusion tapering, and chemical etching. Consequently, many fiber optic sensors have been proposed which are based on specialty optical fibers such as polarization-maintaining fibers, photonic crystal fibers, and multi-core fibers, and the special structure in the fiber is formed during the fabrication and no extra post processing for fabricating a fiber sensing head is needed.

A large number of in-line fiber optic sensor configurations utilize interference between polarization modes [12–16]. Standard highly birefringent (HB) fibers with elliptical-core or stress-applying elements have been successfully used as active elements of fiber optic sensors for measuring numerous physical parameters such as strain, temperature and pressure [12–16]. Some of the sensor configurations are working in the spatial domain and utilize white-light interferometric methods [12–14]. The interferometric systems are available even when the group optical path difference between polarization modes is larger than the source coherence length. In this case a tandem configuration of two interferometers, a sensing fiber interferometer and a birefringent calcite plate to compensate the group delay between the polarization modes introduced by the sensing fiber, can be utilized [12,14]. The other configurations are working in the spectral domain and use two birefringent optical fibers [16] or are based on the shift of the transmission spectrum dip [17]. In some configurations, the phase change to be measured is inscribed in the spectral interference fringes detected by a spectrometer [18–20]. Some of these configurations have been primarily used for measuring the dispersion of birefringence in polarization-maintaining fibers by processing a stationary-phase point spectrum [21] or channeled spectrum [22]. In addition, the principle of channeled spectrum is utilized for optical switching [23,24].

Standard HB fibers exhibit temperature-sensitive birefringence so that when they are used for sensing other parameters than temperature, such as strain, the temperature cross-sensitivity affects the measurement accuracy significantly. To overcome this limitation, HB holey fibers with much higher flexibility in shaping

* Corresponding author. Tel.: +420 597 323 134; fax: +420 597 323 139.
E-mail address: petr.hlubina@vsb.cz (P. Hlubina).

http://dx.doi.org/10.1016/j.optlaseng.2015.03.003
0143-8166/

modal birefringence and significantly less temperature dependence than standard HB fibers have emerged as active elements of fiber optic sensors [25–28].

In this paper, theoretical and experimental analysis of a spectral-domain technique utilizing the interference of polarization modes of an elliptical-core HB fiber to measure temperature is presented. The analysis is motivated by the fact that spectral analysers with a sufficiently high resolution, such as compact spectrometers, are easily accessible. Moreover, a tandem configuration is proposed to resolve spectral interference fringes for a long HB fiber. The method, utilizing a compact spectrometer in a visible spectral range, is based on the wavelength interrogation, i.e., the position of a given interference maximum as a function of temperature is measured. A tandem configuration of a birefringent delay line and a sensing HB fiber is considered and first, the spectral interferograms are modelled for the known spectral dependence of both the phase and group modal birefringence of the HB fiber under test. As the delay line, a birefringent quartz crystal of a suitable thickness is employed to resolve a channeled spectrum in a range as wide as possible. Second, the polarimetric sensitivity to temperature is measured and it is higher at shorter wavelengths so the HB fiber under test is suitable for temperature sensing at a wavelength of about 520 nm. Finally, it is revealed that when a part of the sensing HB fiber, which is placed in a chamber, is exposed to temperature changes, a shift of the wavelength position of a given interference maximum is present. The temperature sensitivity reaches -0.25 nm/K and the resolution is better than 0.5 K.

2. Theoretical background

Consider a sensing HB fiber of length z in an experimental setup shown in Fig. 1. A linearly polarized optical field, propagating along the axis of the HB fiber, in which only the fundamental mode in both x and y polarizations is excited, is disturbed by the external physical quantity – temperature. The spectral intensity at the output of the HB fiber alone with a polarizer and an analyzer adjusted at 45° with respect to the fiber eigenaxes is given as [19]

$$I(z;\lambda) = I_0(\lambda)\{1 + V(z;\lambda)\cos[(2\pi/\lambda)B(\lambda)z]\}, \quad (1)$$

where $I_0(\lambda)$ is the reference spectral intensity, $B(\lambda)$ is the phase modal birefringence and $V(z;\lambda)$ is the visibility term, which is dependent on the group modal birefringence $G(\lambda)$.

The interference of the polarization modes at the output of the experimental setup shows up as the spectral modulation (channeled spectrum) with the period inversely proportional to the group modal birefringence $G(\lambda)$, which means that for the longer sensing HB fiber the period of the spectral modulation is smaller [20].

If the resolving power of a spectrometer is insufficient to resolve the channeled spectrum, the HB fiber in tandem with a birefringent crystal of the group birefringence $G_c(\lambda)$ and the thickness d can be used as shown in Fig. 1. The spectral intensity at the output of the tandem configuration with a polarizer and an analyzer adjusted at 45° with respect to the polarization axes of the HB fiber is for $G(\lambda) > 0$ and $G_c(\lambda) > 0$ given by [19]

$$I(z;\lambda) = I_0(\lambda)\{1 + V(z;\lambda)\cos\{(2\pi/\lambda)[B(\lambda)z - B_c(\lambda)d]\}\}, \quad (2)$$

where $B_c(\lambda)$ is the phase birefringence of the crystal. The period of the spectral modulation depends on the difference $G(\lambda)z - G_c(\lambda)d$, which means that the equalization wavelength is resolvable in the recorded spectrum when the overall group birefringence in the tandem configuration of the birefringent crystal and the HB fiber is zero [20].

2.1. Theoretical spectral interferograms

Consider an elliptical-core PM fiber whose phase and group modal birefringence dispersions are known from previous measurements [22]. The group modal birefringence as a function of the wavelength (see Fig. 2) was measured by a method of spectral tandem interferometry [21] with the precision better than 0.1%. The phase modal birefringence as a function of the wavelength (see Fig. 3) was deduced from the wavelength dependence of the group modal birefringence [22,29] when value $B = 8.55 \times 10^{-5}$

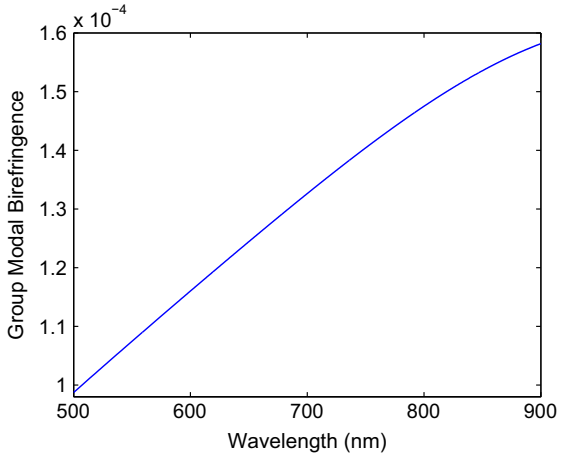

Fig. 2. Measured spectral dependence of the group modal birefringence in the HB fiber under test.

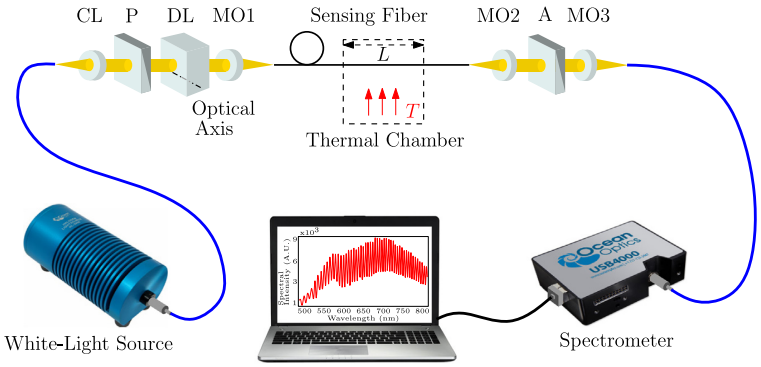

Fig. 1. Experimental setup with a sensing fiber to record channeled spectra; collimating lens (CL), polarizer (P), delay line (DL), analyzer (A) and microscope objectives (MO1–MO3).

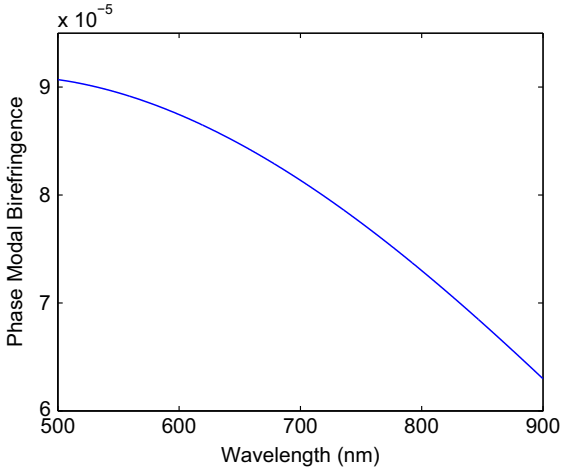

Fig. 3. Measured spectral dependence of the phase modal birefringence in the HB fiber under test.

measured at a wavelength of 637.08 nm by a lateral force method applied in the spectral domain [29] was used. The phase modal birefringence decreases with wavelength and its sign is positive and is the same as the sign of the group modal birefringence specified using a simple procedure [22].

If we consider a spectrometer with the width of the response function $\Delta\lambda_R = 3$ nm and the HB fiber of length $z = 1.6$ m, the period of the spectral modulation is smaller than $\Delta\lambda_R$ and the channeled spectrum is not resolvable by the spectrometer so that the HB fiber alone cannot be used in the sensing applications. If we consider a tandem configuration of a birefringent crystal of a suitable thickness d and the HB fiber, the period of the spectral modulation is larger than $\Delta\lambda_R$ and the channeled spectrum is resolvable by the spectrometer. This effect can be illustrated for a quartz crystal, the birefringence dispersion of which can be represented in the Sellmeier-like form [30]:

$$B_c(\lambda) = H + \frac{I\lambda^2}{\lambda^2 - K} + \frac{J\lambda^2}{\lambda^2 - L}, \tag{3}$$

where λ is wavelength in micrometers and the dispersion coefficients at room temperature are as follows: $H = -29.435688 \times 10^{-3}$, $I = -134.804456 \times 10^{-3}$, $J = -294.96110 \times 10^{-3}$, $K = 2.17641576 \times 10^{-2}$ and $L = 80$. The group birefringence dispersion can be represented as

$$G_c(\lambda) = -\lambda^2 \frac{d[B_c(\lambda)/\lambda]}{d\lambda} = B_c(\lambda) + \frac{2IK\lambda^2}{(\lambda^2 - K)^2} + \frac{2JL\lambda^2}{(\lambda^2 - L)^2}. \tag{4}$$

In Fig. 4 are shown two examples of the theoretical spectra corresponding to overall phases $\phi_1(\lambda) = (2\pi/\lambda)[B(\lambda)z - B_c(\lambda)d]$ and $\phi_2(\lambda) = \phi_1(\lambda) - \pi/2$ when the thickness of the birefringent quartz crystal is $d = 21$ mm. We clearly see that the equalization wavelength $\lambda_0 = 666.46$ nm is resolvable in the spectrum. The phase change, which is inscribed in the spectral interferograms, can be retrieved using a relatively complicated procedure [20].

When the thickness of the birefringent quartz is changed to $d = 13$ mm, the equalization wavelength λ_0 shifts toward shorter wavelengths and in the considered wavelength range a channeled spectrum can be resolved. This is illustrated in Fig. 5 showing two examples of the theoretical channeled spectra corresponding to overall phases $\phi_1(\lambda)$ and $\phi_2(\lambda) = \phi_1(\lambda) - \pi/2$. The phase change, which is inscribed in a shift of the channeled spectrum, can be retrieved using a relatively simple procedure [31]. In addition, the

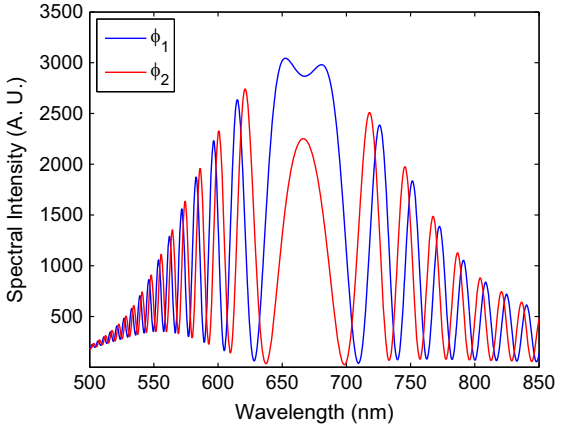

Fig. 4. Two examples of the theoretical spectra corresponding to overall phases ϕ_1 and $\phi_2 = \phi_1 - \pi/2$ when the thickness of the birefringent quartz crystal is $d = 21$ mm.

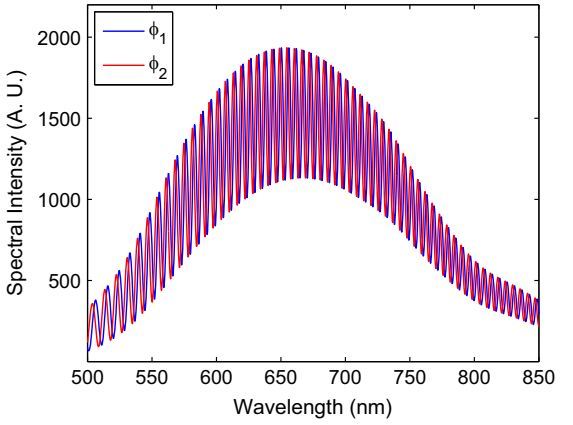

Fig. 5. Two examples of the theoretical spectra corresponding to overall phases ϕ_1 and $\phi_2 = \phi_1 - \pi/2$ when the thickness of the birefringent quartz crystal is $d = 13$ mm.

change of temperature related to the phase change can be deduced from the shift of a given interference maximum or minimum. In the practical implementations of the sensing scheme, it is advantageous to choose the last approach because temperature can be sensed by measuring the position of a single interference maximum in the channeled spectrum.

3. Experimental setup

The experimental setup we used in temperature sensing via recording channeled spectra is shown in Fig. 1. It consists of a broadband source – a halogen lamp (HL-2000, Ocean Optics), light of which is launched into a fiber terminated by a lens. From the lens a collimated beam propagates through a Glan–Taylor calcite polarizer (Thorlabs) and a birefringent delay line represented by a quartz crystal of thickness $d = 14.91$ mm. The transmission azimuth of the polarizer is adjusted at 45° with respect to the birefringent crystal optical axis, which is perpendicular to the beam axis so that the beam in two orthogonal polarizations is present at the output of the crystal. The light beam in two polarizations is focused by a microscope objective into an elliptical-core HB fiber of length

$z=1.78$ m and the polarization axes of the fiber are parallel to the polarization axes of the crystal [19]. A loop of the HB fiber is used to strip off the higher-order modes and to smooth the reference spectrum as much as possible. At the output of the sensing fiber, microscope objectives and a Glan–Taylor calcite analyzer (Thorlabs) are used to easily control the interference signal detected by a fiber optic spectrometer (USB4000, Ocean Optics) connected to a personal computer. The transmission azimuth of the analyzer is oriented at 45° with respect to the polarization axes of the fiber to detect the interference of the polarization modes with the highest contrast. The spectrometer has a spectral operation range from 350 to 1000 nm.

The HB fiber, which was drawn at the Department of Optical Fibers Technology, University of Marie Curie-Sklodowska in Lublin, Poland, has a core made of GeO_2-doped silica glass (19.3 mol%) and a cladding made of pure silica. The dimensions of the fiber elliptical core are approximately 3.2×1.2 μm [22].

4. Experimental results and discussion

In this section, the polarimetric sensitivity of the investigated HB fiber to temperature is presented and the approach to temperature sensing based on the wavelength interrogation is outlined.

4.1. Polarimetric sensitivity to temperature

Using the experimental setup shown in Fig. 1, with the length L of the HB fiber subjected to temperature changes, we measured the polarimetric sensitivity of the fiber to temperature. It is defined by the following relation:

$$K_T(\lambda)=\frac{1}{L}\frac{\mathrm{d}[\phi_x(\lambda)-\phi_y(\lambda)]}{\mathrm{d}T}, \tag{5}$$

and represents an increase in the phase shift between the two polarization modes of the investigated HB fiber induced by the unit change of the temperature acting on the unit fiber length [20].

To determine the polarimetric sensitivity to temperature $K_T(\lambda)$, we recorded a series of channeled spectra for increasing temperature T with a step small enough to assure unambiguity in retrieving the temperature-induced phase changes $\Delta[\phi_x(\lambda)-\phi_y(\lambda)]$. To measure $K_T(\lambda)$, the HB fiber of the length $L=0.164$ m was immersed in water heated in a chamber with increasing temperature up to 373 K. Fig. 6 shows two examples of the recorded spectra corresponding to temperatures $T_1=304$ K and $T_2=324$ K. It is clearly seen from Fig. 6 that the interference of polarization modes in the tandem with the delay line shows up as the channeled spectrum, which shifts with increasing temperature toward shorter wavelengths.

Using a windowed Fourier transform [31], we retrieved from the two channeled spectra the phase functions $[\phi_x(\lambda)-\phi_y(\lambda)]_{T_2}$ and $[\phi_x(\lambda)-\phi_y(\lambda)]_{T_1}$. Their difference is wavelength dependent and decreasing with wavelength and for the known fiber length L and temperature difference $\Delta T=T_2-T_1$ it enables us to determine the absolute value of the polarimetric sensitivity to temperature $K_T(\lambda)$. It is also wavelength dependent and decreasing with wavelength. Repeating this procedure for some other temperatures we obtained the corresponding values of $K_T(\lambda)$. In Fig. 7 is shown the mean value of the polarimetric sensitivity to temperature as a function of the wavelength and its precision is better than 5%. A sign of the polarimetric sensitivity to temperature is determined from the expression [32]

$$K_T(\lambda)=\frac{2\pi}{\lambda}\left[\frac{\mathrm{d}B(\lambda)}{\mathrm{d}T}+B(\lambda)\alpha\right], \tag{6}$$

where α is a thermal expansion coefficient. The first term in Eq. (6), representing the susceptibility of the modal birefringence to temperature [32], has a negative sign for conventional HB fibers with elliptical cores, and is higher at shorter wavelengths [33]. The second term $B(\lambda)\alpha$, representing the fiber elongation, is most often neglected when the temperature sensitivity in conventional HB fibers is considered [32]. As a result, the polarimetric sensitivity to temperature has a negative sign. The absolute value of the mean polarimetric sensitivity to temperature for the investigated HB fiber decreases with wavelength from a value of 1.2 rad m^{-1} K^{-1} to a value of 0.4 rad m^{-1} K^{-1} (in the range from 500 to 850 nm). The absolute value at $\lambda=632.8$ nm is in good agreement with a value of 1.1 rad m^{-1} K^{-1} for elliptical-core fiber, but it is less than that of bow-tie fiber, 7.4 rad m^{-1} K^{-1}, and PANDA fiber, 7.6 rad m^{-1} K^{-1} [34].

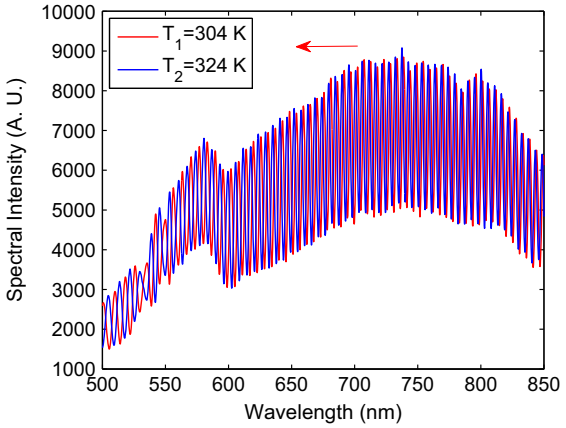

Fig. 6. Two examples of the recorded channeled spectra corresponding to temperatures T_1 and T_2.

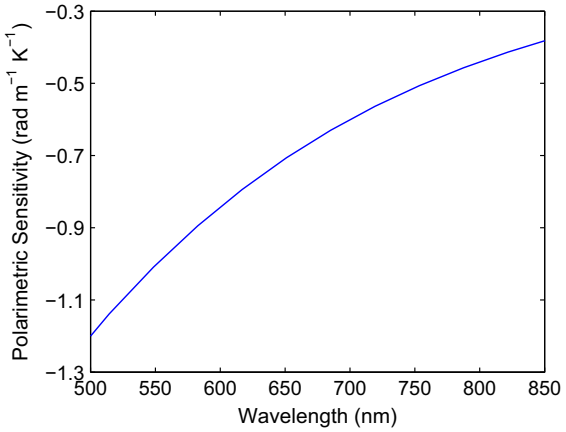

Fig. 7. The spectral dependence of the mean value of the polarimetric sensitivity to temperature for the HB fiber under test.

4.2. Temperature response

Because the interference of polarization modes of the investigated HB fiber shows up as the channeled spectrum, a shift of the wavelength position of a given interference maximum with temperature can be utilized for temperature sensing. In other words, the wavelength interrogation can be used. As an example, in Fig. 8 are shown three channeled spectra in the wavelength range from 510 to 580 nm corresponding to three different temperatures $T_1=304$ K, $T_2=314$ K and $T_3=324$ K. Similarly, in Fig. 9 are shown the same channeled spectra in the wavelength

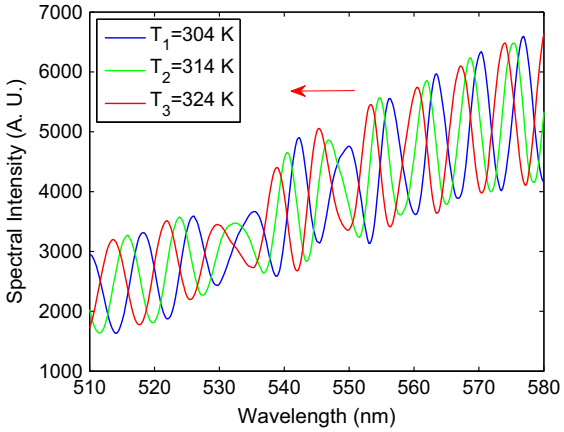

Fig. 8. Three examples of the recorded channeled spectra corresponding to temperatures T_1, T_2 and T_3 (the wavelength range from 510 to 580 nm).

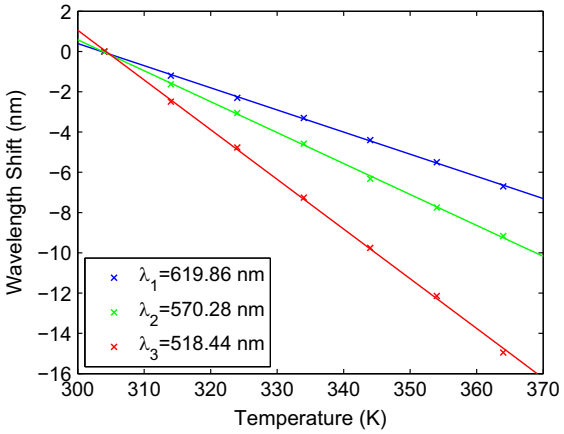

Fig. 10. The wavelength shift of interference maximum as a function of temperature corresponding to three different initial positions λ_1, λ_2 and λ_3.

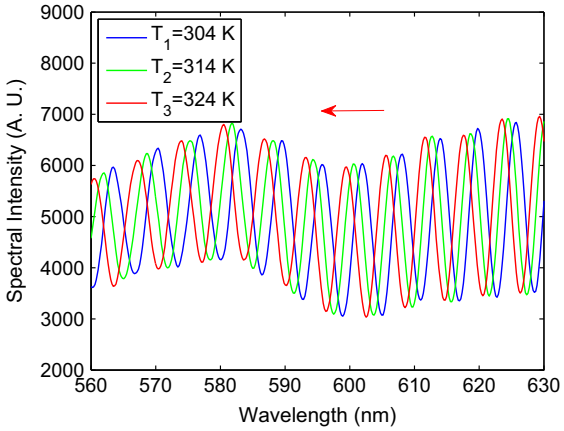

Fig. 9. Three examples of the recorded channeled spectra corresponding to temperatures T_1, T_2 and T_3 (the wavelength range from 560 to 630 nm).

range from 560 to 630 nm. The interference maxima in both wavelength ranges are shifted with temperature toward shorter wavelengths and the shift is smaller for longer wavelengths (560–630 nm). This is due to the lower polarimetric sensitivity of the investigated HB fiber to temperature at longer wavelengths. The shift is also affected by the group birefringence dispersion of the fiber because the temperature sensitivity $S_T(\lambda)$, representing the wavelength shift of the interference maximum induced by the unit change of the temperature, is given by [27]

$$S_T(\lambda) = \frac{d\lambda_{max}}{dT} = \frac{\lambda^2}{2\pi} \frac{K_T(\lambda) L}{G(\lambda) z}. \quad (7)$$

For the investigated HB fiber it reaches -0.20 nm/K at $\lambda = 520$ nm.

The measured wavelength shifts corresponding to the given maxima in the channeled spectra for increasing temperature up to 373 K are shown in Fig. 10 by crosses. The lower crosses correspond to a maximum starting at a wavelength of 518.44 nm, the intermediate crosses correspond to a maximum starting at a wavelength of 570.28 nm and the upper ones correspond to a maximum starting at a wavelength of 619.86 nm. The dependences of the wavelength shift on the temperature are with different slopes (temperature sensitivities): -0.25 nm/K for the lower dependence, -0.15 nm/K for the intermediate dependence and -0.11 nm/K for the upper one. The temperature sensitivity is higher at shorter wavelengths and from the point of view of temperature sensing using this method the position of a maximum should be measured at shorter wavelengths (near 520 nm). To the slopes uncertainties correspond the temperature fluctuations with the root-mean-square amplitudes below 0.5 K demonstrating that the measurement method is of sufficient resolution. Temperature sensitivities of other types of HB fibers are higher due to a higher polarimetric sensitivity. As an example, near $\lambda = 1550$ nm $S_T(\lambda)$ reaches -0.2 nm/K for elliptical-core fiber, -1.2 nm/K for bow-tie fiber, -1.9 nm/K for PANDA fiber [15].

A temperature measurement step is limited by the phase unambiguity (the phase change not exceeding 2π) and reaches $\Delta T = 35$ K in the vicinity of 518.44 nm, and $\Delta T = 48$ K in the vicinity of 619.86 nm. It can be enlarged using the shorter length L of the sensing fiber. However, in a sequential temperature measurement with a step small enough to assure phase unambiguity, the measurement range can be very wide, that is, high-temperature measurements are possible.

5. Conclusions

In this paper, the results of theoretical and experimental analysis of the spectral-domain interference of polarization modes in an elliptical-core HB fiber applicable to temperature sensing are presented. A tandem configuration of a birefringent quartz crystal and a sensing HB fiber is considered and the spectral interferograms are modelled for the known birefringence dispersion of the HB fiber. It is revealed that for a suitable thickness of the birefringent crystal channeled spectra can be resolved and a shift of the position of a given interference maximum can be used to temperature sensing.

The investigated HB fiber is employed in an experiment and from the channeled spectra recorded for different temperatures, the polarimetric sensitivity to temperature is determined in the wavelength range from 500 to 850 nm. It is decreasing with wavelength so that the HB fiber is suitable for temperature sensing in a short wavelength range. Temperature sensing is demonstrated in the range from 300 to 370 K when a shift of the wavelength position of a given interference maximum is measured. The temperature sensitivity reaches -0.25 nm/K and the resolution is better than 0.5 K. In addition, the measurement range can easily be extended

for temperatures greater than 370 K provided that the phase unambiguity is ensured.

The results obtained are important from the point of view of implementation of temperature sensors employing HB fibers and utilizing the spectral interference of polarization modes. A tandem configuration enables one to resolve the spectral interference even for a long HB fiber. Moreover, the sensing is performed in a visible spectral range using a low-cost source and a compact spectrometer, components easily accessible.

Acknowledgements

The research was partially supported by the COST TD1001 action “OFSeSa” through project LD12003.

References

[1] Culshow B, Dakin J. Optical fiber sensors: systems and applications. Boston: Artech House; 1988.
[2] Ball GA, Morey WW, Cheo PK. Single- and multipoint fiber-laser sensors. IEEE Photon Technol Lett 1993;5:267–70.
[3] Koo KP, Kersey AD. Bragg grating-based laser sensors systems with interferometric interrogation and wavelength division multiplexing. J Lightwave Technol 1995;13:1243–9.
[4] Frazão O, Marques LM, Baptista JMT, Santos JL. Simultaneous measurement for strain and temperature based on a long-period grating combined with a high-birefringence fiber loop mirror. IEEE Photon Technol Lett 2006;18:2407–9.
[5] Huang Z, Zhu Y, Chen X, Wang A. Intrinsic Fabry–Perot fiber sensor for temperature and strain measurements. IEEE Photon Technol Lett 2006;18:1879–81.
[6] Nguyen LV, Hwang D, Moon S, Moon DS, Chung Y. High temperature fiber sensor with high sensitivity based on core diameter mismatch. Opt Express 2008;16:11369–75.
[7] Bao H, Wang T, Shen Y. High sensitive coupling evanescent wave temperature sensor. Proc SPIE 2005;5634:558–62.
[8] Chandani SM, Jaeger NAF. Fiber-optic temperature sensor using evanescent fields in D fibers. IEEE Photon Technol Lett 2005;17:2706–8.
[9] Zhu T, Ke T, Rao Y, Chiang KS. Fabry–Perot optical fiber tip sensor for high temperature measurement. Opt Commun 2010;283:3683–5.
[10] Rota-Rodrigo S, Lopez-Amo M, Kobelke J, Schuster K, Santos JL, Frazão O. Simultaneous strain and temperature measure based on a single suspended core photonic crystal fiber. Proc SPIE 2014;9157 915721-1–4.
[11] Pinto AMR, Baptista JM, Santos JL, Lopez-Amo M, Frazão O. Micro-displacement sensor based on a hollow-core photonic crystal fiber. Sensors 2012;12:17497–503.
[12] Rao YJ, Jackson DA. Recent progress in fiber optic low-coherence interferometry. Meas Sci Technol 1996;7:981–99.
[13] Bock WJ, Urbańczyk W. Temperature-desensitization of fibre-optic pressure sensor by simultaneous measurement of pressure and temperature. Appl Opt 1998;37:3897–901.
[14] Urbańczyk W, Bock WJ. Influence of dispersion on sensitivity of highly birefringent fibers to temperature and hydrostatic pressure. Appl Opt 1998;37:3176–80.
[15] Frazão O, Baptista JMT, Santos JL. Recent advances in high-birefringence fiber loop mirror sensors. Sensors 2007;7:2970–83.
[16] Osório JH, Cordeiro MB. Optical sensor based on two in-series birefringent optical fibers. Appl Opt 2013;52:4915–21.
[17] Jin Y, Chan CC, Zhang Y, Dong X, Zu P. Temperature sensor based on a pressure-induced birefringent single-mode fiber loop mirror. Meas Sci Technol 2010;21:065204.
[18] Egorov SA, Mamaev AN, Polyantsev AS. Spectral signal processing in intrinsic interferometric sensors based on birefringent polarization-maintaining optical fibers. J Lightwave Technol 1995;13:1231–6.
[19] Hlubina P, Ciprian D, Knyblová L. Interference of white light in tandem configuration of birefringent crystal and sensing birefringent fiber. Opt Commun 2006;260:535–41.
[20] Hlubina P, Olszewski J, Martynkien T, Mergo P, Makara M, Poturaj K, et al. Spectral-domain measurement of strain sensitivity of a two-mode birefringent side-hole fiber. Sensors 2012;12:12070–81.
[21] Hlubina P, Martynkien T, Urbańczyk W. Dispersion of group and phase modal birefringence in elliptical-core fiber measured by white-light spectral interferometry. Opt Express 2003;11:2793–8.
[22] Hlubina P, Ciprian D. Absolute phase birefringence dispersion in polarization-maintaining fiber or birefringent crystal retrieved from a channeled spectrum. Opt Lett 2010;35:1566–8.
[23] Zang Z, Yang W. Theoretical and experimental investigation of all-optical switching based on cascaded Gs separated by an erbium-doped fiber. J Appl Phys 2011;109:103106.
[24] Zang Z. All-optical switching in Sagnac loop mirror containing an ytterbium-doped fiber and fiber Bragg grating. Appl Opt 2013;52:5701–6.
[25] Woliński TR. Polarimetric optical fibres and sensors. In: Progress in optics, vol. XL; 2000. p. 1–75.
[26] Martynkien T, Statkiewicz G, Szpulak M, Olszewski J, Golojuch G, Urbańczyk W, et al. Measurements of polarimetric sensitivity to temperature in birefringent holey fibers. Meas Sci Technol 2007;18:3055–60.
[27] Szczurowski MK, Martynkien T, Statkiewicz-Barabach G, Urbańczyk W, Webb DJ. Measurements of polarimetric sensitivity to hydrostatic pressure, strain and temperature in birefringent dual-core microstructured polymer fiber. Opt Express 2010;18:12076–87.
[28] Hlubina P, Martynkien T, Olszewski J, Mergo P, Makara M, Poturaj K, et al. Spectral-domain measurements of birefringence and sensing characteristics of a side-hole microstructured fiber. Sensors 2013;13:11424–38.
[29] Hlubina P, Ciprian D. Spectral-domain measurement of phase modal birefringence in polarization-maintaining fiber. Opt Express 2007;15:17019–24.
[30] Ghosh G. Dispersion-equation coefficients for the refractive index and birefringence of calcite and quartz crystal. Opt Commun 1999;163:95–102.
[31] Hlubina P, Luňáček J, Ciprian D, Chlebus R. Windowed Fourier transform applied in the wavelength domain to process the spectral interference signals. Opt Commun 2008;281:2349–54.
[32] Martynkien T, Szpulak M, Urbańczyk W. Modeling and measurement of temperature sensitivity in birefringent photonic crystal holey fibers. Appl Opt 2005;44:7780–8.
[33] Urbańczyk W, Martynkien T, Bock WJ. Dispersion effects in elliptical-core highly birefringent fibers. Appl Opt 2001;40:1911–20.
[34] Zhang F, Lit JWY. Temperature and strain sensitivity measurements of high-birefringent polarization-maintaining fibers. Appl Opt 1993;30:2213–8.